

Declaration

I, Hannah Elizabeth Painter, confirm that the work presented in this thesis is my own. Where information has been derived from other sources, I confirm that this has been indicated in the thesis.

The copyright of this thesis rests with the author and no quotation from it or information derived from it may be published without the prior written consent of the author.

Abstract

The Bacille Calmette–Guérin (BCG) vaccine offers partial protection against tuberculosis (TB). Vaccines able to sufficiently contribute to global TB control are required urgently. The mouse model is an important tool for preclinical evaluation of TB vaccines, however protection in this model is not always predictive of efficacy in humans. TB is caused by various members of the *Mycobacterium tuberculosis* (MTB) complex. Differences in the host response to infection are known; however, incorporation of this diversity into *in vivo* studies is not viable due to the large number of animals required. Currently, vaccines are commonly evaluated against laboratory strains. The evidence of protection gained from these studies is likely to be incomplete. The *ex vivo* mycobacterial growth inhibition assay (MGIA) represents an alternative viable tool to perform head-to-head screening of vaccine-induced immunity. A murine splenocyte MGIA has been established.

This thesis demonstrates the adaptation of the murine MGIA for use with lung cells, as a potential readout of lung immunity. Further, the MGIA was used to determine vaccine-induced growth inhibition against multiple MTB clinical isolates. Comparison of the MGIA and *in vivo* infection was performed for the first time using clinical isolates. Observations indicate that the MGIA may represent a tool to evaluate vaccines against the most prevalent MTB lineages. Further optimisation for other lineages is required. Evaluation of the biological processes underlying growth inhibition was performed by RNA-seq. Vaccine- and lineage-specific gene perturbations were identified. Comparison of correlates of growth inhibition in the MGIA and protection in an *in vivo* dataset revealed that the lung MGIA recapitulates several elements of *in vivo* transcriptional perturbation observed following infection.

Collectively, these observations demonstrate that the MGIA warrants further development as a simplified model of *ex vivo* immunity to infection able to expediate and diversify preclinical TB vaccine testing.

Acknowledgements

I'd firstly like to thank my supervisors, Helen, Andrea and Rajko for their guidance, support and wisdom throughout my PhD project. Helen, thank you for your optimism and trust in my ability to get assays working and learn how code – two cynics in the room would not have got me to this point!

I'd like to express gratitude to the three members of my Advisory Committee, Sam Willcocks, Rachel Tanner and Julius Müller for their support and recommendations throughout this project. An extra special thanks to Sam for being such a great sounding board, extra set of hands during takedowns and friend in the lab. Thank you to lab mates old and new in 420 and 424, and everyone from what was 480. Rachel Gregory and Carolynne Stanley, thank you for your LSHTM wisdom and help with ordering. To Paola Niola and Ayad Eddaoudi at UCL, thank you for your valued assistance with the sequencing and flow cytometry components of this project.

I would like to express particular thanks to the BSF staff, and Greg Bancroft, for all the time invested training me, help with animal experiments and for always being so level-headed. I would like to acknowledge all the animals used in this project and hope that the outcomes of this study will make a contribution to a reduction in use of animals in TB research in the future.

I'd also like to thank the Medical Research Council and Rosetrees Trust for funding this PhD, as well as the administration staff from both funding bodies for their support.

Thank you to the two groups I was welcomed into on placements undertaken during this PhD. To Tom Scriba, Elisa Nemes, Stanley Mbandi Kimbung and all the staff and students at SATVI, as well as Rhea Coler, Sasha Larsen and the Coler Group at SCRI.

And finally to friends and family who have supported me over the last four years, particularly Hadija Uwase-Pottier.

This thesis is dedicated to Adrian Painter (1943 – 2020).

Table of contents

Declaration	3
Abstract	4
Acknowledgements	5
List of figures	13
List of tables	15
List of abbreviations.....	17
1 Introduction.....	21
1.1 Tuberculosis and the <i>Mycobacterium tuberculosis</i> complex	21
1.1.1 History.....	21
1.1.2 Epidemiology	21
1.1.3 The spectrum of TB infection and disease.....	23
1.1.4 TB treatment and drug resistance.....	24
1.1.5 <i>Mycobacterium tuberculosis</i> complex	25
1.2 Immune response to TB infection.....	27
1.2.1 Innate immunity	28
1.2.2 Adaptive immunity	30
1.2.3 The granuloma	31
1.3 Animal models of TB.....	32
1.3.1 Mouse.....	33
1.3.2 Guinea pig	34
1.3.3 Non-human primates.....	35
1.4 TB vaccines.....	35

1.4.1	Current.....	37
1.4.2	Immune targets for the generation of an effective TB vaccine.....	39
1.4.3	Analysis and induction of immunity at the lung mucosa.....	40
1.4.4	The current TB vaccine pipeline.....	44
1.4.4.1	Whole-cell live vaccines.....	47
1.4.4.2	Whole-cell inactivated vaccines.....	49
1.4.4.3	Subunit vaccines.....	50
1.4.5	Evaluation of TB vaccines in animal models.....	53
1.5	Immunological correlates of protection.....	54
1.5.1	A systems biology approach to CoP.....	56
1.5.2	Correlates of risk.....	58
1.6	Mycobacterial growth inhibition assays.....	59
1.6.1	Human MGIAs.....	59
1.6.2	Animal MGIAs.....	62
1.6.2.1	Bovine MGIAs.....	64
1.6.2.2	NHP MGIAs.....	64
1.6.2.3	Murine MGIAs.....	65
1.6.3	Mycobacterial quantification and the BACTEC system.....	68
1.6.4	Immune mechanisms of growth inhibition.....	68
1.6.4.1	Cytokine and chemokine production.....	68
1.6.4.2	T-cell subsets.....	70
1.6.4.3	Other immune cell populations and products.....	71
1.7	Diversity of the MTB complex.....	71
1.7.1	Host response to MTB complex infection.....	71
1.7.2	Vaccine-induced protection against the MTB complex.....	74

1.7.3	Mycobacterial diversity in the MGIA.....	76
1.7.4	Murine MGIA for vaccine evaluation	77
2	Project structure	79
2.1	Study rationale	79
2.2	Hypothesis.....	80
2.3	Study aims and objectives.....	80
2.4	Thesis structure	82
3	Materials and methods	83
3.1	Solutions, reagents, consumables and equipment.....	83
3.2	Ethics statement	83
3.3	Mycobacteria.....	83
3.4	Vaccines	84
3.5	Generation of mycobacterial stocks.....	84
3.6	Assessment of stock stability and estimation of CFU.....	85
3.7	BACTEC MGIT system.....	86
3.8	BACTEC MGIT standard curve	87
3.9	Animals	87
3.10	Vaccine preparation and immunisation.....	88
3.11	Lung cell isolation.....	89
3.12	Spleen cell isolation	90
3.13	Sample pooling	90

3.14	<i>Mycobacterium</i> spp. 2-thiophenecarboxylic acid hydrazide susceptibility	91
3.15	Mycobacterial growth inhibition assay	91
3.15.1	Mycobacteria/murine cell co-culture	91
3.15.2	Direct-to-MGIT set-up	93
3.15.3	Post-culture CFU quantification	93
3.16	Murine infection with MTB	95
3.17	RNA extraction	95
3.18	Quality control	98
3.19	Library preparation and sequencing	99
3.20	RNA-seq data analysis	100
3.20.1	Initial quality control with FASTQC and read trimming with BBDuk	101
3.20.2	Generation of genome index and read alignment with STAR	102
3.20.3	Alignment quality control with RESeQC and Picard Tools	103
3.20.4	Read counting with featureCounts	103
3.20.5	MultiQC report generation	104
3.20.6	Differential gene expression analysis	104
3.20.6.1	DESeq2	105
3.21	Microarray analysis	108
3.22	Mouse lung module enrichment analysis	109
3.23	Flow cytometry	111
3.23.1	Data analysis	113
3.24	Statistical analysis	113

4	Results I – Adaption of the <i>ex vivo</i> mycobacterial growth inhibition assay for use with murine lung cells.....	116
4.1	Chapter background.....	116
4.2	Aims and objectives.....	116
4.3	Abstract.....	116
4.4	Introduction.....	117
4.5	Results.....	120
4.5.1	Number of murine lung cells influences mycobacterial growth inhibition by immunised and control groups.....	120
4.5.2	Comparison of MTB Erdman and BCG growth inhibition.....	122
4.5.3	<i>Mycobacterium</i> spp. TCH susceptibility.....	124
4.5.4	Vaccine-mediated inhibition of mycobacterial growth in lung cell culture	125
4.6	Discussion.....	128
4.6.1	Conclusions.....	134
4.7	Materials and methods.....	134
4.7.1	Ethics statement.....	134
4.7.2	Mycobacteria.....	135
4.7.3	Animals.....	135
4.7.4	Immunisation.....	135
4.7.5	Lung and spleen cell isolation.....	136
4.7.6	<i>Ex vivo</i> mycobacterial growth inhibition assay.....	137
4.7.7	<i>Mycobacterium</i> spp. 2-thiophenecarboxylic acid hydrazide susceptibility	138

4.7.8	Statistical analysis	138
4.8	Supplementary materials	139
5	Results II – The <i>ex vivo</i> murine mycobacterial growth inhibition assay as a tool to expand tuberculosis vaccine testing against representative lineages of the <i>Mycobacterium tuberculosis</i> complex	145
5.1	Introduction	145
5.2	Aims and objectives	149
5.3	Materials and methods	150
5.4	Results	150
5.4.1	Vaccine-mediated growth inhibition of MTB complex clinical isolates in <i>ex vivo</i> lung cell culture.....	150
5.4.2	Head-to-head comparison of the murine <i>ex vivo</i> MGIA with <i>in vivo</i> MTB infection	157
5.4.3	<i>Ex vivo</i> growth of ancient L1 (N0072) in unvaccinated murine lung cells in the MGIA is lower compared with L2	160
5.5	Discussion	161
5.5.1	Limitations and future studies.....	165
5.5.2	Conclusions	166
6	Results III – The biology of growth inhibition in the MGIA.....	167
6.1	Introduction.....	167
6.2	Aims and objectives	169
6.3	Materials and methods	170
6.4	Results	170

6.4.1	Analysis of the host immune cell input in the murine lung MGIA.....	170
6.4.2	Correlates of <i>ex vivo</i> BCG growth inhibition in the BCG-vaccinated murine lung	178
6.4.3	Correlates of protection in the murine lung following <i>in vivo</i> <i>M bovis</i> challenge 184	
6.4.4	Correlates of <i>ex vivo</i> growth inhibition of MTB complex clinical isolates in the BCG-vaccinated murine lung.....	190
6.5	Discussion	197
6.5.1	Limitations and future studies.....	207
6.5.2	Conclusions.....	208
7	Final discussion and conclusions	210
7.1	Final discussion.....	210
7.2	Conclusions.....	220
8	References.....	222
9	Appendix.....	276
9.1	Appendix 1. Published MGIA protocols and results.	277
9.2	Appendix 2. Experimental analysis of host response to infection with strains of the MTB complex and vaccine-induced protection.....	311
9.3	Appendix 3. Solutions, reagents, consumables and equipment.	328
9.3.1	Solutions.....	328
9.3.2	Reagents	329
9.3.3	Antibodies: flow cytometry	331
9.3.4	Consumables	332

9.3.5	Equipment	333
9.4	Appendix 4. MTB complex clinical strains reference set.	334
9.5	Appendix 5. LSR II configuration for flow cytometry panel I.	336
9.6	Appendix 6. RNA-seq I – Library prep input and MultiQC report.	337
9.7	Appendix 7. RNA-seq II – Library prep input and MultiQC report.	339
9.8	Appendix 8. DEG lists from Venn diagram intersections (LFC > 1, padj<0.05).	342
9.9	Appendix 9. DEG lists from Venn diagram intersections (LFC < -1, padj<0.05).	344

List of figures

Chapter 1: Introduction

Figure 1-1. Global TB incidence rate 2019.	22
Figure 1-2. MTB complex.	26
Figure 1-3. Immune response to MTB infection.	27
Figure 1-4. Immune targets for vaccine-induced protection.	41

Chapter 2: Project structure

No figures

Chapter 3: Materials and methods

Figure 3-1. MGIA overview.	92
Figure 3-2. Overview of RNA extraction protocol using the RNeasy mini kit.	98
Figure 3-3. Overview of library preparation process.	99
Figure 3-4. Effect of LFC shrinkage using ash.	108
Figure 3-5. Singhania murine lung transcriptional modules.	110

Chapter 4: Results I – Adaption of the *ex vivo* mycobacterial growth inhibition assay for use with murine lung cells

Figure 4-1. Host-cell density affects growth inhibition in the <i>ex vivo</i> MGIA.	121
Figure 4-2. Residual BCG in murine lung cells following intranasal vaccination in the <i>ex vivo</i> MGIA.	123
Figure 4-3. Optimised <i>ex vivo</i> MGIA comparing MTB Erdman growth inhibition conferred by vaccination in murine lung.	126
Figure S4-1. <i>Ex vivo</i> MGIA comparing BCG growth inhibition conferred by vaccination in murine splenocytes.	139
Figure S4-2. Quantification of MTB Erdman growth inhibition by plating on solid media in the optimised <i>ex vivo</i> MGIA.	140
Figure S4-3. <i>Ex vivo</i> MGIA comparing MTB Erdman growth inhibition conferred by vaccination in murine splenocytes.	141
Figure S4-4. Comparison of inter-assay consistency of MTB Erdman growth inhibition between BACTEC MGIT and plating.	142
Figure S4-5. BACTEC MGIT standard curves.	143

Chapter 5: Results II – The *ex vivo* murine mycobacterial growth inhibition assay as a tool to expand tuberculosis vaccine testing against representative lineages of the *Mycobacterium tuberculosis* complex

Figure 5-1. TCH susceptibility of clinical isolates.	151
Figure 5-2. MTB complex clinical isolate BACTEC MGIT standard curves.	152
Figure 5-3. Growth inhibition of L1–4 by BCG-vaccinated murine lung cells versus unvaccinated control.	154
Figure 5-4. Head-to-head comparison of MGIA and MTB challenge study.	158
Figure 5-5. Mycobacterial growth in control murine lung cells.	160

Chapter 6: Results III – The biology of growth inhibition in the MGIA

Figure 6-1. <i>Ex vivo</i> BCG growth inhibition by BCG-vaccinated murine lung cells versus control lung cells.	171
Figure 6-2. Flow cytometry gating strategy I.	172
Figure 6-3. Cell populations in the murine lung MGIA input.	174
Figure 6-4. Flow cytometry gating strategy II.	175

Figure 6-5. Cell populations in murine lung and spleen MGIA input.	177
Figure 6-6. Study design – RNA-seq I.	178
Figure 6-7. PCA plot of PC1 versus PC2 for all samples in RNA-seq I.	179
Figure 6-8. Venn diagrams – RNA-seq I.	180
Figure 6-9. tmod analysis – RNA-seq I.	182
Figure 6-10. Study design – Aranday–Cortes microarray dataset.	184
Figure 6-11. PCA plot of PC1 versus PC2 for all samples in the Aranday– Cortes microarray dataset.	185
Figure 6-12. tmod analysis – Aranday–Cortes microarray dataset.	187
Figure 6-13. <i>Ex vivo</i> MTB growth inhibition by BCG-vaccinated murine lung cells versus control lung cells.	190
Figure 6-14. Study design – RNA-seq II.	191
Figure 6-15. PCA plots – RNA-seq II.	192
Figure 6-16. Venn diagrams – RNA-seq I.	194
Figure 6-17. tmod analysis – RNA-seq II.	195

Chapter 7: Final discussion and conclusions

No figures

List of tables

Chapter 1: Introduction

Table 1-1. Clinical TB vaccine pipeline.	45
--	----

Chapter 2: Project structure

No tables

Chapter 3: Materials and methods

Table 3-1. Clinical strains selected from the MTB complex reference set for downstream analysis.	85
Table 3-2. Organ- and mycobacteria-specific dilutions for CFU quantification following 96-hour MGIA co-culture.	94

Chapter 4: Results I – Adaption of the *ex vivo* mycobacterial growth inhibition assay for use with murine lung cells

Table S4-1. MGIA intra-assay variability. 144

Chapter 5: Results II – The *ex vivo* murine mycobacterial growth inhibition assay as a tool to expand tuberculosis vaccine testing against representative lineages of the *Mycobacterium tuberculosis* complex

Table 5-1. Comparison of parameters of MGIA versus MTB challenge study for a three-group study design testing against four strains of MTB. 147

Table 5-2. MTB complex clinical isolate non-linear regression analysis. 152

Table 5-3. MGIA intra-assay variability. 156

Chapter 6: Results III – The biology of growth inhibition in the MGIA

Table 6-1. Summarised enrichment analysis results for RNA-seq I analysis and Aranday–Cortes microarray. 188

Chapter 7: Final discussion and conclusions

No tables

List of abbreviations

ACDP	Advisory Committee on Dangerous Pathogens
ACK	Ammonium-chloride-potassium
ACR	Alpha crystallin
AEC	Airway epithelial cell
AM Φ	Alveolar macrophage
ANOVA	Analysis of variance
APC	Antigen-presenting cells
AUROC	Area under the receiver operating curve
BAL	Bronchoalveolar lavage
BAM	Binary alignment map
BCE	Before common era
BCG	Bacille Calmette–Guérin
BED	Browser extensible data
BME	Beta-mercaptoethanol
BMM	Bone marrow-derived macrophages
BSF	Biological Services Facility
BSL	Biosafety level
CCL	Chemokine (C–C motif) ligand
CD	Cluster of differentiation
CERNO	Coincident extreme ranks in numerical observations
CFP-10	Culture filtrate protein 10
CFU	Colony forming units
ChAd	Chimpanzee adenovirus vector
CMV	Cytomegalovirus
CoP	Correlate(s) of protection
CoR	Correlate(s) of risk
CV	Coefficient of variation
CXCL	Chemokine (C–X–C motif) ligand
D2M	Direct-to-MGIT
DC	Dendritic cell
DBD	Dextran-binding domain
DEA	Differential expression analysis
DEGs	Differentially expressed genes
DMSO	Dimethyl sulfoxide
DTP	Days-to-positivity
DURT	Donor-unrestricted T-cell
ELISA	Enzyme-linked immunosorbent assays
ELISpot	Enzyme-linked immune absorbent spot
EMI-TB	Eliciting Mucosal Immunity to Tuberculosis
EPI	Expanded Programme on Immunization

ESAT-6	Early secreted antigenic target 6
ESX-1	ESAT-6 secretion system
FMO	Fluorescence minus one
GEO	Gene Expression Omnibus
GLM	Generalised linear model
GP	Guinea pig
GSK	GlaxoSmithKline
GTF	Gene transfer format
HBHA	Heparin-binding haemagglutinin adhesin
HEV	High endothelial venule
HLA	Human leukocyte antigen
HPC	High-performance computing
IAVI	International AIDS Vaccine Initiative
ICMR	Indian Council of Medical Research
IDRI	Infectious Disease Research Institute
i.d.	Intradermal
i.m.	Intramuscular
i.n.	Intranasal
i.p.	Intraperitoneal
ICH	Institute for Child Health
IFN γ	Interferon gamma
IL	Interleukin
ILC	Innate lymphoid cell
IM Φ	Interstitial macrophage
iNKT	Invariant natural killer T
iNOS	Inducible nitric oxide synthase
ISG	Interferon-stimulated genes
IVC	Individually ventilated cage
L	Lineage
LFC	Log ₂ fold change
LSHTM	London School of Hygiene & Tropical Medicine
LTBI	Latent TB infection
Ly6C	Lymphocyte antigen 6 complex, locus C
Ly6G	Lymphocyte antigen 6 complex, locus G
MAF	<i>Mycobacterium africanum</i>
MAIT	Mucosa-associated invariant T
MDR	multi-drug resistant
M Φ	Macrophage
MGIA	Mycobacterial growth inhibition assay
MGIT	Mycobacterial growth indicator tubes
MHC	Major histocompatibility complex
ML ratio	Monocyte to lymphocyte ratio
MMP	Maximal mappable prefixes

MPIIB	Max Planck Institute of Infection Biology
MTB	<i>Mycobacterium tuberculosis</i>
MVA85A	Modified vaccinia Ankara-expressing Ag85A
NB	Negative binomial
NHP	Non-human primate
NK	Natural killer
NO	Nitrogen oxides
NTM	Nontuberculous mycobacteria
OD	Optical density
PA	Pasteur Aeras
padj	Adjusted p
PAMP	Mycobacterial pathogen-associated molecular pattern
PBMC	Peripheral blood mononuclear cell
PBS	Phosphate-buffered saline
PBS-T80	Phosphate-buffered saline–Tween 80
PCA	Principal component analysis
PGE	Prostaglandin E2
PLH	People living with HIV
PoD	Prevention of disease
PoI	Prevention of infection
PRR	Pattern recognition receptor
QC	Quality control
RAM	Random access memory
RBC	Red blood cell
RD1	Region of difference 1
rBCG	Recombinant BCG
RINe	RNA integrity number equivalent
RLU	Relative light units
ROI	Reactive oxygen intermediates
RR	Rifampicin resistant
SAM	Sequence alignment map
s.c.	Subcutaneous
Siglec	Sialic acid-binding immunoglobulin-type lectins
SII	Serum Institute of India
SSI	Statens Serum Institut
TB	Tuberculosis
TbD1	MmpS6/MmpL6-encoding Mtb-specific deletion 1
TBVI	Tuberculosis Vaccine Initiative
T _C	Cytotoxic T
TCH	2-thiophenecarboxylic acid hydrazide
T _{CM}	Central memory T
T _{EM}	Effector memory T
T _{FH}	Follicular helper T

T _H	T helper
TLR	Toll-like receptor
TNF α	Tumour necrosis factor alpha
T _{reg}	Regulatory T
T _{RM}	Tissue-resident memory T
TTD	Time-to-detection
TTP	Time-to-positivity
uM Φ	Undifferentiated macrophage
VPM	Vakzine Projekt Management
WB	Whole blood
WGCNA	Weighted gene correlation network analysis
WHO	World Health Organization
XDR	Extensively drug resistant

1 Introduction

1.1 Tuberculosis and the *Mycobacterium tuberculosis* complex

1.1.1 History

Tuberculosis (TB) has afflicted humankind throughout the majority of its history. Great epidemics and declines have been noted during this period, with written references to TB in the Old Testament approximately 3,000 years ago [1]. During the seventeenth to nineteenth centuries large epidemics were recorded in North America and Europe, accounting for up to one in four deaths during this period [2]. In 1882, the German physician and microbiologist, Robert Koch, discovered the causative agent of TB: *Mycobacterium* species of the *Mycobacterium tuberculosis* (MTB) complex [3]. Improvements in working and living environments, sanitation and nutrition, as well as significant breakthroughs in understanding of the etiology and pathogenesis of TB, are considered to have contributed to the eventual decline in TB mortality rates in Europe and North America [4].

Despite considerable developments in TB treatment and prevention since, including the development of effective anti-TB drugs and a vaccine, TB remains a major public health concern globally, particularly in low- and middle-income countries [5]. At present, TB is a top ten cause of death globally and a leading cause of death from a single infectious agent [5].

1.1.2 Epidemiology

According to the World Health Organization (WHO), approximately 10 million people developed active TB disease, and 1.4 million people died as a result of TB disease

in 2019. Global TB incidence in 2019 per 100,000 population is shown in Figure 1-1. India (26%), China (8.4%), Indonesia (8.5%), the Philippines (6.0%), Pakistan (5.7%), Nigeria (4.4%), Bangladesh (3.6%) and South Africa (3.6%) accounted for two-thirds of TB cases. Thirty high-burden TB countries accounted for 87% of cases [5].

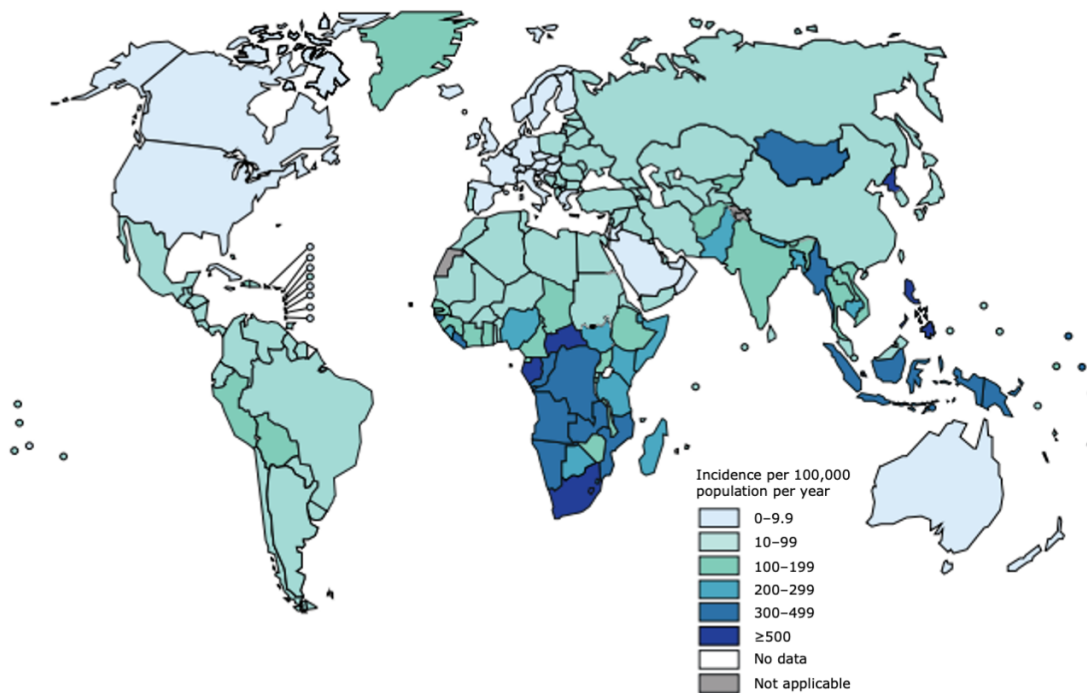


Figure 1-1. Global TB incidence rate 2019. Reproduced from [5].

Unchanged from epidemics more than 100 years ago, socio-economic factors, such as poor living and working conditions, sanitation, air quality, as well as malnutrition, stress and co-infections, continue to impact susceptibility to TB disease [6]. The ongoing HIV pandemic represents a major driver of TB disease, particularly in sub-Saharan Africa. The risk of developing active TB is 18-fold higher in people living with HIV (PLH) compared with HIV-negative individuals [5]. At present, PLH account for 8.2% of active TB cases globally, although rates of co-infection exceed 50% in regions of Southern Africa. In 2019, 14.7% of TB deaths occurred in PLH [5]. In addition to HIV co-infection,

other known risk factors for TB disease include substance abuse, type II diabetes mellitus, use of immunosuppressive drugs and smoking. Men are twice as likely as women to develop active TB disease [5,7].

1.1.3 The spectrum of TB infection and disease

TB is primarily an airborne infection, transmitted from person to person through aerosol-generating actions. TB in adults is commonly, although not exclusively, pulmonary. Forms of extrapulmonary TB include infection of the pleura, lymph nodes, abdomen, genitourinary tract, skin, joints, bones and central nervous system [8]. Widespread dissemination of TB can also occur in which the infection affects multiple organs and may be present in the blood. Extrapulmonary disease largely affects children and immunosuppressed individuals [8,9].

Following MTB exposure, a persistent but asymptomatic infection is most commonly established in which a dynamic relationship of containment between the host and pathogen is introduced. Current estimates predict that one-quarter of the global population are infected with MTB, each with a 5–15% lifetime risk of developing active TB disease [10,11]. Clearance of the infection via an innate or acquired immune response may also occur. At the other end of the spectrum, approximately 5% of infected individuals rapidly progress to active disease on exposure to TB [12].

Historically, asymptomatic infection and disease has been crudely divided into latent TB infection (LTBI) and active TB, respectively; however, an increasingly complex appreciation of the spectrum of the host–pathogen interaction has arisen of late, which translates into a continuum of various asymptomatic states prior to manifestation of active clinical disease [11,12]. This continuum has been proposed to encompass three states, with speed of progression highly variable and cyclic between states in some

instances. LTBI, in which an individual is infected with viable but metabolically inactive MTB. The infection is not expected to progress further without immunological compromise. Incipient infection, in which an individual is infected with viable, metabolically active MTB which does not present radiographically and is not detectable using current microbiological techniques. Subclinical infection, in which an individual is infected with viable, metabolically active MTB which is identifiable radiographically and using microbiological techniques, but has no classical symptoms of TB. Both incipient and subclinical TB are likely to progress to active TB without intervention. In addition to the attributes described for subclinical infection, individuals with active disease present clinical symptoms classically associated with TB disease such as a persistent cough, loss of appetite, unintentional weight loss, night sweats, chills and fever [12]. Within the active disease state, heterogeneity between TB lesions within the same individual is frequently observed, representing a further spectrum of pathology previously underappreciated [13].

1.1.4 TB treatment and drug resistance

Drug-susceptible pulmonary TB is treated using a six-month rifampicin-containing regimen, typically two months of isoniazid, rifampicin, pyrazinamide and ethambutol, followed by four months of isoniazid and rifampicin [14]. The emergence of drug-resistant TB represents a key driving force of the modern TB epidemic, particularly in India, China and the Russian Federation. In 2019, almost 500,000 cases of TB were rifampicin resistant (RR), of which 78% of these cases were multi-drug resistant (MDR), defined as TB resistant to at least isoniazid and rifampicin. Further, extensively drug-resistant (XDR) TB describes additional resistance to any fluoroquinolone and to at least one of the injectable agents used for MDR-TB [5]. Second-line drugs must be introduced

into the treatment regimen of MDR-TB. Treatment is typically 18–24 months; however, a favourable treatment outcome in 90% of patients with XDR-TB or unresponsive MDR-TB has recently been reported using a six-month regimen composed of three oral drugs – bedaquiline, pretomanid, and linezolid [15].

In LTBI individuals at high risk of developing active TB disease, various regimens for the treatment of LTBI are recommended, ranging from shorter course (3–4 months) combination regimens to longer course (6–9 months) monotherapy regimens. Where drug intolerance or interactions are not predicted, short-course rifamycin-based regimens are recommended [16].

1.1.5 *Mycobacterium tuberculosis* complex

High-throughput sequence analysis has enabled in-depth reconstruction of the evolution of the MTB complex with the migration of humans. Current predictions place an early progenitor of current *Mycobacterium* species in circulation today at approximately three million years ago, in coexistence with early hominids in East Africa [17]. The most recent common ancestor of the MTB complex is estimated to have emerged 73,000 before common era (BCE) from an environmental mycobacterium [18]. The MTB complex includes causative agents of both animal and human TB. At least nine animal-adapted lineages are known [19]. Human-adapted organisms include MTB sensu stricto (lineage [L] 1–4 and 7) and *M africanum* (MAF) (L5 and 6) [20]. A sister lineage to the MTB complex, currently referred to as L8, was identified recently in the African Great Lakes region [21]. In a 2020 study analysing the genomes of more than 700 L5 and L6 strains, five unclassified strains were identified and assigned to a new lineage; L9 [22]. The phylogenetic relationship of members of the complex is shown in Figure 1-2.

Lineages of the MTB complex can also be divided into ancient/ancestral (L1, 5–7) and modern (L2–4) lineages. This division is based on the presence/absence of the MmpS6/MmpL6-encoding Mtb-specific deletion 1 (TbD1) region, respectively [23,24]. Loss of this region is hypothesised to have occurred 46,000 BCE [18]. Modern lineages demonstrate a close phylogenetic relationship [25]. Each lineage is associated with and predominates in different global regions; however modern lineages of the MTB complex are currently geographically widespread and considered drivers of the TB pandemic in sub-Saharan Africa, Eastern Europe and Southeast Asia. By contrast, L1 is geographically restricted largely to the Indo-Oceanic region and the Philippines [20,26], L5 and 6 [27] to West Africa, and L7 to Ethiopia [28].

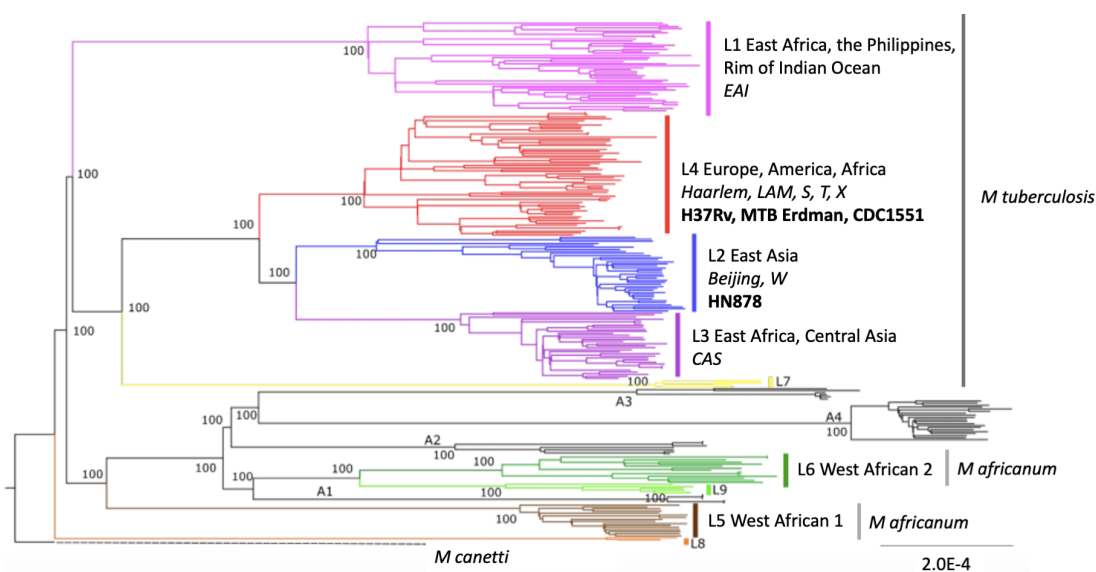


Figure 1-2. MTB complex. Maximum likelihood phylogeny of five previously unclassified genomes analysed together with a reference dataset of 248 MTB complex genomes performed to identify the newest lineage of the MTB complex: lineage 9 (light green). The reference genome set included all eight human-associated lineages (branches indicated in various colours) and four animal-associated lineages (branches indicated in black: A1–A4). The phylogeny was rooted on *M. canetti*. Bootstrap values are shown for clades corresponding to MTB complex lineages. Lineages are labelled according to their dominance in a particular geographical region. Alternative names / lineage-specific

family names identified in the literature are provided in italics for each lineage. The four most commonly used laboratory strains have been added in bold and assigned to their corresponding lineage. Figure adapted from [22]. MTB, *Mycobacterium tuberculosis*.

1.2 Immune response to TB infection

The immune response to infection with MTB is summarised in Figure 1-3. Evidence in humans and animal models of TB demonstrate the importance of cluster of differentiation (CD)4 T cells, as well as interferon gamma (IFN γ), tumour necrosis factor alpha (TNF α) and interleukin (IL)-12, in control of mycobacterial growth [29].

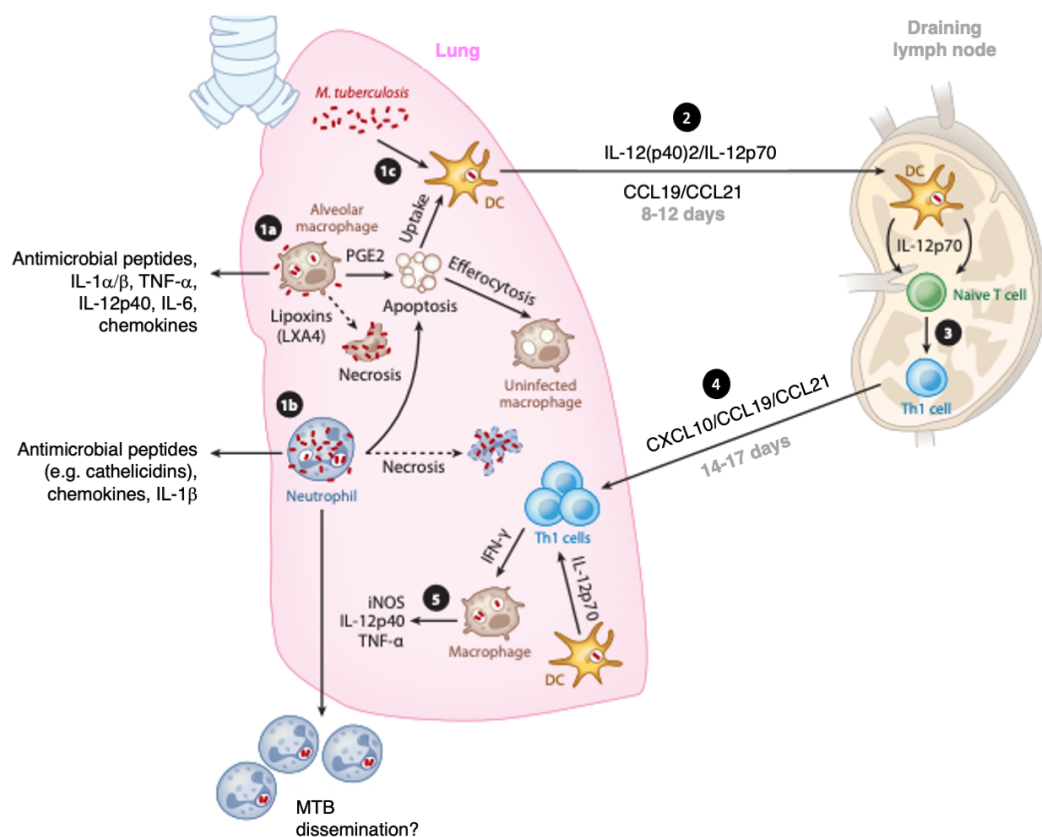


Figure 1-3. Immune response to MTB infection. Small airborne infectious droplets containing MTB are deposited in the alveoli and engulfed by (1a) AM Φ and later (1b) neutrophils and (1c) DCs. Internalisation of MTB by phagocytes induces the production and secretion of cytokines, chemokines and antimicrobial peptides. Lipid mediators determine the induction of AM Φ cell death by either necrosis (in favour of the pathogen)

or apoptosis. Apoptosis of infected cells results in efferocytosis and/or uptake by DCs. (2) Infected DCs mature and migrate to local lung-draining lymph nodes along chemokine gradients in the presence of IL-12, and present mycobacterial antigen to naïve T cells. (3) Presentation of antigen results in the expansion of antigen-specific T-cell populations which (4) migrate to the lungs and (5) activate MΦ. CCL, chemokine (C–C motif) ligand; CXCL, chemokine (C–X–C motif) ligand; DC, dendritic cell; IFN γ , interferon gamma; IL, interleukin; iNOS, inducible nitric oxide synthase; MΦ, macrophages; MTB, *Mycobacterium tuberculosis*; PGE, prostaglandin E2; T_H, T helper; TNF α , tumour necrosis factor alpha. Reproduced from [29].

1.2.1 Innate immunity

The initial host response to infection is dominated by the innate immune system and primarily involves the recognition of mycobacterial pathogen-associated molecular patterns (PAMPs) by pattern recognition receptors (PRRs). PRRs include toll-like receptors (TLRs) and members of the C-type lectin receptor family, on the cell surface of antigen-presenting cells (APCs), as well as cytosolic receptors. Stimulation of PRRs results in enhanced expression of proinflammatory molecules which mobilise local, and later systemic, immune cell populations [30].

Infection occurs when small airborne infectious droplets containing MTB enter the lungs and may be established by a single bacilli [31]. In the alveolar space, MTB can infect and is detected by airway epithelial cells (AECs), resulting in modulation of the liquid composition of the airway surface to improve its antimicrobial properties, as well as production of proinflammatory molecules that recruit and activate phagocytes to the infection site [32].

Mycobacteria are also recognised and engulfed by alveolar macrophages (AMΦs). In response to infection, mycobacterial growth may be controlled and potentially cleared by AMΦs through phagocytosis, the induction of apoptosis and the generation of reactive

oxygen intermediates (ROI), nitrogen oxides (NO) and antimicrobial peptides [29,33]. Many of these processes are mediated and enhanced by the presence of IFN γ (produced by CD4 T helper 1 [T_H1], CD8 cytotoxic T [T_C], natural killer [NK], $\gamma\delta$ T and CD1-restricted T cells), as well as TNF α , which classically activates infected M Φ s and facilitates their antimicrobial functions [34].

However, MTB is a highly adapted facultative intracellular pathogen of phagocytic cells and employs a number of evasion techniques to optimise early establishment in the lung, and modulate the immune response to its advantage. Once internalised, MTB is able to restrict the antimicrobial mechanisms of AM Φ s and generate an intracellular environment where it can remain undetected and replicate, and later infect other cells. These tactics include the prevention of phagolysosome fusion and detoxification of oxygen and nitrogen radicals to evade lysosomal killing and degradation [35,36]; inhibition of cell apoptosis to extend the survival of infected cells and enhance mycobacterial replication [37,38]; reduction in M Φ response to IFN γ [39,40]; reduction in major histocompatibility complex (MHC) II expression, maturation and trafficking for the presentation of mycobacterial peptides to the adaptive immune system [41,42]; and promotion of necrosis and recruitment of uninfected M Φ s via the early secreted antigenic target-6 (ESAT-6) secretion system (ESX)-1 type VII secretion system which facilitates spread of infection to other cells [30,43–45]. Through its prevention of innate immune activation, contact with and recruitment of components of the adaptive immune response is delayed, enabling MTB to gain a foothold in the lung and replicate relatively undisturbed for 2–3 weeks post-infection. This delay occurs in both humans and animal models of TB [46] and is likely to contribute to the inability of the majority of hosts to clear MTB infection.

Infected AMΦs migrate across the interstitial space resulting in access of mycobacteria to the lung interstitium [47]. As the MΦ infection develops, neutrophils, monocyte-derived MΦs and dendritic cells (DCs) also become infected.

1.2.2 Adaptive immunity

DCs form the primary link between the innate and adaptive immune response. Following infection, these cell types undergo maturation which promotes antigen processing and presentation whereby mycobacterial peptides docked onto MHC class I and II molecules are trafficked to the plasma membrane [48,49]. Mature DCs traffic to draining lymph nodes under the influence of IL-12(p40)₂ [50], and the chemokines chemokine (C–C motif) ligand (CCL)19 and CCL21 [29], and present antigen to naïve T cells. This results in the expansion of antigen-specific T-cell populations to generate CD4 and CD8 effector T cells. Effector T-cell populations are attracted to the lung by chemotactic factors such as chemokine (C–X–C motif) ligand (CXCL)10 and migrate from the lymph node via the circulation.

Since MTB is a facultative intracellular pathogen, the CD4 T-cell response is considered to play a vital role in mycobacterial control. Evidence in animal models of TB suggest that mycobacterial growth is rapid for the first three weeks following infection, with inhibition of mycobacterial growth found to correlate with the arrival of CD4 T cells to the lung [51–53]. The importance of CD4 T cells in mycobacterial control is exemplified by the increased susceptibility of PLH to TB [54]. In the mouse model, CD4 or MHCII knockout results in reduced capacity to control mycobacterial growth and decreased survival [55,56]. The phenotype of differentiated T cells is defined by the presence of cytokines in the microenvironment. In the context of TB, release of IL-12p70 in the lymph nodes by infected DCs results in the polarisation of CD4 T cells towards a

predominantly T_H1 phenotype able to produce IFN γ and/or TNF α and/or IL-2. IFN γ has been demonstrated to be necessary for control of MTB growth in humans and animal models [46,57,58]. The downstream targets of IFN γ signalling in the lungs are not fully understood in the context of mycobacterial control, however IFN γ is known to activate M Φ to kill intracellular mycobacteria, inducing cytokine production and antimicrobial activity [59–62]. The production of IL-17 and IL-21 by other CD4 T-cell populations has also been shown to contribute to protective immunity against TB infection [63–66].

CD8 T cells are activated by presentation of antigen in association with MHC I. Activated CD8 T cells are also a source of IFN γ and TNF α . Further, these cell types are also able to kill infected cells through the release of cytotoxic granules or induction of apoptosis via Fas/FasL interactions. Antigen-specific CD8 T cells are generated during MTB infection and recruited to the lungs [67,68], however, the importance of these populations in the context of TB remains unclear. A study in non-human primates (NHPs) found that CD8 T cells may play an important role in anti-TB immunity during reinfection and in vaccine-mediated immunity [69].

A number of other immune populations have been demonstrated to contribute to early defense against MTB infection, including neutrophils, NK cells, B cells, innate lymphoid cells (ILCs), mucosa-associated invariant T (MAIT), CD1-restricted, human leukocyte antigen (HLA)-E-restricted and $\gamma\delta$ T cells [46,70–73].

1.2.3 The granuloma

Recruitment of T-cell populations back to the lungs, as well as additional M Φ populations and B cells, results in the formation of a key characteristic of TB; the granuloma. The granuloma is a highly regulated immune microenvironment maintained by a complex interaction between inflammatory factors, immune cell populations and

hypoxia. Its general structure consists of a central necrotic core of infected MΦs surrounded by additional infected and uninfected MΦ populations, DCs, NK cells, neutrophils, fibroblasts and cells that secrete extracellular matrix components. An outer structure composed of T cells, B cells and epithelial cells is also found [29,40].

The precise role of the granuloma is unclear and its benefit to the host and pathogen is likely to be dynamic in nature, depending on the phenotype of the MTB strain and the health conditions of the host. From the perspective of the host, the granuloma facilitates containment and control of the bacilli in a quiescent state away from the rest of the body, and focuses the immune response to the site of persistence [74]. From the pathogen perspective, the granuloma represents a growing assembly of phagocytic host cells for infection and further mycobacterial replication. In 90% of cases, infection does not progress to disease indicating that granuloma formation is highly effective in the majority of individuals [10,11]. Evidence of healed, and in some cases sterile, granulomas have been identified in individuals who did not have symptoms of active disease [75]. However, where hosts present with existing risk factors, or acquire them following infection, the delicate equilibrium of immune regulation which maintains containment may be disrupted in favour of the pathogen, and active disease ensues. An environment which facilitates active mycobacterial replication and necrosis results in the subsequent breakdown of the granuloma structure and release of bacilli into other regions of the lungs to form additional lesions. Breakdown of the granuloma may also result in release of bacilli into the airways where they can be transmitted to other individuals [76].

1.3 Animal models of TB

Animal models are an integral component of scientific evaluation; however, observations must be interpreted with care. While each model shares physiological and

anatomical similarities with humans, outcomes in animals do not always translate directly. The complete human TB profile and manifestation of lesions has not been identified to be recapitulated in any animal model. The ethical implications of using live animals for scientific discovery must also be considered. Experimental design is guided by the three Rs principle: replace, reduce, refine. Under these principles, experiments must be sufficiently powered to detect reproducible, biological differences using the minimum number of animals (reduction); utilise alternative tools where available which do not require animals (replacement); and utilise experimental procedures and husbandry which minimise suffering and improve animal welfare (refinement) [77]. The use of animals in TB research has contributed to major progress in the field. Mice, NHPs and guinea pigs (GPs) are the most commonly used models at present [78].

1.3.1 Mouse

The mouse does not provide an accurate recapitulation of human TB; however, it does represent a highly manipulatable vertebrate lung and immune system [79]. Its small size, relatively low cost, wide range of reagents and knockout strains available, and well annotated genome, has generated a rich body of literature in this model [80,81].

Although mice and humans do share numerous physiological similarities, differences do exist, including variations in the adaptive and innate immune systems [82]. The most commonly used mouse strains in TB research are the C57BL/6 and BALB/c strains. Experimental infection with these strains is performed by delivery of a low dose of mycobacteria to the lungs which aims to infect 100% of the animals. Cell-mediated immunity is able to control the infection but it is not eliminated, resulting in chronic infection which has been shown to be tolerated for more than one year [83]. Correlates of human TB have been shown, including an important role for CD4 T cells [84], IL-12

[85,86] and TNFa [83,87,88]. A key variation to human TB pathology observed is the absence of progressive disease and advanced lesion types. In the C57BL/6 and BALB/c strains, lesions include high numbers of lymphocytes and macrophages, however the structure of the human TB granuloma is absent. Mycobacteria remain primarily intracellular in non-necrotic inflammatory lesions. By contrast, in advanced disease stages in humans and other animal models, mycobacteria are largely extracellular and situated within necrotic lesions [89,90]. Necrotising responses have been observed in other inbred (C3HeB/FeJ, DBA/2, CBA/J and I/St), inbred crossed (HET3) and outbred mouse strains [91]. Opportunity to model varying levels of susceptibility and resistance to TB does exist in the mouse, with susceptible strains, such as CBA, DBA/2, C3H, 129/SvJ, and resistant strains, such as BALB/c and C57BL/6. This susceptibility is retained following BCG vaccination [92].

Latency does not occur naturally in the mouse model. However, antibiotic treatment (the Cornell model) has been used to establish latency [93] and more recently contained MTB infection was generated in C57BL/6 mice using i.d. delivery of H37Rv to the ear [94]. In addition, heterogeneous mouse stocks are now available which aim to model the diversity of the human immune response and enable study of the contribution of host genetics to disease. The Collaborative Cross [95] and Diversity Outbred [96] populations are an example of such stocks. In both instances, animals exhibit varying susceptibilities and responses to MTB, as well as BCG protection.

1.3.2 Guinea pig

In contrast to the most commonly used mouse strains, GPs are generally considered to be susceptible to TB. GPs exhibit a number of similarities to TB disease in humans, presenting lung necrosis, lymphadenopathy and disease dissemination [78].

Historically, GP research has suffered from a lack of immunological reagents and tools for infection. Improvements have since been made; however, GPs remain more expensive than mice. A far smaller body of literature on TB in the GPs exists, despite representing a seemingly more accurate small animal model of human TB. To this end, low-dose infection of GPs is commonly used to evaluate vaccines following initial screening in mice [90].

1.3.3 Non-human primates

NHPs are our closest relatives phylogenetically and considered to represent the most accurate model of human TB, recapitulating a number of anti-mycobacterial components of the human immune system absent in other animal models [97]. NHPs are naturally susceptible to MTB [83,97], active disease, latency and reactivation can be established, and BCG vaccination provides partial protection [98–100]. However, NHPs are expensive to purchase and house, particularly where containment is required.

Rhesus (*Macaca mulatta*) and cynomolgus (*M fascicularis*) macaques are most commonly used in TB research. The two species display a range of infection outcomes, clinical presentations and pathologies, enabling some recapitulation of human variation. Low (<25 colony-forming units [CFU]) and ultra-low (<10 CFU) dose studies have been performed as more representative models of human infection [101,102], as well as repeated low-dose exposure [103], facilitated by more recent advances in *in vivo* imaging [104].

1.4 TB vaccines

The WHO estimates that between 2010 and 2015, 10 million deaths were prevented by vaccination [105]. Vaccination aims to establish long-lived antigen-specific

immunological memory able to rapidly and effectively eliminate future host infection with its target pathogen. Following infection or vaccination, antigen-specific T cells and B cells undergo clonal expansion and later die off following clearance of the infection. A small population of long-lived memory cells remain which are able to mount a rapid and robust response to secondary exposure to antigen [106]. Focusing on memory T-cell populations, a number of different populations have been identified. T memory stem and central memory T (T_{CM}) cells represent less differentiated populations located in secondary lymphoid organs and exhibit high proliferative capacities. More differentiated populations of memory cells exist in tissues, known as tissue-resident memory T (T_{RM}) cells, and circulating between lymphoid organs and tissues, effector memory T (T_{EM}) cells. These populations are important for rapid protection against pathogens, with the less differentiated populations functioning as a backup where necessary [107].

In the context of TB, vaccination should induce the following in response to MTB infection in order to sufficiently contribute to global TB control: a) a robust and sustained antimycobacterial immune response which circumnavigates elements of natural host immunity to MTB which facilitate mycobacterial infection; and b) timely induction of pulmonary protective mechanisms prior to establishment of MTB infection in the lung and modulation of the environment (persistence), or the ability to eliminate persistent MTB infections [108].

At present, a TB vaccine able to sufficiently contribute to global TB control is not available. The following issues play important roles in achievement of this goal and will be described in detail in the remainder of this chapter: i) BCG offers only partial protection against TB and the reasons for this are poorly understood; ii) the immune mechanisms required to obtain sterilising immunity are unknown; iii) animal models used in preclinical evaluation of TB vaccines are suboptimal representations of the human

immune response to TB infection and disease, and *in vivo* infection studies poorly replicate the conditions of human infection. Observations do not always translate into humans; and v) vaccine efficacy in humans and animal models is confirmed only by the absence of disease. A robust correlate of protection (CoP) has yet to be identified.

1.4.1 Current

Bacille Calmette–Guérin (BCG) remains the only licensed vaccine against TB. BCG has been included in the Expanded Programme on Immunization’s (EPI) infant vaccination schedule since 1974 [109] and is estimated to be administered to 100 million children per year worldwide [110]. In countries with high TB burdens, BCG vaccination is recommended at birth or within one week of life [111].

BCG is a live attenuated strain of *M bovis*, the causative agent of TB in cattle. The vaccine was produced by Calmette and Guèrin over an 11-year period (1908 to 1919) by repeated subculture of a virulent tubercle bacillus isolated from a cow with TB. In 1919, failure to cause progressive TB, and the subsequent attenuation of the strain, was confirmed in various animal models [112]. BCG was later distributed globally where it was cultured further to set up stocks for vaccination programmes, generating many of the daughter strains used at present [113].

Loss of the region of difference 1 (RD1) genomic region in BCG is considered to contribute significantly to attenuation of the vaccine. RD1 encodes two major MTB virulence factors, ESAT-6 and culture filtrate protein 10 (CFP-10), as well as structural components of the complex involved in secretion of the two antigens: the ESX-1 type VII secretion system [24].

BCG offers only partial protection against TB disease. Protection against severe and disseminated forms of TB disease in children is well documented [114] and BCG

vaccination is estimated to reduce the risk of meningeal and miliary TB by approximately 85% [111]. In high-burden countries, this protection typically wanes 10–15 years post vaccination, with increased incidence of TB disease in adolescent and young adult populations [115]. Globally, the vaccine provides highly variable levels of protection against pulmonary disease in both adults and children ranging from 0 to 80% efficacy. Higher levels of efficacy are generally reported in countries situated further from the equator with low incidence of TB [116]. The efficacy against pulmonary TB has been evaluated in numerous trials and observational studies. Two trials commonly referenced to demonstrate the dramatically different outcomes obtained in BCG trials are a UK trial in British schoolchildren and trial in a South Indian population. In the UK trial initiated in 1950, vaccine efficacy was approximately 77% over a 20-year follow-up period [117]. By contrast, in the South Indian population, no evidence of a protective effect of BCG was found 7.5 years following study start [118]. Reasons for these stark variations in pulmonary protection remain poorly understood and are likely to be caused by a number of host, vaccine and environmental factors. Host genotype [119], coinfections [120], previous exposure to MTB, bio-equivalence of BCG strain [121], nutritional and metabolic health [46], the phenotype of circulating MTB strains [122] and environmental sensitisation, such as exposure to specific nontuberculous mycobacteria (NTM) [123], have all been hypothesised to have an effect on BCG immunity [46].

Environmental exposure to NTM and the subsequent establishment of antimycobacterial immunity appears to account for some variation in BCG efficacy in different populations globally. A correlation between latitude and BCG protection has been hypothesised, whereby in tropical regions closest to the equator with an abundance of atypical NTM, BCG protection is at its poorest [123]. Identification of the causative species behind this correlation will be particularly challenging as NTMs are not unique

to the tropics. Hundreds of environmental NTMs have been identified worldwide, each demonstrating individual and collective levels of cross-reactivity with BCG [124,125]. The effect of NTM-mediated immunity on the subsequent impact of BCG vaccination may either block replication of BCG and the subsequent mechanisms involved in establishing BCG protective immunity, or mask a rise in antimycobacterial immunity due to existing background immunity [126]. Further complicating this matter, prior exposure to MTB may also have the same effect on BCG protection [124].

Beyond its TB-specific effects, BCG is considered to function as an immunomodulator and has been shown to mediate cross-protective effects against leprosy and Buruli ulcer, diseases also caused by mycobacteria [127,128], as well as heterologous (non-specific) effects. The non-specific effects of BCG are hypothesised to be mediated by innate immunity-dependent mechanisms [129]. In a recent randomised trial on BCG revaccination, as well as a noted reduction in sustained MTB infection, respiratory tract infections were significantly less common [130]. Intravesical administration of BCG is currently used to treat non-muscle-invasive bladder cancer [131]. There is also evidence that BCG reduces all-cause mortality [132].

1.4.2 Immune targets for the generation of an effective TB vaccine

In order for long-term, robust protection against TB to be generated by vaccination, a well-balanced immune response mediated by multiple arms of the immune system must be induced and sustained systemically and in the lung. Vaccine design has historically focused on induction of ‘conventional’ T_H1 immunity using a limited set of immunodominant antigens. However, more recent advances in understanding of the host response to TB have revealed a considerably more complicated landscape of TB immunity. Targeting and evaluation of immune responses beyond the T_H1 narrative must

be performed in order to generate a vaccination strategy able to sufficiently contribute to global TB control.

Components of the immune response considered to be important targets of TB vaccines are summarised in Figure 1-4. Generation of a multi-dimensional immune response may not be possible using a single vaccine design and may require a combination of vaccine approaches [46].

1.4.3 Analysis and induction of immunity at the lung mucosa

The immune response to infection in the lung remains poorly understood, however, increasing efforts are being made to understand mucosal immunity, as well as how to target it by vaccination. As the main site of MTB entry and infection, the installation of a robust immune response in the lungs as a first line of defence is a core aim of modern TB vaccine design. Administration of BCG via the intradermal (i.d.) route generates a suboptimal immune response in the lung mucosa at best [133].

The localisation of effective anti-mycobacterial adaptive and innate immunity to the lung by vaccination has been hypothesised to represent a viable method of improving vaccine-mediated protection against pulmonary TB. One argument in favour of installation of localised lung immunity in advance of infection, relates to its potential to overcome the known delay in pathogen recognition and recruitment of adaptive immunity to the lung following infection. Where established prior to infection, a capacity to intercept MTB at early stages of infection may be possible prior to initiation of the various immune modulation strategies used by the pathogen to survive and replicate in host cells.

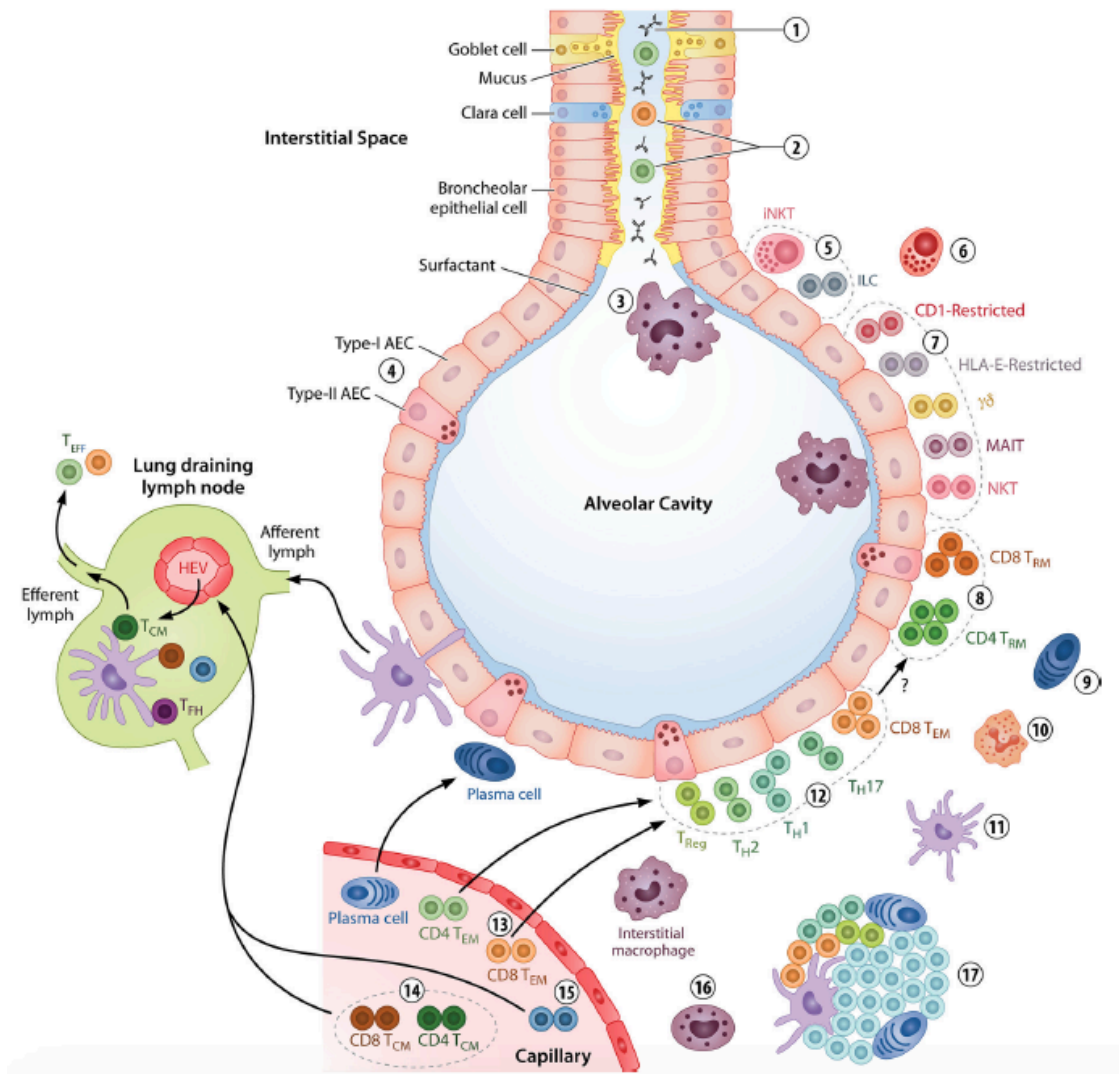


Figure 1-4. Immune targets for vaccine-induced protection. Robust and sustainable vaccine-mediated protection against TB is likely to require an extensive and broad immune response mediated by multiple arms of the immune system. The following components of systemic and lung mucosal immunity have been proposed as important targets of vaccination to generate effective immunity. 1) Protective airway antibodies. 2) Airway T-cell populations with ‘innate-like’ recognition abilities and early effector functions able to produce cytokines which enhance bactericidal properties of AMΦs and recruit monocyte-derived MΦs. 3) Increased microbicidal properties and trained immunity of AMΦs. 4) Increased surfactant secretion and anti-microbial peptide production by AECs. Presence of trained 5) innate lymphoid cells, 6) NK cells, 7) unconventional T cells and vaccine-induced 8) T_{RM} cells at the submucosa functioning as sensory cells, assisting in recruitment of memory T-cell populations and early effectors to enhance mycobacterial killing. 9) Generation of plasma cells able to rapidly secrete

specific antibodies against antigen. 10) Regulation of neutrophil population over infection period to facilitate the antimicrobial environment. 11) Increased activation, capacity to present antigen and speed of migration of DCs to draining lymph nodes to activate T_{CM} and memory B cells. Establishment of long-lived, rapidly deployable and specific 12) airway interstitial T_{EM} , and 13) circulating T_{EM}/T_{EFF} and 14) T_{CM} populations with sustained proliferative and multifunctional capacity. Primed effector populations display specificity to various stages of MTB infection and a capacity for recruitment to the lung where necessary. 15) Long-lived circulating memory B cells able to home to lymph nodes and specific plasma cells. 16) Increased trained immunity of monocytes. 17) Generation of lymphoid follicles as a local site of antigen presentation. AECs, alveolar epithelial cells; $AM\Phi$, alveolar macrophage; DC, dendritic cells; HEV, high endothelial venule; ILC, innate-lymphoid cell; iNKT, invariant natural killer T cell; MAIT, mucosa-associated invariant T cell; NK, natural killer; TB, tuberculosis; T_{CM} , central memory T; T_{EFF} , effector T; T_{EM} , effector memory T; T_{FH} , T follicular helper; T_H , T helper; T_{reg} , T regulatory; T_{RM} , tissue resident memory T. Reproduced with permission [46].

In the mouse, GP and NHP model, delivery of BCG via the respiratory route has been demonstrated to enhance its protective efficacy [103,133–135]. A phase-I human clinical trial of aerosolised BCG administration in healthy, BCG-naïve UK adults is currently underway (NCT02709278). Further, a number of candidate TB vaccine strategies in the clinical [136–143] and preclinical [43,144,153–156,145–152] pipeline are delivered directly to the lung and have been demonstrated to induce superior protection compared with i.d. BCG alone. These include mucosal delivery of BCG, or mucosal boost vaccines which follow parenteral administration of BCG. Described in more detail in section 1.4.4.

Use of a cytomegalovirus (CMV) vector for antigen delivery has been demonstrated to establish T-cell responses outside of lymphoid structures even where administered systemically. In rhesus macaques, the induction and maintenance of tissue-resident MTB-specific CD4 and CD8 memory T-cell responses in the lungs was shown

following subcutaneous (s.c.) delivery of two CMV-vectored TB vaccines [108,157]. The first phase-I clinical trial of a CMV-vectored TB vaccine was planned for 2020 [158].

Regardless of whether vaccine delivery is systemic or mucosal, an ability to assess vaccine-induced immunity at the site of infection during vaccine evaluation is vital. In small animal models, evaluation of lung immunity can be performed using a study design in which groups of animals are culled at various time points following vaccination and/or challenge, and the immune components of the lung can be directly assayed. A study of this design is not feasible in humans or larger animal models, and assessment of potential immunological correlates of TB vaccine efficacy to date has typically been performed in peripheral blood. It is currently unknown whether the immune response in blood represents an informative readout of the lung. Antigen-specific T-cell responses in the blood and lung have been shown to poorly correlate in infected NHPs and humans [159]. These observations emphasise that a robust correlate(s) of vaccine protection against TB may not be detectable in the blood and may represent an immunological readout present in the lung. As an example, in a recent study in the macaque model, immune responses associated with vaccine protection were detected in the lung compartment but were absent in the blood [103].

Evaluation of pulmonary immune responses following vaccination can be performed on airway cells obtained via bronchoalveolar lavage (BAL) and this procedure can be repeatedly performed during NHP studies [160]. Large-scale collection of BAL across a human clinical trial cohort is not currently feasible but is increasingly performed on a smaller scale within human studies. Whether BAL provides a representative readout of tissue-resident immunity remains unknown and should be evaluated further in animal models, particularly NHPs in which the process of BAL acquisition is similar to human sampling [159]. In this context, preclinical animal models represent critically important

tools for the evaluation of mucosal immunity following vaccination and validation of correlates of protection in the lung across different sample types. At present, ethically and financially viable immunological tools and markers to facilitate these studies are lacking.

1.4.4 The current TB vaccine pipeline

Since BCG does provide protection against childhood manifestations of TB and appears to have important non-specific effects, novel TB vaccination strategies build on BCG. Candidate vaccines represent i) replacements for BCG which improve on the safety, strength and/or the duration of the current vaccine-induced immune response or ii) booster vaccines to BCG-generated responses which are able to induce a broader and/or novel vaccine-induced immune response to BCG alone [81].

The current TB vaccine clinical pipeline (Table 1-1) includes vaccines for prophylactic (prevention of infection), postexposure (prevention of disease) and therapeutic use, and can be broadly divided into the following: whole-cell live, whole-cell inactivated, adjuvanted protein subunit and viral-vector subunit vaccines.

Table 1-1. Clinical TB vaccine pipeline.

Vaccine	Type	Components	Mode	Developers	Trial status
MTBVAC	Whole cell (live)	Attenuated MTB Mt103 clinical isolate (L4)	PoI, PoD	University of Zaragoza, Biofabri, TBVI, IAVI	IIa
VPM1002	Whole cell (live)	rBCG: urease C deletion, lysteriolysin insertion	PoI, PoD, therapeutic	SSI, VPM, MPIIB, ICMR	III
BCG (revaccination)	Whole cell (live)	Attenuated <i>M bovis</i>	PoI	IAVI	IIb
BCG (aerosol)	Whole cell (live)	Attenuated <i>M bovis</i>	PoI	University of Oxford	I
RUTI	Whole cell (inactive)	Detoxified, fragmented MTB + liposomes	Therapeutic	Archivel Farma	III
DAR-901	Whole cell (inactive)	<i>M obuense</i> (heat-killed)	PoI, PoD, therapeutic	Geisel School of Medicine, Aeras	IIb
MIP	Whole cell (inactive)	<i>M indicus pranii</i> (inactive)	PoD, therapeutic	ICMR, Cadila Pharmaceuticals	III
Vaccae	Whole cell (inactive)	<i>M vaccae</i> (heat-killed)	PoD, therapeutic	Anhui Zhifei Longcom	III
H56:IC31	Protein / adjuvant	H56: Ag85B + ESAT-6 + Rv2660c	PoI, PoD, therapeutic	SSI, IAVI, Valneva	IIb

		IC31: KLK + ODN1a			
ID93 + GLA- SE	Protein / adjuvant	ID93: Rv1813 + Rv2608 + Rv3619 + Rv3620 GLA-SE: MPL + GLA	PoI, PoD, therapeutic	IDRI, Quratis, Genova Biopharmaceuti cals	Ila
AEC/BCO2	Protein / adjuvant	AEC: Ag85b + ESAT-6 / CFP-10 BCO2: BCG- derived CpG + aluminium salt	PoD	Anhui Zhifei Longcom	I
M72/AS01 _E	Protein / adjuvant	M72: Rv0125 + Rv1196 AS01 _E : MPL- A + QS-21	PoI, PoD	GSK, IAVI	Iib
GamTBvac	Protein / adjuvant	Ag85a + ESAT6– CFP10 + DBD DEAE- dextran + CpG	PoI	Gamaleya Research Institute	Ila
ChAdOx1.85A + MVA85A (i.d., i.m., aerosol)	Viral vector	ChAdOx1 expressing Ag85A MVA expressing Ag85A	PoI, PoD, therapeutic	Oxford University, Birmingham University	I/Ila

Ad5Ag85A (aerosol)	Viral vector	Ad5Ag expressing Ag85A	PoI, PoD	McMaster University, CanSino	I
TB/FLU-04L (i.n.)	Viral vector	Live- attenuated influenza virus expressing ESAT-6 and Ag85A	PoI, PoD	Research Institute for Biological Safety Problems	IIa

ChAd, chimpanzee adenovirus vector; DBD, dextran-binding domain; GSK, GlaxoSmithKline; IAVI, International AIDS Vaccine Initiative; ICMR, Indian Council of Medical Research; i.d., intradermal; IDRI, Infectious Disease Research Institute; i.m. intramuscular; MPIIB, Max Planck Institute for Infection Biology; MVA, modified vaccinia virus Ankara; PoD, prevention of disease; PoI, prevention of infection; rBCG, recombinant bacillus Calmette-Guérin; SII, Serum Institute of India; SSI, Statens Serum Institut; TBVI, Tuberculosis Vaccine Initiative; VPM, Vakzine Projekt Management.

1.4.4.1 Whole-cell live vaccines

Whole-cell live vaccines based on live mycobacteria with attenuated virulence were originally developed as replacement vaccines for BCG in infants but are now also in evaluation as booster vaccines for adolescents and adults. Vaccines within this group are generated through recombinant DNA technology and include MTB deletion mutants and BCG strains with MTB antigen, cytokine or host resistance factor inserts [6]. Approaches in design of vaccines within this category include modification of the evasion strategies of mycobacteria and reduction in persistence or replication following infection. As whole-cell live organisms, these vaccines have intrinsic adjuvant properties and may be capable of generating a broader and more diverse immune response to numerous antigens compared with subunit vaccines in which antigens are selected [161]. However,

as is the case for BCG, efficacy of candidates of this design may be affected by prior exposure to mycobacteria. There are ethical issues associated with vaccines designed to replace BCG and the implications of withholding BCG in an infant cohort in order to evaluate their efficacy; however these candidates may be of value in HIV-positive infants in which BCG is currently contraindicated [46].

Examples currently in the clinical pipeline are VPM1002 and MTBVAC. VPM1002 (BCG Δ ureC::hly) is a recombinant BCG strain in which urease C, which prevents phagosome maturation, is replaced with listeriolysin O, a *Listeria monocytogenes* protein which enables mycobacterial escape from the phagosome and facilitates presentation on MHC class I molecules [6]. Safety and immunogenicity of VPM1002 has been demonstrated in healthy infants and adults, as well as HIV-exposed infants [162,163]. A phase-III trial is planned in newborns receiving either VPM1002 or BCG to assess the efficacy, safety and immunogenicity of VPM1002 as a prophylactic vaccine (NCT04351685). Further, a phase-II/III trial to determine the safety and efficacy of the vaccine in prevention of TB recurrence is currently recruiting (NCT03152903).

MTBVAC is a recombinant MTB deletion mutant strain attenuated by double deletion of two virulence genes, *phoP* and *fadD26* [164]. MTBVAC has been demonstrated to be safe in adults and infants, with an acceptable reactogenicity profile [165]. Further dose-defining studies are recruiting in infant (NCT03536117) and adult populations (NCT02933281), as well as in an adolescent population previously vaccinated with BCG [158].

BCG revaccination has also been evaluated. Previous studies in which the efficacy of BCG revaccination was evaluated reported no or limited additional protection against TB disease to primary BCG alone [166–168]. However, in a recent prevention of infection study in South African adolescents, BCG revaccination was not found to prevent

infection, but was observed to reduce the rate of sustained infection (measured by QuantiFERON conversion + two consecutive positive results) for the follow-up period of two years, by 45.4%, indicating a potential capacity to regulate and/or clear infection. Further, BCG revaccination was found to reduce the frequency of higher QuantiFERON values associated with enhanced risk of developing TB disease [130].

1.4.4.2 Whole-cell inactivated vaccines

Whole-cell inactivated vaccines use killed whole mycobacterial species or extracts, such as lysates or fragments, generated from mycobacterial species. Examples of whole mycobacterial species in the clinical pipeline at present include DAR-901, MIP, RUTI and Vaccae.

The booster vaccine, DAR-901, is composed of heat-killed *M obuense* under evaluation as a prophylactic, postexposure and therapeutic vaccine. In phase-I clinical trials in MTB-infected and -uninfected BCG-vaccinated individuals DAR-901 was safe and immunogenic [169,170], however it did not prevent IGRA conversion in an adolescent population in Tanzania [171]. Evaluation as a postexposure and therapeutic vaccine continues.

MIP (Immunvac) is composed of inactivated *M indicus pranii* and is licensed as a leprosy drug in India. Clinical evaluation of MIP as a therapeutic TB vaccine has been performed with inconclusive results [172,173]. Clinical evaluation as a postexposure vaccine is also underway [46].

RUTI vaccine is made from detoxified cellular fragments of MTB cultured under stress with the aim to mimic internal granuloma conditions and induction of antigens representative of latency [174]. RUTI has been clinically evaluated largely as a

therapeutic vaccine and shown to be immunogenic and safe [175]. A phase-IIa clinical trial in MDR-TB patients is planned (NCT02711735).

The *Vaccae* vaccine is composed of heat-killed *M vaccae* and is approved in China as an adjunct to TB drug therapy. Use of the vaccine in combination with drug treatment has been demonstrated in patients with pulmonary TB disease [176,177]. Results from a phase-III clinical trial have yet to be published (NCT01979900).

1.4.4.3 Subunit vaccines

Subunit vaccines are designed to be administered following BCG vaccination and provide a heterologous boost to existing BCG-primed immune responses. Candidates include viral-vectored vaccines which include live, attenuated, non-replicating viruses engineered to deliver target antigens to host cells, and adjuvanted protein vaccines in which protein antigens are administered with various adjuvant formulations.

Modified vaccinia Ankara-expressing Ag85A (MVA85A) was the first subunit TB vaccine to enter clinical trial and is a viral-vectored subunit vaccine composed of a recombinant strain of modified Vaccinia Ankara virus expressing the immunodominant MTB protein, antigen 85A. Despite demonstrating protection against TB in preclinical animal studies [178,179], MVA85A was safe but did not reduce TB disease in humans. In infants, antigen-specific T_H1 and T_H17 responses were enhanced following MVA85A despite absence of improved protection against TB infection or disease on BCG alone [180]. In HIV-positive adults, MVA85A was also found to enhance antigen-specific T_H1 responses, again in the absence of enhanced protection over BCG alone. Results emphasise the incomplete understanding of what constitutes a protective host immune response to TB in humans and how preclinical observations made in animal models translate into humans [181].

Viral-vectored vaccines in the clinical pipeline at present include ChAdOx1.85A + MVA85A, Ad5Ag85A and TB/FLU-04L, and are designed to be heterologous booster vaccines following BCG priming. These vaccines are under investigation as mucosal vaccines, in addition to administration systemically (ChAdOx1.85A + MVA85A and Ad5Ag85A).

ChAdOx1.85A is a novel chimpanzee adenovirus-vectored vaccine expressing Ag85A. Administered in combination with MVA85A, the regimen is proposed to induce CD4 (MVA85A) and CD8 responses (ChAdOx1.85A) [142]. The ChAdOx1.85A + MVA85A regimen has been evaluated in healthy BCG-vaccinated UK adults and was safe and immunogenic when delivered via the intramuscular (i.m.) route [143]. The safety and immunogenicity profile of i.m. and aerosol administration of ChAdOx1.85A is currently under evaluation in BCG-vaccinated healthy adults (NCT04121494). A phase-I/II dose-escalation and age de-escalation study of the prime–boost combination is recruiting (NCT03681860). In the mouse model, intranasal (i.n.) administration of ChAdOx1.85A + MVA85A following BCG vaccination was found to induce strong immune responses and a higher level of protection against MTB challenge than BCG i.d. alone [142].

Ad5Ag85A is composed of a replication-deficient human adenovirus serotype 5 vector expressing Ag85A. In the mouse model, protection afforded by BCG-prime Ad5Ag85A-boost was higher when Ad5Ag85A was administered i.n. versus i.d. [182]. A phase-I clinical trial in healthy adults found that i.d. administration was safe and immunogenic [136]. Aerosol administration of the vaccine is currently under evaluation in a phase-I trial in healthy BCG-vaccinated adults (NCT02337270).

TB/FLU-04L utilises a replication-deficient live attenuated influenza A virus vector to express Ag85A and ESAT-6 and is delivered via the i.n. route. In a phase-I trial

in Kazakhstan in healthy BCG-vaccinated adults, the vaccine was reported to be safe and immunogenic. Future evaluation as a postexposure vaccine is planned [183].

Adjuvanted protein vaccines in the clinical pipeline at present include H56:IC31, ID93 + GLA-SE, AEC/BCO2, GamTBvac and M72/AS01_E. A number of these vaccines include antigens selected as representative of different stages of MTB early infection and virulence, latency and active disease (listed in Table 1-1). Adjuvants utilised in these vaccines to induce a stronger response to the target antigens were selected largely on the basis of ability to induce cellular immunity and include TLR agonists (TLR4 and 9) in combination with other adjuvants and delivery agents.

H56:IC31 and ID93 + GLA-SE are in development as therapeutic, prophylactic and postexposure vaccines and have been demonstrated to be safe and immunogenic in target populations [46,184–187]. Clinical trials of these candidates are ongoing. GamTBvac was found to be safe and immunogenic in a phase-I trial in healthy adults [188], and is under evaluation in a phase-IIa trial as a prophylactic vaccine in healthy BCG-vaccinated adults (NCT03878004). The safety and immunogenicity of the postexposure vaccine, AEC/BCO2, is under evaluation in a phase-Ib clinical trial in China in healthy adults (NCT04239313).

M72/AS01_E has been extensively tested in phase-I and -II clinical trials as a prophylactic and postexposure vaccine in adults in TB endemic and non-endemic areas [158,189–191], as well as infants and adolescents in endemic areas [192,193]. The vaccine has been found to be safe and immunogenic. In a phase-IIb clinical trial in HIV-negative LTBI adults, a 54.0% reduction in progression to pulmonary TB disease was identified in the M72/AS01_E-vaccinated group at approximately 2.3 years follow up [194]. Vaccine efficacy at three years was more recently reported at 49.7% [195].

1.4.5 Evaluation of TB vaccines in animal models

Systematic screening of the safety, immunogenicity and efficacy of candidate vaccines is performed in various animal models. Efficacy is predominantly assessed by *in vivo* challenge studies in which animals are vaccinated and later infected with MTB via aerosol or i.n. delivery at the peak of the effector T-cell response following vaccination. Efficacy is defined as a significant improvement in disease severity following MTB challenge in vaccinated compared with unvaccinated animals and is quantified by parameters such as bacterial load in the lung and spleen, pathology scores and long-term survival [196]. When evaluating candidate vaccines, BCG is generally included as a positive control. A current challenge in the design of studies to evaluate candidates lies in the risk that the kinetics of one vaccination strategy may vary significantly to other, making it difficult to determine an appropriate vaccine-to-challenge interval and ensure sufficient time has been granted for a memory T-cell response to be established. The timing of boosting vaccines is also an issue [78].

It is recommended that novel TB vaccine candidates are tested in a minimum of two animal species, in at least two laboratories, using sufficiently powered study designs. Head-to-head evaluation of promising candidates is later performed to identify vaccines for testing in NHPs.

At present this is not done. Globally, the capacity to test candidate vaccines in mice far exceeds that of any other animal model, and a vast amount of funding is assigned to this step with seemingly poor return. Further, vaccines are predominantly tested against the MTB laboratory strains H37Rv or MTB Erdman. Where testing expands beyond these strains, isolates used are often poorly characterised and unavailable to the wider community (described in detail in section 1.7). Ideally, a widely accessible reference set

of representative clinical isolates would be utilised in this setting to improve reproducibility and comparison between candidates.

Unfortunately, the current lack of international collaboration and funding in the TB field can make it difficult to progress into head-to-head testing of vaccines and other animal models. MTB challenge experiments are expensive, require a large number of animals and sufficient housing capacity in BSL3 facilities. Where head-to-head testing is performed, and/or where different strains of MTB are introduced, the cost and number of animals required rises further. Establishment of laboratories able to independently evaluate candidates may provide some resolution to this issue. Further, the development of lower cost and more ethically viable tools to perform comparative testing must be developed to accelerate these studies and diversify strains used to evaluate vaccine performance. *Ex vivo* functional assays represent complementary tools to facilitate this expansion and are described further in section 1.6.

1.5 Immunological correlates of protection

An immunological CoP, as defined by the European Medicines Agency, is ‘a type and amount of immunological response that correlates with vaccine-induced protection against a clinically apparent infectious disease and that is considered predictive of clinical efficacy’ [197,198]. This marker may be causally related or unrelated to the mechanisms by which protection is instated in the host [199]. In order to identify a correlate of vaccine protection, the sample population should include protected and unprotected individuals of sufficient size to perform comparisons, for example evaluation of a vaccine in a placebo-controlled clinical trial with a disease endpoint [198].

Effective TB vaccines must induce robust long-lasting immune responses able to eliminate or contain MTB. Ideally, a thorough understanding of the mechanisms by which

vaccine-mediated protection is established, as well as the changes in cell populations and molecules which substantiate this protection, are known. The BCG vaccine was developed empirically approximately 100 years ago. Despite major progression in understanding of human immunology over the century since, an incomplete comprehension of immune protection against TB remains. To this end, current TB vaccine development retains some degree of empiricism [159,200]. TB vaccine development does not have a reliable CoP to predict vaccine efficacy. In the absence of bona fide correlates, rational vaccine design and down selection cannot be performed, and candidates traverse the pipeline to large-scale field trials in humans utilising immune correlates which inadequately model protection against TB [201]. To complicate matters further, where novel CoP are identified, validation in clinical trials in which a vaccine demonstrates efficacy must be performed, representing a ‘chicken and egg’ scenario.

Readouts of protective immunity during the evaluation of TB vaccines have historically focused on the CD4 T-cell response and secretion of IFN γ . A role for CD4 T_{H1} cells and IFN γ in protection against TB has been appreciated for decades [56,202–206], with the majority of subunit vaccines in the current pipeline designed by selection of MTB antigens able to induce IFN γ [159]. However, a shift in this paradigm has occurred of late following conflicting data in human clinical trials on the role of IFN γ [181,207,208], as well as from animal studies in which the shortcomings of a focus on the IFN γ T_{H1} response for protection against TB have been shown [103,209–212]. Measurement of IFN γ alone is now considered to represent an inaccurate CoP.

Emerging evidence from animal and human data highlight roles in protection against TB by other host immune components. These cell types include T_{H17} cells [66,103,144,213], donor-unrestricted T-cells (DURTs) such as NKT cells [214–217] and

$\gamma\delta$ T cells [218–227], and specific antibody isotypes [207,228–234]. The importance of the innate immune system is also gaining traction [129,235–237].

1.5.1 A systems biology approach to CoP

Vaccine evaluation is commonly performed in conjunction with immunological methods, such as enzyme-linked immunosorbent assays (ELISAs), Luminex, enzyme-linked immune absorbent spot (ELISpot) and flow cytometry, to define immune cell phenotypes and secreted proteins. These techniques rely on the predefined and the inevitably biased selection of target readouts which may not include novel CoP. The complex and ever-expanding landscape in which a robust CoP against TB may be identified highlights the value of utilising an unbiased systems biology approach. High-throughput ‘omics’ technologies are able to generate a global view of the status of biological systems at various levels, including the genome, transcriptome, proteome and metabolome [238].

In other disease settings, a systems biology approach has been used to successfully identify early gene signatures predictive of vaccine efficacy. Blood transcriptome profiling following vaccination with YF-17D, a yellow fever vaccine, identified early innate immune signatures predictive of the subsequent adaptive immune response [239]. A study of similar design was also performed using two vaccine candidates against influenza to identify early predictive markers of adaptive immunity which were subsequently mechanistically validated in the mouse model [240].

In the context of TB, it has been suggested that CoP may be vaccine-, strain- and/or population-specific, emphasising the importance of incorporating unbiased methods into evaluation of vaccine-induced protection and head-to-head comparisons of candidates to encompass the range of correlates that may be revealed [241].

Blood samples from the M72/AS01_E [194] trial in which vaccine efficacy was observed were archived, representing an invaluable opportunity for the study of correlates and mechanisms of protection associated with vaccination [159]. However, as was the case in this study, the number of TB disease cases in study cohorts enrolled in vaccine trials is often small, resulting in limited power to perform robust CoP analysis. As a potential solution to this, the utilisation of infection endpoints has been proposed; an outcome which may be ten times higher than disease over the study period [198]. How prevention of infection translates to prevention of disease, and whether this end point is suitable for evaluation of specific vaccine candidates only (i.e. prophylactic) remains to be understood fully. In the 2018 BCG revaccination trial [130], revaccination with BCG was demonstrated to protect against infection. Blood samples were archived and plans to perform CoP analysis on this dataset are in place.

Although CoP cannot be validated in animal models of TB, the incorporation of systems biology approaches into preclinical evaluation of vaccines represents a tool to gain early mechanistic insight into vaccine-induced protection and identify CoP within a specific animal model. CoP may be tracked through to larger animal models and into clinical trials as early indicators of translation of vaccine-induced protection into humans. In a recent evaluation of a CMV-based TB vaccine in rhesus macaques, whole blood (WB) RNA-seq analysis was performed to identify gene expression signatures which correlated with differential outcomes in vaccinated animals following MTB infection. A set of 280 genes were identified which were associated with eventual outcome. Further, transcriptional module and pathway enrichment analysis of samples obtained prior to vaccination revealed unique enrichment of genes in animals later identified to be protected, as well as in susceptible animals [108].

1.5.2 Correlates of risk

Prospective cohort studies and clinical vaccine trials, even in the absence of vaccine efficacy, represent a valuable source of longitudinal patient samples for the evaluation of correlates of risk (CoR) for development of TB disease. To date, more progress has been made in the identification of CoR compared with CoP.

CoR provide the opportunity to improve understanding of the mechanisms of progression from TB infection to disease, and on a practical level to identify individuals for preventative treatment, monitor response to drug therapy and select individuals for clinical evaluation of vaccine and drug candidates [198]. An imbalance in monocyte to lymphocyte ratio (ML) was identified as a CoR in a South African infant cohort using microarray analysis and cellular phenotyping. This observation was validated in additional infant and adult cohorts [198,242,243]. Further, samples from the infant MVA85A phase-IIb trial were used to evaluate CoR. Increased frequency of HLA-DR⁺ CD4 T cells were found to correlate with risk of TB disease which was later confirmed in an independent adolescent cohort. BCG-specific T cells secreting IFN γ and Ag85A IgG were found to correlate with reduced risk [207]. In the same cohort, enhanced risk of developing disease was later found to correlate with CD8 T-cell activation and prior or subclinical infection with CMV [244].

Machine learning and statistical approaches, such as random forest, support vector machine and pair ratio algorithm, have been applied to longitudinal gene expression analysis datasets to derive biosignatures of incipient and LTBI, to determine an individual's risk of progression to active disease, as well as signatures of active TB disease [245]. Evaluation of the performance of a number of these signatures in the mouse and NHP model has also been performed [246] (Painter, manuscript in preparation) as potential tools for the preclinical evaluation of vaccine and drug efficacy.

1.6 Mycobacterial growth inhibition assays

The mycobacterial growth inhibition assay (MGIA) is a functional assay hypothesised to replicate a range of host immune mechanisms and complex interactions *ex vivo*. The summative capacity of a mixed population of host cells to control mycobacterial growth is determined by *ex vivo* culture with mycobacteria for a defined period, followed by quantification of mycobacterial load. Where host phenotype or treatment provides an ability to regulate mycobacterial growth, such as vaccinated versus unvaccinated, a level of growth inhibition is observed compared with a selected control. Human and animal MGIA have been described. A summary of MGIA performed to date is provided in Appendix 1.

Growth inhibition may represent a functional CoP. The assay aims to model natural or *in vivo* infection in a faster and more ethically viable manner. In the context of preclinical vaccine evaluation, the *ex vivo* nature of the assay facilitates head-to-head testing of vaccine-induced protection against a diverse set of MTB strains and may represent an important opportunity to resolve current concerns regarding the translation of preclinical observations made in animal models of TB to the clinical setting.

1.6.1 Human MGIA

The human MGIA represents a potential method of ethically viable experimental infection and surrogate of human challenge. Modern human MGIA perform *ex vivo* mycobacterial co-culture with WB or peripheral blood mononuclear cells (PBMCs) and have been used to evaluate TB drugs [247–253] and vaccines [199,207,261–264,247,254–260], as well as improve understanding of mycobacterial control.

Early human MGIA commonly used monocyte-derived MΦs obtained from PBMCs, stimulated *ex vivo* with lymphokines or recombinant cytokines [265–273]. The

first example of a human MGIA was performed by Crowle *et al* in 1981 as a method for detecting tuberculoimmunity. Lymphokines collected from antigen-stimulated lymphocytes were applied to a MΦ and mycobacteria co-culture. Intracellular mycobacterial replication was inhibited in MΦs cultured with lymphokines from samples from PPD+ individuals only, including those historically vaccinated with BCG [265]. Two vaccine studies were performed by Cheng *et al* using *ex vivo* stimulated autologous lymphocytes, rather than lymphokines. Growth inhibition in both studies was consistent with previous epidemiological observations in each population [115]. In agreement with BCG protection demonstrated in British schoolchildren, *M microti* growth rates were significantly lower in monocytes pulsed daily with stimulated autologous lymphocytes isolated from British schoolchildren after vaccination compared with before [270]. Further, in a South Indian population in which BCG protection was absent, no difference in *M microti* growth rates was noted following vaccination [271].

Modern human MGIAs comprise two forms: WB and PBMCs. Use in vaccine clinical trials has been limited to date [242,256,257].

In WB MGIA, heparinised blood is diluted and co-cultured with mycobacteria for 3–4 days in tubes before mycobacterial load is quantified. During the early twenty-first century, two methods of WB MGIA were published which utilised distinct quantification methods: lux luminescence [254,255,282,274–281] and the BACTEC mycobacterial growth indicator tube (MGIT) system [248,249,284–289,250–253,256,257,259,283].

In 2000, the lux assay, which utilises mycobacterial species engineered to constitutively express luminescent lux genes, was reported by Kampmann *et al*. Following co-culture with blood samples, mycobacterial quantification was performed by reading luminescence and expressed as relative light units (RLU) / second. RLU and

CFU have been demonstrated to correlate [274]. This assay was more recently optimised for investigation of paediatric immunity to TB by reducing the blood input volume required for the assay [280,281], and has been utilised in a study on Gambian children highly exposed to TB [282].

In 2001, Wallis *et al* published a WB MGIA protocol in which mycobacterial quantification was performed using the BACTEC MGIT system (described further in sections 1.6.3 and 3.7). Compared with the lux assay, the BACTEC system offers more flexibility to analyse a range of mycobacterial species and clinical isolates as it does not require bacterial transformation and construction of luminescent strains. With growing interest in the diversity of the MTB complex and recommendations to evaluate TB vaccines against diverse representatives of mycobacteria, WB MGIA developed using the BACTEC system represent a more viable method to incorporate these interests.

Three methods of PBMC MGIA can be found in the literature: i) primary lymphocyte inhibition assay; ii) secondary lymphocyte inhibition assay; and iii) direct. The primary lymphocyte inhibition assay involves separation of adherent and non-adherent PBMC fractions, mycobacterial infection of adherent cells for one hour, followed by addition of non-adherent cells and culture for seven days. In the secondary lymphocyte inhibition assay, total PBMC are rested or stimulated for seven days, added to previously infected MΦs and cultured for three days [290]. Lastly, in the direct assay, the MΦ infection step is eliminated and PBMCs are directly co-cultured with mycobacteria for four days. The latter assay is most commonly performed at present.

The direct PBMC MGIA was developed by Fletcher *et al* in 2013 [256] for use in rotating tubes and has been optimised more recently [263]. Mycobacterial co-culture in 48-well plates was demonstrated to increase host cell viability, and reduce intra- and inter-assay and site variability compared with tubes. Further, in a later study, growth inhibition

demonstrated by the optimised assay was shown to correlate with the protection readout obtained from an *in vivo* human challenge model at the per person and group level [199].

A comparison of the primary and secondary lymphocyte inhibition assay (PBMCs) and the lux WB MGIA was performed by Hoft *et al* in 2003. The three assays were all demonstrated to detect mycobacterial growth inhibition following vaccination, however, readouts were shown to reflect complementary but independent components of immune function [275]. More recently Fletcher *et al* performed a head-to-head comparison of the direct WB and PBMC MGIA in a UK adult population receiving primary BCG vaccination followed by revaccination. Mycobacterial growth inhibition was detected by the PBMC MGIA only following primary BCG vaccination, consistent with clinical trial data. No improvement in mycobacterial control was detected following revaccination in the WB or PBMC MGIA. Later, an association between haemoglobin/iron levels and *in vitro* mycobacterial growth was identified by Tanner *et al* which may account for the disparities observed in growth inhibition between the two assays [259].

1.6.2 Animal MGIA

Animal MGIA have been described for mice, NHPs [259,291] and cattle [292–294]. These MGIA represent complementary tools to classic *in vivo* infection studies. At the timepoint in which animals would be infected with MTB, organs or blood samples are instead obtained and co-cultured with mycobacteria *ex vivo* to assess the ability of host cells to regulate mycobacterial growth. In some animal models, mycobacterial growth inhibition has been demonstrated to correlate with *in vivo* mycobacterial load as a readout of protection against TB.

Compared with *in vivo* MTB challenge studies, MGIA are lower in cost, shorter in study duration and do not require specialised BSL-3 animal containment facilities.

Since animals are not infected with MTB, the severity limit required for the experiment is decreased. For example, MTB infection studies in mice are assigned the highest severity limit ('severe') by the UK Home Office; studies which use vaccination only are assigned a 'moderate' severity limit. Where MGIA's are optimised and growth inhibition is demonstrated to correlate with *in vivo* protection, the assay represents a novel tool to minimise animal suffering and improve welfare in TB studies, in line with the refinement principle of the NC3Rs [77].

Further, the MGIA represents an opportunity to reduce the number of animals required to perform a sufficiently powered study, in line with the reduction principle of the NC3Rs. In comparison to MTB challenge studies where one animal provides one data point per organ, each organ/blood volume harvested for *ex vivo* co-culture in the MGIA represents multiple inputs for the assay. This provides several options for the researcher: i) the number of animals required to test a hypothesis against a single strain of mycobacteria can be reduced by pooling of samples within groups to generate technical replicates for the assay (in-bred animals only); ii) samples can be tested against multiple mycobacterial strains; and/or iii) remaining cells can be utilised in other immunological assays to expand the readout generated from the study.

In murine MGIA's, organs are harvested at the equivalent time point to *in vivo* infection, processed into single cell suspensions and co-cultured *ex vivo* with mycobacteria. In larger animal models, organ harvest can also be performed at the infection time point, however these studies also include the option to acquire blood samples up to and at this time point. To date, animal MGIA's have been exclusively utilised to evaluate TB vaccines and/or manipulate immune components to improve understanding of the host response to TB. Assessment of drug performance has not been performed in animal models using the MGIA.

1.6.2.1 Bovine MGIA

Bovine MGIA have been performed using WB and PBMCs. Three vaccination studies which included a PBMC MGIA have been performed [292–294]. Observations on the ability of cells from BCG-vaccinated cows to control mycobacterial growth compared with unvaccinated animals are conflicting, with only one study demonstrating growth inhibition [293]. In the most recent bovine MGIA study, the direct WB and PBMC MGIA were adapted for use in cattle. Enhanced mycobacterial control was not observed in cells from BCG-vaccinated animals compared with unvaccinated [294]. BCG protection in cattle is not complete and is complicated by exposure to environmental mycobacteria [295]. *In vivo* challenge was not performed alongside any of the described bovine MGIA studies and therefore it is difficult to determine whether observations made are an accurate readout of vaccine-mediated protection or whether the bovine MGIA requires further optimisation to capture this protection.

1.6.2.2 NHP MGIA

To date, WB and PBMC MGIA have been performed in NHPs [259,291]. Both MGIA were utilised by Tanner *et al*, alongside human MGIA, to identify a role for haemoglobin/iron in mycobacterial growth inhibition [259]. The PBMC MGIA was performed by Dijkman *et al* in an MTB infection study using rhesus and cynomolgus macaques. Species-dependent variations in TB pathology and bacterial burden were not reflected in the capacity of PBMCs to control mycobacterial growth, indicating that the NHP MGIA in its current form does not represent a CoP against *in vivo* infection [291].

1.6.2.3 Murine MGIA

Murine MGIA identified in the literature can be broadly divided into two themes:

i) *ex vivo* infection of MΦs from naïve animals with mycobacteria, followed by addition of ‘primed’ immune cell populations or their cytokine products [267,268,304,296–303]; and ii) *ex vivo* co-culture of splenocytes from vaccinated/unvaccinated animals with mycobacteria [174,201,305–308].

Early murine MGIA largely performed *ex vivo* co-culture of mycobacterial species with peritoneal or bone-marrow-derived MΦs (BMM) in combination with adaptive immune cells, or lymphokines, previously exposed to mycobacteria (theme 1). Analysis of growth inhibition in the presence of recombinant IFN γ was also performed [267,268,296–300,302–304]. One of the first examples of the MGIA was performed by Youmens *et al* in 1979 in the mouse model. In this study, isolated splenocytes were stimulated *ex vivo* with MTB and lymphokines collected. MTB-infected peritoneal MΦs were then cultured in the presence/absence of these lymphokines. A reduction in mycobacterial growth was observed in MΦs in the presence of lymphokines [301]. Vaccine-induced mycobacterial growth inhibition was first demonstrated by Rook *et al* in 1985 using the MGIA. Addition of T cells from mice immunised with heat-killed MTB to cultured MΦs infected with MTB was found to induce a bacteriostatic effect [302].

Later, MGIA built on the same concept utilised naïve BMMs and splenocytes to evaluate BCG and a number of novel candidate TB vaccines in the mouse model [296,298–300]. Briefly, naïve BMM were isolated from mice, cultured for seven days and then infected with MTB or BCG (as a surrogate of MTB) for two hours. Spleens from vaccinated/unvaccinated mice were harvested, processed to a single cell suspension and cultured for two hours. Non-adherent cells from the splenocyte culture were collected and co-cultured with infected BMM. BMM–splenocyte cell culture is performed in multi-well

plates, permitting gas exchange and subsequently enabling longer co-culture periods. The length of co-culture by this method is typically seven days but has been performed up to 11 days. Vaccine-induced growth inhibition of MTB Erdman and BCG has been demonstrated to correlate with *in vivo* protection against MTB [299,300].

More recently the murine MGIA has been simplified, eliminating the requirement for BMM and M Φ infection steps prior to addition of splenocytes. In this MGIA, referred to as the ‘direct’ MGIA, splenocytes are harvested from mice, processed and directly co-cultured with mycobacteria for 3–4 days (theme 2). Vaccine-induced growth inhibition of mycobacteria using the direct splenocyte method has been demonstrated to correlate with *in vivo* protection against MTB [201,306,307].

Development of this method was based on the human WB protocol developed by Wallis *et al* [253,309] and splenocyte–mycobacterial co-culture is performed in a closed system using screw-cap tubes. Since gas exchange does not occur, the culture period was shortened to 3–4 days during optimisation. Constant rotation of tubes is used as agitation during mycobacterial culture and has been demonstrated to increase growth [310], and may facilitate splenocyte contact with mycobacteria and increase oxygen availability [305]. Where standing tubes and rotating tubes were compared, growth inhibition by vaccinated splenocytes compared with control splenocytes was enhanced in rotating cultures [309].

Using 1×10^6 splenocytes and an inoculum equivalent to a time-to-positivity (TTP) value of 6.5 days, Marsay *et al* identified a modest but significant reduction in mycobacterial growth in splenocytes from BCG-vaccinated mice compared with control [201]. The direct MGIA was later optimised by Zelmer *et al*. Testing various splenocyte ($1\text{--}5 \times 10^6$) and mycobacterial inputs (100–2,000 CFU), the growth inhibitory effect of vaccination was highest using 5×10^6 splenocytes and 100 CFU BCG. With the aim to

reduce study time, *M smegmatis*, a fast-growing mycobacteria, was used in the MGIA. BCG-vaccinated and control groups were also distinguishable by this method. Vaccine-induced growth inhibition of BCG Pasteur Aeras (PA) and *M smegmatis* in splenocytes was demonstrated to correlate with *in vivo* protection against MTB Erdman in the lung and spleen [306]. In addition to analysis of BCG-induced protection, the optimised splenocyte MGIA has also been used to evaluate candidate TB vaccines, including RUTI [174], a therapeutic vaccine, as well as H56:CAF01 and H56:CAF01 SBS [308].

The direct splenocyte MGIA is predominantly performed using cells from individual mice [174,201,306,308]. However a simplified version using five technical replicates generated from a pooled study group of three mice was reported by Yang *et al* [307]. Using this method, intra-assay variability was reduced, as well as the number of animals required to perform the study. Vaccine-induced growth inhibition by BCG, BCG + adjuvant and SD1 fusion protein compared with unvaccinated animals was comparable to protection in the aerosol challenge model. As utilised in the BMM–splenocyte MGIA, multi-well plates were used in this study instead of rotating tubes. Cell viability was not determined in plates or compared with tubes [307].

In an MGIA study by Jensen *et al* [308] concern regarding splenocyte viability in the protocol reported by Zelmer *et al* [305] was highlighted. Splenocyte viability was increased from 21% to 46% following 96 hours of co-culture in rotating tubes by enriching the standard media used for MGIA with sodium pyruvate, non-essential amino acids and 2-mercaptoethanol. A head-to-head comparison of growth inhibition using enriched and standard media was not performed, therefore the effect of this increase in cell viability on the performance of the assay itself cannot be determined. Since different mycobacterial species were used in the two publications, a crude comparison of values reported cannot be made.

1.6.3 Mycobacterial quantification and the BACTEC system

The mainstay method of bacterial quantification in early human and animal MGIA was incorporation of radiolabelled uracil or thymidine, or plating on solid media. Mycobacterial quantification using the BACTEC MGIT system was first used in the human WB MGIA by Wallis *et al* 2001 [253] but was not used in murine MGIA until 2013 by Marsay *et al* [201]. It is currently the most common method of mycobacterial quantification for animal MGIA and human PBMC MGIA, as well as WB MGIA which do not use reporter gene tagged mycobacteria. Further details of the BACTEC MGIT system are provided in section 3.7.

1.6.4 Immune mechanisms of growth inhibition

To date, mechanisms involved in growth inhibition in the MGIA remain poorly understood and data are sparse. Since each type of MGIA utilises a unique set of immune cells, mechanisms of growth inhibition within each are likely to vary and recapitulate different elements of the immune response to MTB.

1.6.4.1 Cytokine and chemokine production

Analysis of cytokine/chemokine production is often performed alongside the MGIA [199,201,306,308,311,312,255,256,272,274,275,289,296,299]. Consistent with observations in humans and animal models of TB, the role of IFN γ in regulation of mycobacterial growth in the MGIA is unclear.

A number of studies have shown that mycobacterial growth inhibition in human MGIA is independent of IFN γ production [255,256,272,275,311,312]. Others have found an inverse correlation between IFN γ levels and mycobacterial burden [199,272,274,289]. Conflicting reports on the role of TNF α in mycobacterial growth

inhibition in the human MGIA also exist [199,272]. In a study by O'Shea *et al*, increased levels of a cytokine/chemokine cluster, containing Gro, transforming growth factor α , platelet-derived growth factor-BB and -AA, C-X-C motif chemokine ligand 10 (IP-10) and C-C motif chemokine 22, was found to negatively correlate with mycobacterial growth in the direct PBMC MGIA [289].

In mice, IFN γ has been found to play a role in with mycobacterial growth in the simplified splenocyte MGIA [201,306,308]. Zelmer *et al* demonstrated that mycobacterial growth was higher in co-cultures using splenocytes from B6.129S7-*Ifn γ ^{tm1Ts}/J* (IFN γ ^{-/-}) mice compared with wild-type C57BL/6 [306], consistent with observations made *in vivo* using this knockout strain. In this study, a vaccine arm was not included in analyses which utilised the knockout strain and therefore the importance of IFN γ in vaccine-mediated mycobacterial control was not determined [58]. Marsay *et al* performed microarray analysis in tandem with the simplified murine splenocyte MGIA. Following *ex vivo* overnight stimulation with BCG, an enhanced T_H1 response, including increased expression of IFN γ , nitric oxide synthase (NOS2) and IL-17, was observed in BCG-immunised splenocytes compared with splenocytes from unvaccinated animals which correlated with *ex vivo* growth inhibition in the MGIA [201]. The cellular source of IFN γ was not identified in these studies.

IFN γ levels have also been shown to correlate with growth inhibition in the murine bone marrow-derived macrophage (BMM) + lymphocyte MGIA. Parra *et al* reported that expression of IFN γ , as well as TNF α , IL-21 and IL-27, was upregulated in splenocytes from BCG-vaccinated compared with unvaccinated mice, concomitant with enhanced mycobacterial growth control [299]. However, Cowley *et al* found that the enhanced capacity of MTB-primed splenocytes and lung lymphocytes to control mycobacterial growth in macrophages was independent of IFN γ . Despite enhanced levels

of IFN γ in the supernatants of co-cultures using MTB-primed lymphocytes and wild-type C57BL/6 BMM, when BMM from IFN γ R-deficient mice were used, mycobacterial control was retained in the absence of IFN γ . This was also observed *in vivo* whereby IFN γ R-deficient mice primed with BCG developed displayed enhanced protection against MTB aerosol challenge compared with unprime mice [296].

1.6.4.2 T-cell subsets

A role for a number of T-cell subsets in mycobacterial growth control in various MGIA has been demonstrated. In the human WB MGIA, depletion of CD4 and CD8 T cells resulted in loss of growth inhibition of H37Rv in PPD⁺ individuals. Of note, where the clinical isolate, MP-28, was used in the MGIA, depletion of these subsets had no effect on mycobacterial growth [254]. Growth inhibition in the human PBMC MGIA has been found to correlate with a T-cell transcriptional signature [257]. Evidence for a role of CD4 and CD8 T cells in mycobacterial control in the PBMC MGIA is conflicting [260,272,312], as well as the role of polyfunctional T cells [199,258,260]. An inverse correlation between $\gamma\delta$ T cell populations and mycobacterial burden in the PBMC MGIA has been reported [312,313].

Studies on the T-cell subsets involved in growth inhibition in the mouse MGIA are limited. In the murine BMM–splenocyte MGIA, CD4 and CD8 T cells were found to account for a large portion of growth inhibition in the spleen [296]. In the direct splenocyte MGIA, CD4 T cells, as well as cytokine expression and production, were unchanged following four-day co-culture with MTB, despite detection of growth inhibition in vaccinated groups compared with unvaccinated [308].

1.6.4.3 Other immune cell populations and products

A number of studies have communicated a role for humoral immunity in mycobacterial control in human MGIAAs [199,230,289,314]. In addition, an inverse correlation between NK cells [247,273,311] and neutrophil populations [279] and mycobacterial growth has also been reported. Analysis of monocyte populations has been performed in animal and human MGIAAs. Using a systems biology approach, Hoft *et al* identified an inverse correlation between enrichment in monocyte expression modules and anti-mycobacterial activity in the human WB MGIA using RNA-seq [257]. In an additional study incorporating a systems biology approach with the human PBMC MGIA, a relationship between ML ratio and mycobacterial control was reported, in which a concomitant increase in CFU was found with increasing ML ratio. In addition to variations in anti-mycobacterial capacity, different ML ratios were associated with distinct transcriptional monocyte profiles [286]. Increased ML ratio has been shown to be associated with increased risk of TB disease in infant and adult cohorts [315,316]. However, specific monocyte populations, such as non-classical monocytes, have been found to inversely correlate with mycobacterial growth in the human PBMC [260] and the murine splenocyte [174] MGIAAs.

1.7 Diversity of the MTB complex

1.7.1 Host response to MTB complex infection

The ability to genotype patient clinical isolates has enabled analysis of disease phenotype associated with specific members of the MTB complex. Virulence, and the rate of extrapulmonary disease, multi-drug resistance, treatment failure and relapse has been shown to vary by lineage [12,317–319]. To date, robust TB susceptibility genes have not been identified in human populations and the lack of reproducibility of observations

made in genome-wide association studies remains an issue. It has been suggested that this may be due to a historically simplified view of the interplay between human and MTB genomic variability, and consideration of this variability may aid discovery of pathogenic drivers of the TB epidemic [320].

In the laboratory setting, growing interest in MTB genomic variability has resulted in the use of non-laboratory strains in some studies. Differences in the transcriptome, proteome, methylome and metabolome of isolates themselves [321–325] have been found. Lineage- and sublineage-dependent variations in the host response to infection have been identified experimentally and are summarised in Appendix 2.

At present, experimental analyses of MTB most commonly utilise a single laboratory strain, namely H37Rv, Erdman and CDC1551. These strains all belong to L4 of the MTB complex and have been passaged for decades in the laboratory [23,80]. Infection studies in human cell lines and animal models of TB using these strains predominantly demonstrate induction of a protective T_H1 response and high rates of host survival following *in vivo* infection [319,326–328]. By contrast, head-to-head comparison of the host response to infection with laboratory strains and clinical isolates representative of the global diversity of the MTB complex indicate a dramatic range of inflammatory response and cytokine profiles, pathogenicity, capacity for intracellular replication and rates of survival. In general, lineage-specific phenotypes have been broadly identified, albeit with some conflicting observations between studies. Further, heterogeneity within lineages themselves exists which has yet to be understood fully and may, in part, account for contradictory lineage-specific observations made to date. The historical reliance on laboratory MTB strains and lack of diversity in strains used in *in vitro* and *in vivo* studies has been postulated to contribute to the conflicting performance of some vaccine candidates in animal models and humans to date [122].

In regions where MTB and MAF are present, such as The Gambia, epidemiological variations in the populations infected by the two species indicate that MAF lineages may be less virulent than MTB and adapted to a distinct ecological niche. Individuals infected with L6 MAF are often older, immunocompromised and/or have a low body mass index compared with those infected with MTB [329]. MAF grows slower in culture than MTB, has different nutrient requirements and favours microaerobic growth conditions [325,330]. Concomitant with this observation, distinct species-specific T-cell profiles pre- and post-TB treatment were observed following overnight stimulation of WB with TB-specific antigens from MTB- and MAF-infected individuals [331]. At present, a dearth of *in vivo* analysis of MAF exists, with a small number of studies identifying a less virulent phenotype and induction of an early host inflammatory response for MAF strains compared with modern MTB lineages [26,317,332–334]. These observations are shared with the other ancient lineage of the MTB complex, L1. Modern lineages are collectively associated with induction of a heterogeneous but comparatively reduced/delayed host inflammatory response following infection, which has been hypothesised to contribute to the rapid disease progression and transmission associated with these lineages [334].

Beyond utilisation of the laboratory strains, H37Rv, Erdman and CDC1551, Beijing sub-strains of L2 are by far the most well-characterised members of the MTB complex. Beijing strains account for 10% of global TB cases, and 50% of cases across Eastern and Southeast Asia. Prevalence is rising outside of these regions as well, particularly in Russia, Cuba, Bangladesh, South Africa and Western Europe. Beijing strains are frequently associated with drug resistance [335]. *In vivo* studies in various animals models indicate the following phenotypic profile for Beijing strains [333,336]: high virulence, intracellular replication rate and lung pathogenesis score, and low survival;

reduced levels of proinflammatory cytokines, increased levels of anti-inflammatory cytokines; failed or transient induction of a T_H1 response, followed by induction of T_H2 response [326,328]; modulation of DC activation [337] and induction of type I IFN signalling [338,339]. Within lineage/sub-lineage variations for L2 have also been found. A number of studies have shown dramatic heterogeneity between different L2/Beijing isolates, particularly between ‘ancient’ and more ‘modern’ Beijing strains, revealing broad virulence, pathology, bacterial load and delayed hypersensitivity phenotypes [334,340–344]; by contrast, others have found no or very limited differences [345,346]. Phenolic glycolipid has been demonstrated to correlate with hyperlethality in this strain [347,348].

Modern L3 and L4 appear to exhibit an intermediate virulence phenotype situated between L2 and the ancient lineages. High levels of heterogeneity within this intermediate phenotype have been found for both lineages [336,349–351].

It is clear the global population of MTB strains responsible for TB disease is highly diverse and remains poorly understood at present. The heterogeneous observations obtained *in vivo*, indicate that diversity exists at and below lineage level, and may have dramatic implications for vaccine and drug development. Methods to incorporate this diversity experimentally must be developed.

1.7.2 Vaccine-induced protection against the MTB complex

A limited number of studies have performed head-to-head testing of MTB clinical isolates in *in vivo* MTB challenge studies with variations in the protective efficacy of BCG against TB reported in the mouse, rabbit and GP models of TB [24,122,348,349,352–354]. Results of these studies are summarised in Appendix 2.

The majority of studies on vaccine-induced protection against clinical isolates have evaluated BCG performance to date, most commonly using L2 strains [348,349,352]. L4 is almost exclusively represented by the laboratory strains, H37Rv, CDC1551 and Erdman [24,348,349,352,353], in some instances as a laboratory strain and in others as representative of L4 itself. To the best of our knowledge *in vivo* evaluation of vaccines using ancient lineages has not been performed.

BCG-induced protection against strains representative of the modern lineages of the MTB complex has been demonstrated at earlier time points following *in vivo* challenge (up to 60 days). However, in the limited number of studies extending beyond this time point, BCG protection against clinical isolates thereafter appears to wane, concomitant with increased lung pathology [352,353]. At matched timepoints in these studies, protection against infection with laboratory strains remains intact, indicating that the utilisation of these strains for preclinical vaccine testing may represent a poor model of human TB infection and vaccine-induced protection.

Further, in a 2015 study by Henao–Tamayo *et al*, a high level of protection against strains from the Western Cape, the region in which the MVA85A trial was conducted, was found in BCG-vaccinated mice and GPs. By contrast, a relatively modest ‘window of protection’ was found in BCG-vaccinated animals challenged with laboratory strains, facilitating identification of additional protection by boosting regimens. Compared with performance of BCG against laboratory strains, the authors argued that it would be difficult to demonstrate an improvement by boosting above the high protection afforded by BCG against the Western Cape strains, suggesting that this may account for the poor performance of MVA85A in infants. The authors recommended that for future design of clinical trials, strains local to potential sites should be tested in small animal models prior to commencement of trials in humans [122]. However, the dearth of literature on

preclinical evaluation of vaccines against non-laboratory strains suggests that this recommendation remains largely ignored.

To date, two studies have performed head-to-head evaluation of TB vaccines using a range of laboratory and non-laboratory strains. In the first study, protection afforded by BCG and the live attenuated MTB mutant, GC1237 Rv1503c::Tn Δ phoPR, against L2 and L4 strains was tested in mice. Six-weeks post-infection, lung bacterial burden of M4 (a L4 isolate) was reduced in both vaccinated groups. A modest, but significant, reduction of HN878 (L2) was identified in the lungs of GC1237 Rv1503c::Tn Δ phoPR vaccinated animals, with no significant difference between BCG-vaccinated and naïve mice observed [354]. In the second study, at four weeks post challenge with W4, HCU3524 or H37Rv (representative of lineages 2, 3 and 4 respectively) bacterial burden in the lungs of BCG- and MTBVAC-vaccinated mice was significantly reduced compared with naïve animals. Of note, protection against HCU3524 was comparatively lower than other lineages and absent in the spleen [24].

1.7.3 Mycobacterial diversity in the MGIA

Modern MGIA studies are most commonly performed in biosafety level 2 (BSL2) laboratories using BCG strains. Many research facilities do not house specialised BSL3 laboratories in which work using virulent mycobacterial species can be performed, or have space to incorporate the BACTEC system where facilities are available. Where virulent MTB strains are utilised in the MGIA, the laboratory strains, H37Rv and Erdman, are largely used. In the MGIA, growth inhibition of BCG has been demonstrated to correlate with that of Erdman [298] and H37Rv [309]. A limited number of MGIAs have been performed using clinical isolates [252–254,268,283,284,302,355]; however the

majority of these studies were performed more than 15 years ago and used a single clinical isolate in the absence of information on the phenotype of that isolate.

Eighteen clinical isolates and five reference strains, HN878, CDC1551, H37Rv, H37Ra and MP-28, were analysed by Janulionis *et al* using the human WB MGIA. Information on the phenotype of the clinical isolates is lacking. Variability in the ability of mycobacterial strains to replicate in host cells was identified, and did not correlate with growth in liquid medium [283].

1.7.4 Murine MGIA for vaccine evaluation

The fragmented preclinical pipeline in which vaccine candidates are individually evaluated in the mouse model may represent a key contributor to the unreliable translation of vaccine protection in human clinical trials observed to date. Further, candidates are tested against unrepresentative, single strains of MTB which do not recapitulate the diversity of MTB encountered in the clinical setting. In order to develop a TB vaccine able to sufficiently contribute to global TB control, large-scale, head-to-head screening of vaccine candidates against representative lineages of the MTB complex must be performed during vaccine development. Vaccine-induced protection against MTB and the mechanisms behind this protection must be evaluated systemically and at the lung mucosa to generate insight into potential CoP. Further, head-to-head screening of CoP associated with different vaccination strategies is vital to ensure that downstream immunological evaluation is not biased towards a specific component of immunity.

From a clinical perspective, a number of candidate TB vaccines are now progressing to phase-III clinical trials. Evaluation of the performance of these vaccines against strains less prevalent or absent at sites in which trials have been performed will be of high importance to inform future implementation of novel vaccine candidates.

Utilisation of the traditional *in vivo* MTB challenge experiment to perform these early analyses is not feasible due to the high number of mice required. The MGIA may represent a viable method to evaluate vaccine performance against a representative collection of MTB strains, due to its reduced input and option for study group pooling. Complementary to the MGIA readout, *ex vivo* analyses on the remaining host cells may be performed to identify correlates of growth inhibition and generate insight into potential mechanistic variations in vaccine-mediated protection against MTB. In the absence of a robust CoP, analyses must expand beyond the predetermined biased readouts generated at present. The reduced cost and animal requirements of this simplified *ex vivo* method facilitate this extension. Generation of an early extensive overview of vaccine-induced protection using the MGIA, in combination with complementary analyses which generate biological insight into observations made, may represent a powerful tool to inform and improve the design of downstream *in vivo* studies.

2 Project structure

2.1 Study rationale

The disparate translation of vaccine protection against TB in preclinical animal models to human clinical trials may be accounted for, in part, by a historical reliance on vaccine evaluation using homogenous laboratory strains of MTB. An increased awareness of genetic diversity within the MTB complex and its impact on host–pathogen interactions indicates that utilisation of laboratory strains alone is not representative of the global diversity of the MTB complex. As a result, the overview of vaccine protection gained from these studies is likely to be inadequate.

Incorporation of the diversity of the MTB complex into *in vivo* MTB challenge studies, the current mainstay method of TB vaccine evaluation in animal models, is both ethically and financially unfeasible due to the large number of animals required to sufficiently power these studies. The MGIA has been proposed as an ‘*ex vivo* challenge model’. Due to the lower animal input requirements for this assay, the MGIA represents a viable method by which vaccine testing could be expanded beyond single laboratory strains. To date, a splenocyte MGIA has been established for the murine model using laboratory strains of MTB.

This project will adapt the splenocyte MGIA for use with murine lung cells to generate a tool by which lung mucosal immunity can be evaluated. Both the lung and spleen assay will be optimised for use in an increased throughput setting with multiple mycobacterial strains. To develop this tool further, the assay will be incorporated with a systems biology approach to evaluate potential vaccine- and MTB-lineage-specific correlates of growth inhibition. More broadly, this analysis will demonstrate a method by

which early mechanistic insight into vaccine-induced protection can be obtained, with the aim to evaluate CoP within animal models of TB.

2.2 Hypothesis

The global TB epidemic is negatively impacted by a heterogeneous population of MTB strains known to mediate diverse host–pathogen interactions. Vaccine protection against this heterogenous population may be variable but is currently not captured in preclinical evaluation of candidate TB vaccines. We hypothesise that the murine lung and spleen MGIA represents a suitable tool to evaluate the ability of host cells from vaccinated mice to inhibit growth of a diverse set of mycobacterial clinical isolates, as a potential surrogate of vaccine protection. Further, evaluation of the biological mechanisms by which vaccines inhibit growth of different mycobacterial strains alongside the MGIA will generate early insight into vaccine- or strain-specific CoP in animal models of TB.

2.3 Study aims and objectives

The aims of this project are the following:

- a. Establish a murine lung MGIA for the evaluation of vaccine-induced mucosal immunity.
- b. Expand the capacity of the murine lung and spleen MGIA to evaluate vaccine-induced mycobacterial growth inhibition beyond a single laboratory strain of MTB through the utilisation of multiple MTB clinical isolates.
- c. Determine whether mycobacterial growth inhibition in the MGIA is a representative readout of protection in the lung and spleen following *in vivo* infection with clinical isolates of MTB.

- d. Characterise the host cell population input in the MGIA.
- e. Identify transcriptional correlates of *ex vivo* mycobacterial growth inhibition.
- f. Determine whether correlates of *ex vivo* mycobacterial growth inhibition are unique to *ex vivo* mycobacterial culture or also observed following *in vivo* infection.

The objectives of this project are the following:

- a. Adapt the murine splenocyte MGIA for use with murine lung cells.
- b. Evaluate the reproducibility of vaccine-mediated mycobacterial growth inhibition in the MGIA using clinical isolates representative of four lineages of the MTB complex.
- c. Perform head-to-head comparison of the lung and spleen MGIA with an *in vivo* challenge study using clinical isolates.
- d. Perform flow cytometric and transcriptional analysis of the murine lung MGIA input.
- e. Perform analysis of the transcriptome of the murine lung cell MGIA input following overnight stimulation with mycobacteria. Apply identified perturbations in gene expression to a defined set of murine lung modules to identify biological mechanisms which correlate with vaccine-induced growth inhibition in the MGIA.
- f. Compare transcriptional perturbation and modular enrichment following *ex vivo* stimulation and *in vivo* infection.

2.4 Thesis structure

This thesis is composed of seven chapters, beginning with an introduction to the topic of the thesis (Chapter 1), followed by a chapter outlining the structure of this project (Chapter 2), and a materials and methods chapter which covers all work performed in this project (Chapter 3). Results chapters are presented using a hybrid structure which includes one published paper as the first results chapter (Chapter 4) and two additional results chapters in traditional thesis form (Chapters 5 and 6). The text of the published results chapter (Chapter 4) is included in its original published form but has been typeset to fit the formatting requirements of this thesis. References for this chapter have been incorporated into the final reference list at the end of this thesis. Specific aims and objectives are restated within each results chapter, as well as a brief introduction. Chapter 7 provides a final discussion and conclusions. An appendix is included at the end of the thesis and includes two large tables referenced to in Chapter 1. These tables include a full literature review of the two overarching themes of this thesis: i) the MGIA and ii) experimental analysis of the host response to infection with strains of the MTB complex and vaccine-induced protection. A full reference list is included at the end of the thesis.

3 Materials and methods

3.1 Solutions, reagents, consumables and equipment

Full details provided in Appendix 3.

3.2 Ethics statement

Animal experimentation was performed under licence PPL 70/8043 (superseded by P6CA9EB8D) issued by the UK Home Office according to the Animals (Scientific Procedures) Act 1986 and approved by the London School of Hygiene & Tropical Medicine (LSHTM) Animal Welfare and Ethics Review Body. This thesis was prepared in accordance with the ARRIVE guidelines [356].

3.3 Mycobacteria

BCG PA and BCG Danish 1331 were obtained as frozen aliquots (500 μ L and 1 mL respectively). MTB Erdman was obtained as a 1-mL frozen glycerol stock. The reference set of MTB complex clinical strains were donated by Professor Sebastian Gagneux as 1-mL frozen glycerol stocks (refer to Appendix 4 for details of reference set) [23]. All mycobacterial stocks were stored at -70°C . All work using MTB was performed in aerosol-containment BSL-3 laboratories at LSHTM in accordance with guidance from the UK Advisory Committee on Dangerous Pathogens (ACDP).

3.4 Vaccines

Two strains of BCG were used in this project: BCG PA and Danish 1331. BCG PA was used alone throughout assay optimisation, with the incorporation of BCG Danish in later studies as a comparison of vaccine efficacy between the two strains. The strain in use is specified where necessary.

The spore-fusion protein 1 (FP1) vaccine was used during this project as a mucosal boost vaccine following BCG prime. Spore-FP1 is a novel mucosal TB vaccine candidate, developed as part of the Eliciting Mucosal Immunity to Tuberculosis (EMI-TB) Project funded by EU Horizon2020 [357]. Spore-FP1 is composed of *Bacillus subtilis* spores non-covalently coated with FP1. *B. subtilis* is a Gram-positive bacterium found in soil and as a commensal in the human gastrointestinal tract. The spores are safe and tolerated in humans and have been used as a dual adjuvant and antigen delivery system. *B. subtilis* spores exhibit intrinsic adjuvanticity and ability to bind antigen [358]. FP1 is a fusion protein which includes Ag85B, alpha crystallin (ACR) and heparin-binding haemagglutinin adhesin (HBHA). Ag85B and ACR are antigens representative of early and late stages of MTB infection, respectively. HBHA was selected for epithelial targeting in the lungs. Cloning and production of FP1 were previously described by Copland *et al* [146].

3.5 Generation of mycobacterial stocks

Stocks of the laboratory strain, MTB Erdman, as well as clinical strains representative of each lineage of the MTB complex (1–4) from the reference set, were grown up for use in downstream analyses performed during the project (Table 3-1). Clinical strains that had been sequenced to date and those used in existing publications

were prioritised. Isolates fully susceptible to first-line drugs were selected due to biosafety considerations.

Starter cultures were established by adding 50–100 μL mycobacterial stock to 10 mL 7H9 liquid media in a 50 mL conical tube. Cultures were grown to log phase (optical density [OD] 0.3–0.5) on an orbital shaker at 150 rpm and 37°C. OD was checked every 48 hours using a cell density meter. At log phase, starter cultures were subcultured by adding 100 μL starter culture to 10 mL fresh 7H9 media and returned to the shaker until they reached OD 0.6–0.9. To generate aliquots of the stock, mycobacteria were pelleted by centrifuging tubes at $1,650 \times g$ for 10 minutes (room temperature), washing with 10 mL wash buffer and resuspending in half the volume of freezing buffer. Stocks were frozen as 250 μL aliquots in 2-mL screw-cap Eppendorf tubes at -70°C .

Table 3-1. Clinical strains selected from the MTB complex reference set for downstream analysis.

Lineage	Strain
L1	N0072
L2	N0052
L3	N0054
L4	N1283

3.6 Assessment of stock stability and estimation of CFU

Stability testing and estimation of CFU for generated stocks were performed two and four weeks following freezing. CFU was reassessed every 6–9 months for all mycobacterial stocks. Specifically, one vial of mycobacteria was thawed at room temperature and seven 10-fold dilutions were performed in phosphate-buffered saline–Tween 80 (PBS–T80). Two 7H11 agar plates were divided into 3–4 sectors each and 20

µL spots from each dilution plated onto a section in triplicate. Plates were left to dry and then incubated at 37°C in sealable bags to prevent drying out. Colonies were counted when visible (2–3 weeks).

3.7 BACTEC MGIT system

The BACTEC MGIT system is an automated mycobacterial detection system traditionally utilised for mycobacterial liquid culture and susceptibility testing of clinical specimens in TB diagnostic laboratories. The system uses standardised reagents and equipment. Each tube contains modified Middlebrook 7H9 broth base supplemented with MGIT growth supplement and PANTA™ antibiotic mixture (containing polymyxin B, amphotericin B, nalidixic acid, trimethoprim and azlocillin [359]) to suppress contamination. At the bottom of each tube, an oxygen-quenched fluorochrome, tris 4, 7-diphenyl-1, 10-phenanthroline ruthenium chloride pentahydrate, is embedded in silicone. Bacterial growth is quantified using a fluorescence quenching system whereby bacterial growth depletes free oxygen releasing inhibition of the fluorochrome. Tubes are incubated at 37°C and fluorescence intensity is measured automatically every 60 minutes. Fluorescence is directly proportional to the extent of oxygen depletion defined by bacterial concentration. At a fluorescence threshold representative of 1×10^5 – 10^6 CFU MTB / mL, the tube is registered as positive and a TTP value is generated for the tube [359]. TTP may also be referred to as time-to-detection (TTD) or days-to-positivity (DTP). TTP is dependent on the number of mycobacteria added to the MGIT tubes during inoculation; the higher the bacterial load, the lower the TTP.

A standard curve must be generated to enable conversion of experimentally derived TTP values to bacterial count (CFU) for each mycobacterial strain used in the BACTEC system [305]. The BACTEC MGIT system is favoured over colony counting for

mycobacterial quantification as CFU determination is slower and more labour intensive than the BACTEC method, lacks standardised reagents and is associated with an element of subjectivity, particularly person-to-person. Since the BACTEC system is unaffected by clumping and provides an accurate computer-generated readout based on validated technology, inter- and intra-assay variation may be reduced [300,360,361]. TTP values generated by the BACTEC system have been demonstrated to correlate with CFU enumerations from culture on solid media [300].

3.8 BACTEC MGIT standard curve

Individual standard curves were produced for all mycobacterial species. Seven 10-fold serial dilutions of the mycobacterial stock were made using PBS–T80. PANTA antibiotic mixture was prepared by adding one bottle of MGIT growth supplement to one bottle of lyophilised MGIT PANTA. Next, 800 μ L PANTA enrichment was added to each MGIT tube. Two MGIT tubes per dilution were inoculated with 500 μ L diluted culture, recapped and inverted to mix. Tubes were loaded into the BACTEC MGIT instrument and the TTP value recorded when the tubes registered positive. Each mycobacterial dilution was plated (as described in section 3.6) to estimate the corresponding CFU for each dilution. CFU was log transformed and plotted against TTP values obtained from the BACTEC MGIT instrument to generate a standard curve. Non-linear regression analysis was performed to generate an equation which enabled calculation of CFU from TTP values of samples of unknown bacterial count.

3.9 Animals

Female C57BL/6 mice (5–7 weeks old; weight 16–20 g) were obtained from Charles River UK and rested for at least five days before procedure start. Animals were

housed in individually ventilated cages (IVCs) (maximum six animals/cage) in the LSHTM Biological Services Facility (BSF) with access to food and water *ad libitum*. Animals were randomly assigned to cages on arrival by staff in the BSF. Each cage was randomly assigned a group number on commencement of the study.

3.10 Vaccine preparation and immunisation

Under sterile conditions, BCG PA or BCG Danish were thawed at room temperature and washed once with physiological saline solution by centrifugation at $15,900 \times g$ (10 minutes) in a microcentrifuge to remove glycerol. The inoculum was prepared by diluting the washed BCG in physiological saline solution to a final concentration of 1×10^7 CFU/mL.

For formulation of spore-FP1, FP1 was incubated with *B subtilis* spores for one hour at room temperature and administered shortly following formulation (1×10^9 *B subtilis* spores coated with 10 µg prepared in 40 µL volume per animal).

S.c. BCG was administered as 100 µL (1×10^6 CFU) into the right or left leg flap using a sterile 25G needle. For i.n. immunisations, mice were anaesthetised by intraperitoneal (i.p.) injection of ketamine (50 mg/kg) and xylazine (10 mg/kg) in physiological saline solution, followed by delivery of 50 µL BCG (0.5×10^6 CFU) equally administered between the two nostrils. Animals receiving BCG s.c. + spore-FP1 boost were administered BCG s.c. (as described) at week 0, followed by i.n. boosting at week 3 with spore-FP1. Animals were anaesthetised in the manner described for i.n. BCG, followed by delivery of 40 µL spore-FP1 equally between the two nostrils. Control animals received no treatment. BCG CFU input was confirmed by plating the diluted inoculum on 7H11 agar plates. All animals were rested for six weeks following BCG vaccination.

3.11 Lung cell isolation

The protocol for lung cell isolation was based on the splenocyte MGIA protocol published by Zelmer *et al* [305] and adapted for use with lung cells using a number of published protocols for the isolation of single cell suspensions from murine lung [362,363]. Animals were sacrificed by exposure to carbon dioxide gas in a rising concentration. Lungs were removed aseptically and placed in 5-mL Bijou tubes containing 2 mL R0L (described in Appendix 3). Immediately following the organ harvest, lungs were washed in 2 mL R0L, the media discarded, the tissues cut into 1-mm pieces and 2 mL R0L added. Lungs were incubated for 40 minutes at 37°C (5% CO₂) with deoxyribonuclease I from bovine pancreas (final concentration: 12 µg/mL) and Liberase TL (final concentration: 625 µg/mL). DNase degrades extracellular DNA released during tissue dissociation, preventing clumping which could result in cell loss. Liberase TL is a low thermolysin concentration enzyme blend which improves the quality of tissue dissociation and viability of isolated cells. The enzyme reaction was terminated by adding 2.5 mL R10L (described in Appendix 3). Bijou contents were poured into a 100-µm cell strainer in a 5.5-cm Petri dish and mashed using the rubber end of a sterile 5-mL syringe plunger to obtain a single cell suspension. An additional 5 mL R10L was added to the strainer to wash through any remaining cells before the contents of the Petri dish were transferred to a 15-mL Falcon tube using a plastic Pasteur pipette. Lung cell suspensions were then centrifuged for 5 minutes at 412 \times g at 4°C using a bench-top centrifuge. Supernatants were discarded and cell pellets were gently disturbed by dragging the tube across a plastic tube rack 3–4 times. Red blood cell lysis was performed using 3 mL ammonium-chloride-potassium (ACK) lysis buffer. Lysis was performed for 2 minutes, followed by termination of the reaction with R10L (volume up to 15 mL). Cell

suspensions were centrifuged for 5 minutes as above and the lysis step repeated if red blood cells were still present in the pellet.

Following centrifugation, cells were resuspended in 1 mL R10L for counting and visible cell clumps were removed from the suspension with a pipette and discarded. Viable cells were then counted using a microscope by diluting 10 μ L of the 1-mL cell suspension in 90 μ L trypan blue and loading 10 μ L into counting chambers on disposable slides. Cell numbers were adjusted to the required concentration by centrifuging and re-suspending in the appropriate volume of R10L.

3.12 Spleen cell isolation

The protocol for splenocyte isolation was based on protocol published by Zelmer *et al* [305]. Animals were sacrificed by exposure to carbon dioxide gas in a rising concentration. Spleens were removed aseptically and placed in 15-mL Falcon tubes containing 5 mL R10S (described in Appendix 3). The contents of the Falcon tube were homogenised using a 100- μ m cell strainer in the manner described for the lung. Red blood cell lysis was performed using RBC lysis buffer.

Viable cells were counted using a microscope by resuspending in 10 mL R10S, diluting 10 μ L of the cell suspension in 190 μ L trypan blue and loading 10 μ L into counting chambers on disposable slides. Cell numbers were adjusted to the required concentration by centrifuging and re-suspending in the appropriate volume of R10S.

3.13 Sample pooling

All flow cytometry and RNA-seq analyses were performed on samples from individual mice (biological replicates). All MGIA and related optimisation experiments

were performed using pooled lung and spleen cells (technical replicates). A single pool was made for each mouse study group.

Samples were processed and counted individually to assess for quality and allow for aliquots to be acquired for biological replicates, and later pooled for MGIA set up.

3.14 *Mycobacterium* spp. 2-thiophenecarboxylic acid hydrazide susceptibility

To confirm susceptibility of BCG PA and each MTB strain to 2-thiophenecarboxylic acid hydrazide (TCH) in agar plates, 100 CFU BCG PA and/or 100 CFU MTB were plated on 7H11 agar plates in the absence or presence of 2 µg/mL TCH.

Five-fold serial dilutions of a 2 µg/mL TCH stock (0.4, 0.08 and 0.016 µg/mL) were prepared and added to supplemented MGIT tubes. Susceptibility to TCH when using the BACTEC system was determined by adding 100 CFU BCG PA and/or 100 CFU MTB to MGIT tubes. Tubes were placed in the BACTEC MGIT system until registered positive. CFU input was confirmed in the absence of TCH.

3.15 Mycobacterial growth inhibition assay

An overview of the MGIA, including culture and quantification options, is depicted in Figure 3-1.

3.15.1 Mycobacteria/murine cell co-culture

Following cell isolation, cell number was adjusted in the appropriate volume of R10, samples were pooled within groups to generate a single group pool and 300 µL/well of cells were seeded in 48-well plates. A mastermix of the required bacterial input was prepared by diluting bacteria in the appropriate volume of R10 for the cell type tested. The mastermix was vortexed (BSL2 only) and 300 µL was added to each well containing

cells. Plates were placed inside a CelCulture CO₂ incubator at 37°C (5% CO₂) and cultured for 96 hours.

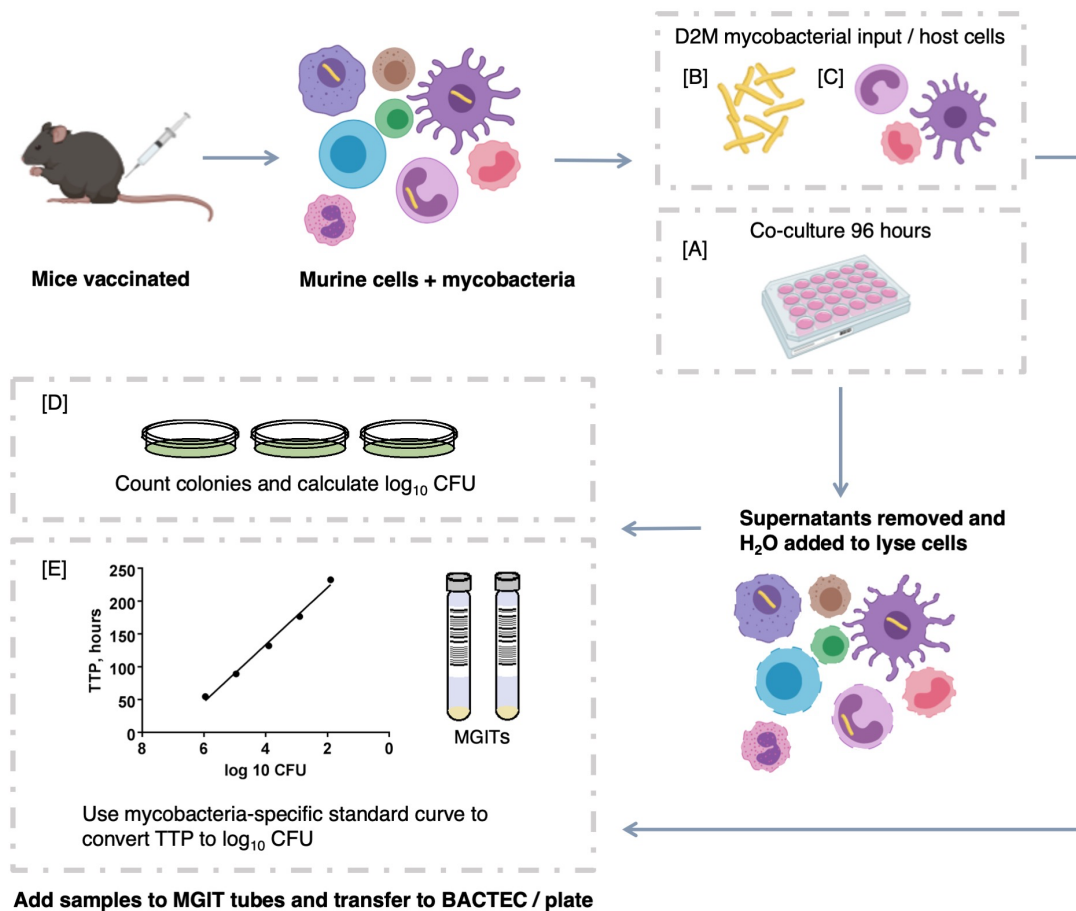


Figure 3-1. MGIA overview. Mice are vaccinated with vaccine of interest or remain unvaccinated (control). At the peak immune response, organs are harvested, typically lung or spleen, and processed to generate a primary cell line. [A] Murine cells are co-cultured at 37°C (5% CO₂) with mycobacteria for 96 hours in 48-well plates. In parallel with this, control D2M samples are set up directly on solid agar or in MGIT tubes with [B] mycobacterial input only, to confirm input at co-culture set up, or [C] murine cells only, to quantify residual mycobacteria in host cells. [A] At 96 hours, supernatants are removed from the wells and water is added to lyse cells and release intracellular mycobacteria. The mycobacterial content of the lysed samples is then quantified by [D] plating on solid agar and counting colonies when visible or [E] using the BACTEC MGIT system to generate TTP values. TTP values are generated from a fluorescence quenching system indicative of mycobacterial oxygen consumption. TTP readouts are converted to CFU using a mycobacteria-specific standard curve. CFU, colony-forming units; D2M,

direct-to-MGIT; MGIA, mycobacteria growth inhibition assay; MGIT, mycobacterial growth indicator tube; TTP, time to positivity. Figure generated using Biorender.

3.15.2 Direct-to-MGIT set-up

For MGIA using the BACTEC MGIT system, ‘direct-to-MGIT’ (D2M) controls were set up to confirm the mycobacterial input CFU, as well as residual mycobacteria present in host cells from animals vaccinated with a live vaccine. Mycobacterial input or host cells were added directly to MGIT tubes supplemented with 800 μ L MGIT PANTA containing bacterial or host cell input alone i.e. 300 μ L input + 200 μ L R10 (required MGIT volume post supplementation = 500 μ L). All MGIT tubes were placed in the BACTEC MGIT system until positive.

For MGIA in which mycobacterial quantification was to be performed by CFU plating, D2M bacterial input controls were set up by plating each bacterial mastermix on agar plates and incubating at 37°C for approximately three weeks. An appropriate volume of host cells was also cultured on agar plates at various dilutions to quantify residual BCG.

3.15.3 Post-culture CFU quantification

Supernatants were removed at 96 hours and 500 μ L sterile water was added to each well and incubated for at least five minutes to lyse cells. Murine cells were further disrupted/lysed by pipetting to release intracellular mycobacteria.

For MGIA using the BACTEC MGIT system, the total volume (500 μ L) from each well was added to a supplemented MGIT tube (800 μ L MGIT PANTA). MGIT tubes were placed in the BACTEC MGIT machine until registered positive and a TTP value was generated. TTP values were used to calculate CFU from standard curves generated previously (Figure S4-5 and Figure 5-2). In studies in which residual BCG from

vaccination was known or predicted to be present in murine lung cells, MGIT tubes contained 0.08 µg/mL TCH.

Where quantification by CFU plating was planned, lysed samples were diluted (refer to Table 3-2 for mycobacteria- and organ-specific dilutions) further in sterile water and 50/100 µL was plated on 7H11 agar plates. 7H11 plates containing 2 µg/mL TCH were used where residual BCG from vaccination was known or predicted to be present in murine lung cells.

Table 3-2. Organ- and mycobacteria-specific dilutions for CFU quantification following 96-hour MGIA co-culture.

Condition (mycobacteria + cell type)	Recommended dilution at day 4	Volume to plate (µL)
BCG PA, murine lung	1 in 5	50
MTB Erdman, murine lung	1 in 2	50
L1 (N0072), murine lung	No dilution	50
L2 (N0052), murine lung	1 in 2	50
L3 (N0054), murine lung	1 in 2	50
L4 (N1283), murine lung	1 in 2	50
BCG PA, murine spleen	No dilution	100
MTB Erdman, murine spleen	1 in 2	100
L1 (N0072), murine spleen	No dilution	100
L2 (N0052), murine spleen	1 in 2	100
L3 (N0054), murine spleen	1 in 2	100
L4 (N1283), murine spleen	1 in 2	100
BCG, Bacille Calmette–Guérin; L, lineage; MTB, <i>Mycobacterium tuberculosis</i> ; PA, Pasteur Aeras.		

3.16 Murine infection with MTB

Six weeks post immunisation, mice were infected intranasally with L1 (N0072) or L2 (N0052) MTB and kept in isolators under BSL-3 containment at LSHTM for the remaining duration of the study. Frozen aliquots of mycobacteria were thawed at room temperature and diluted in physiological saline solution to a concentration of 7.5×10^3 CFU/mL. Mice were anaesthetised by i.p. injection of a combination of ketamine (50 mg/kg) and xylazine (10 mg/kg) in physiological saline solution, followed by delivery of 40 μ L of the inoculum (approximately 300 CFU) equally between the two nostrils. Inoculum CFU was confirmed by plating on 7H11 agar plates.

Confirmation of infectious dose of CFU was performed 24-hours post-infection. Three mice per infection group were sacrificed by cervical dislocation, lungs were aseptically removed and collected in 4 mL sterile PBS–T80. Lungs were homogenised by mashing through 100- μ m sieves using a syringe plunger, and then 200 μ L homogenate was plated in duplicate on 7H11 agar.

Five-weeks post-infection, animals were killed by cervical dislocation. Lungs and spleens were removed aseptically, collected in 4 mL sterile PBS–T80 and homogenised in the manner described for confirmation of infection. To determine organ CFU following five weeks of infection and ensure the ‘window of detection’ was plated, a series of ten-fold dilutions of the tissue homogenates was performed in PBS–T80 and plated on 7H11 agar plates.

All agar plates were incubated at 37°C for approximately three weeks.

3.17 RNA extraction

Lung cells from individual mice (versus pooled for MGIA) were used for RNA-seq analysis. The limitations and explanation for use of pooling (technical replicates) in

the MGIA are discussed in Chapter 4. It was decided that experimental analyses designed to provide insight into the biology of the MGIA would be performed on biological replicates. Conesa *et al* highlight the importance of biological replicates in RNA-seq in the following statement: ‘biological replication is required if inference on the population is to be made, with three replicates being the minimum for any inferential analysis’ [364].

Specifically, 1×10^6 lung cells per mouse were seeded in duplicate (unstimulated/stimulated) in 24-well plates and cultured overnight at 37°C (5% CO₂) in the presence or absence of 1×10^6 CFU mycobacteria (BCG PA [RNA-seq I]; L1 N0072, L2 N0052 or L4 N1283 [RNA-seq II]). The following day, plates were centrifuged for five minutes at 500 \times g in a bench-top centrifuge to collect eukaryotic cells, supernatants were removed and 600 μ L RNeasy Protect Cell Reagent was added to each well and mixed by pipetting to immediately stabilise transcription and prevent RNA degradation. Samples were archived in 2-mL screw-cap tubes at –70°C until RNA extraction.

Centrifugation steps during RNA purification were performed in a microcentrifuge. Samples stabilised in RNeasy Protect Cell Reagent were thawed fully and centrifuged at 5,000 \times g for five minutes. Total RNA purification was performed using the RNeasy Mini Kit and an on-column DNase digestion according to the manufacturer’s instructions. Minor adjustments were made to the protocol for use in a BSL3 laboratory or to increase RNA yield and are outlined below. All adjustments made to the protocol for work in the BSL3 laboratory were confirmed to have no impact on downstream RNA yield in the BSL2 laboratory. The purification process is outlined in Figure 3-2. Briefly, 350 μ L RLT buffer, containing beta-mercaptoethanol (BME; 10 μ L / 1 mL RLT), was added to pelleted cells and mixed by thorough pipetting to lyse and homogenise the sample (vortex step eliminated in BSL3). RLT buffer is a denaturing buffer containing a high concentration of guanidine isothiocyanate. The presence of BME inactivates RNases in

the lysate to retain intact RNA. To ensure complete disruption and homogenisation, the sample in RLT buffer was applied to a QIAshredder spin column and centrifuged at full speed for two minutes. Following centrifugation, an equal volume of 80% molecular grade ethanol was added to the homogenised sample in the QIAshredder collection tube and mixed thoroughly by pipetting. Addition of ethanol is required for binding of RNA to the spin column in the proceeding steps. The total volume was added to the RNeasy spin column and subjected to a series of centrifugation and wash steps, as well as on-column DNase digestion, before elution of purified total RNA (> 200 nucleotides in length) from the column in nuclease-free water.

When extracting RNA in the BSL3 laboratory, the collection tube was replaced with a clean tube following centrifugation, instead of discarding the flow through (as specified by the manufacturer's instructions), to reduce the risk of contamination of the RNeasy column with mycobacteria.

Following the recommendations of JiSook Lee (LSHTM, personal communication) for improvement of RNA yield using the spin column method, the elution of purified RNA from the spin column was performed with adjustments. Briefly, 30 uL of water was added directly to the spin column and incubated for five minutes. The one-minute centrifugation speed was increased to 13,000 \times g. Following centrifugation, the eluted sample was then reapplied to the spin column and subjected to the same incubation and centrifugation steps.

RNA was stored at -70°C until transfer to the Institute for Child Health (ICH; University College London, UK) for quality assessment, library preparation and sequencing.

3.18 Quality control

RNA integrity was assessed, and concentration determined, using the TapeStation system and standard or high-sensitivity RNA ScreenTape device. All samples submitted for downstream library preparation had an RNA integrity number equivalent (RINe) value ≥ 8.2 (Appendix 6 and 7). For both RNA-seq runs, three biological replicates per group, per condition, were submitted for library preparation and sequencing.

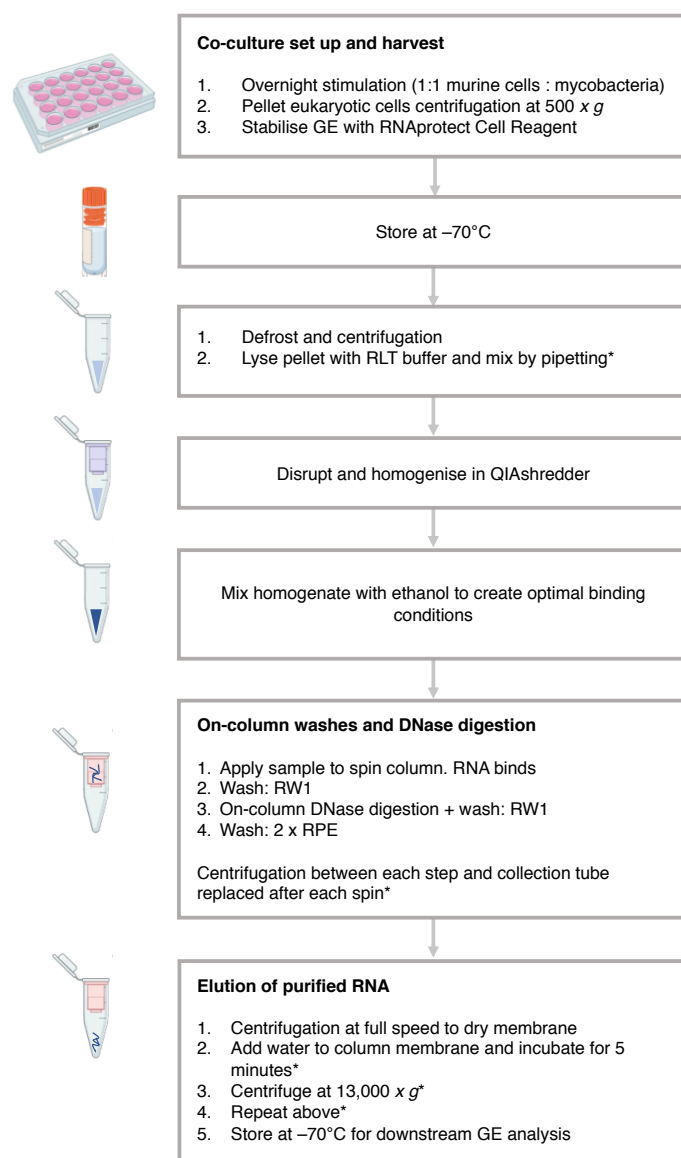


Figure 3-2. Overview of RNA extraction protocol using the RNeasy mini kit. Adaptions made to Qiagen protocol [365] are marked by asterisk and described in the text. GE, gene expression; NFW, nuclease-free water. Figure generated using Biorender.

3.19 Library preparation and sequencing

The NEBNext Ultra II Directional RNA Library Prep Kit and Poly(A) mRNA Magnetic Isolation Module were used to process 200 ng total RNA per sample according to the manufacturer's instructions. Library preparation is summarised in Figure 3-3. Limited cycle PCR was performed with 100 ng for 14 cycles.

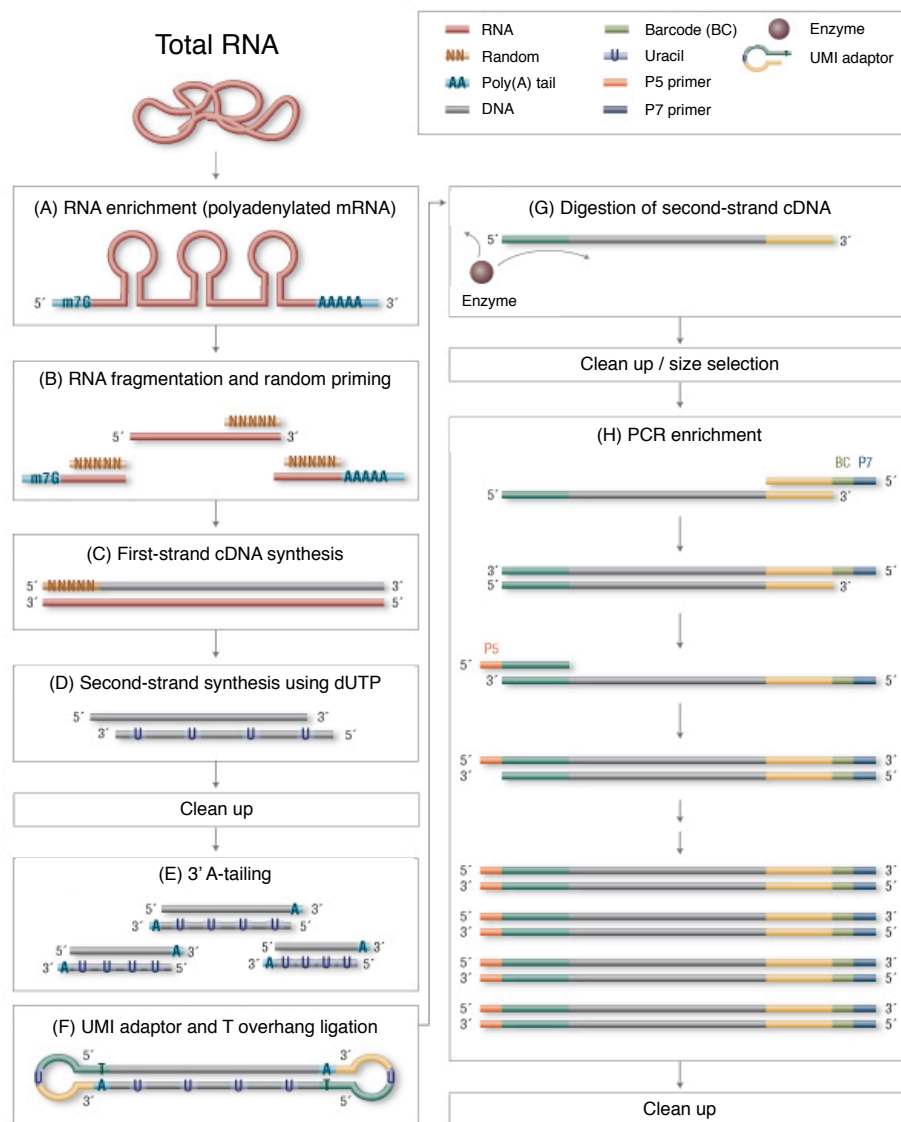


Figure 3-3. Overview of library preparation process. (A) mRNA is isolated from total RNA using oligo-dT beads to pull down polyadenylated mRNA transcripts. (B) Purified mRNA is fragmented using chemical fragmentation (heat and divalent metal cation) and primed with random hexamers. (C) Strand-specific (first strand) cDNA is then generated

using reverse transcriptase and actinomycin-D, allowing for RNA-dependent synthesis while preventing spurious DNA-dependent synthesis. (D) The second cDNA strand is synthesised using dUTP in place of dTTP, to mark the second strand. (E) Resultant cDNA is then ‘A-tailed’ at the 3’ end to prevent self-ligation and adapter dimerisation. (F) Full-length xGen adaptors, containing two unique 8-bp sample specific indexes, a UMI (N8) and a T overhang are ligated to the A-tailed cDNA. (G and H) Successfully ligated cDNA molecules are enriched with limited cycle PCR. The high-fidelity polymerase employed in the PCR is unable to extend through uracil and therefore only the first-strand cDNA is amplified for sequencing, making the library strand specific (first strand). PCR, polymerase chain reaction; UMI, unique molecular identifier. Adapted from [366].

Libraries to be multiplexed in the same run were pooled in equimolar quantities, calculated from Qubit and Bioanalyser fragment analysis. Samples were sequenced on the NextSeq 500 instrument using a 75-bp single read run with a corresponding 8-bp UMI read.

3.20 RNA-seq data analysis

Sample processing from .fastq files from ICH to the generation of a summarised read count matrix and MultiQC report (outlined below) was performed on a central shared Linux-based high-performance computing (HPC) service at LSHTM. Access to the HPC was gained through the SSH client PuTTY (version 0.70, Simon Tatham). Where required, packages were installed and updated using the open-source package management system, Conda (version 4.8.3; Anaconda Inc, USA).

A ‘gold-standard’ RNA-seq analysis pipeline does not exist, and a *large* number of resources and software tools are available for analysis of these data. Instead, analysis pipelines are designed and built based on the research question of a particular study, the genome of interest, the computing facilities available and, most likely, personal or

research group preference. In some cases, upstream analysis decisions can also define downstream ones. The following references were utilised as a starting point for pipeline design and to help navigate the range of analysis options available [364,367].

The decision process for tool selection is outlined in the relevant sections below, as well as recognition of other analysis options. Selection of tools was also based on use of online tutorials for RNA-seq analysis [368–370]. Detail is provided below where non-default settings or run-specific input was required for parameters within commands.

3.20.1 Initial quality control with FASTQC and read trimming with BBDuk

Samples were demultiplexed and converted to .fastq files at ICH. .fastq files were download from the BaseSpace Sequence Hub (Illumina) and uploaded to the LSHTM computing cluster.

Within sample .fastq files were concatenated for downstream processing. FastQC [371] (version 0.11.9) was used for quality control (QC) of raw reads pre- and post-sample adapter/quality trimming and filtering with the BBDuk tool from the BBTools suite (version 38.79) [372]. BBDuk is one of many trimming tools and is known for its speed and efficacy [373]. Other popular tools include Trimmomatic [374] and cutadapt [375]. Adaptor sequences were trimmed (literal=AGATCGGAAGAGCACACGTCTGAACTCCAGTCA, AGATCGGAAGAGCGTCGTGTAGGGAAAGAGTGT), as well as the final 5% 3' bases (ftr=71). Per base sequence quality across all bases at each position in the .fastq file was ≥ 30 .

3.20.2 Generation of genome index and read alignment with STAR

Read processing at this point can take one of two paths: i) alignment dependent (read alignment and counting), using tools such as STAR [376], HISAT2 [377] and Tophat [378]; or ii) alignment independent (pseudocounting), using tools such as Salmon [379], Kallisto [380] or Sailfish [381]. STAR is a popular and well-documented tool which has been found to be a fast and reliable general-purpose aligner where the appropriate amount of random access memory (RAM) is available [382].

Mus musculus genome FASTA (ftp://ftp.ensembl.org/pub/release-99/fasta/mus_musculus/dna/Mus_musculus.GRCm38.dna.primary_assembly.fa.gz) and gene annotation gene transfer format (GTF) (ftp://ftp.ensembl.org/pub/release-99/gtf/mus_musculus/Mus_musculus.GRCm38.99.gtf.gz) files were downloaded from Ensembl [383]. STAR (version 2.7.3a) was used to generate a genome index and subsequently map raw reads in trimmed .fastq files to the *Mus musculus* index (-sjdbOverhang 70). Binary alignment map (.bam) files for each sample were output.

Mapping using STAR is a two-step process: i) seed searching, and ii) clustering, stitching and scoring. In the first step, seed searching is performed by taking each read and searching through the index for the longest location the read maps to (maximal mappable prefixes [MMPs]). The next round of searching starts with the unmapped portion of the read. As each MMP is found, it is assigned a ‘seed’ value, i.e. the longest mapped portion of the read is named ‘seed1’, the second longest ‘seed2’ etc. Where mismatches or indels exist, existing MMPs are extended if possible. In cases where extension results in poor alignment, the sequence is clipped [368,376]. In the second step, whole read alignments are built by clustering seeds by proximity to a set of ‘anchor’ seeds and stitching them together. The decision to stitch is based on an alignment quality score

generated by the presence of matches, mismatches, deletions, insertions and splice junction gaps, indels etc [376].

3.20.3 Alignment quality control with RESeQC and Picard Tools

Prior to input into downstream tools, the ‘strandness’ of aligned reads from the RNA-seq run was confirmed using the `infer_experiment.py` tool (version 3.0.1) from the RESeQC [384] suite. The `infer_experiment.py` tool requires a gene model in browser extensible data (.bed) format. The .gtf file was converted to .bed format using the `gtf2bed` tool (version 2.4.15) from the `ea-utils` suite [385]. Both RNA-seq data sets were confirmed to be stranded.

An additional QC check was performed following mapping using the RNA-seq specific QC tool `CollectRnaSeqMetrics` from the Picard Tools suite [386]. `REF_FLAT` and `RIBOSOMAL_INTERVALS` files were generated to run the `CollectRnaSeqMetrics` tool from the .fa and .gtf files outlined above. The `REF_FLAT` file was generated using the `ucsc-gtftogenepred` tool (version 377) [387]. `CollectRnaSeqMetrics` takes a sequence alignment map (.sam) or .bam file output from the above alignment step and produces metrics describing the distribution of the bases within the transcripts, including an estimation of ribosomal RNA content in the sample.

3.20.4 Read counting with featureCounts

Where alignment-dependant read processing is performed, the two most popular tools for read counting are `featureCounts` [388] and `HTseq` [389].

Read counting was performed using `featureCounts`, a read summarisation function of the SourceForge `Subread` package, which has been demonstrated to be faster, require less memory and accept more input formats than other read count software tools

[388,390]. featureCounts requires an annotation file (for example, the .gtf file used to generate the mouse index during mapping) and input read files from read alignment in .sam or .bam format. The number of reads which map to features (i.e. an exon) or meta-features (i.e. a gene) can be counted and summarised in a counts table. The default settings of featureCounts were used to count meta-features, specifying a stranded dataset (-s 1) [391]. A count matrix is required as input for differential analysis by DESeq2 [392]. The generated featureCounts count matrix was cleaned using the text editor Vim [393] and saved as an Rmatrix.txt file for further analysis in the R environment (version 3.6.1).

3.20.5 MultiQC report generation

As a final step in read processing and counting, MultiQC was used to aggregate the logs from processing and QC steps into a single report for all samples [394] (Appendix 6 and 7).

3.20.6 Differential gene expression analysis

Numerous tools are available for analysis of differential expression analysis (DEA) [395], including DESeq [396], DESeq2 [397], baySeq [398], EBSeq [399], edgeR [400], limma + voom [401], NOIseq [402], SAMseq [403], Cuffdiff 2 [404] and Sleuth [405]. The most consistently recommended tools for bulk RNA-seq analysis appear to be DESeq2, edgeR and limma + voom [367].

Methods for performing DEA can be crudely divided into two categories: parametric and non-parametric. At present, many of the most popular differential analysis methods fit a parametric model to counts data, typically mapping gene expression values onto a negative binomial (NB) distribution [395]. Counts data in general are commonly modelled using Poisson or NB distribution [406]. However, the Poisson distribution

assumes variance and mean are equal. Two inherent qualities of RNA-seq data that make modelling read counts using the Poisson distribution incorrect are: i) variance of the data tends to be higher than the mean expression values, particularly in cases where mean expression is high, and ii) values with low mean expression demonstrate heteroscedasticity, i.e. variation in variance [370,406]. These qualities are known as overdispersion. The NB distribution is a generalisation of the Poisson distribution which includes an additional parameter able to adjust for variance independently of the mean, rendering it more suitable when modelling RNA-seq data [407,408]. Both DESeq2 and edgeR perform DEA using a generalised linear model (GLM) based on an NB distribution [367].

It is important to mention that not all methods fit parametric models to counts data in order to identify significant features. `limma + voom` uses the `limma` empirical Bayes analysis pipeline, classically utilised for microarray analysis, combined with the `voom` method. Instead of modelling the data on a specific distribution, the relationship between mean and variance of log counts is estimated and a precision weight for each count observation is calculated which can be applied to the `limma` pipeline [401]. `limma + voom` has been shown to perform as well, and in some cases better, than RNA-seq analysis methods such as DESeq2 and edgeR [401,406]. However, its performance has been found to be unstable when the number of replicates is low [409], an attribute of many budget-constrained RNA-seq runs, with DESeq2 demonstrating the highest stability [410].

3.20.6.1 DESeq2

Differential gene expression analysis in this project was performed using the R/Bioconductor package DESeq2 (version 1.28.1) in the R environment (version 3.6.1).

The DESeq function performs three core steps on the raw count data: i) size factor estimation using the median of ratios method (taking into consideration depth of sequencing and RNA composition); ii) gene-wise dispersion estimation, and shrinkage where required; and iii) NB GLM fitting for Wald testing or likelihood ratio testing.

A model of the counts is built using the following equation:

$$K_{ij} \sim NB(\mu_{ij}, \alpha_i)$$

Where counts (K) for gene i and sample j are modelled using a NB distribution with a fitted mean (μ_{ij} ; mean composed of two parameters corresponding to sample size and cDNA fragments for each gene in a sample) and dispersion parameter (α_i ; one per gene i) [392,397].

When the DESeq function is run, a design formula is submitted which indicates the main factor or parameter of interest for testing using the model, as well as those to be controlled for. Unnormalised raw read counts were input into the DESeq2 statistical model, and the design formula ‘~group’ (a combination of two factors of interest, stimulation and vaccine, in a single factor) was used to define the variables to be used for modelling. Hypothesis testing in the DESeq function was performed using the Wald test. Results tables for comparisons were built using contrasts to obtain \log_2 fold change (LFC) values and associated statistics for multiple condition effects.

Genome-wide analyses naturally create very large datasets containing thousands of features (i.e. genes) for testing, rendering this type of data open to the multiple comparisons problem. The multiple comparisons problem occurs when statistical inference is measured simultaneously using traditional p-value cut-offs such as 0.05. In this instance, a p value of 0.05, results in 5% of *all* tests being false positives. Where statistical inference is determined at the individual level this is deemed acceptable,

however, in an RNA-seq run where thousands of genes are analysed, 5% of total tests as false positives is high [411].

To overcome this issue, the calculation of adjusted p values can be performed, such as the Benjamini–Hochberg (false discovery rate) adjustment method. By this method, an adjusted p-value threshold of 0.05 will result in 5% of the tests found to have statistically significant p-values being false positives [412]. The Bonferroni approach is another method to reduce false positives, however, it is considered to be highly conservative and it is not recommended for the purpose of DEA [370,413,414].

When generating results tables, the alpha argument was set at 0.05 to filter results. Multiple correction was performed using the default Benjamini and Hochberg method [412], with an adjusted p value of <0.05 considered to be significant.

LFC estimate shrinkage was performed for each results contrast using ‘type=ashr’ [415] after running the DESeq function. ashR was selected as the shrinkage method as it is suitable for use with contrasts [392]. ashR performs ‘adaptive shrinkage’ using an empirical Bayes approach in which the level of shrinkage is not pre-specified and is sensitive to the signal and precision of the data itself [415]. Shrinkage provides more accurate estimates of LFC by bringing counts that are low or have a high level of dispersion back down towards zero. LFC shrinkage is a useful step in DEA where visualisation and ranking of genes is required [392]. Figure 3-4 shows MA plots of the mean of normalised counts plotted against LFC pre- and post-shrinkage.

The R/Bioconductor packages AnnotationDbi [416] and org.Mm.eg.db [417] were used to assign Ensembl gene names to stable identifiers (i.e. ENSMUSG00000102693) in the counts and results tables for visualisation and downstream analysis.

Principal component analysis (PCA) was performed on rlog-normalised counts and plotted using the built-in plotPCA function in DESeq2.

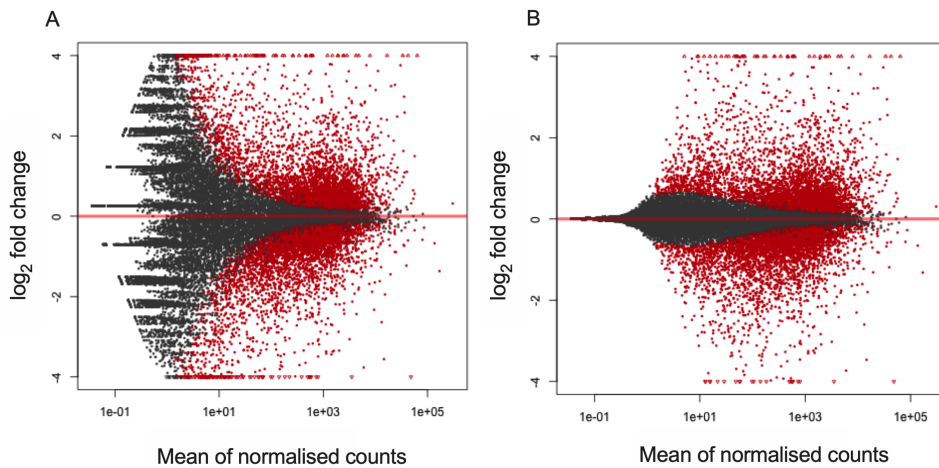


Figure 3-4. Effect of LFC shrinkage using ash. MA plot of mean normalised counts versus LFC for each gene [A] pre and [B] post-shrinkage using ash. Red points indicate an adjusted p value <0.05. LFC, log₂ fold change.

3.21 Microarray analysis

Raw .txt files were downloaded from the Gene Expression Omnibus (GEO) repository for the Agilent dataset GSE21149 (whole mouse genome oligo microarrays 4 x 44K) [418]. Data were processed and DEA was performed using the Bioconductor package limma. Specifically, the dataset was normexp background corrected, quantile normalised and filtered for expressed probes. Next, a linear model was fit to estimate LFC between defined conditions and an empirical Bayes method was used to moderate the standard error of estimated LFC [419,420].

PCA was performed on log₂-normalised expression values using the prcomp function in R and plotted using the ggplot2 package [421].

3.22 Mouse lung module enrichment analysis

A set of 38 murine lung modules generated by Singhania *et al* [422] were used to perform module enrichment analysis on the three gene expression datasets in this study. These defined and biologically meaningful modules were built on RNA-seq data from six disease states using weighted gene correlation network analysis (WGCNA) and downstream functional annotation. Further, modular enrichment of a publicly available dataset containing gene expression profiles of ten isolated immune cell types was performed to identify specific immune cell populations associated with each module [423]. Each module, its perturbation within each disease state, and association with specific immune cell populations is shown in Figure 3-5. An inconsistency in the naming of module 35 (NK vs ILC) between the manuscript and downloaded module annotations used in the present study has been noted but remains uncorrected at present.

Modules were downloaded [424] and pre-processed for use in the tmod package [425]. The makeTmod function was used to generate a tmod object. For LFC data for each condition of interest from both microarray and RNA-seq analyses, a metric score for each DEG gene ($>/< 0$) was calculated using the equation:

$$\text{metric} = -\log_{10}(\text{padj}) \times \text{abs}(\text{LFC}) \text{ [426].}$$

Results were set in descending order to generate ranked Ensembl ID (RNA-seq) or symbol (GEO microarray) lists. Transcriptional module analysis of the lists was performed using the coincident extreme ranks in numerical observations (CERNO) test [427] and visualised using the tmodPanelPlot. tmodPanelPlot generates a heatmap-like representation which includes the effect size (area under the receiver operating curve [AUROC]) and adjusted p (padj) values for modules enriched in one or more of the conditions of interest. All modules from the Singhania set are shown to improve comparison between figures, with an enrichment threshold of $\text{padj} < 0.01$ used.

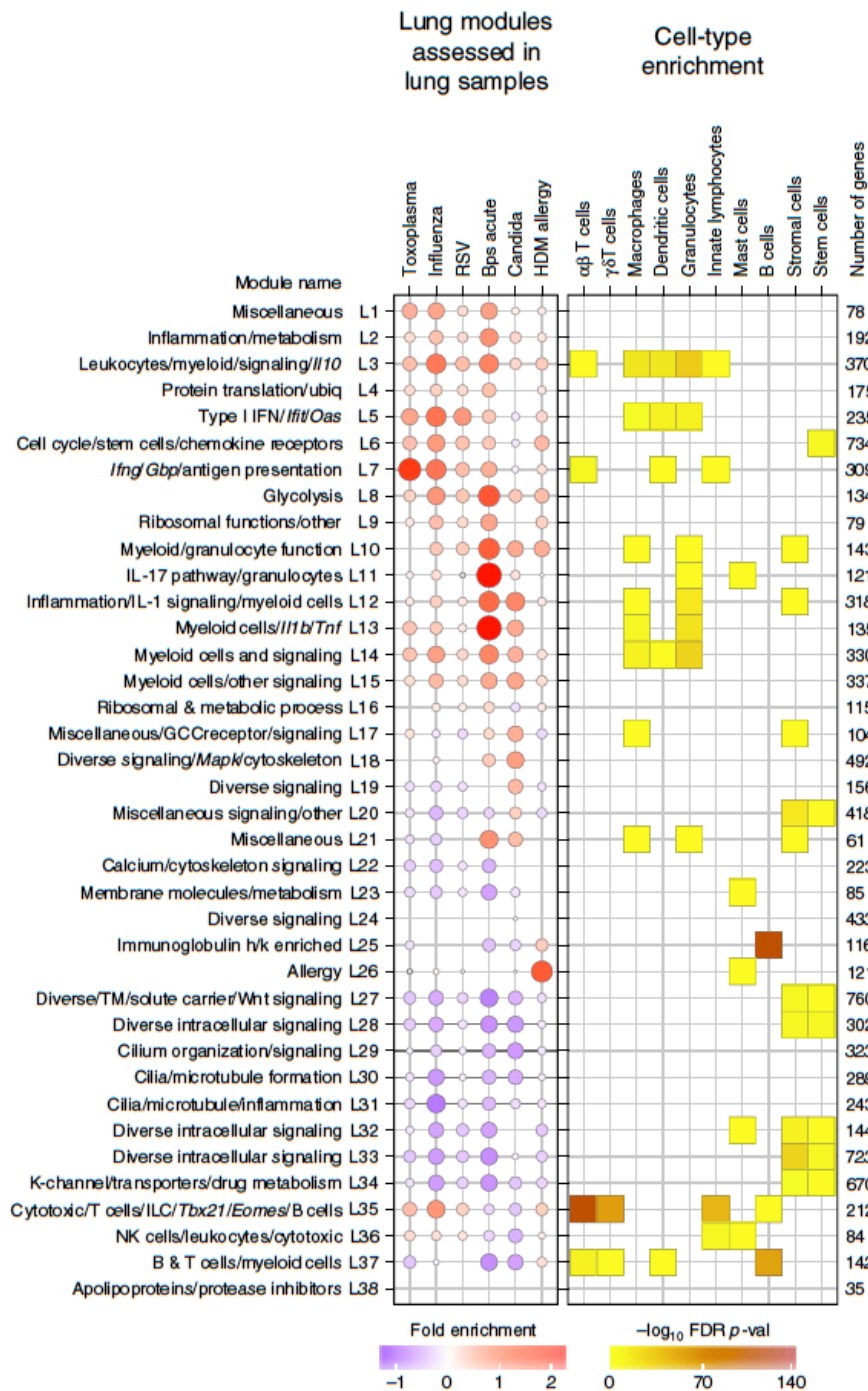


Figure 3-5. Singhania murine lung transcriptional modules. Using six mouse models of infection or inflammation, WGCNA was performed to identify groups of co-expressed genes in the murine lung using RNA-seq expression values. Thirty-eight murine lung modules were derived using this method and then functionally annotated. The module name indicates the biological process(es) annotated to it and the number of genes within each module is shown. Association of specific immune cell types with each module was identified by comparison to a publicly available RNA-seq dataset containing the gene expression profiles of ten isolated immune cell types (right panel). Colour intensity

reflects enrichment significance. Only overrepresented genes were considered cell-type specific [422]. The left panel depicts an example of module enrichment analysis using the 38 lung modules. Enrichment analysis of RNA-seq expression data from the six models and controls was performed using QuSAGE [428]. Over- and under-abundant modules ($p_{adj} < 0.05$) are visualised in red and blue respectively, with size relative to the level of perturbation. p_{adj} , adjusted p; QuSAGE, quantitative set analysis for gene expression; WGCNA, weighted gene co-expression network analysis. Figure reproduced from [422].

Since ordered lists for module enrichment analysis are not generated using a p-value threshold, the proportion of individual genes within each module identified to be significantly up- or downregulated were visualised as a 'pie' using the `tmodDecideTests` function for each result: red, upregulated ($p_{adj} < 0.05$); blue, downregulated ($p_{adj} < 0.05$); grey, not significant.

3.23 Flow cytometry

For test samples, 1×10^6 lung cells from each animal were added to FACS tubes. Cells were centrifuged at $412 \times g$ for 5 minutes (4°C) in a bench-top centrifuge and washed with PBS. LIVE/DEAD fixable blue stain was prepared in dimethyl sulfoxide as per the manufacturer's instructions and each sample was stained for 30 minutes in the dark. Samples were centrifuged at $594 \times g$ for 8 minutes (4°C), and washed and resuspended in PBS before fixing. Ten volumes of prewarmed 1X Phosflow lyze/fix buffer was added to each tube, the sample was mixed by vortexing and then incubated at 37°C for 10 minutes. Following fixation, samples were centrifuged at $594 \times g$ for 8 minutes (4°C), the supernatant removed, and cells washed with FACS buffer. Cells were resuspended in FACS buffer and stored at 4°C until staining.

Staining was performed the day before acquisition. Cells were centrifuged at 594 *x g* for 8 minutes (4°C), the supernatant removed, and cells incubated on ice for 10 minutes with Fc block (0.5 µg / 1 x 10⁶ cells prepared in FACS buffer).

For panel I, the following antibody cocktail was prepared as a mastermix in Brilliant Stain Buffer (as per the manufacturer's instructions): I-E/I-A-APC, Ly6G-BV711, CD11c-PE, CD11b-APC-Cy7, CD45-BUV395, CD64-PECy7, CD24-FITC and SiglecF-BV605. For panel II, the following antibody cocktail was prepared as a mastermix in Brilliant Stain Buffer; CD3-APC/Cy7, Ly6G-BV711, B220-BV510, CD11c-BV605, CD11b-BV650, NK1.1-APC and CD45-PE. Antibodies which had not been previously used in the Fletcher Group were titrated prior to use. Full details of antibodies, including the concentrations used are listed in Appendix 3. Cells were stained for 30 minutes at room temperature in the dark. Following staining, cells were centrifuged at 594 *x g* for 8 minutes (4°C), the supernatant removed, and cells washed with FACS buffer. Cells were then resuspended in FACS buffer and stored at 4°C in the dark until staining.

Fluorescence minus one (FMO) controls (1 x 10⁶ cells per FMO from one age-matched control animal) were stained to guide gating by generating individual antibody cocktails omitting one antibody at a time. Cells were processed in the manner described above.

Antibody compensation was performed by staining OneComp eBeads Compensation Beads with single antibodies as per the manufacturer's instructions. Compensation for the LIVE/DEAD Fixable Blue stain was performed using the Arc Amine Reactive Compensation Bead Kits as per the manufacturer's instructions. The automatic function in FlowJo (v10.4, FlowJo LCC, USA) analytic software was used to

calculate compensation. Compensation was manually checked and adjusted where required.

3.23.1 Data analysis

Cells were acquired on an LSR II flow cytometer (custom configuration - refer to Appendix 5) using FACSDiva Software (BD Biosciences, UK). Data analysis was performed using FlowJo.

3.24 Statistical analysis

Where applicable statistical analysis was carried out using GraphPad Prism software (version 6; GraphPad, USA) or using the R environment. All analyses performed using R were run in RStudio Desktop (version 1.2.5001; RStudio, USA). Specific tests used are indicated in figure legends and results text.

RESEARCH PAPER COVER SHEET

Please note that a cover sheet must be completed **for each** research paper included within a thesis.

SECTION A – Student Details

Student ID Number	LSH1300118	Title	Miss
First Name(s)	Hannah		
Surname/Family Name	Painter		
Thesis Title	Accelerating the preclinical development of effective vaccines for protection against Mycobacterium tuberculosis		
Primary Supervisor	Professor Helen Fletcher		

If the Research Paper has previously been published please complete Section B, if not please move to Section C.

SECTION B – Paper already published

Where was the work published?	Scientific Reports (OPEN ACCESS)		
When was the work published?	24 February 2020		
If the work was published prior to registration for your research degree, give a brief rationale for its inclusion	–		
Have you retained the copyright for the work?*	Yes	Was the work subject to academic peer review?	Yes

*If yes, please attach evidence of retention. If no, or if the work is being included in its published format, please attach evidence of permission from the copyright holder (publisher or other author) to include this work.

SECTION C – Prepared for publication, but not yet published

Where is the work intended to be published?	
Please list the paper's authors in the intended authorship order:	
Stage of publication	Choose an item.

SECTION D – Multi-authored work

For multi-authored work, give full details of your role in the research included in the paper and in the preparation of the paper. (Attach a further sheet if necessary)	I planned and conducted all experiments, with assistance from additional lab members with organ processing. I analysed the data, and wrote and revised the manuscript.
--	--

SECTION E

Student Signature	
Date	12/11/2020

Supervisor Signature	
Date	18th November 2020

4 Results I – Adaption of the *ex vivo* mycobacterial growth inhibition assay for use with murine lung cells

4.1 Chapter background

This chapter is a research paper published in *Scientific Reports* [429] on 24 February 2020. The reference list has been incorporated into the final reference list at the end of this thesis. Supplementary figures and a table are included at the end of the chapter.

4.2 Aims and objectives

Aims

- Establish a murine lung MGIA for the evaluation of vaccine-induced mucosal immunity.

Objectives

- Adapt the murine splenocyte MGIA for use with murine lung cells.

4.3 Abstract

In the absence of a correlate(s) of protection against human tuberculosis and a validated animal model of the disease, tools to facilitate vaccine development must be identified. We present an optimised *ex vivo* mycobacterial growth inhibition assay (MGIA) to assess the ability of host cells within the lung to inhibit mycobacterial growth, including Bacille Calmette–Guérin (BCG) and *Mycobacterium tuberculosis* (MTB) Erdman. Growth of BCG was reduced by 0.39, 0.96 and 0.73 log₁₀ CFU following subcutaneous (s.c.) BCG, intranasal (i.n.) BCG, or BCG s.c. + mucosal boost,

respectively, versus naïve mice. Comparatively, a 0.49 (s.c.), 0.60 (i.n.) and 0.81 (s.c. + mucosal boost) \log_{10} reduction in MTB CFU was found. A BCG growth inhibitor, 2-thiophenecarboxylic acid hydrazide (TCH), was used to prevent quantification of residual BCG from i.n. immunisation and allow accurate MTB quantification. Using TCH, a further 0.58 \log_{10} reduction in MTB CFU was revealed in the i.n. group. In combination with existing methods, the *ex vivo* lung MGIA may represent an important tool for analysis of vaccine efficacy and the immune mechanisms associated with vaccination in the organ primarily affected by MTB disease.

4.4 Introduction

Tuberculosis (TB) is the leading cause of death from a single infectious agent. In 2017, approximately 1.6 million individuals died from TB and 10 million fell ill with the disease [430]. The World Health Organization (WHO)'s End TB Strategy aims to reduce TB deaths by 95% and new cases by 90% between 2015 and 2035 [431]. However, the current tools available for control of TB are inadequate and must be improved if this goal is to be met.

The Bacille Calmette–Guérin (BCG) vaccine remains the only clinically approved vaccine against TB. In high-burden countries the vaccine is administered at birth and protects against severe forms of TB in infants [114]. However, protection against pulmonary forms of the disease in adults varies dramatically between different geographical regions, with prior exposure to mycobacteria, either environmental mycobacteria or *Mycobacterium tuberculosis* (MTB) itself, thought to act as a major influence on this variance [116].

Despite recent progression in the TB vaccine pipeline, with efficacy signals reported from two vaccines in phase 2b trial [130,194], the development and validation

of new TB vaccines remains slow and our understanding of the host immune response to MTB remains poor [46]. One of the reasons for this is that preclinical testing currently relies on head-to-head comparisons of vaccine candidates across a number of animal models. Progression through the preclinical pipeline is largely based on immunogenicity readouts which have been criticised for being oversimplified [200,207,208], and challenge studies which are time consuming and costly, and require a large number of animals for sufficient statistical power. Challenge studies have historically relied on use of MTB laboratory strains to evaluate vaccine protection. However, differences in virulence, fitness and T-cell subset responses in animal models challenged with diverse clinical strains of MTB have been reported [23,122,432], and there is therefore growing interest in preclinical testing of vaccines against MTB isolates representative of the global diversity of the MTB complex (MTBC).

As a potential solution to the growing need for a more rapid and cost-effective method for preclinical vaccine testing, interest in functional assays as readouts of vaccine efficacy has emerged. The mycobacterial growth inhibition assay (MGIA) has been used as an '*ex vivo* challenge model' to analyse the summative capacity of a mixed population of *ex vivo* derived host cells to control mycobacterial growth after vaccination [361]. MTB challenge is not required as host cells are harvested from animals at the peak of the immune response following vaccination. The functional efficacy of the vaccine is then predicted by *ex vivo* co-culture of host cells with mycobacteria. Quantification of mycobacterial growth is predominantly performed using the BACTEC mycobacterial growth indicator tube (MGIT) system, but conventional colony-forming unit (CFU) enumeration from culture on solid media has also been used [300]. The cost and study duration of the MGIA are lower than a comparative MTB challenge study, and animal welfare is also improved. Since each animal provides sufficient cells for multiple assay

inputs, the MGIA offers the potential to analyse multiple lineages of the MTBC in parallel, using considerably fewer animals than a challenge study of the same design [80]. These concepts are in line with the ‘Refinement’ and ‘Reduction’ criteria defined by the UK National Centre for the 3Rs [77].

To date, preclinical MGIA protocols have been established for use with splenocytes [306,308] and BMMs in mice [299], as well as whole blood and peripheral blood mononuclear cells (PBMCs) for larger animal models [275,360]. The MGIA has been performed in tandem with MTB challenge in a number of murine studies to determine how *ex vivo* growth inhibition correlates with protection from *in vivo* infection with MTB. These methods have been reported to correlate at the group level [201,299,306].

Protection against pulmonary TB must be demonstrated by candidate TB vaccines; therefore, to be an effective tool for TB vaccine testing, the MGIA should be able to evaluate protective immunity in the lung. To the best of our knowledge, an MGIA using lung cells from animal models of TB has not been reported. In this report, we present an optimised MGIA protocol for use with murine lung cells, to assess the ability of host lung cells to inhibit mycobacterial growth following vaccination. Following optimisation of host cell and bacterial input number, the lung MGIA was able to detect differences in both BCG (as a surrogate of MTB) and MTB Erdman growth inhibition between vaccine groups. Where residual BCG from immunisation was present in input cells, we found that use of the BCG inhibitor, 2-thiophenecarboxylic acid hydrazide (TCH), revealed additional MTB Erdman growth inhibition. In combination with current methods of preclinical TB vaccine assessment, the *ex vivo* lung MGIA could be used as a tool for analysis of vaccine efficacy and the underlying immune mechanisms associated with vaccination.

4.5 Results

4.5.1 Number of murine lung cells influences mycobacterial growth inhibition by immunised and control groups

A reduction in CFU burden after *in vivo* MTB challenge has been demonstrated in the murine lung in animals administered with BCG and/or various candidate TB vaccines compared with unvaccinated animals [146,201,433]. To determine whether the lung MGIA could be utilised as an ‘*ex vivo* challenge model’ to assess vaccine efficacy in animal models, C57BL/6 mice (six per group) received either BCG Pasteur Aeras subcutaneous (s.c.) or intranasal (i.n.) at week 0, BCG Pasteur Aeras s.c. at week 0 followed by an i.n. boost with the candidate vaccine spore-FP1 at week 3, or received no treatment. At six weeks, lungs were harvested, enzymatically digested and homogenised to generate a single cell suspension. Next, 3×10^6 or 1×10^6 lung cells from one pool of cells generated for each group were co-cultured with 100 CFU BCG Pasteur Aeras in 48-well plates. At 96 hours, cells were lysed and samples transferred to the BACTEC MGIT system until time to positivity (TTP) values were generated. BCG was used as a surrogate for MTB in early assay development as MGIA outcomes have previously been shown to correlate [289,360].

Initially, the lung MGIA was performed with 3×10^6 lung cells (Figure 4-1A), revealing a significant but small reduction ($\Delta 0.26 \log_{10}$ CFU) in growth following BCG s.c. vaccination compared with control animals ($p=0.0075$; one-way ANOVA followed by Tukey's multiple comparison test). No differences in BCG growth were found between the BCG i.n. group and control.

Decreasing the input lung cell count to 1×10^6 resulted in improved sensitivity to detect significant reductions in growth of BCG in all vaccinated groups compared with the control group ($\Delta \log_{10}$ CFU: BCG s.c. 0.39, BCG i.n. 0.96, BCG s.c. + mucosal boost

0.73; $p \leq 0.0001$; one-way ANOVA followed by Tukey's multiple comparison test) (Figure 4-1B). When comparing BCG i.n. to s.c., a 0.57 \log_{10} reduction in CFU was noted when vaccinating intranasally ($p < 0.0001$). Mucosal boosting with spore-FP1 three weeks following BCG s.c. was also found to reduce BCG growth by a further 0.33 \log_{10} CFU compared with BCG s.c. alone ($p = 0.0006$).

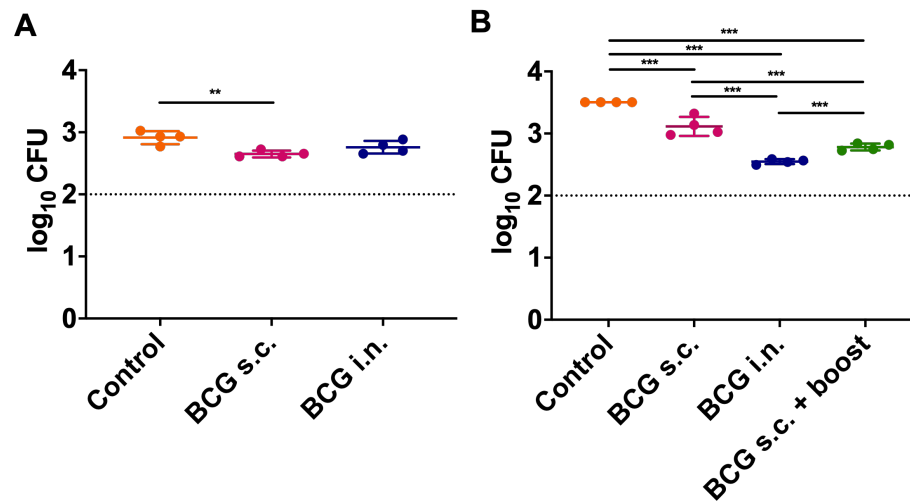


Figure 4-1. Host-cell density affects growth inhibition in the *ex vivo* MGIA. C57BL/6 mice ($n=6$ /group) received s.c. or i.n. BCG Pasteur Aeras at week 0 or no treatment (control). An additional group shown in part B received s.c. BCG Pasteur Aeras at week 0 followed by i.n. boosting with the candidate vaccine spore-FP1 at week 3. At six weeks, (A) 3×10^6 or (B) 1×10^6 lung cells were co-cultured with 100 CFU BCG Pasteur Aeras in 48-well plates. At 96 hours, samples were lysed and transferred to the BACTEC system until TTP values were generated. TTP values were converted to \log_{10} CFU based on a standard curve. Data points ($n=4$ /group) represent samples generated from pooled cells isolated from six mice. Dotted line indicates mycobacterial input at day 0. Statistical significance was tested by one-way ANOVA followed by Tukey's multiple comparison test. Error bars represent mean \pm standard deviation. ** $p < 0.01$ (adjusted); *** $p < 0.001$ (adjusted). ANOVA, analysis of variance; BCG, Bacille Calmette–Guérin; CFU, colony-forming units; i.n., intranasal; MGIA, mycobacterial growth inhibition assay; s.c., subcutaneous; TTP, time to positivity.

Since *ex vivo* mycobacterial growth inhibition following BCG immunisation has previously been demonstrated in murine splenocytes [305,306,308], an MGIA using splenocytes from the same animals was performed as a positive control in parallel with the lung MGIA. Using 3×10^6 splenocytes co-cultured with 100 CFU BCG Pasteur, a 1.04, 0.86 and 0.87 \log_{10} CFU reduction in BCG growth was observed in the BCG s.c., i.n. and BCG s.c. + mucosal boost groups respectively, compared with the control ($p < 0.0001$; one-way ANOVA followed by Tukey's multiple comparison test) (Supplementary Figure S4-1).

4.5.2 Comparison of MTB Erdman and BCG growth inhibition

Next, to determine whether BCG growth inhibition identified in the vaccinated groups above correlates with growth inhibition of MTB Erdman, an MGIA was performed using the same host cell and bacterial input (Figure 4-2A).

Surprisingly, no differences in MTB growth were found between the vaccinated and control groups. In contrast, in the BCG i.n. group, a significant increase in MTB Erdman CFU of 0.49 \log_{10} was noted compared with the BCG s.c. group ($p = 0.03$; one-way ANOVA followed by Tukey's multiple comparison test). When comparing the control and BCG i.n. groups, a trend in increased growth in the i.n. group was observed; however this was not significant. Intra-assay variability was determined by calculating the coefficient of variation (CV): $[\text{standard deviation}/\text{mean}] \times 100$. The CV quantifies the spread of data within each experimental group. When using 100 CFU of MTB Erdman in the MGIA, the CV for control and BCG s.c. was found to be 7.17% and 3.52%, respectively (Supplementary Table S4-1). Of note, the CV in the BCG i.n. group was 0.95%.

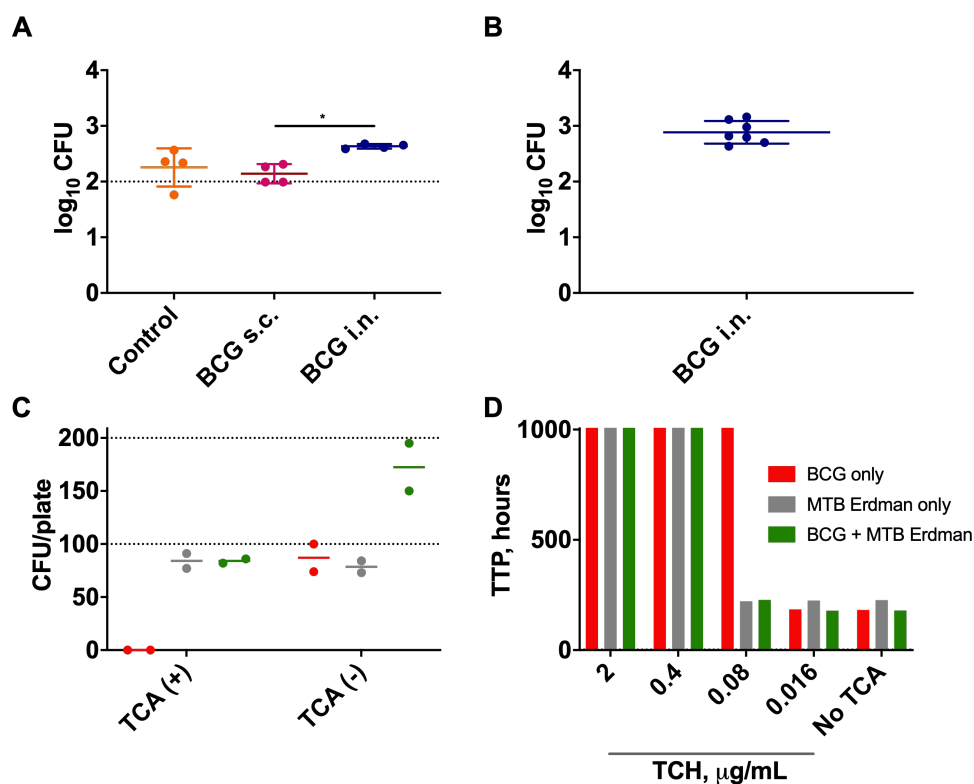


Figure 4-2. Residual BCG in murine lung cells following intranasal vaccination in the *ex vivo* MGIA. (A) C57BL/6 mice (n=6/group) received s.c. or i.n. BCG Pasteur Aeras at week 0 or no treatment (control). At six weeks, 1×10^6 lung cells were co-cultured with 100 CFU MTB Erdman in 48-well plates. At 96 hours, samples were transferred to the BACTEC system until TTP values were generated. TTP values were converted to \log_{10} CFU based on a standard curve. Data points (n=4/group) represent samples generated from pooled cells from six mice. Statistical significance was tested by one-way ANOVA followed by Tukey's multiple comparison test. * $p < 0.05$ (adjusted). (B) Residual BCG in 1×10^6 murine lung cells six weeks following immunisation with i.n. BCG Pasteur Aeras was quantified using the BACTEC MGIT system. Data points represent four pools of cells from four individual mouse experiments (run as duplicate or single). (C and D) 100 CFU BCG Pasteur Aeras or MTB Erdman, or 100 CFU BCG Pasteur Aeras and 100 CFU MTB Erdman were: (C) plated on 7H11 agar plates in the presence or absence of $2 \mu\text{g/mL}$ TCH to confirm the inhibitory properties of TCH on BCG only (n=2/condition); (D) added to MGITs in the absence or presence TCH (five-fold serial dilutions of $2 \mu\text{g/mL}$ stock: 0.4, 0.08, 0.016 $\mu\text{g/mL}$) to determine the optimal concentration of TCH to inhibit BCG growth only (n=1/condition) in the BACTEC system. A TTP value of 1,008 hours (42 days) indicates a negative result (no bacteria

detected). Dotted lines indicate mycobacterial input. Error bars represent mean \pm standard deviation. ANOVA, analysis of variance; BCG, Bacille Calmette–Guérin; CFU, colony-forming units; i.n., intranasal; MGIA, mycobacterial growth inhibition assay; MGIT, mycobacterial growth indicator tube; s.c., subcutaneous; TCH, 2-thiophenecarboxylic acid hydrazide; TTP, time to positivity.

The lack of growth inhibition of MTB led us to hypothesise that residual live BCG from vaccination persisted in *ex vivo* isolated lung cells, potentially confounding CFU enumeration of MTB. To clarify this, 1×10^6 lung cells only were added to supplemented MGITs in the absence of co-culture with mycobacteria to quantify residual BCG at six weeks following vaccination using the BACTEC MGIT system. In the BCG i.n. group, residual BCG at six weeks post-vaccination was $2.87 \log_{10}$ CFU (mean calculated from four individual mouse experiments [run as duplicate or single]; maximum, 3.161; minimum, 2.634; (Figure 4-2B). No residual BCG was detected in samples from the BCG s.c. group (data not shown). To eliminate the confounding effect of residual BCG on MTB growth inhibition, we refined the assay further by addition of TCH, a compound known to specifically inhibit BCG growth.

4.5.3 *Mycobacterium* spp. TCH susceptibility

At defined concentrations, TCH inhibits growth of BCG but not MTB [434]. Addition of $2 \mu\text{g/mL}$ TCH to 7H11 agar plates is standard practice in MTB challenge studies which include i.n. BCG vaccination [135,435]. The inhibitory properties of TCH on BCG, but not MTB Erdman, were confirmed here by plating 100 CFU of each of BCG Pasteur Aeras or MTB Erdman alone, or 100 CFU of BCG Pasteur Aeras and 100 CFU of MTB Erdman together on 7H11 agar plates in the presence or absence of $2 \mu\text{g/mL}$ TCH (Figure 4-2C). MTB Erdman CFU was unchanged in the absence and presence of 2

$\mu\text{g/mL}$ TCH. By contrast, BCG did not grow in the presence of 2 $\mu\text{g/mL}$ TCH, indicating that enumeration of MTB Erdman only could be performed using this concentration of TCH in agar plates.

To date, use of TCH in the MGIA or in the BACTEC MGIT system has not been reported. Therefore, 100 CFU of each of BCG Pasteur Aeras or MTB Erdman alone, or 100 CFU of BCG Pasteur Aeras and 100 CFU MTB Erdman together were added to supplemented MGITs in the presence (five-fold serial dilutions of a 2 $\mu\text{g/mL}$ stock: 0.4, 0.08, 0.016 $\mu\text{g/mL}$) or absence of TCH to determine the optimal concentration of TCH to inhibit growth of BCG, but not MTB Erdman, in the BACTEC system (Figure 4-2D). A concentration of 0.08 $\mu\text{g/mL}$ TCH was found to inhibit growth of BCG only. Growth inhibition of both MTB Erdman and BCG was observed at TCH concentrations of 2 and 0.4 $\mu\text{g/mL}$, and no growth inhibition of either mycobacterial species was found at 0.016 $\mu\text{g/mL}$.

4.5.4 Vaccine-mediated inhibition of mycobacterial growth in lung cell culture

Incorporating the optimised parameters described, an MGIA was performed to determine the vaccine-induced capacity of murine lung cells to control the growth of MTB Erdman. In addition to the aforementioned parameters, the mycobacterial input for the MTB Erdman MGIA was increased to 200 CFU. This was because residual BCG was not identified in lungs harvested from animals receiving BCG s.c., and yet no significant difference in growth inhibition of MTB Erdman was noted in the BCG s.c. group compared with control. Notably, intra-assay variability (CV) in the control and BCG s.c. groups was high using 100 CFU MTB Erdman (Supplementary Table S4-1). We therefore hypothesised that increasing the mycobacterial input may also improve the performance of the assay and decrease variability.

Using the same four-group study design described above for the BCG MGIA, lungs were harvested at six weeks after vaccination and 1×10^6 lung cells from pools of cells generated for each group were co-cultured with 200 CFU MTB Erdman in 48-well plates. At 96 hours, samples were lysed and transferred to the BACTEC MGIT system (Figure 4-3) or plated on solid media (Supplementary Figure S4-2), in the absence and presence of TCH.

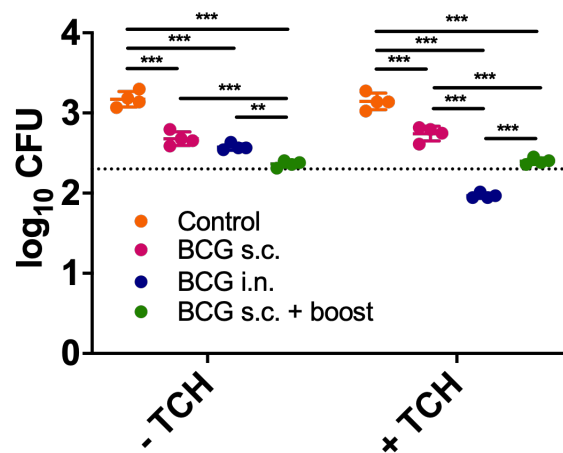


Figure 4-3. Optimised *ex vivo* MGIA comparing MTB Erdman growth inhibition conferred by vaccination in murine lung. C57BL/6 mice ($n=6$ /group) received s.c. or i.n. BCG Pasteur Aeras at week 0, s.c. BCG Pasteur Aeras at week 0 and i.n. boosting with the candidate vaccine spore-FP1 at week 3, or received no treatment (control). At six weeks, 1×10^6 lung cells were co-cultured with 200 CFU MTB Erdman in 48-well plates. At 96 hours, samples were transferred to the BACTEC MGIT system until TTP values were generated. Mycobacterial quantification was performed in the presence and absence of TCH. TTP values were converted to \log_{10} CFU based on a standard curve. Data points ($n=4$ /group) represent samples generated from pooled cells isolated from six mice. Dotted line indicates mycobacterial input at day 0. Statistical significance was tested by one-way ANOVA followed by Tukey's multiple comparison test. Error bars represent mean \pm standard deviation. * $p<0.05$ (adjusted); ** $p<0.01$ (adjusted); *** $p<0.001$ (adjusted). ANOVA, analysis of variance; BCG, Bacille Calmette–Guérin; CFU, colony-forming units; i.n., intranasal; MGIA, mycobacterial growth inhibition assay;

MGIT, mycobacterial growth indicator tube; s.c., subcutaneous; TCH, 2-thiophenecarboxylic acid hydrazide; TTP, time to positivity.

Using the BACTEC MGIT system in the absence of TCH, significant reductions in growth of MTB Erdman were observed in all vaccinated groups compared with the control group ($\Delta \log_{10}$ CFU: BCG s.c. 0.49, BCG i.n. 0.60, BCG s.c. + mucosal boost 0.81; $p < 0.0001$; one-way ANOVA followed by Tukey's multiple comparison test). Mucosal boosting three weeks following BCG s.c. was found to reduce MTB Erdman growth by a further 0.32 \log_{10} CFU compared with BCG s.c. alone ($p = 0.0002$). No significant difference in growth inhibition between the BCG s.c. and i.n. groups was identified. In the presence of TCH, reductions in growth of MTB Erdman were again found in all vaccinated groups compared with controls ($\Delta \log_{10}$ CFU: BCG s.c. 0.40, BCG i.n. 1.18, BCG s.c. + mucosal boost 0.75; $p < 0.0001$), as well as a further reduction in growth associated with BCG s.c. + mucosal boost compared with BCG s.c. alone ($\Delta 0.35 \log_{10}$ CFU; $p = 0.0001$). Of note, a further reduction in MTB Erdman growth of 0.58 \log_{10} CFU was noted in the BCG i.n. group compared with samples without TCH. Intra-assay variability was low in all groups, with a 4.53% and 1.38% reduction in CV in the control and BCG s.c. groups respectively when increasing MTB Erdman to 200 CFU (Supplementary Table S4-1).

An MGIA using splenocytes from the same animals was performed as a positive control in parallel with the lung MGIA. Using 3×10^6 splenocytes co-cultured with 200 CFU MTB Erdman, a 1.12, 0.93 and 1.30 \log_{10} CFU reduction in MTB Erdman growth was observed using the BACTEC MGIT system in the BCG s.c., i.n. and BCG s.c. + mucosal boost groups respectively, compared with the control ($p < 0.0001$; one-way ANOVA followed by Tukey's multiple comparison test) (Supplementary Figure S4-3).

When plating lysates on solid media (Supplementary Figure S4-2) in the absence of TCH, significant reductions in growth of MTB Erdman were also noted in all vaccinated groups compared with the control group ($\Delta \log_{10}$ CFU: BCG s.c. 0.34 [p=0.0362], BCG i.n. 0.37 [p=0.0210], BCG s.c. + mucosal boost 1.05 [p<0.0001]; one-way ANOVA followed by Tukey's multiple comparison test). In the presence of TCH, reductions in growth of MTB Erdman were found in the BCG s.c. ($\Delta 0.37 \log_{10}$ CFU; p=0.0331), BCG i.n. ($\Delta 1.02 \log_{10}$ CFU; p<0.0001) and BCG s.c. + mucosal boost compared with the control group ($\Delta 0.61 \log_{10}$ CFU; p=0.001). Again, a further reduction in MTB Erdman growth of 0.65 \log_{10} CFU was noted in the BCG i.n. group compared with in the absence of TCH.

Using the optimised MGIA conditions described, variations in the ability of *ex vivo* derived host lung cells to inhibit MTB Erdman growth were found following vaccination. These variations were identified using the BACTEC MGIT system and plating on solid media. Use of the BCG inhibitor, TCH, revealed additional MTB Erdman growth inhibition in groups in which residual BCG was present six weeks following vaccination.

4.6 Discussion

The MGIA has been developed as a tool to facilitate preclinical evaluation of TB vaccines using mycobacterial growth inhibition as a surrogate readout of vaccine-induced protection against TB [361]. To date, murine MGIA's have been performed using splenocytes and BMMs, with mycobacterial growth inhibition *ex vivo* reported to correlate with *in vivo* protection in MTB challenge studies at the group level [299,306,308].

TB is predominantly a pulmonary infection, and MTB challenge studies commonly enumerate bacterial burden in the lung and spleen of infected animals. We therefore aimed to develop a lung MGIA as a complementary tool for the preclinical evaluation of existing and experimental TB vaccines. Induction of an earlier, pulmonary, vaccine-induced immune response to infection is a key objective in TB vaccine development, highlighting the importance of development of tools able to analyse this compartment. To date, mycobacterial growth control of cells from human alveolar lavage [261] and alveolar macrophages [268] has been investigated using the MGIA. To the best of our knowledge, an MGIA using total lung cells from animal models of TB has not been reported.

In this study, an MGIA using BCG as a surrogate for MTB was performed in 48-well plates to determine whether this culture method is conducive to assessment of the control of mycobacterial growth by lung cells. Recent MGIA publications have recognised that host cell viability following co-culture in rotating screw-cap tubes is low, hypothesising that the lack of oxygen availability in the tubes and shear forces associated with rotation may be deleterious to cell viability [263,308]. Use of static 48-well plates in the splenocyte MGIA has been reported previously [307]. A mouse study was designed which included s.c. and i.n. administration of BCG, as well as a control unvaccinated arm. The experimental prime-boost vaccine, spore-FP1, was also included at later stages of assay development.

The majority of published MGIA studies use biological replicates (albeit using inbred mice) within each group. In 2016, Yang *et al* presented a simplified splenocyte MGIA using five technical replicates per group from three pooled mice. Pooling was recognised as a limitation; however, it was found that by reducing variability, sensitivity to detect differences in growth inhibition between groups was improved. MGIA outcomes

were reported to correlate with *in vivo* protection [307]. The simplified MGIA was performed in the current study using four technical replicates from each group of six pooled mice.

To date, 5×10^6 splenocytes have been used in murine MGIA [299,306,308]. When comparing host cell input numbers in the MGIA using rotating tubes, a higher number of splenocytes (5×10^6) was found to increase sensitivity to differences in growth inhibition and improve intra-assay variability compared with lower inputs [306]. However, when using 48-well plates in the current study, higher host cell density resulted in considerable yellowing of the media at 96 hours (microscopic evaluation) indicative of nutrient exhaustion and potentially less healthy cells. To this end, we selected a lower input cell number for MGIA performed in this study, with the aim to improve host cell viability and subsequent inhibitory capacity.

As a positive control during assay development, a splenocyte MGIA was run in tandem with the lung MGIA. Significant growth inhibition of BCG was observed in all vaccinated groups compared with the control using 3×10^6 splenocytes and 100 CFU BCG (Supplementary Figure S4-1). In comparison, when using lung cells, a modest reduction in mycobacterial growth was observed only in the s.c. group (vs control group) under the same conditions (Figure 4-1A). No differences were observed between other groups. By contrast, reducing the lung cell input to 1×10^6 resulted in a significant reduction in BCG growth in all vaccination groups (Figure 4-1B), consistent with *in vivo* protection reported in the literature [135,146].

To enable better comparison to *in vivo* MTB challenge experiments, an MGIA was performed using MTB Erdman with the same host and mycobacterial input as the BCG MGIA. Paradoxically, mycobacterial growth was increased in the BCG i.n. group

compared with the BCG s.c. and the control group. No other growth differences were noted (Figure 4-2A). We therefore sought to further optimise the MGIA conditions.

As advised by Zelmer *et al* [306], ‘direct-to-MGITs’ (host cells added directly to MGITs) for all experimental groups receiving a live vaccine were performed for all MGIA. We report that six weeks following i.n. BCG immunisation, $2.87 \log_{10}$ CFU BCG was present in 1×10^6 lung cells (Figure 4-2B), resulting in the hypothesis that residual BCG from the immunisation was also being quantified by the BACTEC MGIT system after the MGIA co-culture, falsely inflating CFU estimates and potentially masking vaccine responses. In our hands, BCG Pasteur Aeras grows faster than MTB Erdman when plated on 7H11 agar plates (data not shown). The BACTEC MGIT system is unable to differentiate between mycobacterial species and CFU input is estimated in the MGIA using a mycobacteria-specific standard curve. Therefore, we hypothesised that in the MTB Erdman MGIA, fast-growing residual BCG from the immunisation would be quantified as MTB Erdman, potentially causing an even larger overestimation of bacterial count than in the BCG MGIA.

Intra-assay variability was considerably higher in the control and BCG s.c. groups when using 100 CFU MTB Erdman compared with BCG in the MGIA (Supplementary Table S4-1). Based on these observations, two adaptations were made to the MTB Erdman MGIA: i) mycobacterial input was increased to 200 CFU; and ii) TCH was added to MGITs/plates to ensure the enumeration of MTB Erdman only. *Mycobacterium bovis*, of which BCG is an attenuated form, is sensitive to low concentrations of TCH (1–5 $\mu\text{g}/\text{mL}$) on solid growth media [436]. Since MTB and other mycobacteria are not sensitive to TCH at these concentrations [436], the compound is routinely added to agar plates in MTB challenge studies which include an i.n. BCG study group [135,435]. We report that a concentration of 2 and 0.08 $\mu\text{g}/\text{mL}$ TCH added to agar plates and MGITs, respectively,

can be used to inhibit growth of BCG Pasteur Aeras but not MTB Erdman (Figure 4-2C and D). It is important to note that TCH sensitivity of members of the MTBC compared with MTB laboratory strains is variable [434,437] and we recommend that sensitivity be determined on a case-by-case basis when using clinical isolates.

Using the adapted lung MGIA protocol, an MGIA was performed using 1×10^6 lung cells and 200 CFU MTB Erdman (Figure 4-3). The assay was performed in the presence or absence of TCH. Significant growth inhibition of MTB Erdman was noted in all vaccinated groups compared with the unvaccinated group and intra-assay variability (CV) was reduced using 200 CFU MTB Erdman compared to 100 CFU (Supplementary Table S4-1). When TCH was added to MGITs, a further reduction in MTB Erdman CFU was observed in the BCG i.n. group. Differences in MTB Erdman growth inhibition following vaccination were consistent with *in vivo* protection reported in the literature [135,146], as well as with growth inhibition observed in the BCG MGIA performed in this study. Using a low-dose MTB aerosol challenge model, Copland *et al* report enhanced control of MTB in murine lung boosted with spore-FP1 following BCG prime compared with BCG alone (0.70 vs 1.44 log₁₀ CFU reduction vs PBS control) [146]. A number of mouse studies have demonstrated superior protection in the lung in challenge studies following BCG i.n. compared with BCG s.c. at comparable time points following vaccination [135,438,439]. While the MGIA aims to model vaccine protection observed in *in vivo* challenge studies, we do not expect log₁₀ CFU values from the BACTEC MGIT system to match those obtained from challenge studies. The number of host cells and CFU associated with *in vivo* studies are different to the MGIA and we predict that the assay is not able to model the full complexity of an *in vivo* system. It is however encouraging to observe that results are consistent at the group level with existing literature. We suggest that future studies using the lung MGIA perform challenge studies in parallel

to confirm that growth inhibition following vaccination translates to protection in the murine model.

Kolibab *et al* previously demonstrated that results obtained by BACTEC MGIT and colony counting for the splenocyte MGIA were comparable. The BACTEC MGIT system is generally favoured over colony counting since CFU determination is slower and more labour intensive than the BACTEC method, and the absence of standardised reagents and element of subjectivity in manual counting may result in increased inter-assay variation [300]. Furthermore, the BACTEC MGIT system is unaffected by clumping and provides an accurate computer-generated readout based on validated technology [360]. However, reagents and equipment for the BACTEC MGIT system are costly. Therefore, to make the lung MGIA more accessible, particularly in resource-limited settings, MTB Erdman enumeration was also performed by culture on solid media. Under the optimised conditions described, comparable results were observed in all groups (Supplementary Figure S4-2). However, consistent with previous reports, a reduction in the sensitivity of the MGIA when plating on solid media has been found between independent assay runs of the optimised lung MGIA presented here (Supplementary Figure S4-4). Where differences in growth inhibition in the lung between vaccinated and non-vaccinated animals are small, for example when administering BCG s.c., a consistent reduction in MTB Erdman growth of $<0.50 \log_{10}$ CFU is noted using the BACTEC MGIT system; however, this difference is inconsistently found on plates in experiments performed in tandem with the BACTEC system. This observation suggests that the BACTEC MGIT system should be used when differences in growth inhibition are expected to be more conservative in the lung, for example when using systemic vaccine regimens, to ensure that smaller differences in growth are detected by the assay.

4.6.1 Conclusions

We present an optimised preclinical MGIA protocol to assess the ability of host lung cells to inhibit mycobacterial growth in this organ following vaccination. We demonstrate that factors including host cell density, *ex vivo* co-culture CFU input, residual live BCG from vaccination and CFU enumeration method all significantly affect the reliability of the MGIA. Furthermore, we present optimised solutions to these challenges and show for the first time the utility of the MGIA to assess TB vaccine efficacy in the lung by virtue of growth inhibition of both BCG and MTB Erdman *ex vivo*.

In the future, the lung MGIA may be applied to refinement of vaccine dose or regimen prior to clinical studies and provide early insight into variations in protection against different lineages of the MTBC. Further optimisation of the assay is required for use with multiple MTBC lineages and *in vivo* challenge studies will need to be performed in parallel with the assay to confirm that growth inhibition following vaccination translates to protection. At present, it is encouraging to see that growth inhibition observed using various vaccination strategies is consistent with existing literature at the group level, indicating that the MGIA may represent a complementary tool to MTB challenge studies and immunogenicity measures for preclinical evaluation of TB vaccine strategies. The assay also represents a viable method for the reduction and refinement of animal studies in the TB field.

4.7 Materials and methods

4.7.1 Ethics statement

Animal experimentation was performed under licence PPL 70/8043 (superseded by P6CA9EB8D) issued by the UK Home Office according to the Animals (Scientific Procedures) Act 1986 and approved by the London School of Hygiene & Tropical

Medicine (LSHTM) Animal Welfare and Ethics Review Body. This manuscript was prepared in accordance with the ARRIVE guidelines [356].

4.7.2 Mycobacteria

BCG Pasteur Aeras was obtained from Aeras (Rockville MD, USA) as 500 µL frozen aliquots. MTB Erdman was obtained from BEI Resources (Manassas, VA, USA) as a 1-mL frozen glycerol stock. MTB Erdman stocks were grown to log phase at 150 rpm and 37°C in Middlebrook 7H9 Broth (Yorlab, York, UK) supplemented with 10% OADC (Yorlab), 0.05% Tween-80 (Sigma, Gillingham, UK) and 0.2% glycerol (Sigma). All work using MTB Erdman was performed in an aerosol containment level-3 laboratory at LSHTM in accordance with guidance from the UK Advisory Committee on Dangerous Pathogens (ACDP). All mycobacterial stocks were stored at –80°C.

4.7.3 Animals

For immunisation experiments, female C57BL/6 mice (5–7 weeks old; weight 16–20 g) were obtained from Charles River UK and rested for at least five days before procedure start. Animals were housed in groups of 5–6 with access to food and water *ad libitum*. Animals were randomly assigned to cages on arrival by staff in the Biological Services Facility at LSHTM. Each cage was randomly assigned a group number on commencement of the study.

4.7.4 Immunisation

BCG Pasteur Aeras was thawed at room temperature and diluted in physiological saline solution for irrigation (Baxter Healthcare, Newbury, UK) to a final concentration of 10⁷ CFU/mL. S.c. BCG Pasteur Aeras was administered as 100 µL (1 x 10⁶ CFU) into

the right or left leg flap using a sterile 25G needle. For i.n. immunisations, mice were anaesthetised by intraperitoneal injection of ketamine (50 mg/kg; Ketalar, Pfizer Ltd, Walton Oaks, UK) and xylazine (10 mg/kg; Rompun, Bayer plc, Newbury, UK) in physiological saline solution for irrigation, followed by delivery of 50 μ L (0.5×10^6 CFU) BCG Pasteur Aeras equally administered between the two nostrils. Animals in the BCG s.c. + spore-FP1 boost arm were administered BCG Pasteur Aeras s.c. (as described) at week 0, followed by i.n. boosting at week 3 with spore-FP1. FP1 is a fusion protein constructed of MTB proteins, ACR, Ag85B and HBHA. Cloning and production of FP1 were previously described by Copland *et al* [146]. For formulation of spore-FP1, FP1 (Lionex GmbH, Braunschweig, Germany) was incubated with *Bacillus subtilis* spores (Sporegen, Egham, UK) for one hour at room temperature and administered shortly following formulation. Animals were anaesthetised in the manner described for i.n. BCG, followed by delivery of 1×10^9 *B subtilis* spores coated with 10 μ g FP1 (delivery volume: 40 μ L/animal) equally between the two nostrils. Control animals received no treatment. BCG CFU input was confirmed by plating the diluted inoculum on Middlebrook 7H11 agar (Yorlab) plates containing 10% OADC supplement and 0.5% glycerol. All animals were rested for six weeks following vaccination and then sacrificed by exposure to carbon dioxide gas in a rising concentration.

4.7.5 Lung and spleen cell isolation

Lungs were removed aseptically, washed in R0L (RPMI-1640 (Sigma) + 2 mM L-Glutamine [Fisher Scientific, Loughborough, UK] + 50 U/mL penicillin [Sigma]) and cut into small pieces with sterile scissors. Lungs were incubated for 40 minutes at 37°C (5% CO₂) with deoxyribonuclease I from bovine pancreas (type IV, Sigma; final concentration: 12 μ g/mL) and Liberase TL (Sigma; final concentration: 625 μ g/mL). The

enzyme reaction was terminated by adding R10L (R0L + 10% heat-inactivated FBS [Sigma]) and homogenised lungs were passed through a 100- μ m cell strainer (VWR International, Lutterworth, UK) to obtain a single cell suspension. Red blood cell lysis was performed using ammonium–chloride–potassium (ACK) lysis buffer. Spleens were removed aseptically and homogenised by passing through a 100- μ m cell strainer. Red blood cell lysis was performed using RBC lysis buffer (Sigma). Processing of spleens was performed in R10S (antibiotic-free R10L). For all assays, samples from six mice were used to generate one pool per group.

4.7.6 *Ex vivo* mycobacterial growth inhibition assay

Following cell isolation, murine cell number was counted, adjusted in R10 and 300 μ L/well added to 48-well plates (Fisher Scientific, Loughborough, UK). A mastermix of the required bacterial input was made by diluting bacteria to the desired concentration in R10 and 300 μ L added to each well containing cells. Plates were incubated at 37°C (5% CO₂) for 96 hours. At 96 hours, supernatants were removed from the plates and 500 μ L sterile water was added to each well and incubated for five minutes. Murine cells were disrupted/lysed by pipetting to release intracellular mycobacteria and then the total volume (500 μ L) was: i) added to a PANTA-supplemented MGIT (BD, Oxford, UK); or ii) plated on 7H11 agar plates supplemented with OADC and glycerol. ‘Direct-to-MGITs’ containing bacteria only were set up to confirm bacterial input, as well as for murine cells from immunised groups to detect residual BCG. All MGITs were placed in the BACTEC MGIT 960 or 320 systems (BD) until registered positive.

Standard curves were produced for BCG Pasteur Aeras and MTB Erdman (Supplementary Figure S4-5) as described previously [305] in order to convert TTP to bacterial count (CFU).

4.7.7 *Mycobacterium* spp. 2-thiophenecarboxylic acid hydrazide susceptibility

To confirm susceptibility of BCG Pasteur Aeras and MTB Erdman to TCH in agar plates, 100 CFU BCG Pasteur Aeras and/or 100 CFU MTB Erdman were plated on 7H11 agar plates (supplemented with OADC and glycerol) in the absence or presence of 2 µg/mL TCH (Sigma). Five-fold serial dilutions of a 2 µg/mL TCH stock (0.4, 0.08 and 0.016 µg/mL) were performed and added to supplemented MGITs. Susceptibility of BCG Pasteur Aeras and MTB Erdman to TCH in MGITs was determined by adding 100 CFU BCG Pasteur Aeras and/or 100 CFU MTB Erdman to the MGITs. Tubes were placed in the BACTEC MGIT system until registered positive. CFU input was confirmed in the absence of TCH.

4.7.8 Statistical analysis

All statistical analyses were carried out using GraphPad Prism Software version 7 (GraphPad, La Jolla, CA, United States). Data sets were found to follow Gaussian (normal) distribution using the D'Agostino-Pearson omnibus test. One-way analysis of variance (ANOVA) followed by Tukey's multiple comparison test was used to determine whether there were any statistically significant differences between groups. A p value (adjusted) of <0.05 was considered statistically significant.

4.8 Supplementary materials

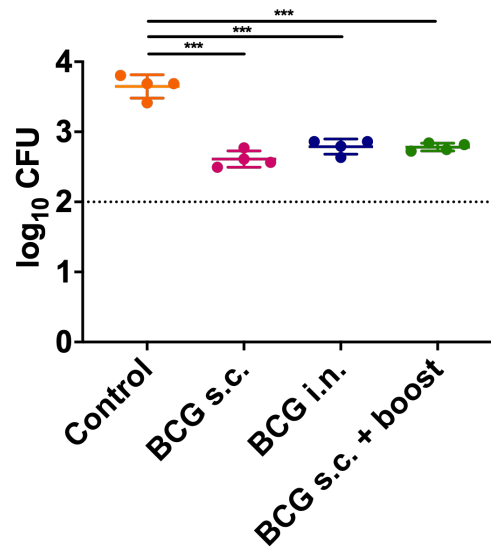


Figure S4-1. *Ex vivo* MGIA comparing BCG growth inhibition conferred by vaccination in murine splenocytes. C57BL/6 mice (n=6/group) received s.c. or i.n. BCG Pasteur Aeras at week 0, s.c. BCG Pasteur Aeras at week 0 and i.n. boosting with the candidate vaccine spore-FP1 at week 3, or received no treatment (control). At six weeks, 3×10^6 spleen cells were co-cultured with 100 CFU BCG Pasteur Aeras in 48-well plates. At 96 hours, samples were transferred to the BACTEC system until TTP values were generated. TTP values were converted to log₁₀ CFU based on a standard curve. Data points (n=4/group) represent samples generated from pooled cells isolated from six mice. Dotted line indicates mycobacterial input at day 0. Statistical significance was tested by one-way ANOVA followed by Tukey's multiple comparison test. Error bars represent mean \pm standard deviation. *** p<0.001 (adjusted). ANOVA, analysis of variance; BCG, Bacille Calmette–Guérin; CFU, colony-forming units; i.n., intranasal; MGIA, mycobacterial growth inhibition assay; s.c., subcutaneous; TTP, time to positivity.

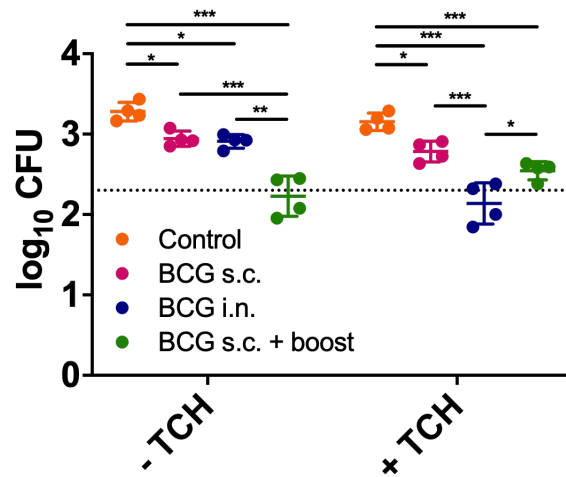


Figure S4-2. Quantification of MTB Erdman growth inhibition by plating on solid media in the optimised *ex vivo* MGIA. C57BL/6 mice (n=6/group) received s.c. or i.n. BCG Pasteur Aeras at week 0, s.c. BCG Pasteur Aeras at week 0 and i.n. boosting with the candidate vaccine spore-FP1 at week 3, or received no treatment (control). At six weeks, 1×10^6 lung cells were co-cultured with 200 CFU MTB Erdman in 48-well plates. At 96 hours, samples were plated on 7H11 agar plates and incubated at 37°C for approximately three weeks. Mycobacterial quantification was performed in the presence and absence of TCH. Data points (n=4/group) represent samples generated from pooled cells isolated from six mice. Dotted line indicates mycobacterial input at day 0. Statistical significance was tested by one-way ANOVA followed by Tukey's multiple comparison test. Error bars represent mean \pm standard deviation. * p<0.05 (adjusted); ** p<0.01 (adjusted); *** p<0.001 (adjusted). ANOVA, analysis of variance; BCG, Bacille Calmette–Guérin; CFU, colony-forming units; i.n., intranasal; MGIA, mycobacterial growth inhibition assay; s.c., subcutaneous; TCH, 2-thiophenecarboxylic acid hydrazide.

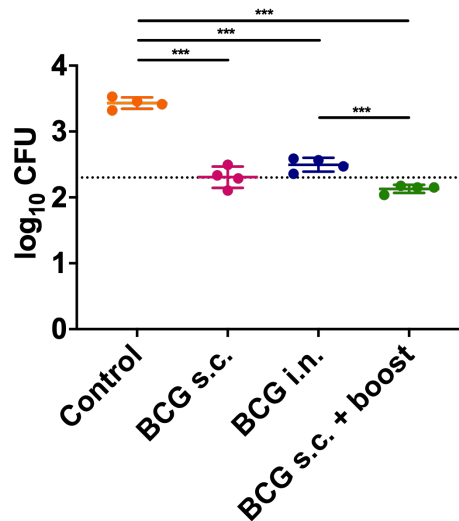


Figure S4-3. *Ex vivo* MGIA comparing MTB Erdman growth inhibition conferred by vaccination in murine splenocytes. C57BL/6 mice (n=6/group) received s.c. or i.n. BCG Pasteur Aeras at week 0, s.c. BCG Pasteur Aeras at week 0 and i.n. boosting with the candidate vaccine spore-FP1 at week 3, or received no treatment (control). At six weeks, 3×10^6 spleen cells were co-cultured with 200 CFU MTB Erdman in 48-well plates. At 96 hours, samples were transferred to the BACTEC system until TTP values were generated. TTP values were converted to log₁₀ CFU based on a standard curve. Data points (n=4/group) represent samples generated from pooled cells isolated from six mice. Dotted line indicates mycobacterial input at day 0. Statistical significance was tested by one-way ANOVA followed by Tukey's multiple comparison test. Error bars represent mean \pm standard deviation. *** p<0.001 (adjusted). ANOVA, analysis of variance; BCG, Bacille Calmette–Guérin; CFU, colony-forming units; i.n., intranasal; MGIA, mycobacterial growth inhibition assay; s.c., subcutaneous; TTP, time to positivity.

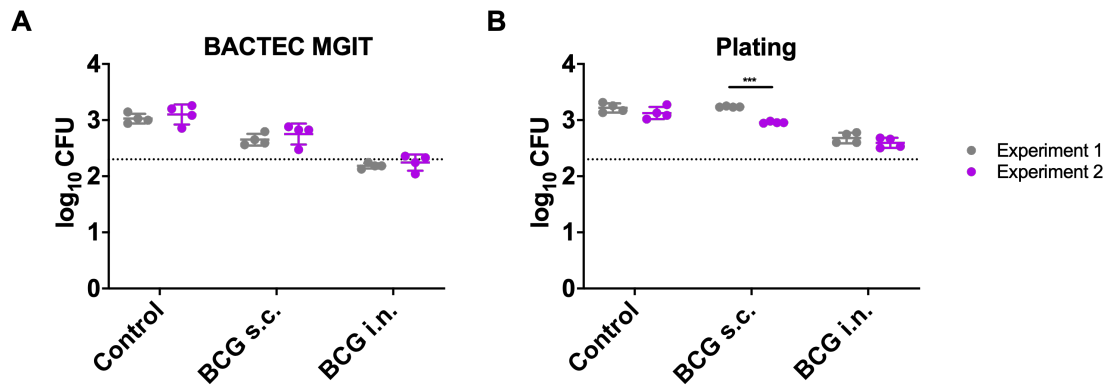


Figure S4-4. Comparison of inter-assay consistency of MTB Erdman growth inhibition between BACTEC MGIT and plating. C57BL/6 mice (n=6/group) received s.c. or i.n. BCG Pasteur Aeras at week 0 or received no treatment (control). At six weeks, 1×10^6 lung cells were co-cultured with 200 CFU MTB Erdman in 48-well plates. At 96 hours, samples were (A) transferred to the BACTEC system until TTP values were generated or (B) plated on 7H11 agar plates and incubated at 37°C for approximately three weeks. TTP values were converted to log₁₀ CFU based on a standard curve. Mycobacterial quantification was performed in the presence of TCH. Two independent assay repeats of the optimised lung MGIA (quantification by BACTEC MGIT system and plating) were performed from two separate mouse experiments. Data points (n=4/group) represent samples generated from pooled cells isolated from six mice. Dotted line indicates mycobacterial input at day 0. Statistical significance between the two experiment runs at the group level was tested by unpaired t-test. Error bars represent mean \pm standard deviation. *** p<0.001 (adjusted). BCG, Bacille Calmette–Guérin; CFU, colony-forming units; i.n., intranasal; MGIA, mycobacterial growth inhibition assay; MGIT, mycobacterial growth indicator tube; s.c., subcutaneous; TCH, 2-thiophenecarboxylic acid hydrazide; TTP, time to positivity.

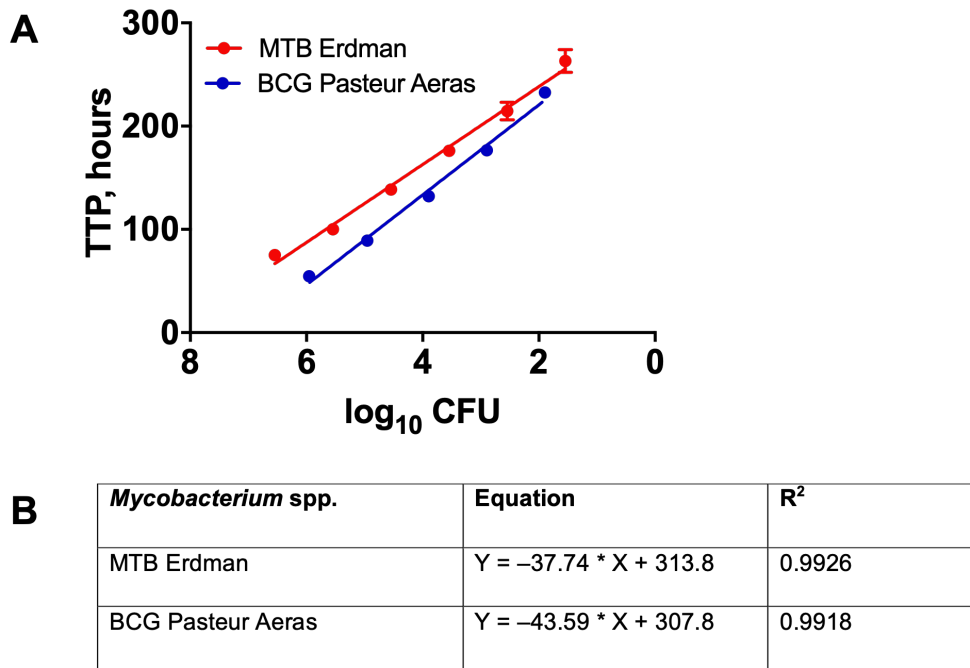


Figure S4-5. BACTEC MGIT standard curves. Serial ten-fold dilutions of MTB Erdman or BCG Pasteur Aeras were added to supplemented MGITs in duplicate to generate TTP values. Inoculum size was determined by plating the bacterial dilutions on 7H11 agar plates to calculate total CFU. (A) Total CFU was converted to log₁₀ CFU and plotted against TTP. Error bars represent mean ± standard deviation. (B) Subsequent non-linear regression analysis was performed by fitting a semi-log line. R² value indicates goodness of fit. BCG, Bacille Calmette–Guérin; CFU, colony-forming units; MGIT, mycobacterial growth indicator tube; TTP, time to positivity.

Table S4-1. MGIA intra-assay variability.

MGIA	CV, %			
	Control	BCG s.c.	BCG i.n.	BCG s.c. + boost
MTB Erdman BACTEC MGIT (100 CFU; -TCH)	7.17	3.52	0.95	–
MTB Erdman BACTEC MGIT (200 CFU; -TCH)	2.48	1.96	0.89	0.83
MTB Erdman BACTEC MGIT (200 CFU; +TCH)	2.64	2.14	0.64	0.84

C57BL/6 mice (n=6/group) received s.c. or i.n. BCG Pasteur Aeras at week 0, s.c. BCG Pasteur Aeras at week 0 and i.n. boosting with the candidate vaccine spore-FP1 at week 3, or received no treatment (control). At six weeks, 1×10^6 lung cells were co-cultured with MTB Erdman (CFU specified in rows) in 48-well plates. Four technical replicates per group were generated from pooled cells isolated from six mice. At 96 hours, samples were transferred to the BACTEC system until TTP values were generated. CV values were calculated for all groups under various MGIA conditions using raw TTP values ($CV = (\text{standard deviation}/\text{mean}) \times 100$). BCG, Bacille Calmette–Guérin; CFU, colony-forming units; CV, coefficient of variation; i.n., intranasal; MGIA, mycobacterial growth inhibition assay; MGIT, mycobacterial growth indicator tube; s.c., subcutaneous; TCH, 2-thiophenecarboxylic acid hydrazide; TTP, time to positivity.

5 Results II – The *ex vivo* murine mycobacterial growth inhibition assay as a tool to expand tuberculosis vaccine testing against representative lineages of the *Mycobacterium tuberculosis* complex

5.1 Introduction

Advances in DNA sequencing have facilitated the study of large collections of MTB clinical isolates representative of the global diversity of the MTB complex. A higher level of genetic diversity than originally considered has been found, leading researchers to reconsider the impact that this may have on the spectrum of TB infection and disease [20,23]. Furthermore, growing interest in these variations has resulted in some diversification of strains utilised in the laboratory setting, revealing differences at the transcript, protein and metabolite levels in isolates themselves [321–325,336,440], as well as the host response to infection, including in animal models of TB [303,319,329,333,334,344,441,442].

In the context of vaccine evaluation in animal models, very little progress has been made in diversification of strains, with the majority of *in vivo* MTB challenge studies using a single laboratory strain of MTB. The three most commonly used strains, Erdman, CDC1551 and H37Rv, all belong to L4 of the MTB complex and have been passaged for decades in the laboratory [23,80]. The historical reliance on the use of laboratory strains of MTB in animal models may explain, in part, why observations in these models can translate poorly into humans. As a specific example, the use of H37Rv, Erdman [178,443–446] and *M bovis* [447] in the preclinical evaluation of MVA85A was hypothesised to play a contributing role in the subsequent poor translation of vaccine

protection seen on clinical evaluation of this vaccine. Henao–Tamayo *et al* hypothesised that MVA85A boosting was observed in animal models against these laboratory strains as the window of protection afforded by BCG is modest compared with strains prevalent in the Western Cape where the vaccine was tested in humans. The authors recommended that prior to clinical evaluation in humans, vaccines should be tested against strains representative of those found at potential clinical sites [122].

Studies which have evaluated vaccine-induced protection against strains other than H37Rv, Erdman and CDC1551 have reported variations in protection against isolates representative of different lineages and sublineages of the MTB complex, indicating that incorporation of mycobacterial diversity into preclinical vaccine testing may be vital to improve translation into clinical studies [24,122,348,349,352–354].

However, key contributors to the absence of change in the preclinical pipeline relate to the ethical and financial feasibility of performing sufficiently powered *in vivo* infection studies with multiple mycobacterial strains. MTB challenge studies using single strains of MTB are already expensive, require specialised BSL-3 animal facilities, and a large number of animals on a protocol of the highest severity defined by the UK Home Office [448].

The preclinical MGIA represents a potential tool to incorporate mycobacterial diversity into the evaluation of TB vaccines. In comparison to challenge studies where one animal provides one data point per organ, each organ harvested for *ex vivo* co-culture in the MGIA provides multiple inputs for the assay, enabling samples to be tested head-to-head against multiple mycobacterial strains. Table 5-1 provides a summary of the parameters of an MGIA and MTB challenge study to evaluate two vaccines (plus unvaccinated control) against four strains of mycobacteria, to highlight the potential of

the MGIA to reduce the cost, length, severity and number of mice required to expand early evaluation of vaccine efficacy.

Table 5-1. Comparison of parameters of MGIA versus MTB challenge study for a three-group study design testing against four strains of MTB.

Parameter	MGIA	MTB challenge study
Mice, n/group	Minimum 3	8–10 per MTB strain ^a
Total mice for proposed study design, n	9	96 + 8 ^b (lower range limits used)
<i>In vivo</i> experiment duration	6 weeks ^c	6 ^c (pre-challenge) + 5 ^d (post-challenge) weeks
<i>Ex vivo</i> experiment duration	4 days	–
Time to results post-takedown	11–15 days	~3 weeks
Home Office severity limit	Moderate	Severe
BSL-3 animal research laboratory required?	No	Yes
BSL-3 microbiology research laboratory required?	Yes	Yes
Information in rows 1–5 is specific to the study design: three group design (BCG + novel candidate vaccine + unvaccinated) with four MTB strains and should be adjusted accordingly. ^a The Lamorte power calculation tool was used to approximate sample size [449]; ^b 2–3 mice per strain for confirmation of infection; ^c MGIA takedown/MTB infection timepoint defined by vaccine-specific immune response peak; ^d duration of infection should be adjusted for factors such as CFU of infection dose, mouse strain and mycobacterial strain virulence, and be based on defined humane end points. BCG, Bacille Calmette–Guérin; BSL-3, biosafety level-3; CFU, colony-forming units; MGIA, mycobacterial growth inhibition assay; MTB, <i>Mycobacterium tuberculosis</i> .		

Focusing on murine MGIA, both lung (Chapter 4) [429] and spleen [306] assays have been developed, and may be representative of vaccine-induced immunity at the lung mucosa and systemically. In the spleen MGIA, vaccine-mediated mycobacterial growth inhibition has been shown to correlate with protection in *in vivo* MTB challenge in a number of studies [201,299,306,307]. A direct comparison of the lung MGIA with MTB challenge has not been performed, however, observations made in the MGIA with respect to growth inhibition correlate at the group level with published *in vivo* studies [429].

Only two studies, dating back more than 30 years, have used clinical isolates in murine MGIA [268,302], with the vast majority of studies to date using a single, often laboratory, strain of mycobacteria. In light of growing interest in the genetic diversity of the MTB complex and variations in the host response to infection, the murine lung and spleen MGIA represent a potential tool to diversify the readout feasibly obtained from MTB challenge studies. To the best of our knowledge, the suitability of the simplified murine MGIA to test vaccines against multiple mycobacterial strains has not been determined.

Where mycobacterial diversity is introduced into preclinical studies, reproducibility is an important consideration. Studies which have included multiple mycobacterial strains to date generally suffer from a lack of standardisation. Many of these studies utilised poorly characterised and/or research-group-specific sets of clinical isolates. MTB complex reference sets, such as the Gagneux set of 20 clinical strains (deposited in the Belgian Coordinated Collections of Microorganisms), represent an important tool to the TB research community. The reference set is made up of multiple sequenced clinical isolates representative of seven lineages of the MTB complex (L1–7). Within each lineage, representatives of various sublineages are included. Use of publicly available, well-characterised reference sets such as the Gagneux set enables incorporation

of the diversity of the MTB complex into studies in a standardised manner, facilitating future comparison with other research findings which is otherwise challenging to perform using research-group-specific clinical isolates [23].

In this chapter, the murine MGIA is used to test TB vaccines against four lineages of the MTB complex. The performance of the assay is further investigated by performing a head-to-head comparison of the MGIA and an MTB challenge study using clinical isolates representative of two lineages.

The generation of a platform able to test vaccines head-to-head against a well-characterised set of MTB clinical isolates represents an important tool to improve and inform the design of downstream MTB challenge studies. By gaining early insight into the performance of vaccine candidates against a diverse set of mycobacterial species, outputs from challenge studies may better represent the clinical setting and potentially aid selection of clinical sites at later stages of vaccine development.

5.2 Aims and objectives

Aims

- Expand the capacity of the murine MGIA to evaluate vaccine-induced mycobacterial growth inhibition beyond a single laboratory strain of MTB through the utilisation of multiple MTB clinical isolates.
- Determine whether mycobacterial growth inhibition in the MGIA is a representative readout of protection in the lung and spleen following *in vivo* infection with clinical isolates of MTB.

Objectives

- Evaluate the reproducibility of vaccine-mediated mycobacterial growth inhibition in the MGIA using clinical isolates representative of four lineages of the MTB complex.
- Perform head-to-head comparison of the lung and spleen MGIA with the *in vivo* challenge study using clinical isolates.

5.3 Materials and methods

Materials and methods for the experiments described in this chapter are outlined in full in Chapter 3.

5.4 Results

5.4.1 Vaccine-mediated growth inhibition of MTB complex clinical isolates in *ex vivo* lung cell culture

Vaccine-mediated growth inhibition of the laboratory MTB Erdman strain by murine lung cells has been previously demonstrated by MGIA [429]. To determine whether the lung MGIA could be expanded to explore potential differences in vaccine-mediated growth inhibition beyond a single laboratory strain of MTB, four clinical isolates (N0072, N0052, N0054 and N1283), representative of L1–4 of the MTB complex, were selected from a well-characterised reference set [23]. Frozen stocks of each isolate were established for downstream use and the sensitivity of each isolate to TCH was assessed (Figure 5-1).

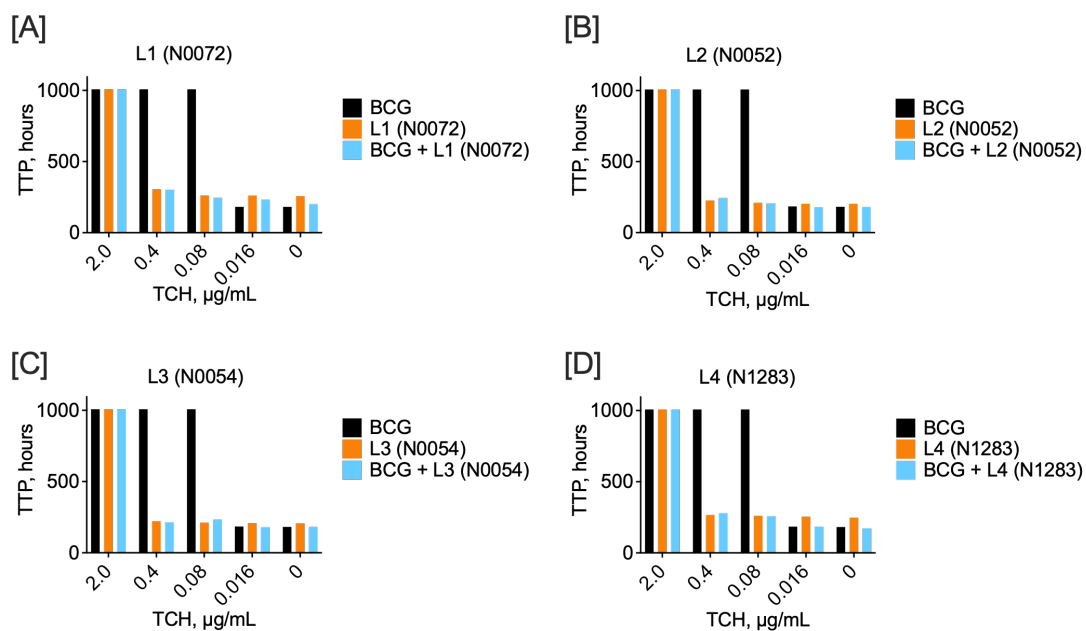


Figure 5-1. TCH susceptibility of clinical isolates. Susceptibility to the BCG inhibitor, TCH, was determined for [A] L1 (N0072), [B] L2 (N0052), [C] L3 (N0054) and [D] L4 (N1283) at a final concentration of 2, 0.4, 0.08 and 0.016 µg/mL in MGITs. Either 100 CFU BCG PA or clinical isolate, or 100 CFU BCG PA and 100 CFU clinical isolate were added to MGITs in the absence or presence of TCH to determine the optimal concentration of TCH to inhibit BCG growth only (n=1/condition) in the BACTEC system. A TTP value of 1,008 hours (42 days) indicates a negative result (no bacteria detected). BCG, Bacille Calmette–Guérin; CFU, colony-forming units; L, lineage; MGIT, mycobacterial growth indicator tube; PA, Pasteur Aeras; TCH, 2-thiophenecarboxylic acid hydrazide; TTP, time to positivity.

Standard curves were generated for each isolate to enable experimental TTP values to be converted to CFU. The results of non-linear regression analysis and generated standard curves are presented in Table 5-2 and Figure 5-2.

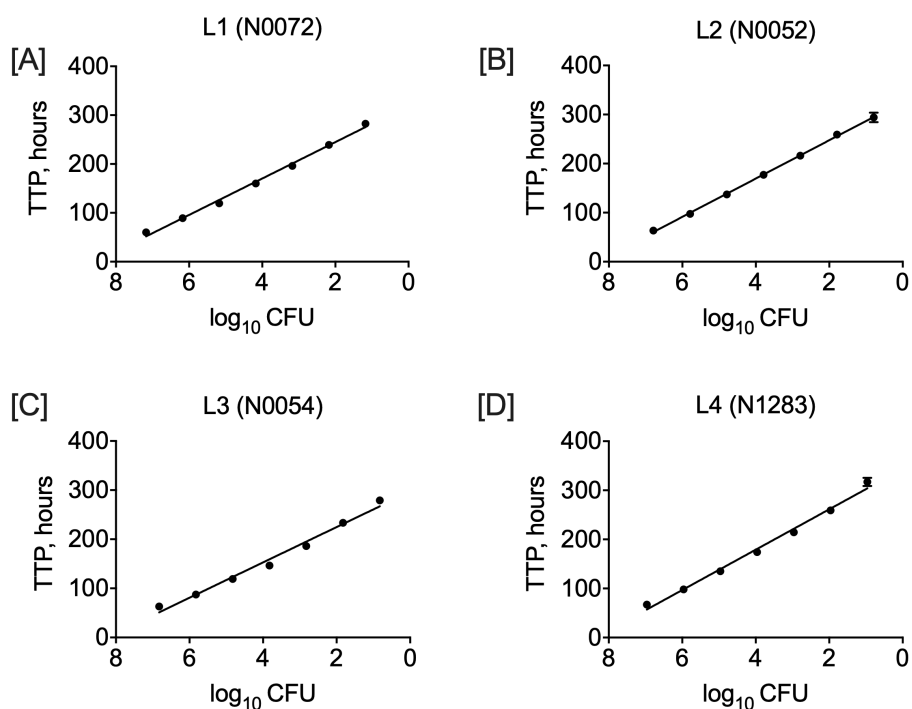


Figure 5-2. MTB complex clinical isolate BACTEC MGIT standard curves. Serial ten-fold dilutions of the clinical isolates were added to supplemented MGITs in duplicate to generate TTP values. Inoculum size was determined by plating the bacterial dilutions on 7H11 agar plates to calculate total CFU. Total CFU was converted to log₁₀ CFU and plotted against TTP. Standard curves are shown for [A] L1 (N0072), [B] L2 (N0052), [C] L3 (N0054) and [D] L4 (N1283). Error bars represent mean ± standard deviation. CFU, colony-forming units; L, lineage; MGIT, mycobacterial growth indicator tube; MTB, *Mycobacterium tuberculosis*; TTP, time to positivity.

Table 5-2. MTB complex clinical isolate non-linear regression analysis.

<i>Mycobacterium</i> spp.	Equation	R ²
L1 (N0072)	$Y = -37.29 * X + 319.4$	0.9948
L2 (N0052)	$Y = -39.05 * X + 325.8$	0.9993
L3 (N0054)	$Y = -35.96 * X + 296.7$	0.9851
L4 (N1283)	$Y = -41.13 * X + 343.6$	0.9917
R ² value indicates goodness of fit. L, lineage; MTB, <i>Mycobacterium tuberculosis</i> .		

C57BL/6 mice (six per group) were vaccinated with BCG PA via the s.c. or i.n. route, BCG Danish s.c., or received no treatment. At six weeks, lungs were harvested, enzymatically digested and homogenised to generate a single cell suspension. Next, 1×10^6 lung cells from one pool of cells generated for each group were co-cultured with 200 CFU L1 (N0072), L2 (N0052), L3 (N0054) or L4 (N1283) in 48-well plates. At 96 hours, cells were lysed and samples transferred to the BACTEC MGIT system until TTP values were generated.

When performing MGIA with a single strain of mycobacteria, data are most commonly presented as \log_{10} CFU. However, Zelmer *et al* recommend that when comparing more than one experiment, and in this case more than one strain of mycobacteria, normalisation should be performed to improve comparison. This can be done by a number of different methods: i) \log_{10} (sample CFU / D2M (mycobacteria) CFU) to generate a 'growth ratio' [263,305]; ii) mean (control group \log_{10} CFU) – \log_{10} CFU individual immunised samples [308]; or iii) sample \log_{10} CFU – D2M (mycobacteria) \log_{10} CFU [308]. Data in this chapter were normalised using method iii.

Under the conditions outlined for the lung MGIA using MTB Erdman [429], consistent levels of growth inhibition of modern (L2–4) lineages of the MTB complex were observed across two experimental repeats when comparing lung cells from BCG PA s.c. animals and the unvaccinated group (Figure 5-3). Specifically, L2 (N0052) growth was reduced by $\sim 0.46 \log_{10}$ CFU in the BCG s.c. group ($p < 0.01$); no significant difference in growth of L3 (N0054) was found between the two groups; L4 (N1283) growth was reduced by $\sim 0.33 \log_{10}$ CFU in the BCG s.c. group ($p < 0.01$). For ancient L1 (N0072), inconsistent levels of mycobacterial growth in co-culture with BCG s.c. lung cells were observed. In experiment 1, a $0.49 \log_{10}$ CFU reduction in L1 (N0072) was found

($p=0.011$); by contrast, no significant difference in mycobacterial growth was found in experiment 2.

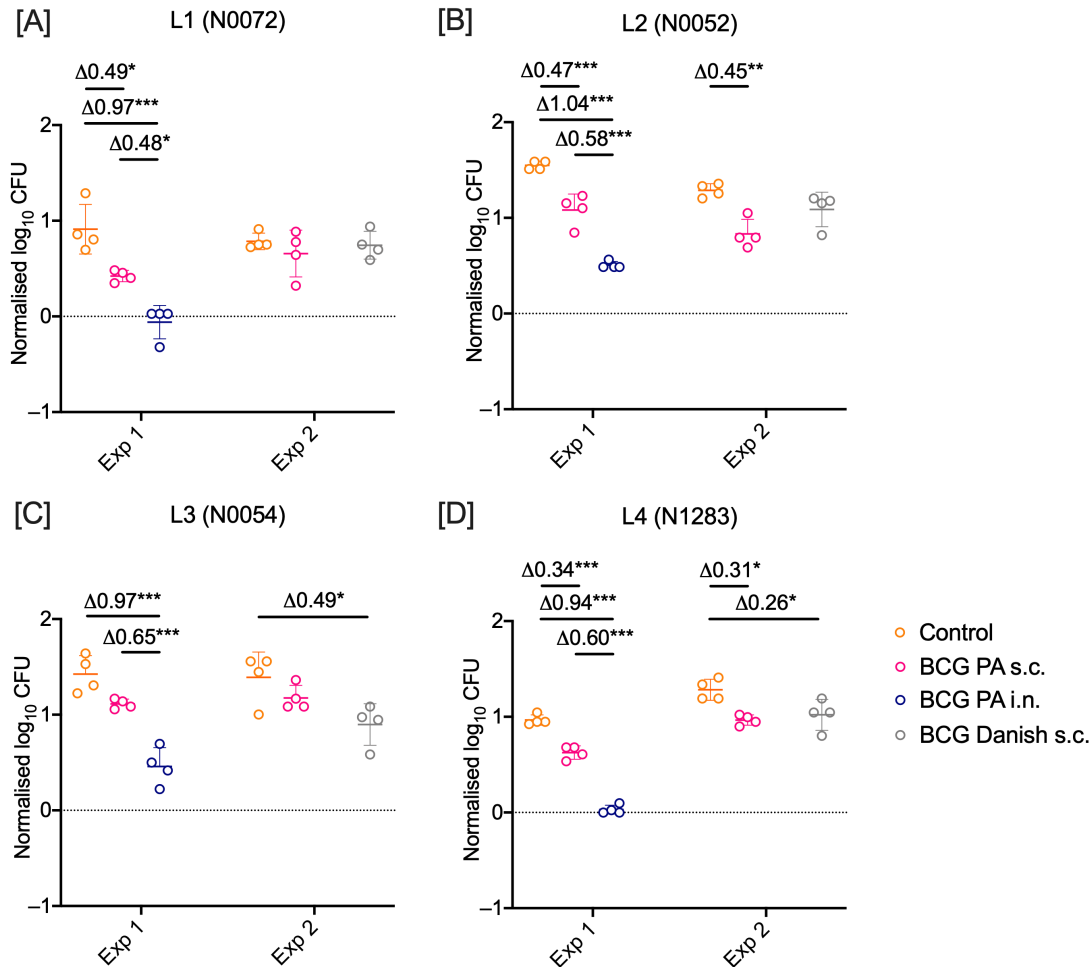


Figure 5-3. Growth inhibition of L1–4 by BCG-vaccinated murine lung cells versus unvaccinated control. C57BL/6 mice ($n = 6/\text{group}$) in experiment 1 received s.c. or i.n. BCG PA at week 0 or no treatment (control). C57BL/6 mice ($n = 6/\text{group}$) in experiment 2 received s.c. BCG PA or BCG Danish at week 0 or no treatment (control). At six weeks, lung cells were co-cultured with 200 CFU [A] N0072, [B] N0052, [C] N0054 or [D] N1283 clinical isolate. At 96 hours, samples were lysed and transferred to the BACTEC system until TTP values were generated. TTP values were converted to log₁₀ CFU based on a clinical-isolate-specific standard curve. Normalisation of each MGIA was performed by subtracting the log₁₀ CFU value obtained for the specific mycobacterial input D2M tube from all log₁₀ CFU data points. Data points ($n = 4/\text{group}$) represent samples generated from pooled cells isolated from six mice. Statistical significance was

tested by one-way ANOVA followed by Tukey's multiple comparison test. Error bars represent mean \pm standard deviation. * $p < 0.05$ (adjusted); ** $p < 0.01$ (adjusted); *** $p < 0.001$ (adjusted). ANOVA, analysis of variance; BCG, Bacille Calmette–Guérin; CFU, colony-forming units; D2M, direct-to-MGIT; exp, experiment; i.n., intranasal; L, lineage; MGIA, mycobacterial growth inhibition assay; PA, Pasteur Aeras; s.c., subcutaneous; SSI, Statens Serum Institute; TTP, time to positivity.

In experiment 1, an $\sim 1 \log_{10}$ CFU reduction in mycobacterial growth of all four lineages (Figure 5-3) was observed following co-culture with lung cells from BCG PA i.n. mice compared with unvaccinated mice ($p < 0.001$). TCH, a BCG inhibitor, was used across the assay to prevent quantification of residual BCG from i.n. vaccination.

In experiment 2, the ability of lung cells from BCG Danish s.c. vaccinated mice to inhibit growth of L1–4 in co-culture was also tested. Lung cells from BCG Danish vaccinated mice inhibited growth of L3 (N0054) and L4 (N1283) by 0.49 ($p = 0.023$) and 0.26 ($p = 0.028$) \log_{10} CFU respectively, compared with unvaccinated (Figure 5-3). Growth of L1 (N0072) and L2 (N0052) was unchanged.

Intra-assay variability was determined by calculating the coefficient of variability (CV): (standard deviation/mean) $\times 100$. CV quantifies the spread of data within each experimental group. CV ranged between 0.71 and 5.06% across the lineage MGIA in the two experiments; however, a high/low level of variability was not associated with a specific lineage (Table 5-3).

Table 5-3. MGIA intra-assay variability.

Experiment	Lineage	CV, %			
		Control	BCG PA s.c.	BCG PA i.n.	BCG Danish s.c.
1	1 (N0072)	4.62	0.98	2.65	–
	2 (N0052)	1.01	3.43	0.71	–
	3 (N0054)	3.86	0.96	3.29	–
	4 (N1283)	1.09	1.32	0.78	–
2	1 (N0072)	1.51	4.21	–	2.55
	2 (N0052)	1.50	2.96	–	3.68
	3 (N0054)	5.06	2.40	–	3.79
	4 (N1283)	2.35	1.09	–	3.28
3	1 (N0072)	1.90	4.74	–	–
	2 (N0052)	2.15	1.15	–	–

C57BL/6 mice (n=6/group) received s.c. or i.n. BCG (PA or Danish) at week 0, or received no treatment (control). At six weeks, lung cells were co-cultured with mycobacteria in 48-well plates. Four technical replicates per group were generated from pooled cells isolated from six mice. At 96 hours, samples were transferred to the BACTEC system until TTP values were generated. CV values were calculated using raw TTP values ($CV = (\text{standard deviation}/\text{mean}) \times 100$). BCG, Bacille Calmette–Guérin; CV, coefficient of variation; i.n., intranasal; MGIA, mycobacterial growth inhibition assay; MGIT, mycobacterial growth indicator tube; L, lineage; PA, Pasteur Aeras; s.c., subcutaneous; TTP, time to positivity.

5.4.2 Head-to-head comparison of the murine *ex vivo* MGIA with *in vivo* MTB infection

To determine how the growth inhibition readout from the lung and spleen MGIA compares with bacterial burden following *in vivo* infection with MTB clinical isolates, an MGIA and MTB challenge study were performed in tandem using an ancient (L1 N0072) and modern (L2 N0052) lineage of the MTB complex. L1 (N0072) was selected as inconsistent results had been obtained in the MGIA; by contrast, consistent results across two experiments were found for L2 (N0052). In addition, we were keen to test performance of the MGIA using an ancient and modern lineage of the MTB complex.

Figure 5-4A depicts an overview of this analysis. Briefly, C57BL/6 mice received BCG s.c. or no vaccine (n=23/group) and were rested for six weeks. For mice in the MGIA arm of the study (n=3/group), animals were sacrificed, and single cell suspensions were generated from the lung and spleen for co-culture with 200 CFU L1 (N0072) or L2 (N0052) for 96 hours. CFU at 96 hours was quantified using the BACTEC MGIT system.

Growth of L1 (N0072) was not found to be significantly different in spleen or lung cells from BCG-vaccinated compared with unvaccinated animals (Figure 5-4C and D). A significant reduction in growth of L2 (N0052) was observed in co-cultures with lung ($0.42 \log_{10}$ CFU, $p=0.0010$) and spleen ($0.27 \log_{10}$ CFU, $p=0.0025$) cells from BCG-vaccinated compared with unvaccinated animals (Figure 5-4E and F). Growth inhibition of L2 (N0052) by lung cells from BCG s.c. animals was consistent with that observed in experiments 1 and 2.

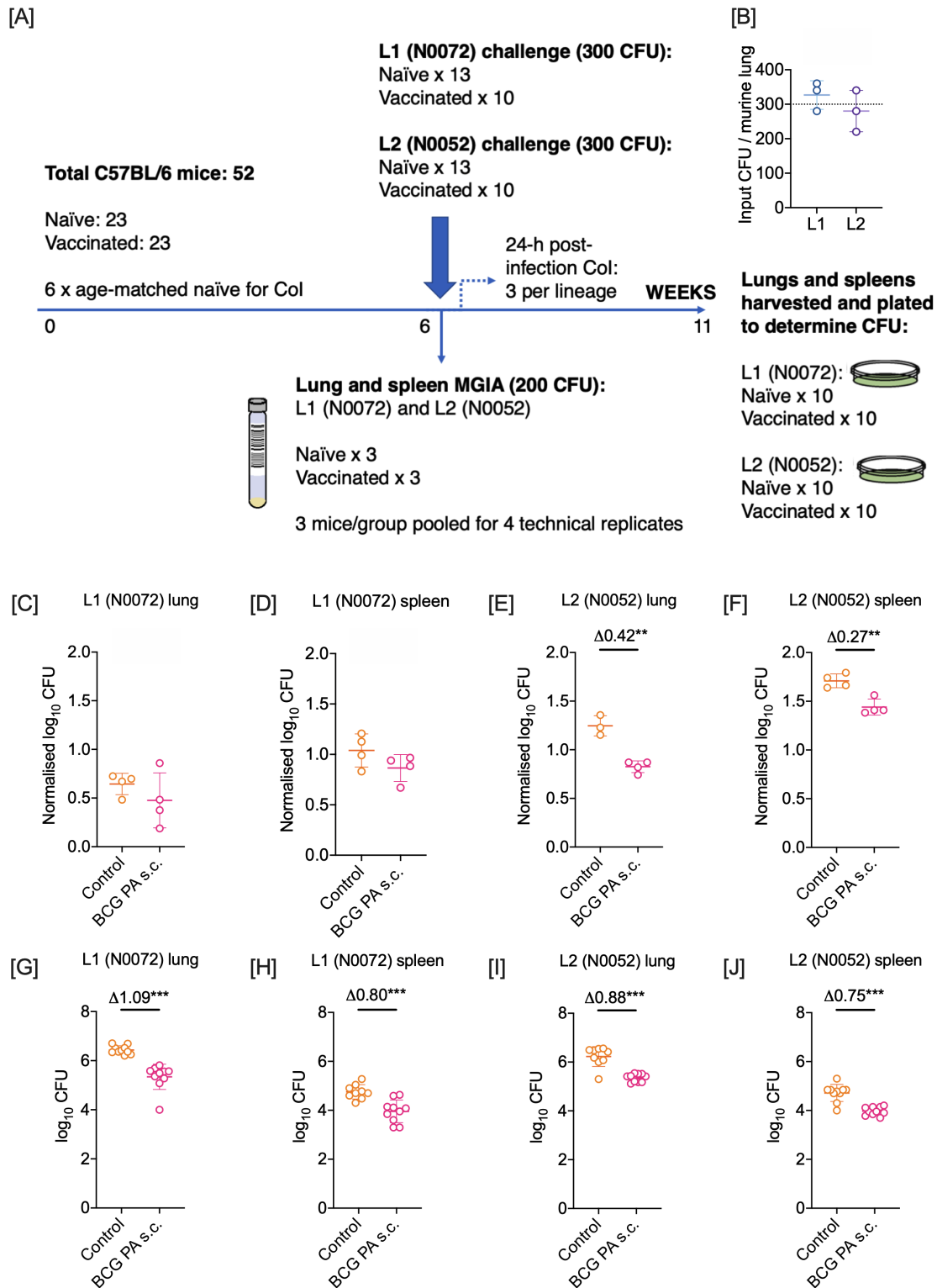


Figure 5-4. Head-to-head comparison of MGIA and MTB challenge study.

[A] Visualisation of MGIA and MTB challenge study design, including number of animals per group. C57BL/6 mice received s.c. BCG PA at week 0 or no treatment (control). [C–F] For mice in the MGIA arm of the study, lungs and spleens were harvested at six weeks from three mice per group, processed to single cell suspensions and co-

cultured with 200 CFU L1 (N0072) or L2 (N0052). At 96 hours, samples were lysed and transferred to the BACTEC system until TTP values were generated. TTP values were converted to \log_{10} CFU based on a clinical-isolate-specific standard curve. Normalisation was performed by subtracting the \log_{10} CFU value obtained for the specific mycobacterial input D2M tube from all \log_{10} CFU data points. Data points (n = 4/group) represent samples generated from pooled cells isolated from three mice. [G–J] At the same six-week time point, mice in the MTB challenge arm were i.n. infected with 300 CFU L1 (N0072) or L2 (N0052). CFU per organ was determined five-weeks post-infection in the lung and spleen (n=9–10/group). [B] Age-matched naïve C57BL/6 mice were i.n. infected with 300 CFU L1 (N0072) or L2 (N0052). CFU per organ was determined 24-hours post-infection in the lung. Each data point represents an individual animal. For both datasets, statistical significance was tested by unpaired t test. Error bars represent mean \pm standard deviation. ** p < 0.01; *** p < 0.001. BCG, Bacille Calmette–Guérin; CFU, colony-forming units; CoI, confirmation of infection; D2M, direct-to-MGIT; i.n., intranasal; L, lineage; MGIA, mycobacterial growth inhibition assay; ns, not significant; PA, Pasteur Aeras; s.c., subcutaneous; TTP, time to positivity.

Animals in the MTB challenge arm were i.n. infected six-weeks post vaccination with 300 CFU L1 (N0072) or L2 (N0052) (each lineage: n=9–10/group + n=3 naïve age-matched controls). At 24-hours post-infection no significant difference in mycobacterial load between L1 (N0072) and L2 (N0052) was identified in the lung, indicating that both groups received a similar inoculum (~300 CFU) of mycobacteria (Figure 5-4B). Five-weeks post-infection, CFU was determined in the lung and spleen. Compared with unvaccinated animals, a significant reduction in L1 (N0072) and L2 (N0052) bacterial burden was observed in the lung and spleen of BCG-vaccinated animals (Figure 5-4G–J): L1 (N0072) lung, 1.09 \log_{10} CFU, p<0.0001; L1 (N0072) spleen, 0.80 \log_{10} CFU, p=0.0004; L2 (N0052) lung, 0.88 \log_{10} CFU, p<0.0001; L2 (N0052) spleen, 0.75 \log_{10} CFU, p<0.0001).

5.4.3 *Ex vivo* growth of ancient L1 (N0072) in unvaccinated murine lung cells in the MGIA is lower compared with L2

Figure 5-5A depicts data from control animals from Figure 5-3 and Figure 5-4 to demonstrate differences in *ex vivo* mycobacterial growth observed in culture with unvaccinated murine lungs at 96 hours by L1 (N0072) and L2 (N0052).

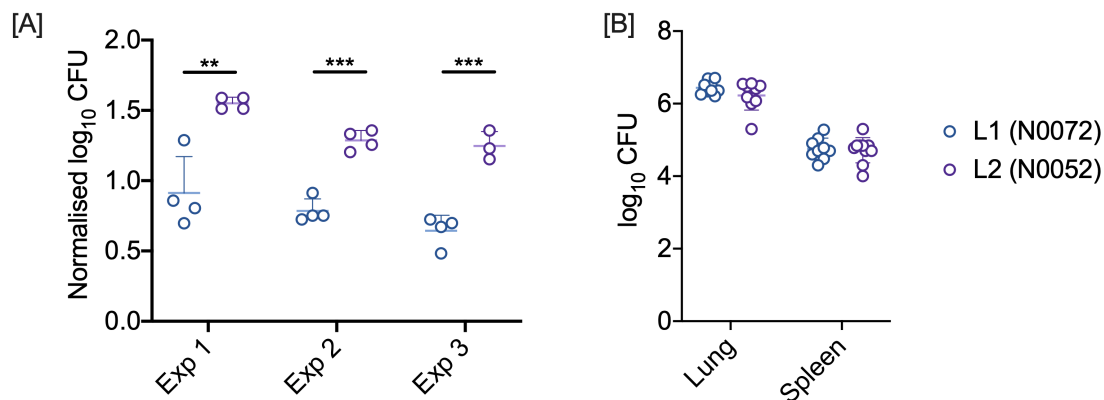


Figure 5-5. Mycobacterial growth in control murine lung cells. [A] Normalised log₁₀ CFU values across the three experimental repeats shown to visualise mycobacterial growth of L1 (N0072) and L2 (N0052) at 96 hours in unvaccinated (control) murine lung cells in the MGIA. Mycobacterial input was 200 CFU mycobacteria. Normalisation was performed by subtracting the log₁₀ CFU value obtained for the specific mycobacterial input D2M tube from all log₁₀ CFU data points. [B] log₁₀ CFU in the unvaccinated murine lung and spleen five weeks following *in vivo* i.n. infection with L1 (N0072) or L2 (N0052). Statistical significance was tested by unpaired t test. Error bars represent mean ± standard deviation. ** p < 0.01; *** p < 0.001. CFU, colony-forming units; D2M, direct-to-MGIT; i.n., intranasal; L, lineage; MGIA, mycobacterial growth inhibition.

Despite using a mycobacterial input of 200 CFU for both lineages at assay set up, a significantly lower level of L1 growth following *ex vivo* co-culture was observed in all three experimental repeats of the MGIA. By contrast, in the *in vivo* MTB challenge study in which animals were i.n. infected with 300 CFU L1 or L2, bacterial burden at five weeks

post-challenge was not found to be different between lineages in the lung or spleen (Figure 5-5B).

5.5 Discussion

There is growing interest in the expansion of TB vaccine testing beyond standard laboratory strains of MTB, with the recommendation that preclinical evaluation should be performed against multiple strains of MTB representative of the global diversity of this pathogen. Currently, limited resources within the TB research field, and an emphasis on reducing, refining and replacing animal techniques, render the traditional MTB challenge study an unsuitable tool to routinely generate a sufficiently powered readout of this size.

The preclinical MGIA was developed as an ‘*ex vivo* challenge model’ to facilitate evaluation of TB vaccines. The assay uses mycobacterial growth inhibition as a surrogate readout of protection against TB, representing a complementary tool to MTB challenge studies. Murine MGIA has been established for use with murine splenocytes [306] and lung cells (Chapter 4) using laboratory strains of MTB. Mycobacterial growth inhibition by spleen cells harvested from vaccinated mice has been directly compared, and shown to correlate, with vaccine-induced protection against *in vivo* MTB challenge in the lung and spleen. To date, growth inhibition observed in lung cells from vaccinated mice has been compared only with published MTB challenge studies; a side-by-side comparison of the two methods has not been performed. In its current design, the readout of the MGIA has been compared previously with bacterial burden 4–6 weeks post-challenge [306,308]. To the best of our knowledge, use of non-laboratory strains in the murine MGIA has been limited [268,302], with no study performing head-to-head comparison of more than one strain.

In this chapter, four clinical isolates from a well characterised MTB complex reference set were used in the lung MGIA. MTB isolates representative of L1–4 of the MTB complex were selected and included one ancient (L1 [N0072]) and three modern (L2–4 [N0052, N0054 and N1283]) strains. The L2 isolate selected for this project was a Beijing sub-strain (L2.2) of the lineage [450]. Three BCG vaccine regimens were tested in the MGIA – BCG PA s.c., BCG PA i.n. and BCG Danish s.c. – with a focus on BCG PA s.c. downstream.

Data for modern strains were reproducible across two experimental repeats for BCG PA s.c., with a significant reduction in growth inhibition of L2 and L4 observed in vaccinated lung cells compared with control. The ability of BCG s.c. lung cells to regulate growth of the ancient strain, L1, was inconsistent across the two studies (Figure 5-3).

Studies in which animal models are infected *in vivo* with strains representative of MTB lineages 1–4 have been performed. However, to date, the evaluation of TB vaccines against non-laboratory strains has focused on the modern lineages of the MTB complex following administration of BCG via the s.c. or i.d. route. Beijing strains are the most frequently tested. It is common for ‘representatives’ of L4 to be MTB Erdman or H37Rv. Vaccination with BCG Danish and Pasteur has been demonstrated to provide protection against these strains at 4–6 weeks post-infection in murine studies [24,306,349]. An analysis of BCG-induced protection against L1 strains has not been identified in the literature.

A number of studies have performed *in vivo* murine MTB challenge studies with L2 clinical isolates [24,122,349,353,354,451] using BCG Pasteur. BCG Danish has not been tested against L2. Consistent with our own observations using the MGIA, bacterial burden in the lung and spleen has been found to be significantly lower than controls at 4–5 weeks following challenge with various Beijing strains in mice vaccinated with BCG

Pasteur in a number of studies [24,122,349,353,451]. By contrast, in an analysis by Levillain *et al* BCG Pasteur provided protection in mice six weeks post-challenge with MTB M2, a L4 strain; however, no protection was found against HN878, a highly virulent L2 Beijing strain [354].

In a study by Perez *et al* [24], live attenuated TB vaccines, as well as BCG Pasteur, were evaluated four weeks post-challenge with W4 (L2), HCU3524 (L3) or H37Rv (L4) in the mouse model. The highest reduction in bacterial burden in the lung and spleen of BCG-vaccinated animals was found following infection with W4 (L2). The most conservative reduction was observed in mice infected with HCU3524 (L3). The low level of protection afforded by BCG against L3, may be consistent with the absence of growth inhibition observed in the MGIA between the control and BCG-vaccinated groups in the current study.

To determine whether growth inhibition observed in the lung MGIA is an accurate readout of protection observed in challenge studies, two clinical isolates were selected for analysis in a head-to-head comparison of performance of the MGIA versus that of MTB challenge. Comparison of all four lineages was not performed due to study costs, the capacity of the animal facility and size of the research group.

Compared with unvaccinated animals, a robust reduction in L1 and L2 bacterial burden five weeks post-infection was found in the lungs and spleens of vaccinated animals. Growth inhibition of L2 in the MGIA by BCG-vaccinated murine cells was observed and correlated with *in vivo* protection against L2. Growth inhibition of L1 in the MGIA was not observed, inconsistent with *in vivo* observations using this lineage. It was noted that the bacterial burden of L1 and L2 in the lungs and spleens of control animals five weeks post-infection was not significantly different. By contrast, in the *ex vivo* MGIA, L1 CFU following 96 hours of co-culture with control murine cells was significantly

lower than L2, indicating that the growth conditions afforded by the current MGIA protocol may not be conducive for growth of L1.

The importance of experimental standardisation when using clinical isolates to account for the inherent differences in growth rates is emphasised by Coscolla and Gagneux [452]. Variations in the growth rate of MTB lineages *in vitro* and *ex vivo* have been reported previously [26,333,342,441,453–455]. Focusing specifically on L1 and L2, a lower replication rate of L1 isolates compared with modern lineages was observed in human PBMC-derived and alveolar macrophages [26,333] consistent with behaviour observed in the MGIA in this study. The *ex vivo* MGIA is a simplified model of the *in vivo* mouse lung and is not able to replicate recruitment of immune responses outside of the spleen or lung in response to infection. Further, processing of murine cells for *ex vivo* culture may impact the viability of specific immune cell populations. It is possible that the MGIA in its current form, and the immune cell population used in the assay, may be suitable for testing modern, but not ancient lineages of the MTB complex, with immune cell populations required to effectively model infection and BCG-mediated protection against L1 absent from the system.

In the murine aerosol infection model, reports on the *in vivo* growth rate of L1 compared with modern strains are conflicting and are likely, in part, to reflect diversity at the sub-lineage level. Strains of varying susceptibility have been utilised across these studies. In agreement with their own observations in human macrophages *in vitro*, Reiling *et al* report a reduced growth rate *in vivo* in the lungs of DBA/2 mice for L1 compared with modern strains at 3- and 12-weeks post-infection [333]. This observation is inconsistent with the current study where a reduced growth rate was only seen *ex vivo*. By contrast, at 2-weeks post-infection, Krishnan *et al* observed a significantly lower lung

and spleen bacterial burden in BALB/c mice following i.n. infection with L1 compared with L2; however, at later time points (7 and 14 weeks) this difference was not seen [441].

L2 is made up of two sublineages, L2.1 (proto-Beijing) and L2.2 (Beijing), with the latter sublineage further categorised into different strains referred to as ancient or modern Beijing strains [456,457]. Hypervirulent phenotypes have been observed in humans and animal models within the Beijing strains [432]. A study by Ribeiro *et al* in which bacterial burden was determined in the lungs of C57BL/6 mice 28 days following i.t. infection with 100 CFU of six sublineages of L2 (three modern, three ancient Beijing strains) provides an example of the range of virulence found with strains of L2. Bacterial load ranged from $6-8 \log_{10}$ CFU, with ancient Beijing strains associated with lower CFU.

The disparities outlined in *in vivo* infection studies and vaccine studies to date are likely to be a reflection of the diversity of the lineages and sublineages of the MTB complex and emphasise the importance of analysis platforms able to incorporate this diversity in a standardised manner. As well as providing insight into *in vivo* variations in L2 versus L1 growth described above, these observations emphasise that the evaluation of TB vaccines using multiple non-laboratory strains may need to extend further than single representative isolates of lineages in some instances. It also highlights the importance of incorporating a standardised reference set of clinical isolates into the MGIA to improve reproducibility.

5.5.1 Limitations and future studies

We hypothesise that where *ex vivo* growth of MTB is unrepresentative of *in vivo* behaviour, such as that observed with L1, the MGIA does not accurately model BCG-mediated protection. We propose a number of future studies to improve understanding of this observation: i) increased CFU input at co-culture set up; ii) use of log-phase stocks

at co-culture set-up [344]; iii) use of another L1 clinical isolate in the MGIA and MTB challenge study to determine whether this observation is specific to this isolate or to the lineage itself; iv) extension of the MGIA co-culture period and time course analysis to determine whether growth inhibition is observed beyond 96 hours; and v) phenotypic analysis of cells infected with L1 and L2.

We were not able to investigate MGIA results for BCG PA i.n. or BCG Danish s.c. further in this study. Following clarification and potential optimisation of the MGIA for use with L1 isolates, validation of these observations may further demonstrate the value of the MGIA for the informed expansion of preclinical TB vaccine testing. Future studies should also incorporate other ancient members of the MTB complex such as MAF.

5.5.2 Conclusions

As it stands, we have shown reproducible MGIA readouts for isolates representative of the modern lineages (L2–4) of the MTB complex. Data indicate that growth inhibition in the lung and spleen MGIA could be used as a surrogate readout of protection in MTB challenge studies using L2 of the MTB complex. At present, the MGIA does not accurately model the protection afforded by BCG against infection with ancient L1 in the mouse model. Inconsistencies in results were not only observed in the head-to-head comparison of MGIA and challenge, but also between three experimental repeats of L1 using the lung MGIA developed in Chapter 4.

The generation of a platform which is able to provide an accurate preclinical assessment of vaccine performance against strains representatives of the global diversity of the MTB complex, may represent an invaluable tool to streamline the design of MTB challenge studies, as well as guide clinical trial site selection.

6 Results III – The biology of growth inhibition in the MGIA

6.1 Introduction

TB is highly complex and reliable CoPs against TB have not been identified to date. An unbiased systems biology approach to CoP identification, rather than a study design in which immune targets of interest are preselected such as multi-colour flow cytometry, may aid identification of novel CoPs to facilitate and expediate vaccine evaluation. Novel CoP must be defined in placebo-controlled clinical vaccine trials with a disease endpoint [198]; however preclinical studies using animal models of TB may represent an important tool for early exploration of potential CoP associated with TB vaccines and validation of novel CoP identified in humans.

In Chapters 4 and 5 the murine lung MGIA was optimised and subsequently used to evaluate vaccine-induced protection against multiple MTB lineages. The *ex vivo* MGIA represents a platform to expand the current readout of vaccine performance in a more financially and ethically viable manner than can currently be achieved using *in vivo* MTB challenge. As described, the *ex vivo* nature of the MGIA enables a considerable reduction in the number of mice required during the evaluation of vaccine performance, which subsequently enables expansion of testing against a larger panel of vaccines and/or beyond a single strain of mycobacteria. Vaccine evaluation may be expanded further by performing the MGIA in tandem with high-throughput unbiased methods, such as RNA-seq, able to generate insight into the biological mechanisms associated with observations in the MGIA.

An unbiased preclinical readout of the biological mechanisms behind vaccine-induced growth inhibition, and whether mechanisms vary by mycobacterial strain, may

help expand downstream readouts of immunogenicity beyond the parameters currently utilised. To the best of our knowledge, the incorporation of an unbiased whole-genome approach when evaluating TB vaccines in preclinical animal models *in vivo* has been limited to date [98,108,145,418,458], particularly in the mouse model. Considering the cost of *in vivo* studies, it is unsurprising that no evidence of expansion beyond use of a single laboratory MTB strain in studies which incorporate a systems biology approach has been found. Orme and Henao-Tamayo emphasise that our understanding of memory immunity to TB is complicated further by the notion that different types of vaccines may mediate protection by different methods [459], highlighting the importance of early elucidation of mechanisms associated with vaccine candidates.

In this chapter, we expand on the information generated from vaccine studies using the MGIA by incorporating flow cytometry and RNA-seq analysis into the lung MGIA workflow. The same homogenised host cell preparations utilised in the MGIA were analysed. Part I focuses on the two routes of BCG administration analysed by MGIA in Chapter 4. The aim was to identify differential gene expression and immune cell populations associated with the growth inhibition profiles of lung cells harvested following s.c. and i.n. BCG vaccination. A comparison with a published murine *in vivo* dataset is made to determine whether correlates of growth inhibition are representative of transcriptional perturbation following *in vivo* infection. In part II, RNA-seq analysis of murine lung cells in response to stimulation with three of the MTB clinical isolates used in the MGIA in Chapter 5 was performed. Gene expression in BCG-vaccinated (s.c.) and unvaccinated groups was compared to determine whether correlates of growth inhibition vary by MTB strain.

In addition to improving understanding of the biology of the MGIA as it stands, outputs of this analysis could be approached from two directions. Firstly, ‘back-

translation' of potential correlates of BCG-induced protection identified in other animal models and human studies can be performed, with the aim to evaluate the performance and limitations of the lung MGIA as a model of *in vivo* infection, and its potential as a tool for mechanistic evaluation of vaccines. Secondly, novel perturbations in gene expression and immune cell composition identified by *ex vivo* analysis may provide new targets for validation in larger *in vivo* studies as potential CoP.

In the absence of a robust CoP, as well as the potential for such correlates to vary by vaccine and/or mycobacterial strain, tools for use in early preclinical stages of vaccine selection must be improved. The MGIA represents a potential platform to gain early mechanistic insight into vaccine-induced protection, as well as broader testing of vaccines against clinical isolates of the MTB complex. In the future, readouts from these analyses may inform design of clinical studies and selection of immunogenicity readouts during TB vaccine evaluation.

6.2 Aims and objectives

Aims

- Characterise the host cell population input in the MGIA.
- Identify transcriptional correlates of *ex vivo* mycobacterial growth inhibition in the BCG s.c. and i.n. vaccinated murine lung.
- Determine whether correlates of *ex vivo* mycobacterial growth inhibition are unique to *ex vivo* mycobacterial culture or also observed following *in vivo* infection (CoP in the mouse model).
- Compare transcriptional correlates of *ex vivo* mycobacterial growth inhibition of three different lineages of MTB in the BCG s.c. murine lung.

Objectives

- Perform flow cytometric analysis of the host cell phenotype of the murine lung MGIA input.
- Analysis of the transcriptome of the murine lung cell input (unvaccinated versus BCG s.c./i.n.).
- Analysis of the transcriptome of the murine lung cell MGIA input (unvaccinated versus BCG s.c./i.n.) following overnight stimulation with BCG.
- Analysis of the transcriptome of the murine lung cell MGIA input (unvaccinated versus BCG s.c.) following overnight stimulation with three different lineages of the MTB complex.
- Compare transcriptional perturbation following *ex vivo* stimulation and *in vivo* infection.
- Apply identified perturbations in gene expression to a defined set of murine lung modules.

6.3 Materials and methods

Materials and methods for the experiments described in this chapter are outlined in full in Chapter 3.

6.4 Results

6.4.1 Analysis of the host immune cell input in the murine lung MGIA

In Chapters 4 and 5, *ex vivo* co-culture of lung cells processed from BCG-vaccinated mice at the peak immune response of vaccination was demonstrated to significantly inhibit growth of various mycobacteria compared with unvaccinated animals in the murine lung MGIA. To date, the cell composition of the host input for the MGIA

has not been evaluated. To determine whether BCG vaccination induces changes in the lung immune cell population which correlate with reduced mycobacterial burden observed in the MGIA, flow cytometric analysis of the lung cell composition of C57BL/6 mice six weeks following s.c. and i.n. BCG PA vaccination was performed and compared with unvaccinated (control) mice. The composition of the lung and spleen MGIA input was also compared.

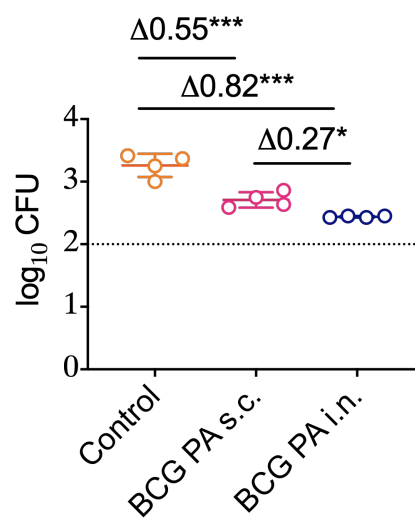


Figure 6-1. *Ex vivo* BCG growth inhibition by BCG-vaccinated murine lung cells versus control lung cells. C57BL/6 mice (n = 4–5/group) received s.c. or i.n. BCG PA at week 0 or no treatment (control). At six weeks, lungs were processed and used in the MGIA. Lung cells were co-cultured with 100 CFU BCG PA for 96 hours and then transferred to the BACTEC system until TTP values were generated. TTP values were converted to log₁₀ CFU based on a standard curve. Data points (n = 4/group) represent samples generated from pooled cells isolated from six mice. Dotted line indicates mycobacterial input at day 0. Statistical significance was tested by one-way ANOVA followed by Tukey’s multiple comparison test. Error bars represent mean ± standard deviation. * p<0.05 (adjusted); *** p<0.001 (adjusted). PA, Pasteur Aeras; ANOVA, analysis of variance; BCG, Bacille Calmette–Guérin; CFU, colony-forming units; i.n., intranasal; MGIA, mycobacterial growth inhibition assay; s.c., subcutaneous; TTP, time to positivity.

Lungs were enzymatically digested and mashed to generate a single cell suspension. As a positive control, the ability of lung cells from BCG s.c. and i.n. vaccinated mice to inhibit mycobacterial growth compared with control murine lung cells was confirmed by *ex vivo* MGIA (Figure 6-1).

For flow cytometry, lung cells were fixed and stained. The gating strategy is shown in Figure 6-2 and was developed using a combination of two published gating strategies [460,461].

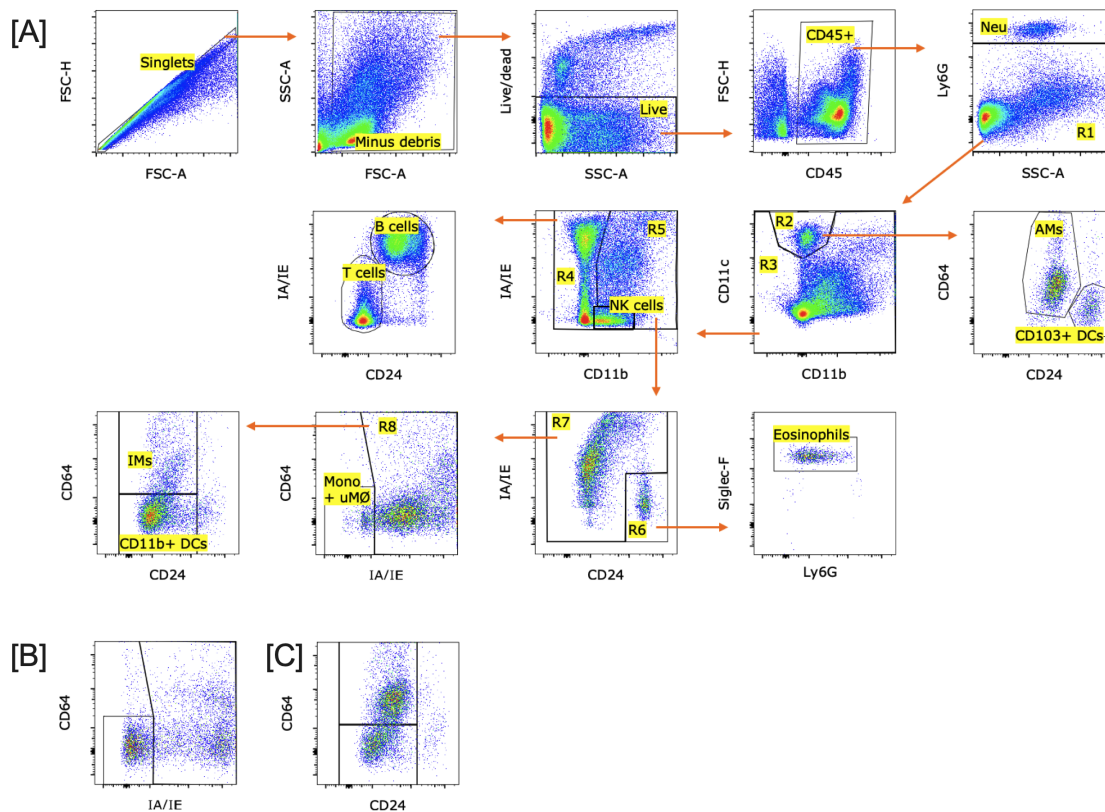


Figure 6-2. Flow cytometry gating strategy I. [A] Gating strategy shown for representative sample. After exclusion of doublets and debris, live CD45⁺ cells were identified, and a sequential gating strategy was used. Neutrophils were discriminated from all other leukocytes (R1) by Ly6G. From R1, CD11c⁺ CD11b⁻ AMΦs and CD103⁺ DCs [460] were identified (R2) and further separated by CD64 and CD24 expression. Lymphoid and myeloid cells (R3) were then separated based on CD11b expression: T and B cells (R4; CD11b⁻), NK cells (CD11b^{int}) and CD11b^{hi} myeloid cells. T and B cells

(R4) were differentiated using IA/IE and CD24 expression. Remaining myeloid cells (R5) were identified as eosinophils (R6; CD24⁺ Siglec-F⁺), mono and uMΦ (R7; CD64^{low} CD24^{low} IA/IE⁻), IMΦs (R7–R8; CD64^{high} IA/IE⁺ CD24⁻) and CD11b⁺ DCs (CD64⁻ IA/IE⁺ CD24⁺). Additional plots depict gating of other samples in the dataset to clarify location of [B] mono and uMΦ populations and [C] IMΦ and CD11b⁺ DC. AMΦ, alveolar macrophage; CD, cluster of differentiation; DC, dendritic cell; IMΦ, interstitial macrophage; mono, monocytes; Ly6C, lymphocyte antigen 6 complex, locus C; Ly6G, lymphocyte antigen 6 complex, locus G; NK, natural killer; Siglec-F, sialic acid-binding immunoglobulin-type lectin F; uMΦ, undifferentiated macrophage.

Figure 6-3A depicts the relative frequencies of nine major immune cell populations as a percentage of the total live cell population for 4–5 mice per group. The relative frequency of CD45-negative cells is also shown. The mean group frequency of each population is visualised in pie charts in Figure 6-3B.

Focusing on the BCG s.c. lung cell population, a significant increase (7.9 vs 2.5%, $p=0.0006$) in the proportion of DCs in the total live cell population was observed in the BCG s.c. lung versus control. Pie charts indicate an increased proportion of NK cells in the BCG s.c. group compared with both control (11.5 vs 8.4%) and BCG i.n. (11.5 vs 6.5%) groups; however, this observation was only significant when compared with the BCG i.n. group ($p=0.0106$).

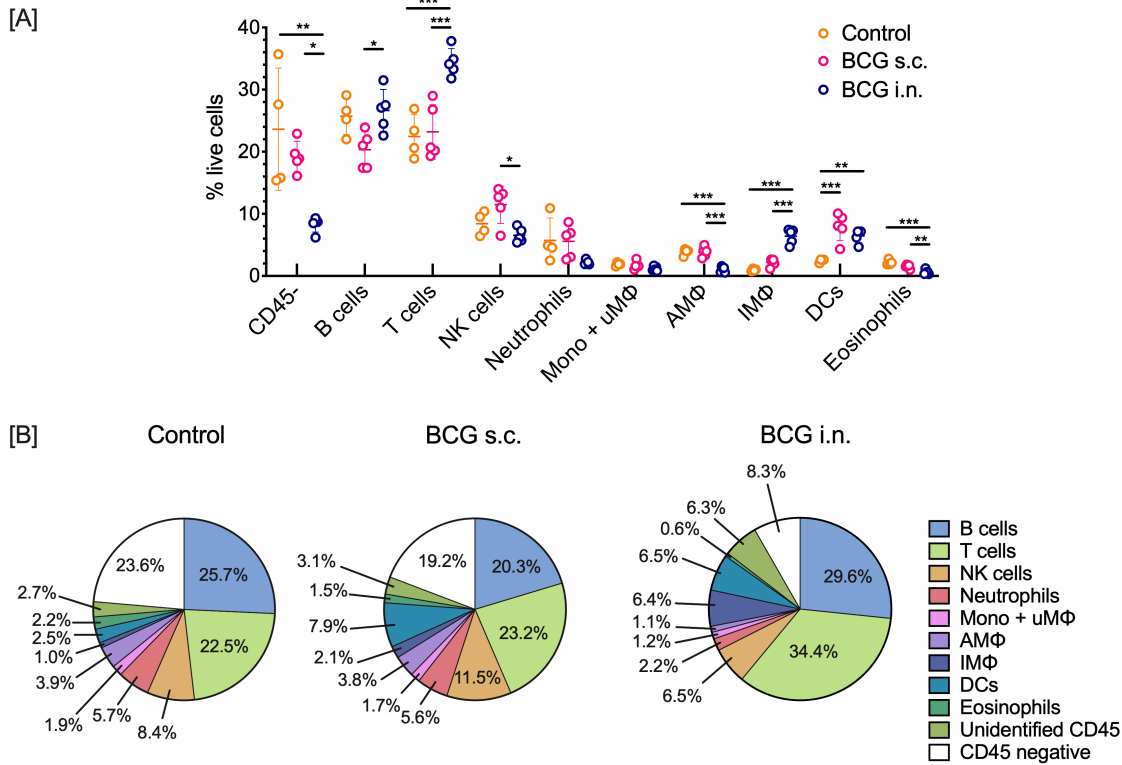


Figure 6-3. Cell populations in the murine lung MGIA input. C57BL/6 mice (n = 4–5/group) received s.c. or i.n. BCG PA at week 0 or no treatment (control). Six weeks post-vaccination, lungs were enzymatically digested and mashed to generate a single cell suspension which was fixed and stained. [A] Identified cell populations as a percentage of live cells are shown. Statistical significance was tested by one-way ANOVA followed by Tukey’s multiple comparison test. Error bars represent mean ± standard deviation. * p<0.05; ** p<0.01; *** p<0.001. [B] Pie charts depict the relative frequencies of identified immune cell types as a percentage of live cells in control and BCG-vaccinated lung (mean of individual mice shown in A). ANOVA, analysis of variance; AMΦ, alveolar macrophages; BCG, Bacille Calmette–Guérin; CD, cluster of differentiation; DC, dendritic cell; IMΦ, interstitial macrophages; i.n., intranasal; mono, monocytes; MGIA, mycobacterial growth inhibition; NK, natural killer; PA, Pasteur Aeras; s.c., subcutaneous; uMΦ, undifferentiated macrophages.

In the BCG i.n. lung cell population, the proportion of T cells was significantly increased compared with the control (34.4 vs 22.5%, p=0.0009) and BCG s.c. (34.4 vs 23.2%, p=0.0010) groups. The DC population was also significantly increased in the

BCG i.n. group compared with control (6.5 vs 2.5%, $p=0.0057$). A significant reduction in the proportion of alveolar macrophages (AM Φ s) and increase in interstitial macrophages (IM Φ s) in the BCG i.n. lung compared with the control (AM Φ , 1.1 vs 2.8%, $p<0.0001$; IM Φ , 6.4 vs 1.0%, $p<0.0001$) and BCG s.c. (AM Φ , 1.1 vs 2.8%, $p<0.0001$; IM Φ , 6.4 vs 2.1%, $p<0.0001$) lung was also noted. Further, eosinophils were reduced compared with the control (0.6 vs 2.2%, $p=0.0002$) and BCG s.c. (0.6 vs 1.5, $p=0.0058$) groups.

Using a different flow cytometry panel, both the lung and spleen cell MGIA input from BCG-vaccinated (s.c. and i.n.) and unvaccinated mice was also analysed. The gating strategy was based on a published strategy by Zelmer *et al* [462] and is shown in Figure 6-4.

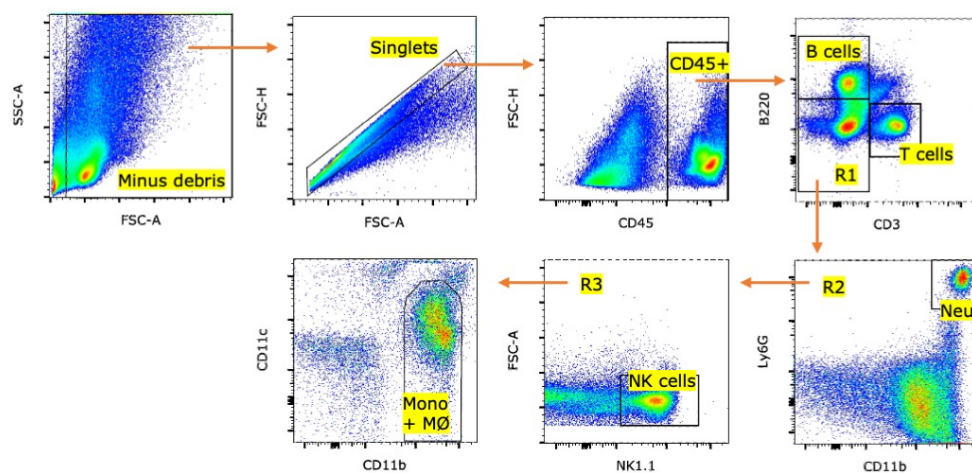


Figure 6-4. Flow cytometry gating strategy II. Gating strategy shown for representative sample. After exclusion of debris and doublets, CD45⁺ cells were identified and a sequential gating strategy was used to identify T cells (CD3⁺), B cells (B220⁺), neutrophils (CD11b⁺ Ly6G⁺), NK cells (NK1.1) and mono/M Φ (CD11b⁺ CD11c^{low-int}). CD, cluster of differentiation; mono, monocytes; Ly6G, lymphocyte antigen 6 complex, locus G; M Φ , macrophage; NK, natural killer.

Figure 6-5A and B depicts the relative frequencies of five major immune cell populations as a percentage of the total single cell population for 5 mice per group. The relative frequency of CD45-negative cells is also shown. The mean group frequency of each cell population in the lung and spleen MGIA input is visualised in pie charts in Figure 6-5C and D, respectively. The composition of the splenocyte MGIA cell input was not analysed using panel I, therefore data from this less extensive panel are included to facilitate comparison between the cell populations present in the lung and spleen MGIA.

The cell composition of the lung MGIA input identified using flow cytometry panel II revealed similar differences between each vaccine group to that observed in panel I. Again, an increase in NK cells in the lung cell population from BCG s.c. vaccinated mice was found compared with those vaccinated via the i.n. route (14.3 vs 7.2%, $p=0.0259$). Consistent with results obtained using panel I, the proportion of B and T cells was increased in lung cells obtained from mice administered BCG via the i.n. route compared with the control (B cells: 29.3 vs 36.8%, $p=0.0012$; T cells: 20.5 vs 35.0%, $p<0.0001$) and BCG s.c. vaccinated (B cells: 27.4 vs 36.8%, $p=0.0002$; T cells; 18.7 vs 35.0%, $p<0.0001$) groups.

Analysis of the cell composition of the spleen MGIA input demonstrated that the proportion of B cells was significantly higher in the spleen MGIA input from mice vaccinated i.n. compared with control or BCG s.c. vaccinated mice. In contrast to an increase in the proportion of T cells in the lung MGIA input, the proportion of T cells in the spleen input was significantly reduced in the i.n. group versus the control and s.c. groups. The panel identified no significant differences in the composition of the splenocyte MGIA input from control and s.c. vaccinated mice.

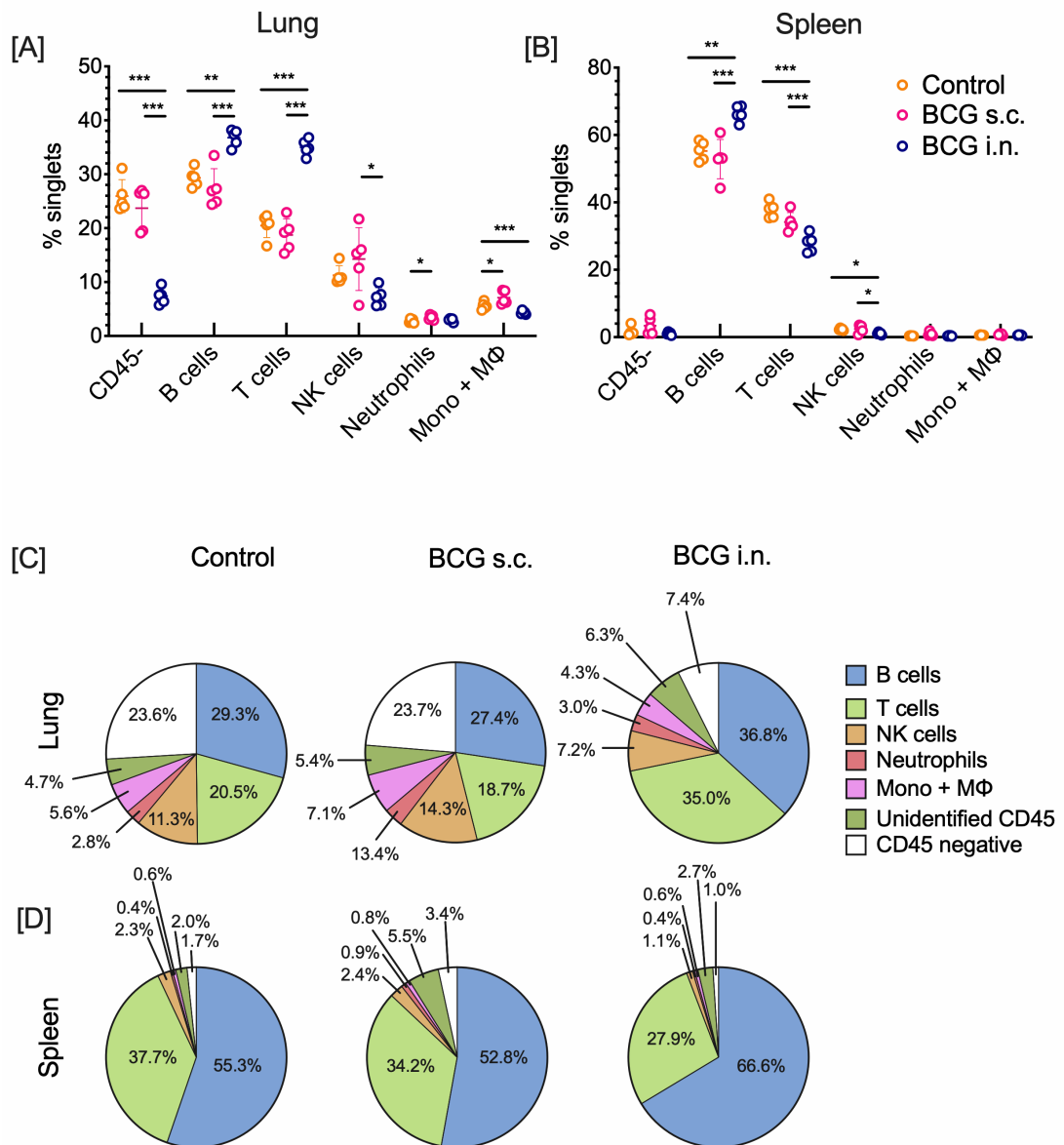


Figure 6-5. Cell populations in murine lung and spleen MGIA input. C57BL/6 mice (n = 5/group) received s.c. or i.n. BCG PA at week 0 or no treatment (control). Six weeks post-vaccination, spleens were mashed, and lungs were enzymatically digested and mashed, to generate a single cell suspension which was fixed and stained. Identified cell populations in the [A] lung and [B] spleen as a percentage of singlets are shown. Statistical significance was tested by one-way ANOVA followed by Tukey's multiple comparison test. Error bars represent mean \pm standard deviation. * p<0.05; ** p<0.01; *** p<0.001. Pie charts depict the relative frequencies of identified immune cell types in the [C] lung and [D] spleen as a percentage of singlets in control and BCG-vaccinated lung (mean of five individual mice). ANOVA, analysis of variance; BCG, Bacille Calmette–Guérin; CD, cluster of differentiation; i.n., intranasal; mono, monocytes;

MGIA, mycobacterial growth inhibition; NK, natural killer; PA, Pasteur Aeras; s.c., subcutaneous; MΦ, macrophages.

6.4.2 Correlates of *ex vivo* BCG growth inhibition in the BCG-vaccinated murine lung

To study the murine lung transcriptome at the peak immune response following BCG vaccination (six weeks) [435], lung cells were processed from BCG PA-vaccinated (s.c. and i.n.) and unvaccinated (control) mice and cultured overnight in the absence or presence of BCG (1:1). Eukaryotic RNA was purified and analysed by RNA-seq. Figure 6-6 provides an overview of the study design and the comparisons made in downstream data analysis.

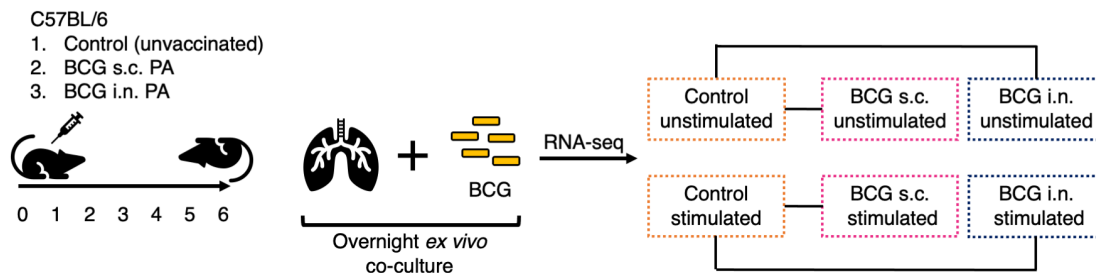


Figure 6-6. Study design – RNA-seq I. C57BL/6 mice ($n = 3/\text{group}$) received s.c. or i.n. BCG PA at week 0 or no treatment (control). Six weeks post-vaccination, lungs were processed and cells (1×10^6) were co-cultured overnight $\pm 1 \times 10^6$ CFU BCG PA. Purified RNA was analysed by RNA-seq. A visualisation of the groups included in the study is shown on the right. Black lines indicate the group comparisons made during bioinformatic analyses to generate lists of DEGs. BCG, Bacille Calmette–Guérin; CFU, colony-forming units; DEGs, differentially expressed genes; i.n. intranasal; PA, Pasteur Aeras; s.c., subcutaneous.

DESeq2 was used to determine differentially expressed genes (DEGs) between conditions of interest. Comparisons made in this dataset focused on baseline differences

in the transcriptional profile of control and BCG-vaccinated samples, as well as in the response to *ex vivo* BCG stimulation, with the aim to identify correlates of growth inhibition.

PCA plots can be used to cluster samples based on their similarity and are useful tools to visualise complex biological datasets.

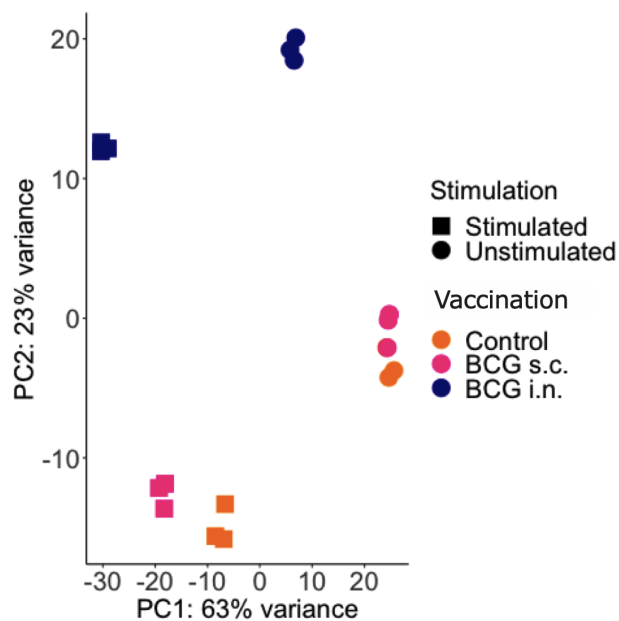


Figure 6-7. PCA plot of PC1 versus PC2 for all samples in RNA-seq I. BCG, Bacille Calmette–Guérin; i.n. intranasal; PCA, principal component analysis; s.c., subcutaneous.

A PCA plot of data from this study demonstrates the largest variation (PC1) in the global gene expression profile of all samples in the dataset is defined by the presence/absence of *ex vivo* BCG stimulation (accounting for 63% of variation in the dataset), and the second by vaccination (PC2) (23% of variation) (Figure 6-7). Complete separation from control and BCG s.c. samples was observed in the *ex vivo* unstimulated and stimulated BCG i.n. group indicative of a distinct transcriptional signature. Some overlap in the global gene expression profile is seen for PC1 and PC2 between

unstimulated control and BCG s.c. lung; however, on stimulation, separation of BCG s.c. samples from control is shown on both PCA dimensions.

To identify potential correlates of mycobacterial growth inhibition, differential expression analysis focused on genes identified as up- or downregulated in the vaccinated (BCG i.n. or s.c.) groups compared with the control group under both the unstimulated and stimulated conditions. In the unstimulated (baseline) samples, representative of six-weeks following vaccination, 338 and 56 genes were found to be significantly ($p_{adj} < 0.05$) upregulated and downregulated in lung cells from mice vaccinated with BCG s.c., respectively. In lung cells from BCG i.n. vaccinated mice, 4,227 and 4,159 genes were found to be significantly ($p_{adj} < 0.05$) upregulated and downregulated respectively. Following *ex vivo* stimulation with BCG, 1,768 and 1,051 genes were found to be significantly ($p_{adj} < 0.05$) upregulated and downregulated in lung cells from mice vaccinated with BCG s.c., respectively. In lung cells from BCG i.n. vaccinated mice stimulated *ex vivo* with BCG, 4,902 and 4,777 genes were found to be significantly ($p_{adj} < 0.05$) upregulated and downregulated respectively.

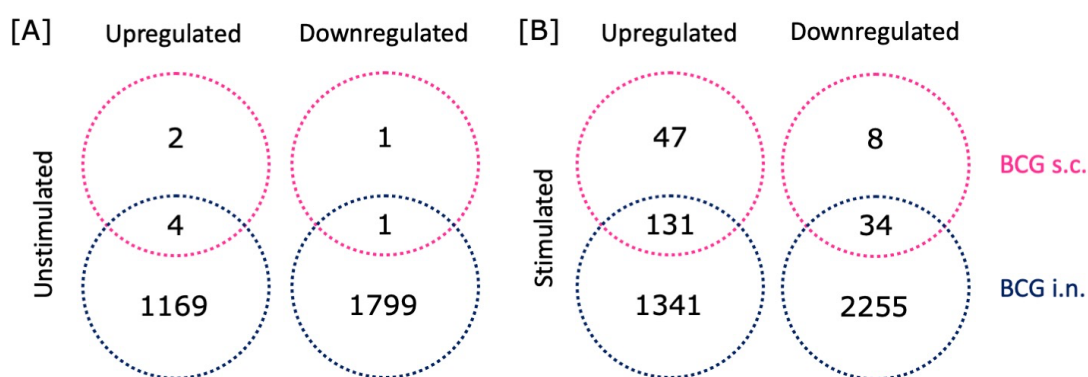


Figure 6-8. Venn diagrams – RNA-seq I. Venn diagrams visualising the relationship between genes identified as significantly ($p_{adj} < 0.05$) up- (LFC = 1) or downregulated (LFC = -1) in lung cells from BCG s.c. or i.n. vaccinated mice versus unvaccinated mice. Results for [A] unstimulated and [B] BCG-stimulated *ex vivo* culture conditions are

shown. BCG, Bacille Calmette–Guérin; i.n. intranasal; LFC, log₂ fold change; padj, adjusted p value; s.c., subcutaneous.

Venn diagrams in Figure 6-8 depict the number of genes identified to be significantly (padj<0.05) up- or downregulated by an LFC of 1/-1 (equal to a 2-fold increase or 0.5-fold decrease in gene expression) under these conditions.

To determine whether condition-specific gene perturbation was associated with a defined biological process or pathway, 38 murine lung transcriptional modules generated by Singhania *et al* [422] were downloaded and processed for use in the Bioconductor package, tmod, in R. A detailed description of the generation of these modules, as well as the methods performed by Singhania *et al* to elucidate the specific immune cell populations associated with each module, is included in Chapter 3. Data generated in the current project are presented alongside a simplified reproduction of the immune cell populations reported to be associated with each module in the original manuscript.

Ordered gene lists for tmod were generated using results tables from DESeq2 analysis. A metric was calculated for all DEGs (>/<0), metric = $-\log_{10}(\text{padj}) \times \text{abs}(\text{LFC})$, and used to order lists of gene names for transcription module analysis using the tmod CERNO test. Enrichment analysis of four comparisons was performed: unstimulated BCG s.c. vs control; unstimulated BCG i.n. vs control; *ex vivo* BCG-stimulated BCG s.c. vs control; and *ex vivo* BCG-stimulated BCG i.n. vs control. Results are shown in Figure 6-9. Significantly enriched modules (padj <0.01) are shown as grey ‘pies’ with the degree of significance indicated by colour intensity and the effect size by the size of the pie. Ordered lists for module enrichment analysis are not generated using a p-value threshold, therefore, the proportion of individual genes within each module identified to be significantly up- or downregulated (padj <0.05) is indicated in red and blue, respectively.

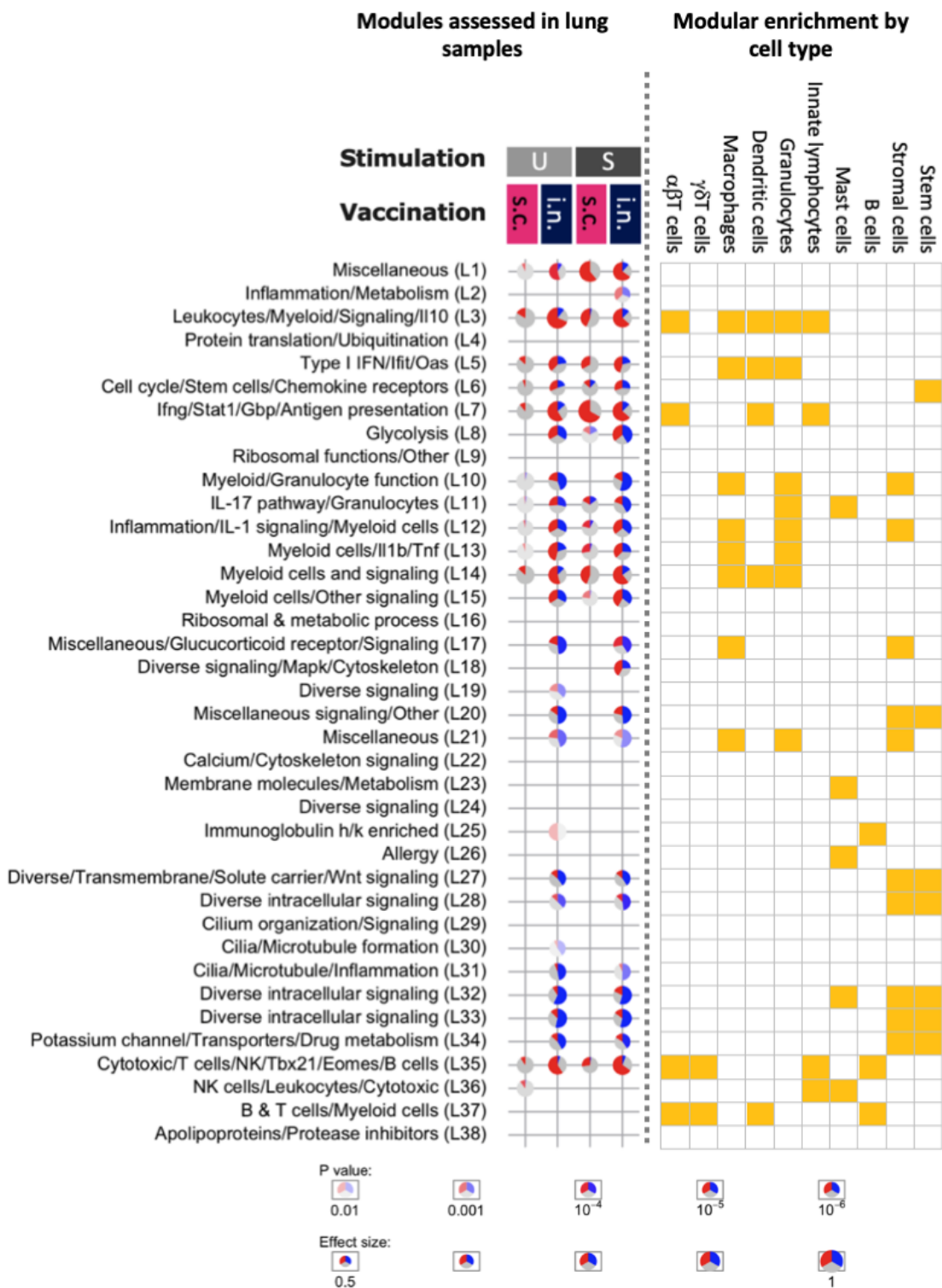


Figure 6-9. tmod analysis – RNA-seq I. Left panel – tmodPanelPlot visualising enrichment in defined murine lung modules for DEGs in BCG i.n. lung versus unvaccinated, or BCG s.c. lung versus unvaccinated. Results for unstimulated (U) and BCG-stimulated (S) *ex vivo* culture conditions are shown. Each row contains one module.

Modules found to be significantly enriched ($\text{padj} < 0.01$) are indicated by a grey circle (pie), with the degree of significance indicated by colour intensity and the effect size (AUROC) by size. The proportion of individual genes within each module found to be significantly ($\text{padj} < 0.05$) up- or downregulated are marked in each pie in red or blue respectively. Right panel – a simplified reproduction of the immune cell populations reported to be associated with each module by Singhania *et al.* AUROC, area under the receiver operating curve; BCG, Bacille Calmette–Guérin; i.n. intranasal; DEGs, differentially expressed genes; LFC, \log_2 fold change; padj , adjusted p value; s.c., subcutaneous.

Across all four conditions comparing the BCG-vaccinated lung to control, enrichment of modules dominated by macrophage-, granulocyte-, and myeloid-specific genes (modules 3, 11–14) was found. Enrichment of module 35, a module annotated as Cytotoxic/T cells/NK/Tbx21/Eomes/B cell, was also common to all conditions, as well as the Type I IFN/Ifit/Oas (module 5) and Miscellaneous (module 1) modules. Module 7, annotated as Ifng/Stat1/Gbp/Antigen presentation, was enriched in all four conditions, with a higher proportion of significantly enriched genes within each module observed on stimulation of BCG s.c. and in both BCG i.n. comparisons.

An additional module associated with NK cells was found to be enriched in the unstimulated BCG s.c. lung compared with the control lung (module 36).

Enrichment of genes associated with Glycolysis (module 8) was observed following stimulation of BCG s.c. lung cells, and in both unstimulated and stimulated BCG i.n. lung cells.

Modules associated with signalling (modules 17, 20, 27, 28, 32 and 33), Cilia/Microtubule/Inflammation (module 31) and drug metabolism (module 34) were enriched in both the unstimulated and stimulated BCG i.n. lung. Focusing on module enrichment differentiating the unstimulated and stimulated i.n. lung, a module associated

with immunoglobulins (module 25) was enriched in the unstimulated i.n. lung only. In the stimulated i.n. lung, a module associated with inflammation and metabolism (module 2) was identified.

6.4.3 Correlates of protection in the murine lung following *in vivo M bovis* challenge

With the aim to determine whether modular enrichment identified when comparing the vaccinated lung transcriptome to that of the control was unique to *ex vivo* mycobacterial culture, or also observed following *in vivo* infection, a murine *M bovis* challenge microarray dataset deposited in the GEO repository by Aranday-Cortes *et al* [418] was downloaded. The dataset, visualised in Figure 6-10, included a BCG Danish s.c. vaccinated and unvaccinated arm in which lung cells were isolated from BALB/c mice at three timepoints: pre *M bovis* infection (6-weeks post-vaccination), and 3- and 14-days post *M bovis* infection. For this project, raw data were downloaded and DEA was performed using Limma.

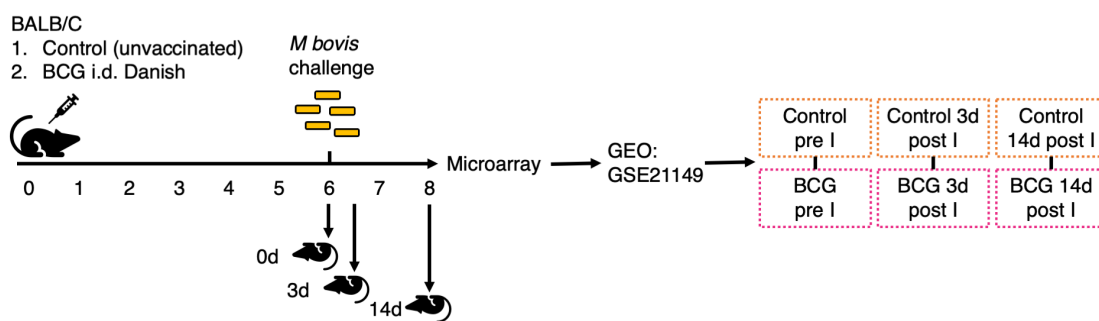


Figure 6-10. Study design – Aranday-Cortes microarray dataset. BALB/c mice received s.c. BCG Danish at week 0 or no treatment (control). Six weeks post-vaccination, mice were intranasally challenged with *M bovis*. Lungs were harvested at pre-I, and 3- and 14 days post-I and processed to generate a single cell suspension. RNA was purified and hybridised to microarrays. A visualisation of the groups included in the study is shown on the right. Black lines indicate the group comparisons made during

bioinformatic analyses to generate lists of DEGs. BCG, Bacille Calmette–Guérin; CFU, colony-forming units; DEGs, differentially expressed genes; i.d., intradermal; pre-I, pre-infection; post-I, post-infection.

Bacterial burden was determined at 28-days post-infection in the original study. A 1.48 ($p < 0.005$) and 1.88 ($p < 0.0005$) \log_{10} CFU reduction in *M bovis* was found in the spleen and lungs of BCG-vaccinated mice, respectively, compared with unvaccinated [418].

The PCA plot in Figure 6-11 demonstrates the largest variation (PC1) in the global gene expression profiles of all samples in the dataset is defined by time point (accounting for 34% of variation).

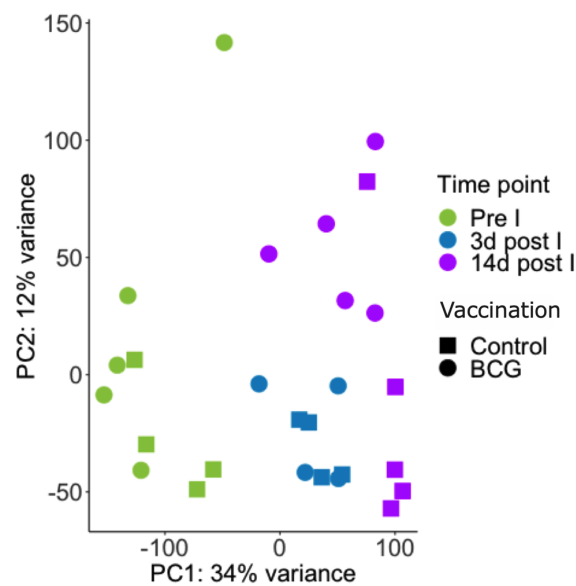


Figure 6-11. PCA plot of PC1 versus PC2 for all samples in the Aranday–Cortes microarray dataset. BCG, Bacille Calmette–Guérin; PCA, principal component analysis; pre-I, pre-infection; post-I, post-infection.

The second (PC2) largest source of variation in the dataset (accounting for 12% of variation) is less clear but may, in part, be defined by vaccination; some sample clustering, particularly at the 14-day post-infection time point, can be seen.

As performed for RNA-seq analyses, ordered gene lists of DEGs in the BCG-vaccinated lung versus control were generated and module enrichment analysis was performed by tmod using the *Singhania murine lung* modules (Figure 6-12).

No module enrichment was found in the lung when comparing gene expression in the BCG-vaccinated group with the control group six-weeks following vaccination (pre-infection). At the post-infection time points, consistent with enrichment previously observed in the *ex vivo* experiment, enrichment of genes annotated to the Cell cycle/Stem cells/Chemokine receptors (module 6), *Ifng/Stat1/Gbp/Antigen presentation* (module 7), *IL-17/Granulocytes* (module 11) and *Cytotoxic/T cells/NK/Tbx21/Eomes/B cells* (module 35) modules was observed in the BCG-vaccinated lung versus control 3- and 14-days following *in vivo M bovis* infection.

Enrichment of genes annotated to a number of signalling modules, including modules 17, 20, 22, 24, 27, 28, 32 and 33, and a drug metabolism module (module 34) were also found post-infection. In *ex vivo* studies, these modules were enriched in the BCG i.n. lung only.

At the 14-day post-infection time point, enrichment of genes annotated to the *Leukocytes/Myeloid/Signalling/IL-10* (module 3) and *Type I IFN/Ifit/Oas* (module 5) modules was also found in the BCG-vaccinated lung.



Figure 6-12. tmod analysis – Aranday–Cortes microarray dataset. Left panel – tmodPanelPlot visualising enrichment in defined murine lung modules for DEGs in BCG-vaccinated lung versus control. Results for pre-I and 3 and 14-days post-I are shown. Each row contains one module. Modules found to be significantly enriched ($\text{padj} < 0.01$) are indicated by a grey circle (pie), with the degree of significance indicated by colour intensity and the effect size (AUROC) indicated by size. The proportion of individual

genes within each module found to be significantly ($p_{adj} < 0.05$) up- or downregulated are marked in each pie in red or blue respectively. Right panel – a simplified reproduction of the immune cell populations reported to be associated with each module by Singhanian *et al.* AUROC, area under the receiver operating curve; BCG, Bacille Calmette–Guérin; DEGs, differentially expressed genes; GEO, Gene Expression Omnibus; LFC, \log_2 fold change; p_{adj} , adjusted p value; PCA, principal component analysis; pre-I, pre-infection; post-I, post-infection.

To facilitate comparisons across the two gene expression datasets, the absence/presence of module enrichment following *ex vivo* stimulation with BCG and *in vivo* infection with *M bovis* is summarised in Table 6-1. Modules identified to be enriched in the BCG s.c. vaccinated murine lung following *ex vivo* co-culture with BCG and *in vivo* infection with *M bovis* are highlighted in grey.

Table 6-1. Summarised enrichment analysis results for RNA-seq I analysis and Aranday–Cortes microarray.

Module	Biological process	<i>Ex vivo</i> BCG stimulation		<i>In vivo</i> <i>M bovis</i> challenge	
		BCG s.c.	BCG i.n.	3-d post-I	14-d post-I
1	Miscellaneous	X	X		
2	Inflammation / Metabolism		X		
3	Leukocytes / Myeloid / Signaling / Il10	X	X		X
4	Protein translation / Ubiquitination				
5	Type I IFN / Ifit / Oas	X	X		X
6	Cell cycle / Stem cells / Chemokine receptors	X	X	X	X
7	Ifng / Stat1 / Gbp / Antigen presentation	X	X	X	X
8	Glycolysis	X	X		
9	Ribosomal functions / Other				

10	Myeloid / Granulocyte function		X		
11	IL-17 pathway / Granulocytes	X	X	X	X
12	Inflammation / IL-1 signaling / Myeloid cells	X	X		
13	Myeloid cells / Il1b / Tnf	X	X		
14	Myeloid cells and signaling	X	X		X
15	Myeloid cells / Other signaling	X	X		
16	Ribosomal & metabolic process				
17	Miscellaneous / Glucocorticoid receptor / Signaling		X		X
18	Diverse signaling / Mapk / Cytoskeleton		X		
19	Diverse signaling				
20	Miscellaneous signaling / Other		X		X
21	Miscellaneous		X		
22	Calcium / Cytoskeleton signaling			X	X
23	Membrane molecules / Metabolism			X	
24	Diverse signaling			X	
25	Immunoglobulin h/k enriched				
26	Allergy			X	
27	Diverse / Transmembrane / Solute carrier / Wnt signaling		X		X
28	Diverse intracellular signaling		X	X	X
29	Cilium organization / Signaling				
30	Cilia / Microtubule formation				
31	Cilia / Microtubule / Inflammation		X		
32	Diverse intracellular signaling		X		X
33	Diverse intracellular signaling		X		X
34	Potassium channel / Transporters / Drug metabolism		X		X
35	Cytotoxic / T cells / NK / Tbx21 / Eomes / B cells	X	X	X	X
36	NK cells / Leukocytes / Cytotoxic				
37	B & T cells / Myeloid cells			X	X

38	Apolipoproteins / Protease inhibitors				
<p>Modules identified to be enriched in the BCG s.c.-vaccinated murine lung following <i>ex vivo</i> co-culture with BCG and <i>in vivo</i> infection with <i>M bovis</i> are highlighted in grey. BCG, Bacille Calmette–Guérin; i.n., intranasal; post-I, post-infection; s.c., subcutaneous.</p>					

6.4.4 Correlates of *ex vivo* growth inhibition of MTB complex clinical isolates in the BCG-vaccinated murine lung

Since BCG is administered systemically at present, further analysis of DEGs unique to BCG vaccination focused on s.c. administration and was expanded to study potential variation in the response to *ex vivo* stimulation with clinical isolates of the MTB complex.

A mouse vaccination study of similar design to that described for the RNA-seq I dataset was performed with a control (unvaccinated) and BCG s.c. vaccinated arm. MGIA data for lung cells from the same animals used in this run are shown in Figure 6-13.

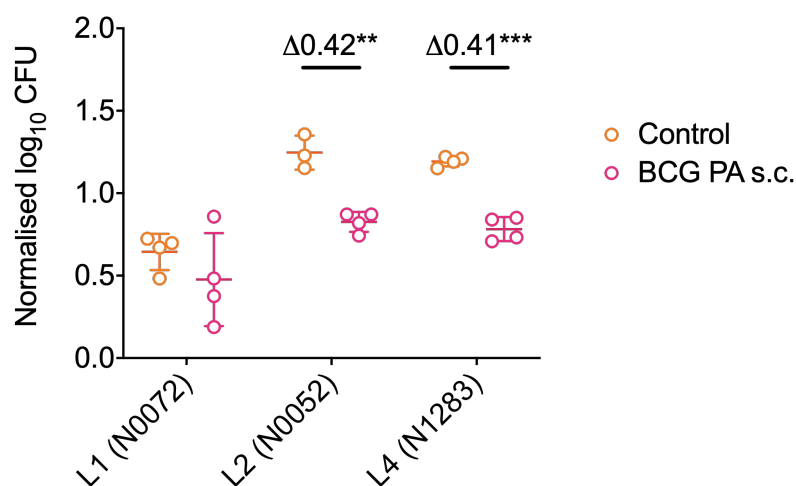


Figure 6-13. *Ex vivo* MTB growth inhibition by BCG-vaccinated murine lung cells versus control lung cells. C57BL/6 mice (n = 4–5/group) received s.c. BCG PA at week 0 or no treatment (control). At six weeks, lungs were processed and used in the MGIA. Lung cells were co-cultured with 200 CFU MTB complex L1 (N0072), L2 N0052 or L4

(N1283) for 96 hours and then transferred to the BACTEC system until TTP values were generated (L1 and L2), or plated on solid agar (L4). TTP values were converted to log₁₀ CFU based on a standard curve. Data points (n = 4/group) represent samples generated from pooled cells isolated from six mice. Statistical significance was tested by unpaired t test. Error bars represent mean ± standard deviation. Data for L1 and L2 are reproduced from Chapter 5. ** p<0.01 (adjusted); *** p < 0.001 (adjusted). BCG, Bacille Calmette–Guérin; CFU, colony-forming units; i.n., intranasal; L, lineage; MGIA, mycobacterial growth inhibition assay; MTB, *Mycobacterium tuberculosis*; PA, Pasteur Aeras; s.c., subcutaneous; TTP, time to positivity.

At six weeks, lung cells were again processed from groups and cultured overnight in the absence or presence of one of three selected MTB complex clinical isolates representative of three lineages: L1 (N0072); L2 (N0052); or L4 (N1283). Eukaryotic RNA was purified and analysed by RNA-seq. Figure 6-14 provides an overview of the study design and the comparisons made in downstream data analysis.

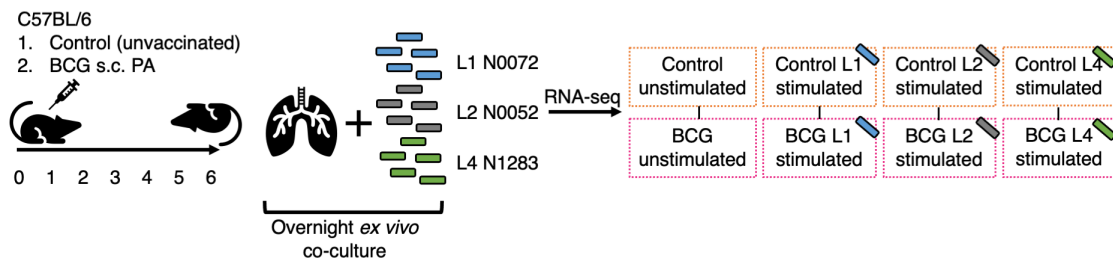


Figure 6-14. Study design – RNA-seq II. C57BL/6 mice (n = 3/group) received s.c. BCG PA at week 0 or no treatment (control). Six weeks post-vaccination, lungs were processed and 1×10^6 cells were co-cultured overnight $\pm 1 \times 10^6$ CFU MTB complex L1 (N0072), L2 (N0052) or L4 (N1283). Purified RNA was analysed by RNA-seq. A visualisation of the groups included in the study is shown on the right. Black lines indicate the group comparisons made during bioinformatic analyses to generate lists of DEGs. BCG, Bacille Calmette–Guérin; CFU, colony-forming units; L, lineage; MTB, *Mycobacterium tuberculosis*; PA, Pasteur Aeras; padj; s.c. subcutaneous.

Data were analysed and visualised by the same methods used in the first RNA-seq run. Since this dataset also included unstimulated (baseline) control and BCG s.c. lung samples, differences in the transcriptional profile identified in the first RNA-seq run between these two groups could be validated in this second run.

The response of BCG s.c. vaccinated and control lung cells to *ex vivo* stimulation with three MTB clinical isolates was compared to identify whether BCG-mediated differential gene expression varies depending on the mycobacteria of interest.

The PCA plot in Figure 6-15A demonstrates the largest variation (PC1) in the global gene expression profiles of all samples in the dataset is defined by the presence/absence of *ex vivo* mycobacterial stimulation (accounting for 81% of variation in the dataset).

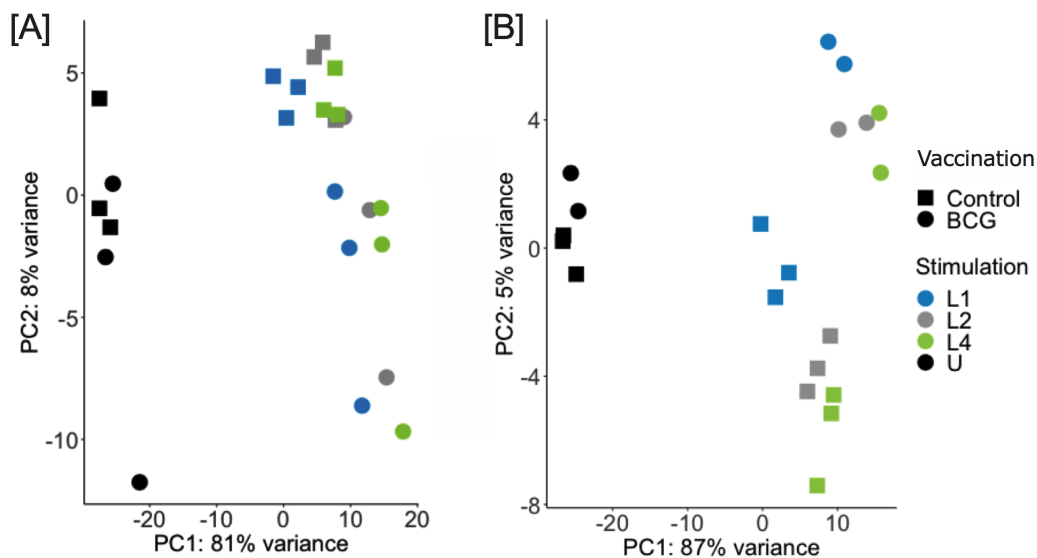


Figure 6-15. PCA plots – RNA-seq II. [A] PCA plot of PC1 versus PC2 for all samples. [B] PCA of PC1 and PC2 for 20/24 samples (outliers removed for PCA plot visualisation only). BCG, Bacille Calmette–Guérin; L, lineage; PCA, principal component analysis; U, unstimulated.

In this instance the second largest variation in the dataset is defined by lung samples from one BCG-vaccinated mouse (8% of variation) suggesting that these four samples may represent outliers. Since the number of samples in the RNA-seq run was small (n=3) these samples were retained in downstream analyses as it was considered that loss of power would be larger with two samples than with the inclusion of outliers. An additional PCA was performed on samples excluding the outlier (Figure 6-15B) to determine whether sample clustering based on vaccination or lineage stimulation could be identified. In the absence of the four outliers, the second largest variation in the dataset (5%) was defined by vaccination. Within each vaccination cluster, separation by lineage stimulation can also be seen, particularly in the BCG s.c. lung.

To identify potential correlates of mycobacterial growth inhibition, differential expression analysis focused on genes identified as up- or downregulated in BCG-vaccinated lung cells versus lung cells from unvaccinated mice following *ex vivo* stimulation with lineage 1, 2 and 4 of the MTB complex. Following *ex vivo* stimulation with L1, 346 and 144 genes were found to be significantly ($p_{adj}<0.05$) up- and downregulated in lung cells from mice vaccinated with BCG s.c., respectively. Following *ex vivo* stimulation with L2, 126 and 39 genes were found to be significantly ($p_{adj}<0.05$) up- and downregulated in lung cells from mice vaccinated with BCG s.c., respectively. Following *ex vivo* stimulation with L4, 319 and 127 genes were found to be significantly ($p_{adj}<0.05$) up- and downregulated in lung cells from mice vaccinated with BCG s.c., respectively. Venn diagrams in Figure 6-16 depict the number of genes identified to be significantly ($p_{adj}<0.05$) up- or downregulated by an LFC of 1/-1 (equal to a 2-fold increase or 0.5-fold decrease in gene expression) under these conditions. A list of the up- and downregulated genes depicted in each intersection of the Venn diagrams is provided in Appendix 8 and 9, respectively.

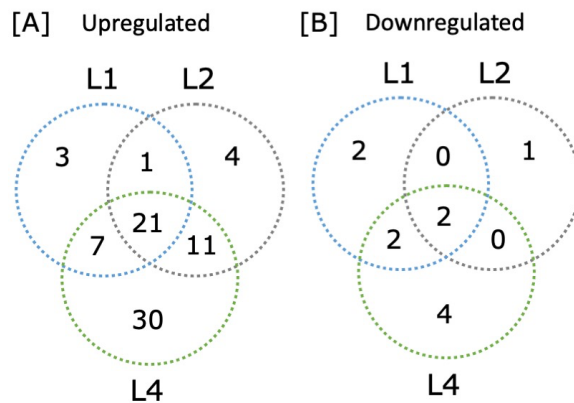


Figure 6-16. Venn diagrams – RNA-seq II. Venn diagrams visualising the relationship between genes identified as significantly ($p_{adj} < 0.05$) [A] up- ($LFC = 1$) or [B] downregulated ($LFC = -1$) in lung cells from BCG s.c. vaccinated mice versus unvaccinated mice stimulated *ex vivo* with MTB L1, L2 or L4. BCG, Bacille Calmette–Guérin; LFC, \log_2 fold change; L, lineage; MTB, *Mycobacterium tuberculosis*; p_{adj} , adjusted p value; s.c., subcutaneous.

Again, to determine whether gene perturbation was associated with a defined biological process or pathway, tmod analysis was performed using the 38 murine lung transcriptional modules [422] in the manner reported for the previous RNA-seq run (Figure 6-17).

Focusing on validation of the baseline comparison made between the BCG s.c. and control lung six weeks following vaccination in the previous RNA-seq run, enrichment of modules dominated by macrophage-, granulocyte-, and myeloid-specific genes were again found (modules 3, 13 and 14), as well as module 7 (*Ifng/Stat1/Gbp/Antigen* presentation). Enrichment of genes associated with Type I IFN/*Ifit/Oas* (module 5), as well as NK cells and cytotoxicity (modules 35 and 36) were confirmed in this dataset, with enrichment in module 36 again appearing to be unique to

unstimulated BCG s.c. lung cells. Enrichment of module 37 (B & T cells/Myeloid cells), which had not been identified in the previous dataset, was also observed.

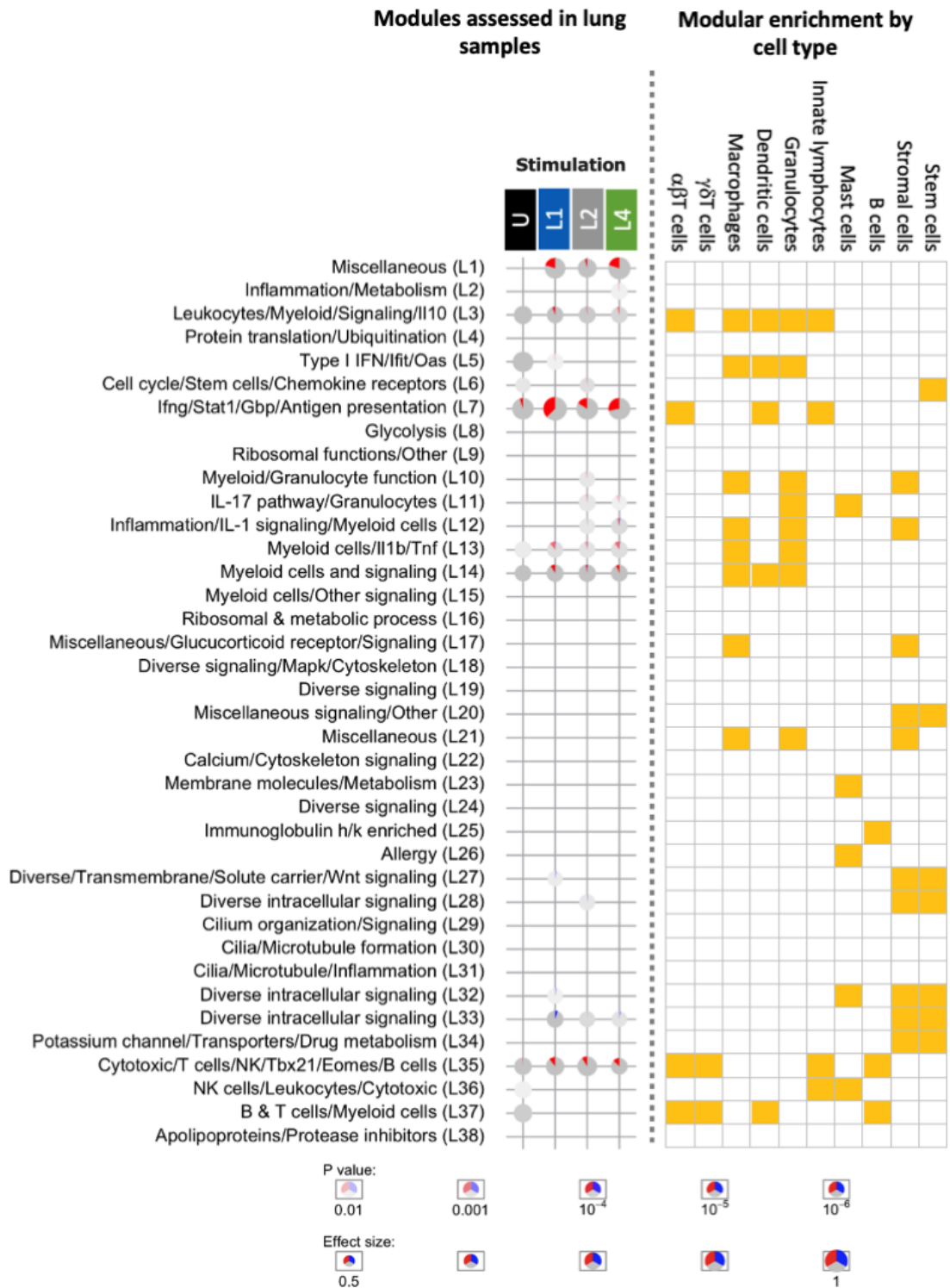


Figure 6-17. tmod analysis – RNA-seq II. Left – tmodPanelPlot visualising enrichment in defined murine lung modules for DEGs in BCG-vaccinated lung versus control.

Results for unstimulated (U) and MTB-stimulated (L1, L2 or L4) *ex vivo* culture conditions are shown. Modules found to be significantly enriched ($\text{padj} < 0.01$) are indicated by a grey circle (pie), with the degree of significance indicated by colour intensity and the effect size (AUROC) indicated by size. The proportion of individual genes within each module found to be significantly ($\text{padj} < 0.05$) up- or downregulated are marked in each pie in red or blue respectively. Right panel – a simplified reproduction of the immune cell populations reported to be associated with each module by Singhania *et al.* AUROC, area under the receiver operating curve; BCG, Bacille Calmette–Guérin; DEGs, differentially expressed genes; L, lineage; LFC, \log_2 fold change; MTB, *Mycobacterium tuberculosis*; padj , adjusted p value; PCA, principal component analysis; U, unstimulated.

Across the three MTB lineages, *ex vivo* stimulation was associated with enrichment of modules 1, 3, 7, 13, 14 and 35 in BCG s.c. lung cells compared with control. These modules were also enriched following *ex vivo* BCG-stimulation (Figure 6-9). Despite enrichment observed in all three lineages, variations in the number of significantly ($\text{padj} < 0.05$) enriched genes within the modules themselves were found, as indicated by the red/blue sections of the pies.

A number of modules were enriched in the BCG-vaccinated lung following stimulation with one lineage only. *Ex vivo* stimulation of BCG-vaccinated lung cells with L1 was uniquely associated with perturbation of genes enriched in Type I IFN/Ifit/Oas (module 5) and two modules associated with cell signalling (modules 27 and 32). L2 stimulation was associated with Cell cycle/Stem cells/Chemokine receptors (module 6), Myeloid/Granulocyte function (module 10) and an intracellular signalling module (module 28). A module related to inflammation and metabolism (module 2) was unique to L4 stimulation. Together, L2 and L4 were associated with enrichment of genes in granulocyte-related modules 11 and 12, annotated as IL-17 pathway/granulocytes and Inflammation/IL-1 signalling/Myeloid cells, respectively.

6.5 Discussion

In the absence of a comprehensive understanding of the determinants of long-term vaccine-induced protection against TB, vaccine development remains time consuming, financially risky and ultimately unattractive to investment. Studies testing vaccine performance against multiple clinical strains indicate that a current limitation in the use of animal models may lie in a historical reliance on vaccine testing against single laboratory strains of MTB, emphasising that vaccines must be tested preclinically against strains representative of the global diversity of the MTB complex [122,354]. In addition, analysis of potential variations in the mechanisms by which vaccines mediate protection against diverse strains must be performed early during vaccine development.

A robust CoP against TB has yet to be identified; however, an increasing awareness of the complexity of the immune response to TB indicates that candidate CoP are likely to represent a context-dependent combination of biological parameters, rather than a numerical readout of a single marker [463]. The complex landscape in which a CoP may be identified lends itself well to unbiased genome-wide analysis approaches such as RNA-seq. Despite a considerable reduction in the cost of sequencing in the last decade, these techniques remain comparatively high cost compared with immunological assays traditionally performed alongside *in vivo* infection studies.

The *ex vivo* MGIA is a low-cost, versatile tool, which may be used prior to and alongside *in vivo* studies, to improve and expand preclinical evaluation of TB vaccines. In this chapter, the murine MGIA was performed in tandem with RNA-seq and flow cytometry to determine the biological mechanisms modelled by the *ex vivo* MGIA and how these compare with *in vivo* studies. More broadly we aimed to establish an *ex vivo* platform with the future potential to generate preliminary vaccine-induced growth

inhibition data for representative strains of the MTB complex, in combination with unbiased mechanistic insight into vaccine-mediated mycobacterial growth regulation.

Flow cytometry and RNA-seq were used to analyse the baseline immune cell composition and transcriptome of lung cells used as input in the MGIA (unstimulated). Transcriptional perturbation following *ex vivo* overnight co-culture of lung cells with BCG (stimulated) was also determined by RNA-seq. BCG was used as a surrogate of MTB in this analysis. For each stimulation condition, DEGs between control and vaccinated mice were identified as potential correlates of growth inhibition. Following identification of DEGs, module enrichment analysis was performed using murine lung transcriptional modules generated by Singhania *et al* [422] to determine whether condition-specific gene perturbation was associated with a defined biological process or pathway.

Flow cytometric analysis of the cell composition of the murine host input in the MGIA identified perturbations in several cell populations in vaccinated groups in which mycobacterial growth inhibition was observed. Two panels were utilised in the project: panel I – characterisation of nine immune cell populations (lung MGIA input only); panel II – characterisation of five immune cell populations (lung and spleen MGIA input).

Indicative of a role for immune cell types of the innate arm of the immune system in mycobacterial control in the MGIA, an enhanced proportion of NK cells and DCs was found in the population generated from the lungs of BCG s.c. vaccinated mice compared with the population obtained from naïve mice. By contrast, in the population generated from lungs of BCG i.n. vaccinated mice perturbations in cell populations were indicative of a role for both adaptive and innate immune cells. An enhanced proportion of T cells, B cells and DCs was found in the MGIA input generated from BCG i.n. vaccinated mice compared with naïve. Further, a shift in the MΦ population was found in which an

enhanced proportion of IM Φ was noted, concomitant with a decreased proportion of AM Φ .

The spleen MGIA composition was also evaluated by flow cytometry, albeit using a panel targeting a smaller number of immune cell phenotypes (T cells, B cells, NK cells, neutrophils, and monocytes and M Φ). This panel was also used to analyse the lung cell population, demonstrating that MGIA inputs generated from both the lung and the spleen include substantial B and T cell populations, particularly in the spleen where these populations comprise between 87 and 95% of the total live cell population. In the lung, B and T cells comprised between 46 and 72% of the total live cell population. Of the immune cell populations analysed, no significant differences between the composition of the splenocyte input from BCG s.c. vaccinated and naïve mice were found. This may be due to the following: i) markers able to identify cell populations which drive growth inhibition in this population were absent in the limited panel used to analyse the splenocyte inputs; and/or ii) mechanisms of growth inhibition are more subtle than changes in the proportion of broadly defined immune cell populations. Consistent with the lung cell population from BCG i.n. vaccinated mice, the proportion of B cells was also enhanced in the splenocyte population. By contrast, the T cell population in the spleen of i.n. vaccinated mice was significantly reduced compared with naïve animals, and may be indicative of recruitment of systemic T-cell populations to the lung mucosa at the site of BCG infection.

Concomitant with mycobacterial growth inhibition observed in co-cultures with lung cells obtained from mice vaccinated with BCG s.c. or i.n., enrichment of genes associated with myeloid cells (modules 3 and 12–15), granulocytes (modules 10 and 11), IL-1b and IL-1 (modules 12 and 13), IFN γ (module 7), IL-17 (module 11) and type I IFNs (module 5) were identified in the vaccinated lung cells compared with control cells.

The type I IFN module (module 5) includes genes associated with innate immune responses, and classical interferon-stimulated genes (ISGs), such as IFNB1, IFIT1 and 3, OAS1A, 2 and 3, OASL1 and 2, MX1, STAT2, and IRF7 and 9. The type II IFN γ -inducible module (module 7) includes IFN γ , IRF1, 2 and 8, and other downstream targets IL-12RB1 and 2, TAP1 and 2, and genes associated with APC function such as H2-MHC molecules, and host defence, such as guanylate binding proteins [422]. The role of type I IFNs in TB is controversial. Type I IFNs are often associated with pathogenesis during infection with hypervirulent strains in humans and the experimental mouse model [339,464–467], and type I IFN-inducible genes feature in a number of human blood diagnostic and risk biosignatures of TB [468–471]. By contrast, and consistent with observations in the current study, protective roles for type I IFNs have been demonstrated in mice infected with avirulent mycobacteria such as BCG, *M avium* and *M smegmatis* [472–474]. Further, type I IFNs have been shown to induce differentiation and activation of DCs in humans and mice [475] which may account for the observed increase in DCs in the BCG s.c. and i.n. vaccinated lung by flow cytometry.

Again, in agreement with flow cytometric analysis (Figure 6-3), enrichment of genes associated with cytotoxicity and NK cells (modules 35 and 36) were also identified in the vaccinated lung. Of note, enrichment of module 36 (NK cells/Leukocytes/Cytotoxic) was unique to unstimulated BCG s.c. lung cells and was not identified under any other conditions. Analysis of module 35 and 36 gene lists using enrichR [476] did not provide clarification on functional differences between the two modules. However, modules were annotated by Singhania *et al* using a publicly available RNA-seq dataset in which transcriptional analysis of ten separate immune cell populations had been performed. Genes in module 35 were identified to be upregulated (LFC >1 and padj <0.05) in both $\alpha\beta$ and $\gamma\delta$ T cells, ILCs and B cells; genes in module

36 were upregulated in ILCs and mast cells [422]. A role for NK cells during the protective immune response to MTB infection has been described previously and NK cells have been shown to exhibit adaptive features of innate immunity to MTB in humans and the mouse model [477–480]. Further, an interplay between DCs and NK cells has been demonstrated in mice in response to viral and bacterial pathogens [481]. In vaccination studies in the mouse model, the NK cell population in the lung prior to *in vivo* challenge has not been analysed to date.

Since the second RNA-seq run also included analysis of unstimulated control and BCG s.c. lung cells six weeks following vaccination we were able to validate these observations (Figure 6-17). Due to an outlier sample in the BCG s.c. group, a degree of power was lost in this run, however, enrichment of genes associated with type I IFN (module 5), NK cells and cytotoxicity (modules 35 and 36), IFN γ (module 7) and myeloid cells (modules 3, 13 and 14) were identified again in this group.

The majority of modules identified as enriched in the unstimulated BCG s.c. lung cells were also enriched following *ex vivo* stimulation with BCG. However, following stimulation the number of genes significantly up- or downregulated was higher than at baseline and may reflect expansion of populations generated by vaccination in response to *ex vivo* infection. We hypothesise that the ability of lung cells from BCG s.c. vaccinated mice to inhibit mycobacterial growth that we have demonstrated is indicative of *in vivo* changes in the lung prior to takedown and are reflected in the perturbation found at baseline in these cells. Changes identified in the immune cell population and the transcriptome compared with lung cells from control mice may represent a continued immune response to a low level of BCG present in the organ, or a degree of lung-resident immune memory in response to dissemination of BCG following vaccination [482,483].

Focusing on modular enrichment specific to *ex vivo* stimulation with BCG, enrichment of genes associated with a glycolysis module (module 8) was identified following *ex vivo* BCG stimulation in both BCG-vaccinated groups. Human [484] and murine [485] macrophages have been shown to induce metabolic reprogramming as a basic defence mechanism to infection with mycobacteria, shifting metabolism of glucose from oxidative phosphorylation to aerobic glycolysis. This shift has also been shown to induce IL-1 β and is required for control of intracellular mycobacterial replication [484]. In the current enrichment analysis this effect may be demonstrated by a concomitant enrichment of modules 12 and 13 (annotated as IL-1b and IL-1, respectively) and module 8. Metabolically distinct states within AM Φ s and IM Φ s have been shown to affect mycobacterial growth. Upregulation of fatty acid oxidation in AM Φ s has been found to provide a nutrient source for MTB and facilitate MTB Erdman replication. By contrast, replication in IM Φ s was restricted by high levels of glycolysis in this M Φ population [486]. Although not significant in the BCG s.c. lung, in both vaccinated groups, a decreased AM Φ population, concomitant with an increased IM Φ population, was identified by flow cytometry six weeks following vaccination and may account for the glycolysis signal following infection with BCG. However, this hypothesis requires further verification since a glycolysis signal in the BCG-vaccinated lung was not observed following infection with any of the MTB lineage strains.

The ongoing ‘infection’ of residual BCG in the BCG i.n. cells rendered analysis of both the unstimulated and stimulated transcriptome by this study design less informative than for the BCG s.c. group. When gene expression in the BCG-vaccinated lung was compared with control to identify changes which correlate with growth inhibition, enrichment in the unstimulated and stimulated conditions was very similar (Figure 6-9). *Ex vivo* stimulation of BCG i.n. lung cells at the six-week time point appears

to predominantly induce higher levels of the same gene perturbation observed in unstimulated BCG i.n. lung cells. However, an Inflammation/Metabolism module (module 2) was uniquely enriched following *ex vivo* stimulation in this group.

In addition to identification of transcriptional perturbation which correlates with growth inhibition observed in the MGIA, results were compared with an *in vivo* challenge study of similar design (modular enrichment results for the RNA-seq I and microarray datasets are shown together in Table 6-1 to facilitate comparison). Modular analysis using the Singhanian murine lung modules was performed on a mouse microarray dataset from a murine *M bovis* challenge study performed by Aranday-Cortes *et al* which included an unvaccinated and BCG Danish s.c. vaccinated group challenged six weeks following immunisation [418] (Figure 6-12).

In the Aranday-Cortes study, RNA was not extracted directly from tissue. Instead lungs were enzymatically digested and mashed to single cell suspensions prior to RNA extraction. Therefore, the pre-infection time point is a replicate dataset to our own unstimulated lung cells from control and BCG s.c. vaccinated mice. In contrast to our own dataset, no module enrichment was found in the lung when comparing gene expression in the BCG-vaccinated group with the control group six-weeks following vaccination. Since we have reproduced our own findings which demonstrate gene perturbation in unstimulated cells (Figure 6-17), inconsistencies may be due to RNA quality (Aranday-Cortes RIN 6.8–9.5; standard RIN for transcriptome analysis >8), choice of platform to perform transcriptional analysis and choice of tool to model differential analysis. RNA-seq has a superior ability to detect low abundance transcripts and differences in expression of these transcripts under conditions of interest compared with microarrays [487] and is not limited by preselected probe sets. The RNA-seq and microarray datasets both have small sample sizes (<5). DEA of the RNA-seq datasets was

performed using DESeq2, a method specifically selected for its superior sensitivity to other analysis methods when handling small sample sets [409,410]; by contrast the microarray dataset was analysed using the Limma method which although recognised as a high performing tool for analysis of microarray datasets [488], is not specifically suited to smaller data sets and therefore may be less sensitive.

Module enrichment was identified in the BCG-vaccinated group 3- and 14-days post *M bovis* infection. Validating a number of our own observations following *ex vivo* stimulation with BCG, BCG-mediated protection in the *in vivo* study was found to correlate with enrichment of genes associated with Cell cycle/Stem cells/Chemokine receptors (module 6), Ifng/Stat1/Gbp/Antigen presentation (module 7), Il-17 pathway/Granulocytes (module 11) and cytotoxic/T cells/NK/Tbx21/Eomes/B cells (module 35) at both time points; as well as Leukocytes/Myeloid/Signalling/Il10 (module 3), Type I IFN/Ifit/Oas (module 5) and Myeloid cells and signalling (module 14) 14-days post-infection. Of note, a number of modules identified to be enriched in the *in vivo* dataset in the BCG s.c.-vaccinated lung following infection were only identified in our own dataset in the BCG i.n. lung (modules 17, 20, 27, 28 and 32–34) and may be indicative of biological processes in the lung in response to mycobacterial presence which require recruitment of cells from outside of the lung.

Where correlates of growth inhibition were identified in part I of the study using BCG as a surrogate for virulent MTB, in part II of the study, an RNA-seq run was performed using murine lung cells from BCG s.c. vaccinated and unvaccinated mice and three MTB clinical isolates used in the MGIA in Chapter 5. L1 (N0072), an ancient MTB lineage, and two modern lineages, L2 (N0052) and L4 (N1283), were selected. The aim of this analysis was to compare gene perturbation in the BCG-vaccinated lung in response

to *ex vivo* stimulation with different lineages of MTB, as a correlate of growth inhibition observed in the MGIA.

Lineage-specific growth kinetics, virulence, disease presentation, and induction of innate and adaptive immune responses have been reported in human and animal studies on infection. Compared with ancient MTB strains, modern lineage strains induce a reduced and delayed proinflammatory response to infection, as well as increased pathogenicity in the mouse model [26,333,334,336,339,344,441]. Evaluation of vaccine-induced protection has been tested against different strains of MTB [24,122,349,353,354], however, to the best of our knowledge, comparative analysis of the mechanisms mediating vaccine-induced protection against different strains has not been performed.

Comparison of gene perturbation identified in the BCG-vaccinated lung following *ex vivo* stimulation with MTB clinical isolates revealed a proportion of genes up- or downregulated under all stimulated conditions. Gene perturbation associated with myeloid cells (modules 3, 13 and 14), *Ifng/Stat1/Gbp/Antigen presentation* (module 7) and *Cytotoxic/T cells/NK/Tbx21/Eomes/B cells* (module 35) was found to correlate with growth inhibition of the three lineages by BCG-vaccinated lung cells. These modules were also found to be enriched in the BCG-vaccinated lung following *ex vivo* stimulation with BCG.

A number of modules were found to be enriched in specific lineages only, indicative of potential variations in the mechanisms by which BCG mediates protection against different lineages. Gene enrichment in the *Type I IFN/Ifit/Oas* (module 5) was identified in BCG-vaccinated lung cells following *ex vivo* stimulation with L1 only. In RNA-seq run I and the *in vivo* infection dataset, enrichment of this module was found to correlate with growth inhibition of BCG by BCG-vaccinated lung cells and with *in vivo* protection in the lung against *M bovis*. As described, a protective role for type I IFNs

against avirulent mycobacteria [472–474] has been described in mice. By contrast, hypervirulence of the Beijing strain, HN878, has been hypothesised to be associated with failure to stimulate T_H1 immunity as a result of increased induction of type I IFNs [339]. Ancient lineages of the MTB complex are generally considered to be less virulent than modern lineages [317,333,339] and type I IFNs may therefore also play a protective role against L1 MTB strains as observed for avirulent strains. The gene perturbation underlying enrichment of this module should be explored further to determine its value in BCG-mediated protection against this lineage. Should a protective role for type I IFNs be identified, a review of the value of human blood diagnostic and risk biosignatures of TB which include ISG transcripts should be considered for individuals infected with L1. Further, the role of type I IFNs in protection against other ancient MTB complex lineages such as L5–7 should also be examined.

Enrichment of genes associated with IL-17 pathway/Granulocytes (module 11) and Inflammation/IL-1 signalling/Myeloid cells (module 12) was also identified in BCG-vaccinated lung cells following *ex vivo* stimulation with the two modern MTB strains only. In the mouse model, Gopal *et al* previously identified that early protective immunity against the hypervirulent Beijing MTB strain, HN878, is driven by high levels of IL-17 induced by production of IL-1 β via a TLR2-dependent mechanism. IL-17 was found to be disposable for protection against less virulent laboratory strains such as H37Rv and CDC1550 (both L4), however, non-laboratory L4 strains or strains representative of other MTB lineages were not tested [63].

6.5.1 Limitations and future studies

Observations made in this analysis represent a starting point for design of more targeted downstream analyses which evaluate the importance of specific components of the immune system on protection against TB.

An extensive analysis of the cell composition of C57Bl/6JN lung by FACS and scRNA-seq was previously reported by the Tabula Muris Consortium [489]. Using both methods, >50% of the cell composition of the murine lung was identified as CD45⁻, including stromal cells, type II pneumocytes, endothelial cells and ciliated columnar cell of tracheobronchial tree (supplementary table 1 [489]). The considerable difference between the cell composition of the lung MGIA input reported in this thesis (in which approximately 76% of cells were identified as CD45⁺ by flow cytometry [panel I] in the lung cell population generated from a naïve C57BL/6 mouse), and the Tabula Muris Consortium publication may be caused by the following: i) substantial blood contamination in the lung MGIA input despite lysis of RBCs using ACK lysis buffer during organ processing and lyse/fix buffer; ii) processing differences which favour immune cells, such as method of dissociation and/or choice of proteolytic enzyme preparations ie thermolysin concentration. As a future study, the degree of blood contamination in the lung cell preparation for the MGIA could be determined by i.v. delivery of an anti-CD45.2 monoclonal antibody immediately prior to organ harvest in order to identify intravascular leukocytes.

To further determine correlates of growth inhibition in the MGIA by flow cytometry, more detailed characterisation of the immune cell populations used in the assay should be performed, as well as analysis of growth inhibition in the MGIA following depletion of specific immune cell populations.

A major limitation of the RNA-seq lineage dataset at present relates to the performance of L1 in the MGIA. The requirement for further optimisation of MGIA using L1 was described in Chapter 5 since, to date, observations on the ability of lung cells from BCG-vaccinated mice to inhibit growth of this lineage have been inconsistent between experimental repeats and with *in vivo* observations. A reduced bacterial burden was detected in the lungs of BCG-vaccinated mice compared with control, five-weeks following i.n. challenge with L1. Since we have not been able to reliably reproduce this outcome in the MGIA, we are currently not able to determine whether transcriptional perturbation identified in BCG-vaccinated lung cells following *ex vivo* stimulation with L1 represents mechanisms of vaccine-induced protection observed following *in vivo* challenge or simply a readout of the unoptimised conditions in the MGIA. To this end, results related to this lineage should be interpreted with caution and validated in future studies.

6.5.2 Conclusions

In this chapter, the *ex vivo* murine lung MGIA was performed in tandem with RNA-seq and flow cytometry to determine the biological mechanisms modelled by the *ex vivo* MGIA and how these compare with *in vivo* studies. Focusing on changes in the immune cell population and transcriptional perturbation identified in the BCG-vaccinated lung only, growth inhibition in the MGIA was found to be associated with both adaptive and innate processes of immunity and varied by vaccine route and MTB strain. A number of processes found to correlate with BCG-mediated growth inhibition in the MGIA were also found to be associated with BCG-induced protection in an *in vivo* dataset of similar design. These observations demonstrate that the MGIA may represent a simplified model

of *in vivo* infection and should be optimised further to expediate and diversify preclinical TB vaccine testing, as well as improve design of downstream *in vivo* studies.

7 Final discussion and conclusions

7.1 Final discussion

At present, candidate TB vaccines are tested in animal models in *in vivo* infection studies against a limited and largely homogeneous set of MTB strains. Three MTB strains, passaged for decades in the laboratory, are overwhelmingly favoured for these studies and all belong to a single lineage of the nine known lineages of the MTB complex [22]. To this end, the evidence for vaccine protection gained from studies of this design is likely to be incomplete.

The historical reliance on these laboratory strains stems in part from a previously underappreciated awareness of genetic diversity within the MTB complex and its impact on host–pathogen interactions. Further, a sufficiently powered MTB challenge study, in which vaccine performance is evaluated against multiple MTB strains, would require an ethically and financially unfeasible number of animals (an example of a sufficiently powered study design is provided in Table 5-1). To this end, novel tools able to incorporate the diversity of the MTB complex into vaccine evaluation at early stages of development are urgently required. When developing these tools, suitability for resource-poor settings and improvements in animal welfare must be considered and prioritised.

The MGIA has been proposed as an ‘*ex vivo* challenge model’, generating a readout of the summative capacity of a mixed population of *ex vivo* derived host cells to control mycobacterial growth following vaccination. Modern MGIA's utilise the ‘direct’ method of *ex vivo* culture and murine splenocyte protocols of this design have been published to date [306–308]. Mycobacterial growth inhibition in the murine splenocyte MGIA has been shown to correlate with protection following *in vivo* infection in the lung

and spleen at the group level [306–308]. Mycobacterial growth inhibition observed in the *ex vivo* splenocyte MGIA is hypothesised to represent a readout of established systemic immunity. An increasing recognition of the need for establishment of anti-mycobacterial immunity at the lung mucosa in advance of MTB infection has led to an expansion of research into mucosal immunity. Concomitant with this interest, tools to evaluate mucosal immunity are required. The adaptation of the murine splenocyte MGIA protocol for use with lung cells represents a viable method by which mucosal immunity may be evaluated following vaccination. Further, with optimisation for larger scale use with BSL3 mycobacterial species, the optimised splenocyte and lung MGIA may represent a lower cost, ethically sustainable platform to expand systemic and mucosal evaluation of TB vaccines against multiple clinical isolates of the MTB complex.

In the project described in this thesis, an optimised murine spleen and lung cell MGIA was established to generate a platform in which vaccine-mediated mycobacterial control could be evaluated using a reference set of clinical isolates representative of the global diversity of the MTB complex. In tandem with the MGIA, flow cytometry and RNA-seq analysis were performed to identify biological correlates of growth inhibition in the MGIA.

The first objective of this thesis was to establish a murine lung MGIA able to detect vaccine-induced mycobacterial growth inhibition. The existing splenocyte MGIA protocol published by Zelmer *et al* [306] was optimised for use in multi-well plates and adapted for murine lung cells in Chapter 4. General optimisation steps were performed for both the murine splenocyte and lung MGIA, including i) performance of the 96-hour co-culture step in 48-well static plates instead of rotating screw-capped tubes, and ii) host cell pooling within groups.

Transition from rotating tubes to static plates was driven by the downstream aim to expand the MGIA for use with multiple strains. The laboratory space in the BSL3 facility was predicted to restrict this expansion should the use of tubes be retained. Further, static plates were considered a safer alternative to rotating tubes when using MTB. Within the MGIA community, a general movement towards use of plates has occurred of late due to the observation that cell viability is lower in tubes [263].

Pooling of host cells within groups is accepted as a limitation but was performed to minimise variability within the assay and enable a reduced number of mice to be used. It was found that by reducing variability, sensitivity to detect differences in growth inhibition between groups was improved using four technical replicates. The MGIA set-up developed during this project represents a starting point to improve the design of downstream experiments. Where results of interest are observed, specific mycobacterial strains and/or vaccine candidates could be evaluated further in the MGIA using biological replicates and/or outbred mouse populations, and further, to improve the design of *in vivo* challenge experiments.

Focusing on the lung MGIA specifically, set-up of this assay was performed alongside the splenocyte MGIA as a positive control of successful murine BCG vaccination, whereby mycobacterial growth inhibition by BCG-vaccinated splenocytes was required. Two routes of BCG administration were included, s.c. and i.n.. Inclusion of i.n. BCG was based on the hypothesis that it may function as a positive control for vaccine-induced growth inhibition in the lung assay specifically. During assay set-up it was unclear whether s.c. BCG would target sufficient anti-mycobacterial immunity to the lung to subsequently inhibit *ex vivo* growth of mycobacteria.

Following optimisation of host cell and bacterial input number, the lung MGIA was able to detect differences in BCG and MTB Erdman growth inhibition between

experimental groups. The lung MGIA represents a simplified model of infection, generating a readout of the immune response to infection in lung cells only. The *ex vivo* nature of the assay provides no opportunity for recruitment from other immune compartments in response to infection, however, lung cells from BCG-vaccinated mice, including animals vaccinated systemically, were able to inhibit growth of mycobacteria when compared with cells from unvaccinated animals.

Residual BCG in the lung six weeks following vaccination was found to mask growth inhibition by BCG-vaccinated lung cells, particularly following i.n. vaccination where approximately $2.9 \log_{10}$ CFU of residual BCG was found six weeks following vaccination. To ensure quantification of MTB only following co-culture with murine lung cells, the BCG inhibitor, TCH, was incorporated into the assay protocol. Vaccine-induced growth inhibition in the lung MGIA was consistent at the group level with *in vivo* protection in the lung reported in published studies. In order for research groups without access to a BACTEC MGIT system to utilise the murine MGIA, plating on solid media was also used to perform mycobacterial quantification alongside the BACTEC system. Mycobacterial growth inhibition was detectable by this method however it was found that variability was higher, rendering the detection of smaller differences in mycobacterial burden unreliable.

In Chapter 5, the established lung MGIA was utilised to evaluate vaccine-mediated growth inhibition against clinical strains selected from a well characterised MTB complex reference set. This reference set is available to researchers from the Belgian Coordinated Collections of Microorganisms. A publicly available reference set was selected to facilitate technology transfer of this assay where required and to enable future inter-laboratory comparisons to be made. Isolates representative of L1–4 of the MTB complex were selected for analysis in this project. Reproducible readouts of growth

inhibition for the three modern lineages (2–4) were obtained using the MGIA across 2–3 experimental repeats, with vaccine-induced growth inhibition found to differ between lineages. By contrast, vaccine-induced growth inhibition of L1, an ancient lineage, was not reproducible.

Next, a direct comparison of *ex vivo* growth inhibition in the lung and spleen MGIA and protection in an *in vivo* MTB challenge study was performed. Due to funding restrictions, only two lineages were included in this analysis. L1 and 2 were selected as a modern and ancient representative of the MTB complex and to further understand the variability observed using L1 *ex vivo*. This was the first time a head-to-head comparison with *in vivo* challenge had been performed for the lung MGIA, as well as the first time a comparison using a non-laboratory strain had been performed in any animal MGIA.

In BCG-vaccinated animals, growth inhibition of L2 in the lung and spleen MGIA was consistent with a reduction in bacterial burden observed in these organs following *in vivo* infection. By contrast, growth inhibition of L1 in the lung and spleen MGIA was not observed in vaccinated animals, inconsistent with a robust reduction in bacterial burden observed following *in vivo* infection. It was noted that replication of L1 in the *ex vivo* co-culture from control animals was comparatively low when compared with L2. In the *in vivo* study, bacterial burden in control animals was not found to be significantly different between L1 and 2. This disparity may be due to the absence of a specific host cell type(s) required for L1 replication in the processed spleen and lung cell population utilised in the MGIA.

Further studies to address this observation are described in Chapter 5 and include use of log phase stocks in the MGIA to confirm that the lack of growth observed over the 96-hour co-culture period is not simply due to a poorly established stock at the start of this project. Further, extension of the MGIA culture period to provide a longer window

of opportunity for vaccine-mediated growth inhibition should be performed. In studies using static plates, a co-culture period of up to 10 days has been reported previously [296,298]. Should results in L1 remain inconsistent under these conditions, phenotypic characterisation of infected host cells in the *ex vivo* culture and *in vivo* using different lineages may reveal distinct host cell niches for specific members of the MTB complex.

In its current form, the *ex vivo* MGIA demonstrates an inconsistent capacity to model *in vivo* protection against different strains of the MTB complex and requires further optimisation. The murine lung and spleen MGIA may represent a valuable tool for use with L2 isolates. This lineage includes the Beijing sub-strain, a strain of particular interest due to its high virulence and global distribution. The L2 isolate used in this project was a Beijing strain. Reproducible *ex vivo* growth inhibition of L3 and 4 was observed in this project suggesting that the MGIA may represent a valuable tool to analyse modern lineages of the MTB complex, however, *in vivo* studies using these lineages must be performed to in order to confirm this hypothesis.

When developing tools to evaluate vaccine-induced protection against diverse strains of the MTB complex it will be important not to initially apply isolate-specific observations across an entire lineage. Within L2 in particular, considerable heterogeneity has been shown in the virulence of strains of this lineage [344], and this heterogeneity may extend to vaccine-induced protection. Low-cost, low-animal input tools such as the MGIA represent a method to address these research questions and to build a representative panel of MTB isolates to be utilised in preclinical vaccine evaluation.

In the final chapter of this thesis (Chapter 6), correlates of growth inhibition in the lung MGIA were analysed by RNA-seq to demonstrate a potential capacity for early mechanistic insight of vaccines against different mycobacterial strains to be ascertained in combination with the MGIA. Phenotypic characterisation of the lung MGIA input was

also performed by flow cytometry with the aim to identify perturbations in immune cell populations which correlate with observed growth inhibition by cells from vaccinated mice using the MGIA. Since the gene expression modules used in this study had been annotated previously using ten distinct immune cell types, a degree of cross comparison between the transcriptome and immune cell population identified by flow cytometry could be performed.

Flow cytometric analysis of the cell composition of the murine host input in the MGIA identified perturbations in several cell populations in vaccinated groups in which mycobacterial growth inhibition was observed. This analysis suggested that growth inhibition by lung cells from mice vaccinated with BCG via the s.c. route may be driven by alterations in innate immune cells, namely DCs and NK cells. Perturbations in the spleen cell population from this group were not identified using the limited panel utilised to analyse these cells. By contrast, in the i.n. vaccinated lung, perturbations in cells of both innate and adaptive immunity were observed and are likely to be representative of the on-going BCG infection in the lungs of mice in this group.

The importance of these immune cell types to mycobacterial growth inhibition observed in these vaccine groups should be evaluated further in future studies through targeted depletion of these cell populations and further assessment of mycobacterial regulation in their absence. Future characterisation of this population would benefit from the inclusion of more detailed T-cell phenotyping, to facilitate comparison with the gene expression data generated in this project. Characterisation of the MGIA host cell composition over the 96-hour culture period by flow cytometry would also provide additional insight into the biological mechanisms mediating growth inhibition.

Variations in the transcriptome of processed lung MGIA input obtained from unvaccinated, BCG s.c. vaccinated and BCG i.n. vaccinated mice six weeks following

vaccination were identified, a number of which were consistent with previously described roles in mycobacterial control. Consistent with growth inhibition observed following s.c. or i.n. BCG vaccination, enrichment of genes associated with myeloid cells, granulocytes, IL-1, IFN γ , IL-17, type I IFNs, and cytotoxic T and NK cells were identified by RNA-seq in vaccinated lung cells compared with control cells. A number of these observations were consistent with the flow cytometric analysis also performed on the lung MGIA input and are discussed further in Chapter 6. Since the second RNA-seq run performed in this study included analysis of the transcriptome of BCG s.c. vaccinated lung cells at the same time point, validation of a number of enriched modules was possible.

RNA-seq analysis was also performed on *ex vivo* lung cells stimulated overnight with BCG with the aim to identify gene perturbations which correlate with *ex vivo* growth inhibition. Further, a published murine microarray dataset in which a BCG-vaccinated and unvaccinated group were intranasally challenged with *M bovis* was re-processed and analysed using the same lung module set used for the RNA-seq data in the current project. The dataset included a vaccinated and unvaccinated group with lung cells processed at three time points: 6-weeks post-vaccination, and 3- and 14-days post-infection. The aim of this reanalysis was to determine whether modular enrichment found to correlate with *ex vivo* growth inhibition in the BCG-vaccinated lung was also representative of *in vivo* infection. As described in Chapter 6, the microarray dataset appeared to exhibit a higher level of sample variation which may have resulted in loss of sensitivity to detect some of the more subtle changes found by RNA-seq. For example, at the six-weeks post-vaccination timepoint in the microarray (a matched timepoint to the ‘unstimulated’ samples in the RNA-seq study), no modular enrichment was found. However, following *in vivo* infection, modular enrichment was found, including a number of processes also identified to correlate with BCG-mediated growth inhibition in the MGIA. This

observation provides early indication that the *ex vivo* MGIA recapitulates some of the protective processes observed in *in vivo* studies. However, it was also noted that a proportion of the modules found to be enriched in the *in vivo* dataset following infection were only identified in the RNA-seq dataset in the BCG i.n. lung. They were not observed following *ex vivo* stimulation of BCG s.c. vaccinated lung cells. This observation may reflect biological processes in the lung in response to mycobacterial presence which require recruitment of cells from outside of the lung. Since a high level of residual BCG was found in the lungs six weeks following i.n. BCG vaccination, these cells may have already been recruited to the lung prior to animal culling and organ processing. By contrast, following BCG s.c. vaccination, installation of mucosal immunity prior to infection is known to be weakly induced [133], and therefore the immune cell population processed from animals vaccinated systemically with BCG would be unlikely to fully recapitulate transcriptional perturbation following *in vivo* infection. Since this comparison was made between two separate gene expression datasets, these preliminary observations require further confirmation by direct comparison of the transcriptome of lung tissue processed from animals infected *in vivo* and lung cells stimulated *ex vivo*.

To the best of our knowledge, comparative analysis of the mechanisms mediating vaccine-induced protection against different strains of MTB has not been performed. In this study we identified common and lineage-specific transcriptional correlates of growth inhibition in the MGIA which warrant further validation *in vivo*. Variations in correlates of growth inhibition in this analysis emphasise that it may be important to phenotype circulating strains when defining novel CoP in placebo-controlled clinical vaccine trials, since CoP may demonstrate lineage or sublineage specificity.

In BCG-vaccinated lung cells, genes associated with a number of murine lung modules were found to be consistently enriched across all three lineages. These included modules associated with myeloid cells, IFN γ signalling, and cytotoxic T and NK cells.

Focusing on lineage-specific perturbation, enrichment of genes associated with IL-17 and IL-1 signalling were found to correlate with vaccine-induced growth inhibition of modern lineages, L2 and L4. This observation may be consistent with a previous report in which IL-17 and IL-1 were found to play important roles in early protection against emerging hypervirulent MTB isolates. In the report, this role was demonstrated using the hypervirulent HN878 L2 Beijing strain. IL-17 signalling was found to be dispensable in strains of lower virulence or lab-adapted strains [63]. As is currently common in studies which describe use of strains representing multiple lineages, the L4 strains used in this study were the laboratory strains, CDC1551 and H37Rv. Since these laboratory strains are considered to be less virulent than clinical isolates, it is difficult to draw conclusions in relation to the L4 clinical isolate used in the current study with respect to its requirement for IL-17 signalling.

Consistent with observations made in the BCG-vaccinated lung following co-culture with BCG and *in vivo* infection with *M bovis*, enrichment of genes associated with type I IFN signalling was found in BCG-vaccinated lung cells following co-culture with L1 only. In Chapter 6, the protective role of type I IFN signalling reported for avirulent mycobacterial strains such as *M bovis*, *M smegmatis* and BCG is described. We hypothesise that type I IFN signalling may also play a protective role against infection with L1 and discuss the implications this may have on specific TB biosignatures of risk and diagnosis currently in development which include ISG transcripts. However, observations made in relation to L1 do require further exploration and validation. *Ex vivo* growth inhibition of L1 by BCG-vaccinated lung cells was not consistently demonstrated;

however robust *in vivo* protection against L1 was demonstrated in BCG-vaccinated mice. It is not currently clear whether transcriptional perturbations identified in the BCG-vaccinated lung following overnight *ex vivo* co-culture with L1 correlate with presence or absence of mycobacterial control. The future MGIA studies outlined to understand the inconsistent performance of BCG-vaccinated murine cells to control growth of L1 will hopefully provide clarity to the meaning of this signal.

7.2 Conclusions

This thesis demonstrates the adaptation and optimisation of the murine MGIA for use with lung cells, to facilitate early head-to-head screening of vaccine-induced immunity at the lung mucosa using a reduced number of animals and procedure severity.

Further, the murine lung MGIA was used to determine BCG-induced growth inhibition against multiple clinical isolates. Growth inhibition of three isolates representative of the modern MTB lineages was reproducible across experimental repeats. Results to date using ancient MTB L1 have not been reproducible and require further evaluation. In addition, head-to-head comparison of the performance of the MGIA against *in vivo* infection was carried out for the first time using two clinical isolates. A correlation between *ex vivo* growth inhibition and *in vivo* protection was observed at the group level in the lung and spleen for L2 only. Observations made in this project indicate that the MGIA in its current form may represent a valuable tool to evaluate vaccine protection against modern lineages of MTB, the most prevalent lineages globally. Further optimisation for use with ancient lineages is required.

Lastly, evaluation of the biological processes underlying growth inhibition by two routes of BCG vaccination and against three MTB clinical isolates was performed by RNA-seq. Vaccine-specific and lineage-specific gene perturbations were found to

correlate with growth inhibition, emphasising the importance of expanding TB vaccine testing and the concomitant identification of preclinical CoP beyond single, arguably unrepresentative, laboratory strains using an unbiased systems biology approach. Comparison of correlates of growth inhibition in the MGIA and protection in an *in vivo* murine dataset revealed that the MGIA is able to recapitulate a number of elements of *in vivo* transcriptional perturbation observed following infection in the murine vaccinated lung.

The MGIA warrants further optimisation and investigation as a simplified model of *in vivo* infection able to expediate and diversify preclinical TB vaccine testing, as well as improve design of downstream *in vivo* studies. From a clinical perspective, a number of candidate TB vaccines are approaching or currently under evaluation in phase-III clinical trials. Determination of vaccine-induced protection against strains less prevalent or absent at sites in which trials have been performed to date will be of high importance to inform future implementation of TB vaccine candidates.

8 References

1. Daniel, V. S. & Daniel, T. M. Old testament biblical references to tuberculosis. *Clin. Infect. Dis.* **29**, 1557–1558 (1999).
2. Barberis, I., Bragazzi, N. L., Galluzzo, L. & Martini, M. The history of tuberculosis: from the first historical records to the isolation of Koch’s bacillus. *J. Prev. Med. Hyg.* **58**, 9–12 (2017).
3. Koch, R. Die Aetiologie der Tuberkulose. *Berliner Klin. Wochenschrift* **15**, 221–230 (1882).
4. Daniel, T. M. The history of tuberculosis. *Respir. Med.* **100**, 1862–1870 (2006).
5. World Health Organization. *Global Tuberculosis Report 2020*. (2020).
6. Nieuwenhuizen, N. E. & Kaufmann, S. H. E. Next-generation vaccines based on Bacille Calmette-Guérin. *Front. Immunol.* **9**, 121 (2018).
7. Pai, M. *et al.* Tuberculosis. *Nat. Rev. Dis. Primers.* **2**, 16076 (2016).
8. Lee, J. Y. Diagnosis and treatment of extrapulmonary tuberculosis. *Tuberc. Respir. Dis. (Seoul)* **78**, 47–55 (2015).
9. Swaminathan, S. & Ramachandran, G. Challenges in childhood tuberculosis. *Clin. Pharmacol. Ther.* **98**, 240–244 (2015).
10. Houben, R. M. G. J. & Dodd, P. J. The global burden of latent tuberculosis infection: a re-estimation using mathematical modelling. *PLoS. Med.* **13**, e1002152 (2016).
11. Behr, M. A., Edelstein, P. H. & Ramakrishnan, L. Revisiting the timetable of

- tuberculosis. *BMJ* **362**, k2738 (2018).
12. Drain, P. K. *et al.* Incipient and subclinical tuberculosis: A clinical review of early stages and progression of infection. *Clin. Microbiol. Rev.* **31**, e00021-18 (2018).
 13. Cadena, A. M., Fortune, S. M. & Flynn, J. L. Heterogeneity in tuberculosis. *Nat. Rev. Immunol.* **17**, 691–702 (2017).
 14. World Health Organization. *Treatment of tuberculosis guidelines: fourth edition.* (2010). doi:10.1016/S0011-5029(56)80012-6.
 15. Conradie, F. *et al.* Treatment of highly drug-resistant pulmonary tuberculosis. *N. Engl. J. Med.* **382**, 893–902 (2020).
 16. Sterling, T. R. *et al.* Guidelines for the treatment of latent tuberculosis infection: Recommendations from the national tuberculosis controllers association and CDC, 2020. *MMWR. Recomm. Reports* **69**, 1–11 (2020).
 17. Gutierrez, M. C. *et al.* Ancient origin and gene mosaicism of the progenitor of *Mycobacterium tuberculosis*. *PLoS. Pathog.* **1**, e5 (2005).
 18. Cardona, P. J., Català, M. & Prats, C. Origin of tuberculosis in the Paleolithic predicts unprecedented population growth and female resistance. *Sci. Rep.* **10**, 1–20 (2020).
 19. Brites, D. *et al.* A new phylogenetic framework for the animal-adapted *Mycobacterium tuberculosis* complex. *Front. Microbiol.* **9**, 2820 (2018).
 20. Coscolla, M. & Gagneux, S. Consequences of genomic diversity in *Mycobacterium tuberculosis*. *Semin. Immunol.* **26**, 431–444 (2014).
 21. Ngabonziza, J. C. S. *et al.* A sister lineage of the *Mycobacterium tuberculosis* complex discovered in the African Great Lakes region. *Nat. Commun.* **11**, 2917 (2020).

22. Coscolla, M. *et al.* Phylogenomics of *Mycobacterium africanum* reveals a new lineage and a complex evolutionary history. *bioRxiv.* **17**, 19 (2020).
23. Borrell, S. *et al.* Reference set of *Mycobacterium tuberculosis* clinical strains: a tool for research and product development. *PLoS. One.* **14**, e0214088 (2019).
24. Pérez, I. *et al.* Live attenuated TB vaccines representing the three modern *Mycobacterium tuberculosis* lineages reveal that the Euro–American genetic background confers optimal vaccine potential. *EBioMedicine.* **55**, 1–10 (2020).
25. Comas, I. *et al.* Out-of-Africa migration and Neolithic coexpansion of *Mycobacterium tuberculosis* with modern humans. *Nat. Genet.* **45**, 1176–1182 (2013).
26. Romagnoli, A. *et al.* Clinical isolates of the modern *Mycobacterium tuberculosis* lineage 4 evade host defense in human macrophages through eluding IL-1 β -induced autophagy article. *Cell. Death. Dis.* **9**, 1–12 (2018).
27. Zumla, A. *et al.* Learning from epidemiological, clinical, and immunological studies on *Mycobacterium africanum* for improving current understanding of host–pathogen interactions, and for the development and evaluation of diagnostics, host-directed therapies, and vaccines for tuberculosis. *Int. J. Infect. Dis.* **56**, 126–129 (2017).
28. Yimer, S. A. *et al.* *Mycobacterium tuberculosis* lineage 7 strains are associated with prolonged patient delay in seeking treatment for pulmonary tuberculosis in Amhara region, Ethiopia. *J. Clin. Microbiol.* **53**, 1301–1309 (2015).
29. O’Garra, A. *et al.* The immune response in tuberculosis. *Annu. Rev. Immunol.* **31**, 475–527 (2013).
30. Ernst, J. D. The immunological life cycle of tuberculosis. *Nat. Rev. Immunol.* **12**, 581–59 (2012).

31. Shaler, C. R., Horvath, C., Lai, R. & Xing, Z. Understanding delayed T-cell priming, lung recruitment, and airway luminal T-cell responses in host defense against pulmonary tuberculosis. *Clin. Dev. Immunol.* **2012**, 628293 (2012).
32. Li, Y., Wang, Y. & Liu, X. The role of airway epithelial cells in response to mycobacteria infection. *Clin. Dev. Immunol.* **2012**, 791392 (2012).
33. Flynn, J. L. & Chan, J. Immunology of tuberculosis. *Annu. Rev. Immunol.* **19**, 93–129 (2001).
34. Bhat, K. H. & Yaseen, I. *Mycobacterium tuberculosis: Macrophage Takeover and Modulation of Innate Effector Responses. Mycobacterium - Research and Development* (2018). doi:10.5772/intechopen.75003.
35. Barker, L. P., George, K. M., Falkow, S. & Small, P. L. C. Differential trafficking of live and dead *Mycobacterium marinum* organisms in macrophages. *Infect. Immun.* **65**, 1497–1504 (1997).
36. Hasan, Z. *et al.* Isolation and characterization of the mycobacterial phagosome: segregation from the endosomal/lysosomal pathway. *Mol. Microbiol.* **24**, 545–53 (1997).
37. Divangahi, M., Desjardins, D., Nunes-Alves, C., Remold, H. G. & Behar, S. M. Eicosanoid pathways regulate adaptive immunity to *Mycobacterium tuberculosis*. *Nat. Immunol.* **11**, 751–8 (2010).
38. Kelly, D. M., Ten Bokum, A. M. C., O’Leary, S. M., O’Sullivan, M. P. & Keane, J. Bystander macrophage apoptosis after *Mycobacterium tuberculosis* H37Ra infection. *Infect. Immun.* **76**, 351–60 (2008).
39. Pai, R. K., Convery, M., Hamilton, T. A., Boom, W. H. & Harding, C. V. Inhibition of IFN- γ -induced class II transactivator expression by a 19-kDa lipoprotein from *Mycobacterium tuberculosis*: a potential mechanism for immune evasion. *J.*

- Immunol.* **171**, 175–184 (2003).
40. Ramakrishnan, L. Revisiting the role of the granuloma in tuberculosis. *Nat. Rev. Immunol.* **12**, 352–66 (2012).
 41. Gehring, A. J., Dobos, K. M., Belisle, J. T., Harding, C. V. & Boom, W. H. *Mycobacterium tuberculosis* LprG (Rv1411c): a novel TLR-2 ligand that inhibits human macrophage class II MHC antigen processing. *J. Immunol.* **173**, 2660–8 (2004).
 42. Pancholi, P., Mirza, A., Bhardwaj, N. & Steinman, R. M. Sequestration from immune CD4⁺ T cells of mycobacteria growing in human macrophages. *Science.* **260**, 984–6 (1993).
 43. D’Agostino, M. R. *et al.* Airway macrophages mediate mucosal vaccine-induced trained innate immunity against *Mycobacterium tuberculosis* in early stages of infection. *J. Immunol.* **205**, 2750–2762 (2020).
 44. Davenne, T. & McShane, H. Why don’t we have an effective tuberculosis vaccine yet? *Expert Rev. Vaccines* **15**, 1009–13. (2016).
 45. Brazier, B. & McShane, H. Towards new TB vaccines. *Semin. Immunopathol.* **42**, 315–331 (2020).
 46. Sable, S. B., Posey, J. E. & Scriba, T. J. Tuberculosis vaccine development: progress in clinical evaluation. *Clin. Microbiol. Rev.* **33**, e00100-19 (2020).
 47. Cohen, S. B. *et al.* Alveolar macrophages provide an early *Mycobacterium tuberculosis* niche and initiate dissemination. *Cell Host Microbe* **24**, 439–446 (2018).
 48. Tian, T., Woodworth, J., Sköld, M. & Behar, S. M. *In vivo* depletion of CD11c⁺ cells delays the CD4⁺ T cell response to *Mycobacterium tuberculosis* and exacerbates the outcome of infection. *J. Immunol.* **175**, 3268–72 (2005).

49. Barber-Mayer, K. D. & Barber, D. L. Innate and adaptive cellular immune responses to *Mycobacterium tuberculosis* infection. *Cold. Spring. Harb. Perspect. Med.* **5**, a018424 (2015).
50. Khader, S. A. *et al.* Interleukin 12p40 is required for dendritic cell migration and T cell priming after *Mycobacterium tuberculosis* infection. *J. Exp. Med.* **203**, 1805–1815 (2006).
51. Wolf, A. J. *et al.* *Mycobacterium tuberculosis* infects dendritic cells with high frequency and impairs their function *in vivo*. *J. Immunol.* **179**, 2509–19 (2007).
52. Wolf, A. J. *et al.* Initiation of the adaptive immune response to *Mycobacterium tuberculosis* depends on antigen production in the local lymph node, not the lungs. *J. Exp. Med.* **205**, 105–15 (2008).
53. Chackerian, A. A., Perera, T. V. & Behar, S. M. Gamma interferon-producing CD4⁺ T lymphocytes in the lung correlate with resistance to infection with *Mycobacterium tuberculosis*. *Infect. Immun.* **69**, 2666–74 (2001).
54. Pawlowski, A., Jansson, M., Sköld, M., Rottenberg, M. E. & Källenius, G. Tuberculosis and HIV co-infection. *PLoS. Pathog.* **8**, e1002464 (2012).
55. Saunders, B. M., Frank, A. A., Orme, I. M. & Cooper, A. M. CD4 is required for the development of a protective granulomatous response to pulmonary tuberculosis. *Cell. Immunol.* **216**, 65–72 (2002).
56. Caruso, A. M. *et al.* Mice deficient in CD4 T cells have only transiently diminished levels of IFN-g, yet succumb to tuberculosis. *J. Immunol.* **162**, 5407–16 (1999).
57. Boisson-Dupuis, S. *et al.* Inherited and acquired immunodeficiencies underlying tuberculosis in childhood. *Immunol. Rev.* **264**, 103–20 (2015).
58. Flynn, J. L. *et al.* An essential role for interferon γ in resistance to *Mycobacterium tuberculosis* infection. *J. Exp. Med.* **178**, 2249–2254 (1993).

59. Macmicking, J. D. *et al.* Identification of nitric oxide synthase as a protective locus against tuberculosis. *Proc. Natl. Acad. Sci. U. S. A.* **94**, 5243–8 (1997).
60. Choi, H. S., Rai, P. R., Chu, H. W., Cool, C. & Chan, E. D. Analysis of nitric oxide synthase and nitrotyrosine expression in human pulmonary tuberculosis. *Am. J. Respir. Crit. Care Med.* **166**, 178–86 (2002).
61. MacMicking, J. D., Taylor, G. A. & McKinney, J. D. Immune control of tuberculosis by IFN- γ -inducible LRG-47. *Science.* **302**, 654–9 (2003).
62. Gutierrez, M. G. *et al.* Autophagy is a defense mechanism inhibiting BCG and *Mycobacterium tuberculosis* survival in infected macrophages. *Cell* **119**, 753–66 (2004).
63. Gopal, R. *et al.* Unexpected role for IL-17 in protective immunity against hypervirulent *Mycobacterium tuberculosis* HN878 infection. *PLoS. Pathog.* **10**, 1004099 (2014).
64. Scriba, T. J. *et al.* Distinct, specific IL-17- and IL-22-producing CD4 + T cell subsets contribute to the human anti-mycobacterial immune response. *J. Immunol.* **180**, 1962–70 (2008).
65. Booty, M. G. *et al.* IL-21 signaling is essential for optimal host resistance against *Mycobacterium tuberculosis* infection. *Sci. Rep.* **6**, 36720 (2016).
66. Khader, S. A. *et al.* IL-23 and IL-17 in the establishment of protective pulmonary CD4+ T cell responses after vaccination and during *Mycobacterium tuberculosis* challenge. *Nat. Immunol.* **8**, 369–377 (2007).
67. Kamath, A. B. *et al.* Cytolytic CD8+ T cells recognizing CFP10 are recruited to the lung after *Mycobacterium tuberculosis* infection. *J. Exp. Med.* **200**, 1479–89 (2004).
68. Serbina, N. V., Liu, C.-C., Scanga, C. A. & Flynn, J. L. CD8 + CTL from lungs of

- Mycobacterium tuberculosis*-infected mice express perforin *in vivo* and lyse infected macrophages. *J. Immunol.* **165**, 353–63 (2000).
69. Chen, C. Y. *et al.* A critical role for CD8 T cells in a nonhuman primate model of tuberculosis. *PLoS Pathog.* **5**, e1000392 (2009).
70. Rothchild, A. C., Jayaraman, P., Nunes-Alves, C. & Behar, S. M. iNKT cell production of GM-CSF controls *Mycobacterium tuberculosis*. *PLoS. Pathog.* **10**, e1003805 (2014).
71. Godfrey, D. I., Uldrich, A. P., Mccluskey, J., Rossjohn, J. & Moody, D. B. The burgeoning family of unconventional T cells. *Nat. Immunol.* **16**, 1114–23 (2015).
72. Orme, I. M., Robinson, R. T. & Cooper, A. M. The balance between protective and pathogenic immune responses in the TB-infected lung. *Nat. Immunol.* **16**, 57–63 (2015).
73. Ardain, A. *et al.* Group 3 innate lymphoid cells mediate early protective immunity against tuberculosis. *Nature.* **570**, 528–532 (2019).
74. Remot, A., Doz, E. & Winter, N. Neutrophils and close relatives in the hypoxic environment of the tuberculous granuloma: New avenues for host-directed therapies? *Front. Immunol.* **10**, 417 (2019).
75. Opie, E. & Aronson, J. Tubercle bacilli in latent tuberculous lesions and in lung tissue without tuberculous lesions. *Arch. Pathol. Lab. Med.* **4**, 1–17 (1927).
76. Guirado, E. & Schlesinger, L. S. Modeling the *Mycobacterium tuberculosis* granuloma - the critical battlefield in host immunity and disease. *Front. Immunol.* **22**, 98 (2013).
77. Burden, N., Chapman, K., Sewell, F. & Robinson, V. Pioneering better science through the 3Rs: an introduction to the national centre for the replacement, refinement, and reduction of animals in research (NC3Rs). *J. Am. Assoc. Lab. Anim.*

- Sci.* **54**, 198–208 (2015).
78. Williams, A. & Orme, I. M. Animal models of tuberculosis: an overview. *Microbiol. Spectr.* **4**, (2016).
79. Cooper, A. M. Mouse model of tuberculosis. *Cold. Spring. Harb. Perspect. Med.* **5**, a018556–a018556 (2014).
80. Tanner, R. & Mcshane, H. Replacing, reducing & refining the use of animals in tuberculosis vaccine research. *ALTEX* **34**, 157–166 (2017).
81. Cardona, P. J. & Williams, A. Experimental animal modelling for TB vaccine development. *Int. J. Infect. Dis.* **56**, 268–273 (2017).
82. Mestas, J. & Hughes, C. C. W. Of mice and not men: differences between mouse and human immunology. *J. Immunol.* **172**, 2731–2738 (2004).
83. Capuano, S. V. *et al.* Experimental *Mycobacterium tuberculosis* infection of cynomolgus macaques closely resembles the various manifestations of human *M. tuberculosis* infection. *Infect. Immun.* **71**, 5831–5844 (2003).
84. Scanga, C. A. *et al.* Depletion of CD4⁺ T cells causes reactivation of murine persistent tuberculosis despite continued expression of interferon γ and nitric oxide synthase 2. *J. Exp. Med.* **192**, 347–358 (2000).
85. Cooper, A. M., Magram, J., Ferrante, J. & Orme, I. M. Interleukin 12 (IL-12) is crucial to the development of protective immunity in mice intravenously infected with *Mycobacterium tuberculosis*. *J. Exp. Med.* **186**, 39–45 (1997).
86. De Jong, R. *et al.* Severe mycobacterial and *Salmonella* infections in interleukin-12 receptor-deficient patients. *Science.* **280**, 1435–1438 (1998).
87. Keane, J. *et al.* Tuberculosis associated with infliximab, a tumor necrosis factor α -neutralizing agent. *N. Engl. J. Med.* **345**, 1098–1104 (2001).

88. Mohan, V. P. *et al.* Effects of tumor necrosis factor alpha on host immune response in chronic persistent tuberculosis: Possible role for limiting pathology. *Infect. Immun.* **69**, 1847–1855 (2001).
89. Hoff, D. R. *et al.* Location of intra- and extracellular *M. tuberculosis* populations in lungs of mice and guinea pigs during disease progression and after drug treatment. *PLoS. One.* **6**, e17550 (2011).
90. Singh, A. K. & Gupta, U. D. Animal models of tuberculosis: lesson learnt. *Indian. J. Med. Res.* **147**, 456–463 (2018).
91. Kramnik, I. & Beamer, G. Mouse models of human TB pathology: roles in the analysis of necrosis and the development of host-directed therapies. *Semin. Immunopathol.* **38**, 221–237 (2016).
92. Medina, E. & North, R. J. Genetically susceptible mice remain proportionally more susceptible to tuberculosis after vaccination. *Immunology.* **96**, 16–21 (1999).
93. Scanga, C. A. *et al.* Reactivation of latent tuberculosis: Variations on the Cornell murine model. *Infect. Immun.* **67**, 4531–4538 (1999).
94. Kupz, A., Zedler, U., Stäber, M. & Kaufmann, S. H. E. A mouse model of latent tuberculosis infection to study intervention strategies to prevent reactivation. *PLoS. One.* **11**, e0158849 (2016).
95. Noll, K. E., Ferris, M. T. & Heise, M. T. The Collaborative Cross: a systems genetics resource for studying host-pathogen interactions. *Cell. Host. Microbe.* **25**, 484–498 (2019).
96. Churchill, G. A., Gatti, D. M., Munger, S. C. & Svenson, K. L. The Diversity Outbred mouse population. *Mamm. Genome.* **23**, 713–718 (2012).
97. Flynn, J. L., Gideon, H. P., Mattila, J. T. & Lin, P. ling. Immunology studies in non-human primate models of tuberculosis. *Immunol. Rev.* **264**, 60–73 (2015).

98. Wareham, A. S. *et al.* Evidence for a role for interleukin-17, Th17 cells and iron homeostasis in protective immunity against tuberculosis in cynomolgus macaques. *PLoS. One.* **9**, e88149 (2014).
99. Langermans, J. A. M. *et al.* Divergent effect of bacillus Calmette-Guérin (BCG) vaccination on *Mycobacterium tuberculosis* infection in highly related macaque species: implications for primate models in tuberculosis vaccine research. *Proc. Natl. Acad. Sci. U. S. A.* **98**, 11497–11502 (2001).
100. Barry, C. E. *et al.* The spectrum of latent tuberculosis: Rethinking the biology and intervention strategies. *Nat. Rev. Microbiol.* **7**, 845–855 (2009).
101. Darrah, P. A. *et al.* Prevention of tuberculosis in macaques after intravenous BCG immunization. *Nature* **577**, 95–102 (2020).
102. Sharpe, S. *et al.* Ultra low dose aerosol challenge with *Mycobacterium tuberculosis* leads to divergent outcomes in rhesus and cynomolgus macaques. *Tuberculosis.* **96**, 1–12 (2016).
103. Dijkman, K. *et al.* Prevention of tuberculosis infection and disease by local BCG in repeatedly exposed rhesus macaques. *Nat. Med.* **25**, 255–262 (2019).
104. Coleman, M. T. *et al.* Early changes by ¹⁸Fluorodeoxyglucose positron emission tomography coregistered with computed tomography predict outcome after *Mycobacterium tuberculosis* infection in cynomolgus macaques. *Infect. Immun.* **82**, 2400–2404 (2014).
105. Chan, M. *Ten years in Public Health 2007-2017.* World Health Organisation (2017).
106. Pepper, M. & Jenkins, M. K. Origins of CD4+ effector and central memory T cells. *Nat. Immunol.* **12**, 467–471 (2011).
107. Khader, S. A. *et al.* Targeting innate immunity for tuberculosis vaccination. *J. Clin.*

- Invest.* **129**, 3482–3491 (2019).
108. Hansen, S. G. *et al.* Prevention of tuberculosis in rhesus macaques by a cytomegalovirus-based vaccine. *Nat. Med.* **24**, 130–143 (2018).
 109. Fine, P. E. M., Carneiro, I. A. M., Milstien, J. B. & Clements, C. J. *Issues relating to the use of BCG in immunization programmes A discussion document.* World Health Organization (1999).
 110. Trunz, B. B., Fine, P. & Dye, C. Effect of BCG vaccination on childhood tuberculous meningitis and miliary tuberculosis worldwide: a meta-analysis and assessment of cost-effectiveness. *Lancet.* **367**, 1173–1180 (2006).
 111. Roy, P. *et al.* Potential effect of age of BCG vaccination on global paediatric tuberculosis mortality: a modelling study. *Lancet. Glob. Health.* **7**, e1655–e1663 (2019).
 112. Luca, S. & Mihaescu, T. History of BCG vaccine. *Maedica. (Buchar).* **8**, 53–8 (2013).
 113. Monteiro-Maia, R. & De Pinho, R. T. Oral bacillus Calmette-Guérin vaccine against tuberculosis: why not? *Mem. Inst. Oswaldo. Cruz.* **109**, 838–845 (2014).
 114. Roy, A. *et al.* Effect of BCG vaccination against *Mycobacterium tuberculosis* infection in children: systematic review and meta-analysis. *BMJ.* **349**, 1–11 (2014).
 115. Abubakar, I. *et al.* Systematic review and meta-analysis of the current evidence on the duration of protection by bacillus Calmette-Guerin vaccination against tuberculosis. *Health. Technol. Assess. (Rocky).* **17**, 1–4 (2013).
 116. Fine, P. E. M. Variation in protection by BCG: implications of and for heterologous immunity. *Lancet* **346**, 1339–1345 (1995).
 117. Hart, P. D. A. & Sutherland, I. A. N. BCG and vole bacillus vaccines in the prevention of tuberculosis in adolescence and early adult life. *Bull. World. Health.*

- Organ.* **46**, 371–385 (1972).
118. Tuberculosis Prevention Trial. Trial of BCG vaccines in south India for tuberculosis prevention: first report. *Bull. World. Health. Organ.* **57**, 819–827 (1979).
 119. Newport, M. J. *et al.* Genetic regulation of immune responses to vaccines in early life. *Gene.s Immun.* **5**, 122–129 (2004).
 120. Biraro, I. A. *et al.* Impact of co-infections and BCG Immunisation on immune responses among household contacts of tuberculosis patients in a Ugandan cohort. *PLoS. One.* **9**, e111517 (2014).
 121. Schaltz-Buchholzer, F. *et al.* Early vaccination with bacille Calmette-Guérin-Denmark or BCG-Japan versus BCG-Russia to healthy newborns in Guinea-Bissau: a randomized controlled trial. *Clin. Infect. Dis.* **71**, 1883–1893 (2020).
 122. Henao-Tamayo, M. *et al.* The efficacy of the BCG vaccine against newly emerging clinical strains of *Mycobacterium tuberculosis*. *PLoS. One.* **10**, 1–15 (2015).
 123. Mangtani, P. *et al.* Protection by BCG vaccine against tuberculosis: a systematic review of randomized controlled trials. *Clin. Infect. Dis.* **58**, 470–480 (2014).
 124. Andersen, P. & Scriba, T. J. Moving tuberculosis vaccines from theory to practice. *Nat. Rev. Immunol.* **19**, 550–562 (2019).
 125. Hoefsloot, W. *et al.* The geographic diversity of nontuberculous mycobacteria isolated from pulmonary samples: an NTM-NET collaborative study. *Eur. Respir. J.* **42**, 1604–1613 (2013).
 126. McShane, H. Editorial commentary: understanding BCG is the key to improving it. *Clin. Inf. Dis.* **58**, 481–482 (2014).
 127. Phillips, R. O. *et al.* Effectiveness of routine BCG vaccination on buruli ulcer disease: a case-control study in the Democratic Republic of Congo, Ghana and

- Togo. *PLoS Negl. Trop. Dis.* **9**, e3457 (2015).
128. Merle, C. S., Cunha, S. S. & Rodrigues, L. C. BCG vaccination and leprosy protection: Review of current evidence and status of BCG in leprosy control. *Expert. Rev. Vaccines.* **9**, 209–222 (2010).
 129. Netea, M. G. & Van Crevel, R. BCG-induced protection: effects on innate immune memory. *Semin. Immunol.* **26**, 512–517 (2014).
 130. Nemes, E. *et al.* Prevention of *M. tuberculosis* infection with H4:IC31 vaccine or BCG revaccination. *N. Engl. J. Med.* **379**, 138–149 (2018).
 131. Guallar-Garrido, S. & Julián, E. Bacillus Calmette-Guerin (BCG) therapy for bladder cancer: an update. *ImmunoTargets. Ther.* **9**, 1–11 (2020).
 132. Curtis, N. BCG vaccination and all-cause neonatal mortality. *Pediatr. Infect. Dis. J.* **38**, 195–197 (2019).
 133. Perdomo, C. *et al.* Mucosal BCG vaccination induces protective lung-resident memory T cell populations against tuberculosis. *MBio.* **7**, e01686-16 (2016).
 134. Garcia-Contreras, L. *et al.* Immunization by a bacterial aerosol. *Proc. Natl. Acad. Sci. U. S. A.* **105**, 4656–4660 (2008).
 135. Derrick, S. C., Kolibab, K., Yang, A. & Morris, S. L. Intranasal administration of *Mycobacterium bovis* BCG induces superior protection against aerosol infection with *Mycobacterium tuberculosis* in mice. *Clin. Vaccine. Immunol.* **21**, 1443–1451 (2014).
 136. Smaill, F. *et al.* A human type 5 adenovirus-based tuberculosis vaccine induces robust T cell responses in humans despite preexisting anti-adenovirus immunity. *Sci. Transl. Med.* **5**, 205ra134 (2013).
 137. Wang, J. *et al.* Single mucosal, but not parenteral, immunization with recombinant adenoviral-based vaccine provides potent protection from pulmonary tuberculosis.

- J. Immunol.* **173**, 6357–6365 (2004).
138. Santosuosso, M. *et al.* Mechanisms of Mucosal and parenteral tuberculosis vaccinations: adenoviral-based mucosal immunization preferentially elicits sustained accumulation of immune protective CD4 and CD8 T Cells within the airway lumen. *J. Immunol.* **174**, 7986–7994 (2005).
139. Xing, Z. *et al.* Intranasal mucosal boosting with an adenovirus-vectored vaccine markedly enhances the protection of BCG-primed guinea pigs against pulmonary tuberculosis. *PLoS. One.* **4**, e5856 (2009).
140. Pérez De Val, B. *et al.* Goats primed with *Mycobacterium bovis* BCG and boosted with a recombinant adenovirus expressing Ag85A show enhanced protection against tuberculosis. *Clin. Vaccine. Immunol.* **19**, 1339–1347 (2012).
141. Vordermeier, H. M., Huygen, K., Singh, M., Hewinson, R. G. & Xing, Z. Immune responses induced in cattle by vaccination with a recombinant adenovirus expressing mycobacterial antigen 85A and *Mycobacterium bovis* BCG. *Infect. Immun.* **74**, 1416–1418 (2006).
142. Stylianou, E. *et al.* Improvement of BCG protective efficacy with a novel chimpanzee adenovirus and a modified vaccinia Ankara virus both expressing Ag85A. *Vaccine.* **33**, 6800–6808 (2015).
143. Wilkie, M. *et al.* A phase I trial evaluating the safety and immunogenicity of a candidate tuberculosis vaccination regimen, ChAdOx1 85A prime – MVA85A boost in healthy UK adults. *Vaccine.* **38**, 779–789 (2020).
144. Ahmed, M. *et al.* A novel nanoemulsion vaccine induces mucosal interleukin-17 responses and confers protection upon *Mycobacterium tuberculosis* challenge in mice. *Vaccine.* **35**, 4983–4989 (2017).
145. Kaushal, D. *et al.* Mucosal vaccination with attenuated *Mycobacterium*

- tuberculosis* induces strong central memory responses and protects against tuberculosis. *Nat. Commun.* **6**, 8533 (2015).
146. Copland, A. *et al.* Mucosal delivery of fusion proteins with *Bacillus subtilis* spores enhances protection against tuberculosis by bacillus Calmette-Guérin. *Front. Immunol.* **9**, 346 (2018).
147. Stylianou, E. *et al.* Identification and evaluation of novel protective antigens for the development of a candidate tuberculosis subunit vaccine. *Infect. Immun.* **86**, (2018).
148. Hart, P. *et al.* Nanoparticle-fusion protein complexes protect against *Mycobacterium tuberculosis* infection. *Mol. Ther.* **26**, 822–833 (2018).
149. Woodworth, J. S. *et al.* Mucosal boosting of H56:CAF01 immunization promotes lung-localized T cells and an accelerated pulmonary response to *Mycobacterium tuberculosis* infection without enhancing vaccine protection. *Mucosal. Immunol.* **12**, 816–826 (2019).
150. Uranga, S., Marinova, D., Martin, C. & Aguilo, N. Protective efficacy and pulmonary immune response following subcutaneous and intranasal BCG administration in mice. *J. Vis. Exp.* **2016**, 54440 (2016).
151. Griffiths, K. L. *et al.* Cholera toxin enhances vaccine-induced protection against *Mycobacterium tuberculosis* challenge in mice. *PLoS. One.* **8**, e78312 (2013).
152. Lagranderie, M. *et al.* BCG-induced protection in guinea pigs vaccinated and challenged via the respiratory route. *Tuber. Lung Dis.* **74**, 38–46 (1993).
153. Gupta, T. *et al.* Evaluation of a temperature-restricted, mucosal tuberculosis vaccine in guinea pigs. *Tuberculosis.* **113**, 179–188 (2018).
154. Kaushal, D. *et al.* Reduced immunopathology and mortality despite tissue persistence in a *Mycobacterium tuberculosis* mutant lacking alternative σ factor,

- SigH. *Proc. Natl. Acad. Sci. U. S. A.* **99**, 8330–8335 (2002).
155. Hall, L. J. *et al.* Characterisation of a live *Salmonella* vaccine stably expressing the *Mycobacterium tuberculosis* Ag85B-ESAT6 fusion protein. *Vaccine*. **27**, 6894–6904 (2009).
 156. Jeyanathan, M. *et al.* Novel chimpanzee adenovirus-vectored respiratory mucosal tuberculosis vaccine: overcoming local anti-human adenovirus immunity for potent TB protection. *Mucosal Immunol.* **8**, 1373–1387 (2015).
 157. Hansen, S. G. *et al.* Cytomegalovirus vectors violate CD8⁺ T cell epitope recognition paradigms. *Science*. **340**, 10.1126 (2013).
 158. Schragar, L. K., Harris, R. C. & Vekemans, J. Research and development of new tuberculosis vaccines: a review. *F1000Research*. **7**, 1732 (2019).
 159. Nemes, E., Khader, S. A., Swanson, R. V. & Hanekom, W. A. Targeting unconventional host components for vaccination-induced protection against TB. *Front. Immunol.* **11**, 1452 (2020).
 160. Silver, R. F. *et al.* Diversity of human and macaque airway immune cells at baseline and during tuberculosis infection. *Am. J. Respir. Cell Mol. Biol.* **55**, 899–906 (2016).
 161. Porcelli, S. A., Ng, T. W., Saavedra-Ávila, N. A., Kennedy, S. C. & Carreño, L. J. Current efforts and future prospects in the development of live mycobacteria as vaccines. *Expert. Rev. Vaccines* **14**, 1493–1507 (2015).
 162. Grode, L. *et al.* Safety and immunogenicity of the recombinant BCG vaccine VPM1002 in a phase 1 open-label randomized clinical trial. *Vaccine*. **31**, 1340–1348 (2013).
 163. Loxton, A. G. *et al.* Safety and immunogenicity of the recombinant *Mycobacterium bovis* BCG vaccine VPM1002 in HIV-unexposed newborn infants

- in South Africa. *Clin. Vaccine. Immunol.* **24**, e00439-16 (2017).
164. Arbues, A. *et al.* Construction, characterization and preclinical evaluation of MTBVAC, the first live-attenuated *M. tuberculosis*-based vaccine to enter clinical trials. *Vaccine.* **31**, 4867–4873 (2013).
 165. Tameris, M. *et al.* Live-attenuated *Mycobacterium tuberculosis* vaccine MTBVAC versus BCG in adults and neonates: a randomised controlled, double-blind dose-escalation trial. *Lancet. Respir. Med.* **7**, 757–770 (2019).
 166. Fine, P. E. M. Randomised controlled trial of single BCG, repeated BCG, or combined BCG and killed *Mycobacterium leprae* vaccine for prevention of leprosy and tuberculosis in Malawi. *Lancet.* **348**, 17–24 (1996).
 167. Rodrigues, L. C. *et al.* Effect of BCG revaccination on incidence of tuberculosis in school-aged children in Brazil: the BCG-REVAC cluster-randomised trial. *Lancet.* **366**, 1290–1295 (2005).
 168. Barreto, M. L. *et al.* Evidence of an effect of BCG revaccination on incidence of tuberculosis in school-aged children in Brazil: second report of the BCG-REVAC cluster-randomised trial. *Vaccine.* **29**, 4875–4877 (2011).
 169. Masonou, T. *et al.* CD4+ T cell cytokine responses to the DAR-901 booster vaccine in BCG-primed adults: a randomized, placebo-controlled trial. *PLoS. One.* **14**, e0217091 (2019).
 170. Von Reyn, C. F. *et al.* Safety and immunogenicity of an inactivated whole cell tuberculosis vaccine booster in adults primed with BCG: a randomized, controlled trial of DAR-901. *PLoS. One.* **12**, e0175215 (2017).
 171. Munseri, P. *et al.* DAR-901 vaccine for the prevention of infection with *Mycobacterium tuberculosis* among BCG-immunized adolescents in Tanzania: a randomized controlled, double-blind phase 2b trial. *Vaccine.* **38**, 7239–7245

(2020).

172. Sharma, A., Bloss, E., Heilig, C. M. & Click, E. S. Tuberculosis caused by *Mycobacterium africanum*, United States, 2004-2013. *Emerg. Infect. Dis.* **22**, 396–403 (2016).
173. Mayosi, B. M. *et al.* Prednisolone and *Mycobacterium indicus pranii* in tuberculous pericarditis. *N. Engl. J. Med.* **371**, 1121–1130 (2014).
174. Prabowo, S. A. *et al.* RUTI vaccination enhances inhibition of mycobacterial growth *ex vivo* and induces a shift of monocyte phenotype in mice. *Front. Immunol.* **10**, 894 (2019).
175. Nell, A. S. *et al.* Safety, tolerability, and immunogenicity of the novel antituberculous vaccine RUTI: randomized, placebo-controlled phase II clinical trial in patients with latent tuberculosis infection. *PLoS. One.* **9**, e89612 (2014).
176. Dlugovitzky, D. *et al.* Immunotherapy with oral, heat-killed, *Mycobacterium vaccae* in patients with moderate to advanced pulmonary tuberculosis. *Immunotherapy.* **2**, 159–169 (2010).
177. Huang, C. Y. & Hsieh, W. Y. Efficacy of *Mycobacterium vaccae* immunotherapy for patients with tuberculosis: a systematic review and meta-analysis. *Hum. Vaccines. Immunother.* **13**, 1960–1971 (2017).
178. Goonetilleke, N. P. *et al.* Enhanced immunogenicity and protective efficacy against *Mycobacterium tuberculosis* of bacille Calmette-Guerin vaccine using mucosal administration and boosting with a recombinant modified vaccinia virus ankara. *J. Immunol.* **171**, 1602–1609 (2003).
179. Verreck, F. A. W. *et al.* MVA.85A boosting of BCG and an attenuated, *phoP* deficient *M. tuberculosis* vaccine both show protective efficacy against tuberculosis in rhesus macaques. *PLoS. One.* **4**, e5264 (2009).

180. Kaufmann, S. H. E. *et al.* Progress in tuberculosis vaccine development and host-directed therapies-a state of the art review. *Lancet. Respir. Med.* **2**, 301–320 (2014).
181. Tameris, M. D. *et al.* Safety and efficacy of MVA85A, a new tuberculosis vaccine, in infants previously vaccinated with BCG: a randomised, placebo-controlled phase 2b trial. *Lancet.* **381**, 1021–1028 (2013).
182. Santosuosso, M., McCormick, S., Zhang, X., Zganiacz, A. & Xing, Z. Intranasal boosting with an adenovirus-vectored vaccine markedly enhances protection by parenteral *Mycobacterium bovis* BCG immunization against pulmonary tuberculosis. *Infect. Immun.* **74**, 4634–4643 (2006).
183. Li, J. *et al.* Tuberculosis vaccine development: from classic to clinical candidates. *Eur. J. Clin. Microbiol. Infect. Dis.* **39**, 1405–1425 (2020).
184. Suliman, S. *et al.* Dose optimization of H56:IC31 vaccine for tuberculosis-endemic populations a double-blind, placebo-controlled, dose-selection trial. *Am. J. Respir. Crit. Care. Med.* **199**, 220–231 (2019).
185. Luabeya, A. K. K. *et al.* First-in-human trial of the post-exposure tuberculosis vaccine H56: IC31 in *Mycobacterium tuberculosis* infected and non-infected healthy adults. *Vaccine* **33**, 4130–4140 (2015).
186. Penn-Nicholson, A. *et al.* Safety and immunogenicity of the novel tuberculosis vaccine ID93 + GLA-SE in BCG-vaccinated healthy adults in South Africa: a randomised, double-blind, placebo-controlled phase 1 trial. *Lancet. Respir. Med.* **6**, 287–298 (2018).
187. Coler, R. N. *et al.* The TLR-4 agonist adjuvant, GLA-SE, improves magnitude and quality of immune responses elicited by the ID93 tuberculosis vaccine: first-in-human trial. *NPJ. Vaccines.* **3**, 34 (2018).
188. Vasina, D. V. *et al.* First-in-human trials of gamtbvac, a recombinant subunit

- tuberculosis vaccine candidate: safety and immunogenicity assessment. *Vaccines*. **7**, 166 (2019).
189. Montoya, J. *et al.* A randomized, controlled dose-finding phase II study of the M72/AS01 candidate tuberculosis vaccine in healthy PPD-positive adults. *J. Clin. Immunol.* **33**, 1360–1375 (2013).
190. Thacher, E. G. *et al.* Safety and immunogenicity of the M72/AS01 candidate tuberculosis vaccine in HIV-infected adults on combination antiretroviral therapy: a phase I/II, randomized trial. *AIDS*. **28**, 1769–1781 (2014).
191. Day, C. L. *et al.* Induction and regulation of T-cell immunity by the novel tuberculosis vaccine M72/AS01 in South African adults. *Am. J. Respir. Crit. Care Med.* **188**, 492–502 (2013).
192. Penn-Nicholson, A. *et al.* Safety and immunogenicity of candidate vaccine M72/AS01E in adolescents in a TB endemic setting. *Vaccine*. **33**, 4025–4034 (2015).
193. Idoko, O. T. *et al.* Safety and immunogenicity of the M72/AS01 candidate tuberculosis vaccine when given as a booster to BCG in Gambian infants: an open-label randomized controlled trial. *Tuberculosis*. **94**, 564–578 (2014).
194. Van Der Meeren, O. *et al.* Phase 2b controlled trial of M72/AS01E vaccine to prevent tuberculosis. *N. Engl. J. Med.* **379**, 1621–1634 (2018).
195. Tait, D. R. *et al.* Final analysis of a trial of M72/AS01E vaccine to prevent tuberculosis. *N. Engl. J. Med.* **381**, 2429–2439 (2019).
196. McShane, H. & Williams, A. A review of preclinical animal models utilised for TB vaccine evaluation in the context of recent human efficacy data. *Tuberculosis*. **94**, 105–110 (2014).
197. European Medicines Agency. *Guideline on clinical evaluation of vaccines*. (2018).

198. Fletcher, H. A. Systems approaches to correlates of protection and progression to TB disease. *Semin. Immunol.* **39**, 81–87 (2018).
199. Tanner, R. *et al.* Tools for assessing the protective efficacy of TB vaccines in humans: *in vitro* mycobacterial growth inhibition predicts outcome of *in vivo* mycobacterial infection. *Front. Immunol.* **10**, 2983 (2020).
200. Abebe, F. Is interferon-gamma the right marker for bacille Calmette-Guérin-induced immune protection? The missing link in our understanding of tuberculosis immunology. *Clin. Exp. Immunol.* **169**, 213–219 (2012).
201. Marsay, L. *et al.* Mycobacterial growth inhibition in murine splenocytes as a surrogate for protection against *Mycobacterium tuberculosis* (M. tb). *Tuberculosis.* **93**, 551–557 (2013).
202. Barnes, P. F., Bloch, A. B., Davidson, P. T. & Snider Jr, D. E. Tuberculosis in patients with human immunodeficiency virus infection. *New. Engl. J. Med.* **324**, 1644–1650 (1991).
203. Geldmacher, C., Zumla, A. & Hoelscher, M. Interaction between HIV and *Mycobacterium tuberculosis*: HIV-1-induced CD4 T-cell depletion and the development of active tuberculosis. *Curr. Opin. HIV. AIDS.* **7**, 268–275 (2012).
204. Marchant, A. *et al.* Newborns develop a Th1-Type immune response to *Mycobacterium bovis* bacillus Calmette-Guérin vaccination. *J. Immunol.* **163**, 2249–2255 (1999).
205. Cooper, A. M. *et al.* Disseminated tuberculosis in interferon γ gene-disrupted mice. *J. Exp. Med.* **178**, 2243–2247 (1993).
206. Newport, M. J. *et al.* A mutation in the interferon- γ -receptor gene and susceptibility to mycobacterial infection. *N. Engl. J. Med.* **335**, 1941–1949 (1996).
207. Fletcher, H. A. *et al.* T-cell activation is an immune correlate of risk in BCG

- vaccinated infants. *Nat. Commun.* **7**, 11290 (2016).
208. Kagina, B. M. N. *et al.* Specific T cell frequency and cytokine expression profile do not correlate with protection against tuberculosis after bacillus Calmette-Guérin vaccination of newborns. *Am. J. Respir. Crit. Care. Med.* **182**, 1073–1079 (2010).
209. Sakai, S. *et al.* CD4 T Cell-derived IFN- γ plays a minimal role in control of pulmonary *Mycobacterium tuberculosis* infection and must be actively repressed by PD-1 to prevent lethal disease. *PLoS. Pathog.* **12**, e1005667 (2016).
210. Mittrücker, H. W. *et al.* Poor correlation between BCG vaccination-induced T cell responses and protection against tuberculosis. *Proc. Natl. Acad. Sci. U. S. A.* **104**, 12434–12439 (2007).
211. Leal, I. S., Smedegård, B., Andersen, P. & Appelberg, R. Failure to induce enhanced protection against tuberculosis by increasing T-cell-dependent interferon- γ generation. *Immunology.* **104**, 157–161 (2001).
212. Mollenkopf, H.-J., Kursar, M. & Kaufmann, S. H. E. Immune response to postprimary tuberculosis in mice: *Mycobacterium tuberculosis* and *Mycobacterium bovis* bacille Calmette-Guérin induce equal protection. *J. Infect. Dis.* **190**, 588–597 (2004).
213. Monin, L. *et al.* Immune requirements for protective Th17 recall responses to *Mycobacterium tuberculosis* challenge. *Mucosal. Immunol.* **8**, 1099–1109 (2015).
214. Wu, C. *et al.* Antigen-specific human NKT cells from tuberculosis patients produce IL-21 to help B cells for the production of immunoglobulins. *Oncotarget.* **6**, 28633–28645 (2015).
215. Pandey, P. *et al.* Insights in tuberculosis immunology: Role of NKT and T regulatory cells. *Int. J. Mycobacteriology.* **8**, 333–340 (2019).
216. Venkataswamy, M. M. *et al.* Incorporation of NKT Cell-activating glycolipids

- enhances immunogenicity and vaccine efficacy of *Mycobacterium bovis* bacillus Calmette-Guérin. *J. Immunol.* **183**, 1644–1656 (2009).
217. Rozot, V. *et al.* Multidimensional analyses reveal modulation of adaptive and innate immune subsets by tuberculosis vaccines. *Commun. Biol.* **3**, 563 (2020).
218. Zufferey, C., Germano, S., Dutta, B., Ritz, N. & Curtis, N. The contribution of non-conventional T cells and NK cells in the mycobacterial-specific IFN γ response in bacille Calmette-Guérin (BCG)-Immunized infants. *PLoS. One.* **8**, (2013).
219. Meraviglia, S., El Daker, S., Dieli, F., Martini, F. & Martino, A. $\gamma\delta$ T cells cross-link innate and adaptive immunity in *Mycobacterium tuberculosis* infection. *Clin. Devel. Immunol.* **2011**, 11 (2011).
220. Janis, E. M., Kaufmann, S. H. E., Schwartz, R. H. & Pardoll, D. M. Activation of $\gamma\delta$ T cells in the primary immune response to *Mycobacterium tuberculosis*. *Science.* **244**, 713–716 (1989).
221. Davey, M. S. *et al.* Human neutrophil clearance of bacterial pathogens triggers anti-microbial $\gamma\delta$ T cell responses in early infection. *PLoS. Pathog.* **7**, e1002040 (2011).
222. Shen, Y. *et al.* Adaptive immune response of V γ 2V δ 2⁺ T cells during mycobacterial infections. *Science.* **295**, 2255–2258 (2002).
223. Chen, Z. W. Multifunctional immune responses of HMBPP-specific V γ 2V δ 2 T cells in *M. tuberculosis* and other infections. *Cell. Mol. Immunol.* **10**, 58–64 (2013).
224. Kabelitz, D. *et al.* The primary response of human γ/δ ⁺ T cells to *Mycobacterium tuberculosis* is restricted to V γ 9-bearing cells. *J. Exp. Med.* **173**, 1331–1338 (1991).
225. Dieli, F. *et al.* Granulysin-dependent killing of intracellular and extracellular *Mycobacterium tuberculosis* by V- γ 9/V δ 2 T lymphocytes. *J. Infect. Dis.* **184**, 1082–1085 (2001).

226. Wozniak, T. M., Saunders, B. M., Ryan, A. A. & Britton, W. J. *Mycobacterium bovis* BCG-specific Th17 cells confer partial protection against *Mycobacterium tuberculosis* infection in the absence of gamma interferon. *Infect. Immun.* **78**, 4187–4194 (2010).
227. Shen, L. *et al.* Immunization of V γ 2V δ 2 T cells programs sustained effector memory responses that control tuberculosis in nonhuman primates. *Proc. Natl. Acad. Sci. U. S. A.* **116**, 6371–6378 (2019).
228. Phuah, J. Y., Mattila, J. T., Lin, P. L. & Flynn, J. L. Activated B cells in the granulomas of nonhuman primates infected with *Mycobacterium tuberculosis*. *Am. J. Pathol.* **181**, 508–514 (2012).
229. Tanner, R., Villarreal-Ramos, B., Vordermeier, H. M. & McShane, H. The humoral immune response to BCG vaccination. *Front. Immunol.* **10**, 1317 (2019).
230. Chen, T. *et al.* Association of human antibodies to arabinomannan with enhanced mycobacterial opsonophagocytosis and intracellular growth reduction. *J. Infect. Dis.* **214**, 300–310 (2016).
231. Li, H. *et al.* Latently and uninfected healthcare workers exposed to TB make protective antibodies against *Mycobacterium tuberculosis*. *Proc. Natl. Acad. Sci. U. S. A.* **114**, 5023–5028 (2017).
232. Zimmermann, N. *et al.* Human isotype-dependent inhibitory antibody responses against *Mycobacterium tuberculosis*. *EMBO. Mol. Med.* **8**, 1325–1339 (2016).
233. Encinales, L. *et al.* Humoral immunity in tuberculin skin test anergy and its role in high-risk persons exposed to active tuberculosis. *Mol. Immunol.* **47**, 1066–1073 (2010).
234. Lu, L. L. *et al.* IFN- γ -independent immune markers of *Mycobacterium tuberculosis* exposure. *Nat. Med.* **25**, 977–987 (2019).

235. Choreño-Parra, J. A., Weinstein, L. I., Yunis, E. J., Zúñiga, J. & Hernández-Pando, R. Thinking outside the box: innate- and B cell-memory responses as novel protective mechanisms against tuberculosis. *Front. Immunol.* **11**, 226 (2020).
236. Verrall, A. J. *et al.* Early clearance of *Mycobacterium tuberculosis* is associated with increased innate immune responses. *J. Infect. Dis.* **221**, 1342–1350 (2019).
237. Koeken, V. A. C. M., Verrall, A. J., Netea, M. G., Hill, P. C. & van Crevel, R. Trained innate immunity and resistance to *Mycobacterium tuberculosis* infection. *Clin. Microbiol. Infect.* **25**, 1468–1472 (2019).
238. Bhatt, K., Verma, S., Ellner, J. J. & Salgame, P. Quest for correlates of protection against tuberculosis. *Clin. Vaccine Immunol.* **22**, 258–266 (2015).
239. Querec, T. D. *et al.* Systems biology approach predicts immunogenicity of the yellow fever vaccine in humans. *Nat. Immunol.* **10**, 116–125 (2009).
240. Nakaya, H. I. *et al.* Systems biology of vaccination for seasonal influenza in humans. *Nat. Immunol.* **12**, 786–795 (2011).
241. McShane, H. *et al.* BCG: myths, realities, and the need for alternative vaccine strategies. *Tuberculosis.* **92**, 283–288 (2012).
242. Fletcher, H. A. *et al.* Human newborn bacille Calmette–Guérin vaccination and risk of tuberculosis disease: a case-control study. *BMC Med.* **14**, 76 (2016).
243. Hawkridge, A. *et al.* Efficacy of percutaneous versus intradermal BCG in the prevention of tuberculosis in South African infants: randomised trial. *BMJ.* **337**, a2052 (2008).
244. Müller, J. *et al.* Cytomegalovirus infection is a risk factor for tuberculosis disease in infants. *JCI. Insight.* **4**, e130090 (2019).
245. Gupta, R. K. *et al.* Concise whole blood transcriptional signatures for incipient tuberculosis: a systematic review and patient-level pooled meta-analysis. *Lancet.*

- Respir. Med.* **8**, 395–406 (2020).
246. Ahmed, M. *et al.* Immune correlates of tuberculosis disease and risk translate across species. *Sci. Transl. Med.* **12**, eaay0233 (2020).
247. Prabowo, S. A., Smith, S. G., Seifert, K. & Fletcher, H. A. Impact of individual-level factors on *ex vivo* mycobacterial growth inhibition: associations of immune cell phenotype, cytomegalovirus-specific response and sex with immunity following BCG vaccination in humans. *Tuberculosis.* **119**, 101876 (2019).
248. Cross, G. B. *et al.* Impact of selective immune-cell depletion on growth of *Mycobacterium tuberculosis* (Mtb) in a whole-blood bactericidal activity (WBA) assay. *PLoS. One* **14**, e0216616 (2019).
249. Naftalin, C. M. *et al.* Adjunctive use of celecoxib with anti-tuberculosis drugs: evaluation in a whole-blood bactericidal activity model. *Sci. Rep.* **8**, 1–8 (2018).
250. Naftalin, C. M. *et al.* Coadministration of allopurinol to increase antimycobacterial efficacy of pyrazinamide as evaluated in a whole-blood bactericidal activity model. *Antimicrob. Agents. Chemother.* **61**, e00482-17 (2017).
251. Gurumurthy, M. *et al.* Activity of faropenem with and without rifampicin against *Mycobacterium tuberculosis*: evaluation in a whole-blood bactericidal activity trial. *J. Antimicrob. Chemother.* **72**, 2012–2019 (2017).
252. Wallis, R. S. *et al.* Whole blood bactericidal activity during treatment of pulmonary tuberculosis. *J. Infect. Dis.* **187**, 270–278 (2003).
253. Wallis, R. S. *et al.* A whole blood bactericidal assay for tuberculosis. *J. Infect. Dis.* **183**, 1300–1303 (2001).
254. Cheon, S. H. *et al.* Bactericidal activity in whole blood as a potential surrogate marker of immunity after vaccination against tuberculosis. *Clin. Diagn. Lab. Immunol.* **9**, 901–907 (2002).

255. Kampmann, B. *et al.* Novel human *in vitro* system for evaluating antimycobacterial vaccines. *Infect. Immun.* **72**, 6401–6407 (2004).
256. Fletcher, H. A. *et al.* Inhibition of mycobacterial growth *in vitro* following primary but not secondary vaccination with *Mycobacterium bovis* BCG. *Clin. Vaccine. Immunol.* **20**, 1683–1689 (2013).
257. Hoft, D. F. *et al.* Safety and immunogenicity of the recombinant BCG vaccine AERAS-422 in Healthy BCG-naïve adults: a randomized, active-controlled, first-in-human phase 1 trial. *EBioMedicine.* **7**, 278–286 (2016).
258. Smith, S. G., Zelmer, A., Blitz, R., Fletcher, H. A. & Dockrell, H. M. Polyfunctional CD4 T-cells correlate with *in vitro* mycobacterial growth inhibition following *Mycobacterium bovis* BCG-vaccination of infants. *Vaccine.* **34**, 5298–5305 (2016).
259. Tanner, R. *et al.* The influence of haemoglobin and iron on *in vitro* mycobacterial growth inhibition assays. *Sci. Rep.* **7**, 43478 (2017).
260. Joosten, S. A. *et al.* Mycobacterial growth inhibition is associated with trained innate immunity. *J. Clin. Invest.* **128**, 1837–1851 (2018).
261. Radloff, J. *et al.* Mycobacterium growth inhibition assay of human alveolar macrophages as a correlate of immune protection following *Mycobacterium bovis* bacille Calmette-Guérin vaccination. *Front. Immunol.* **9**, 1708 (2018).
262. Lee, H. *et al.* *In vitro* mycobacterial growth inhibition in South Korean adults with latent TB infection. *Front. Immunol.* **10**, 896 (2019).
263. Tanner, R. *et al.* Optimisation, harmonisation and standardisation of the direct mycobacterial growth inhibition assay using cryopreserved human peripheral blood mononuclear cells. *J. Immunol. Methods.* **469**, 1–10 (2019).
264. Harris, S. A. *et al.* Evaluation of a human BCG challenge model to assess

- antimycobacterial immunity induced by BCG and a candidate tuberculosis vaccine, MVA85A, alone and in combination. *J. Infect. Dis.* **209**, 1259–1268 (2014).
265. Crowle, A. J. & May, M. Preliminary demonstration of human tuberculoimmunity in vitro. *Infect. Immun.* **31**, 453–464 (1981).
266. Rook, G. A. *et al.* Vitamin D3, gamma interferon, and control of proliferation of *Mycobacterium tuberculosis* by human monocytes. *Immunology.* **57**, 159–63 (1986).
267. Rook, G. A. W., Steele, J., Ainsworth, M. & Champion, B. R. Activation of macrophages to inhibit proliferation of *Mycobacterium tuberculosis*: comparison of the effects of recombinant gamma-interferon on human monocytes and murine peritoneal macrophages. *Immunology.* **59**, 333–338 (1986).
268. Steele, J. *et al.* Inhibition of virulent *Mycobacterium tuberculosis* by murine peritoneal macrophages and human alveolar lavage cells: The effects of lymphokines and recombinant gamma interferon. *Tubercle.* **67**, 289–294 (1986).
269. Crowle, A. J., Ross, E. J. & May, M. H. Inhibition by 1,25(OH)₂-vitamin D₃ of the multiplication of virulent tubercle bacilli in cultured human macrophages. *Infect. Immun.* **55**, 2945–2950 (1987).
270. Cheng, S. H. *et al.* Demonstration of increased anti-mycobacterial activity in peripheral blood monocytes after BCG vaccination in British school children. *Clin. Exp. Immunol.* **74**, 20–5 (1988).
271. Cheng, S. H. *et al.* Monocyte antimycobacterial activity before and after *Mycobacterium bovis* BCG vaccination in Chingleput, India, and London, United Kingdom. *Infect. Immun.* **61**, 4501–4503 (1993).
272. Silver, R. F., Li, Q., Boom, W. H. & Ellner, J. J. Lymphocyte-dependent inhibition of growth of virulent *Mycobacterium tuberculosis* H37Rv within human

- monocytes: requirement for CD4 + T Cells in purified protein derivative-positive, but not in purified protein derivative-negative subjects. *J. Immunol.* **160**, 2408–2417 (1998).
273. Brill, K. J. *et al.* Human natural killer cells mediate killing of intracellular *Mycobacterium tuberculosis* H37Rv via granule-independent mechanisms. *Infect. Immun.* **69**, 1755–1765 (2001).
274. Kampmann, B. *et al.* Evaluation of human antimycobacterial immunity using recombinant reporter mycobacteria. *J. Infect. Dis.* **182**, 895–901 (2000).
275. Hoft, D. F. *et al.* Investigation of the relationships between immune-mediated inhibition of mycobacterial growth and other potential surrogate markers of protective *Mycobacterium tuberculosis* immunity. *J. Infect. Dis.* **186**, 1448–1457 (2002).
276. Tena, G. N. *et al.* Failure to Control growth of mycobacteria in blood from children infected with human immunodeficiency virus and its relationship to T cell function. *J. Infect. Dis.* **187**, 1544–1551 (2003).
277. Kampmann, B., Tena-Coki, G. N., Nicol, M. P., Levin, M. & Eley, B. Reconstitution of antimycobacterial immune responses in HIV-infected children receiving HAART. *AIDS.* **20**, 1011–1018 (2006).
278. Martineau, A. R. *et al.* A single dose of vitamin D enhances immunity to mycobacteria. *Am. J. Respir. Crit. Care. Med.* **176**, 208–213 (2007).
279. Martineau, A. R. *et al.* Neutrophil-mediated innate immune resistance to mycobacteria. *J. Clin. Invest.* **117**, 1988–1994 (2007).
280. Burl, S., Holder, B. S., Lo, B. K. M. & Kampmann, B. Optimisation of a functional mycobacterial growth-inhibition assay to improve its suitability for infant TB vaccine studies. *J. Immunol. Methods.* **394**, 121–124 (2013).

281. Roy, R. B. *et al.* An auto-luminescent fluorescent BCG whole blood assay to enable evaluation of paediatric mycobacterial responses using minimal blood volumes. *Front. Pediatr.* **7**, 151 (2019).
282. Basu Roy, R. *et al.* Protection against mycobacterial infection: a case-control study of mycobacterial immune responses in pairs of Gambian children with discordant infection status despite matched TB exposure. *EBioMedicine.* **59**, 102891 (2020).
283. Janulionis, E. *et al.* Survival and replication of clinical *Mycobacterium tuberculosis* isolates in the context of human innate immunity. *Infect. Immun.* **73**, 2595–2601 (2005).
284. Wallis, R. S., Vinhas, S. & Janulionis, E. Strain specificity of antimycobacterial immunity in whole blood culture after cure of tuberculosis. *Tuberculosis.* **89**, 221–224 (2009).
285. Harris, S. A. *et al.* Process of assay selection and optimization for the study of case and control samples from a phase IIb efficacy trial of a candidate tuberculosis vaccine, MVA85A. *Clin. Vaccine. Immunol.* **21**, 1005–1011 (2014).
286. Naranbhai, V. *et al.* Distinct transcriptional and anti-mycobacterial profiles of peripheral blood monocytes dependent on the ratio of monocytes: lymphocytes. *EBioMedicine.* **2**, 1619–1626 (2015).
287. Baguma, R. *et al.* Application of a whole blood mycobacterial growth inhibition assay to study immunity against *Mycobacterium tuberculosis* in a high tuberculosis burden population. *PLoS. One.* **12**, e0184563 (2017).
288. O’Shea, M. K. *et al.* Human hookworm infection enhances mycobacterial growth inhibition and associates with reduced risk of tuberculosis infection. *Front. Immunol.* **9**, 2893 (2018).
289. O’Shea, M. K. *et al.* Immunological correlates of mycobacterial growth inhibition

- describe a spectrum of tuberculosis infection. *Sci. Rep.* **8**, 1–13 (2018).
290. Worku, S. & Hoft, D. F. *In vitro* measurement of protective mycobacterial immunity: antigen-specific expansion of T cells capable of inhibiting intracellular growth of bacille Calmette-Guérin. *Clin. Infect. Dis.* **30**, S257–S261 (2000).
291. Dijkman, K. *et al.* Disparate tuberculosis disease development in macaque species is associated with innate immunity. *Front. Immunol.* **10**, 2479 (2019).
292. Carpenter, E., Fray, L. & Gormley, E. Cellular responses and *Mycobacterium bovis* BCG growth inhibition by bovine lymphocytes. *Immunol. Cell. Biol.* **75**, 554–560 (1997).
293. Denis, M., Wedlock, D. N. & Buddle, B. M. Ability of T cell subsets and their soluble mediators to modulate the replication of *Mycobacterium bovis* in bovine macrophages. *Cell. Immunol.* **232**, 1–8 (2004).
294. Pepponi, I. *et al.* A mycobacterial growth inhibition assay (MGIA) for bovine TB vaccine development. *Tuberculosis.* **106**, 118–122 (2017).
295. Buddle, B. M., Vordermeier, H. M., Chambers, M. A. & de Klerk-Lorist, L. M. Efficacy and safety of BCG vaccine for control of tuberculosis in domestic livestock and wildlife. *Front. Vet. Sci.* **5**, 259 (2018).
296. Cowley, S. C. & Elkins, K. L. CD4 + T cells mediate IFN- γ -independent control of *Mycobacterium tuberculosis* infection both *in vitro* and *in vivo*. *J. Immunol.* **171**, 4689–4699 (2003).
297. Sada-Ovalle, I., Chiba, A., Gonzales, A., Brenner, M. B. & Behar, S. M. Innate invariant NKT cells recognize *Mycobacterium tuberculosis*-infected macrophages, produce interferon- γ , and kill intracellular bacteria. *PLoS. Pathog.* **4**, e1000239 (2008).
298. Kolibab, K., Parra, M., Yang, A. L., Perera, L. P., Derrick, S. D. & Morris, S. L.

- A practical *in vitro* growth inhibition assay for the evaluation of TB vaccines. *Vaccine*. **28**, 317–322 (2009).
299. Parra, M. *et al.* Development of a murine mycobacterial growth inhibition assay for evaluating vaccines against *Mycobacterium tuberculosis*. *Clin. Vaccine Immunol.* **16**, 1025–1032 (2009).
300. Kolibab, K., Yang, A., Parra, M., Derrick, S. C. & Morris, S. L. Time to detection of *Mycobacterium tuberculosis* using the MGIT 320 system correlates with colony counting in preclinical testing of new vaccines. *Clin. Vaccine Immunol.* **21**, 453–455 (2014).
301. Youmans, G. P. Mechanisms of immunity in tuberculosis. *Pathobiol. Annu.* **9**, 137–62 (1979).
302. Rook, G. A. W., Champion, B. R., Steele, J., Vareyt, A. M. & Stanford, J. L. I-A restricted activation by T cell lines of anti-tuberculosis activity in murine macrophages. *Clin. Exp. Immunol.* **59**, 414–420 (1985).
303. Flesch, I. & Kaufmann, S. H. Mycobacterial growth inhibition by interferon-gamma-activated bone marrow macrophages and differential susceptibility among strains of *Mycobacterium tuberculosis*. *J. Immunol.* **138**, 4408–13 (1987).
304. Denis, M. Interferon-gamma-treated murine macrophages inhibit growth of tubercle bacilli via the generation of reactive nitrogen intermediates. *Cell. Immunol.* **132**, 150–157 (1991).
305. Zelmer, A. *et al.* *Ex vivo* mycobacterial growth inhibition assay (MGIA) for tuberculosis vaccine testing - a protocol for mouse splenocytes. *bioRxiv.* **2015**, 1–10 (2015).
306. Zelmer, A., Tanner, R., Stylianou, E., Damelang, T. & Morris, S. A new tool for tuberculosis vaccine screening: *ex vivo* Mycobacterial growth inhibition assay

- indicates BCG- mediated protection in a murine model of tuberculosis. *BMC Infect. Dis.* **16**, 412 (2016).
307. Yang, A. L., Schmidt, T. E., Stibitz, S. & Morris, S. L. A simplified mycobacterial growth inhibition assay (MGIA) using direct infection of mouse splenocytes and the MGIT system. *J. Microbiol. Methods.* **131**, 7–9 (2016).
308. Jensen, C., Lindebo Holm, L., Svensson, E., Aagaard, C. & Ruhwald, M. Optimisation of a murine splenocyte mycobacterial growth inhibition assay using virulent *Mycobacterium tuberculosis*. *Sci. Rep.* **7**, 2830 (2017).
309. Tanner, R. Development of mycobacterial growth inhibition assays for the early evaluation and gating of novel TB vaccine candidates. (University of Oxford, 2015).
310. Jackson, K., Sievers, A. & Dwyer, B. Effect of agitation of BACTEC 13A blood cultures on recovery of *Mycobacterium avium* complex. *J. Clin. Microbiol.* **29**, 1801–1803 (1991).
311. Prabowo, S. A. *et al.* Historical BCG vaccination combined with drug treatment enhances inhibition of mycobacterial growth *ex vivo* in human peripheral blood cells. *Sci. Rep.* **9**, 4842 (2019).
312. Worku, S. & Hoft, D. F. Differential effects of control and antigen-specific T cells on intracellular mycobacterial growth. *Infect. Immun.* **71**, 1763–1773 (2003).
313. Spencer, C. T. *et al.* Granzyme A produced by γ 9 δ 2 T cells induces human macrophages to inhibit growth of an intracellular pathogen. *PLoS. Pathog.* **9**, e1003119 (2013).
314. De Vallière, S., Abate, G., Blazevic, A., Heuertz, R. M. & Hoft, D. F. Enhancement of innate and cell-mediated immunity by antimycobacterial antibodies. *Infect. Immun.* **73**, 6711–6720 (2005).

315. Naranbhai, V. *et al.* Ratio of monocytes to lymphocytes in peripheral blood identifies adults at risk of incident tuberculosis among HIV-infected adults initiating antiretroviral therapy. *J. Infect. Dis.* **209**, 500–509 (2014).
316. Naranbhai, V. *et al.* The association between the ratio of monocytes: lymphocytes at age 3 months and risk of tuberculosis (TB) in the first two years of life. *BMC. Med.* **12**, 120 (2014).
317. Via, L. E. *et al.* Differential virulence and disease progression following *Mycobacterium tuberculosis* complex infection of the common marmoset (*Callithrix jacchus*). *Infect. Immun.* **81**, 2909–2919 (2013).
318. Wampande, E. M. *et al.* Genetic variability and consequence of *Mycobacterium tuberculosis* lineage 3 in Kampala-Uganda. *PLoS. One.* **14**, e0221644 (2019).
319. Mourik, B. C. *et al.* *Mycobacterium tuberculosis* clinical isolates of the Beijing and East-African Indian lineage induce fundamentally different host responses in mice compared to H37Rv. *Sci. Rep.* **9**, 1–11 (2019).
320. Correa-Macedo, W., Cambri, G. & Schurr, E. The interplay of human and *Mycobacterium tuberculosis* genomic variability. *Front. Genet.* **10**, 1–9 (2019).
321. Zhu, L. *et al.* Precision methylome characterization of *Mycobacterium tuberculosis* complex (MTBC) using PacBio single-molecule real-time (SMRT) technology. *Nucleic. Acids. Res.* **44**, 730–743 (2016).
322. Chiner-Oms, Á. *et al.* Genome-wide mutational biases fuel transcriptional diversity in the *Mycobacterium tuberculosis* complex. *Nat. Commun.* **10**, 3994 (2019).
323. Rose, G. *et al.* Mapping of genotype-phenotype diversity among clinical isolates of *Mycobacterium tuberculosis* by sequence-based transcriptional profiling. *Genome. Biol. Evol.* **5**, 1849–1862 (2013).

324. Banaei-Esfahani, A. *et al.* Network analysis identifies regulators of lineage-specific phenotypes in *Mycobacterium tuberculosis*. *bioRxiv*. **2020**, 1–39 (2020).
325. Ofori-Anyinam, B. *et al.* Comparative genomics shows differences in the electron transport and carbon metabolic pathways of *Mycobacterium africanum* relative to *Mycobacterium tuberculosis* and suggests an adaptation to low oxygen tension. *Tuberculosis*. **120**, 792762 (2020).
326. Manca, C. *et al.* Differential monocyte activation underlies strain-specific *Mycobacterium tuberculosis* pathogenesis. *Infect. Immun.* **72**, 5511–5514 (2004).
327. Ordway, D. *et al.* The hypervirulent *Mycobacterium tuberculosis* strain HN878 induces a potent TH1 Response followed by rapid down-regulation. *J. Immunol.* **179**, 522–531 (2007).
328. Kim, W. S. *et al.* Virulence-dependent alterations in the kinetics of immune cells during pulmonary infection by *Mycobacterium tuberculosis*. *PLoS. One.* **10**, e0145234 (2015).
329. Tientcheu, L. D. *et al.* Differences in T-cell responses between *Mycobacterium tuberculosis* and *Mycobacterium africanum*-infected patients. *Eur. J. Immunol.* **44**, 1387–1398 (2014).
330. de Jong, B. C., Antonio, M. & Gagneux, S. *Mycobacterium africanum* - review of an important cause of human tuberculosis in West Africa. *PLoS. Negl. Trop. Dis.* **4**, e744 (2010).
331. Tientcheu, L. D. *et al.* Host Immune responses differ between *M. africanum*- and *M. tuberculosis*-infected patients following standard anti-tuberculosis treatment. *PLoS. Negl. Trop. Dis.* **10**, e0004701 (2016).
332. Homolka, S., Niemann, S., Russell, D. G. & Rohde, K. H. Functional genetic diversity among *Mycobacterium tuberculosis* complex clinical isolates:

- delineation of conserved core and lineage-specific transcriptomes during intracellular survival. *PLoS. Pathog.* **6**, e1000988 (2010).
333. Reiling, N. *et al.* Clade-specific virulence patterns of *Mycobacterium tuberculosis* complex strains in human primary macrophages and aerogenically infected mice. *MBio.* **4**, e00250-13 (2013).
334. Portevin, D., Gagneux, S., Comas, I. & Young, D. Human macrophage responses to clinical isolates from the *Mycobacterium tuberculosis* complex discriminate between ancient and modern lineages. *PLoS. Pathog.* **7**, e1001307 (2011).
335. Reed, M. B., Gagneux, S., DeRiemer, K., Small, P. M. & Barry, C. E. The W-Beijing lineage of *Mycobacterium tuberculosis* overproduces triglycerides and has the DosR dormancy regulon constitutively upregulated. *J. Bacteriol.* **189**, 2583–2589 (2007).
336. Sarkar, R., Lenders, L., Wilkinson, K. A., Wilkinson, R. J. & Nicol, M. P. Modern lineages of *Mycobacterium tuberculosis* exhibit lineage-specific patterns of growth and cytokine induction in human monocyte-derived macrophages. *PLoS. One.* **7**, 6–13 (2012).
337. Reyes-Martínez, J. E. *et al.* Differential activation of dendritic cells by *Mycobacterium tuberculosis* Beijing genotype. *Immunol. Invest.* **43**, 436–446 (2014).
338. Manca, C. *et al.* Virulence of a *Mycobacterium tuberculosis* clinical isolate in mice is determined by failure to induce Th1 type immunity and is associated with induction of IFN- α/β . *Proc. Natl. Acad. Sci. U. S. A.* **98**, 5752–5757 (2001).
339. Manca, C. *et al.* Hypervirulent *M. tuberculosis* W/Beijing strains upregulate type I IFNs and increase expression of negative regulators of the jak-stat pathway. *J. Interf. Cytokine. Res.* **25**, 694–701 (2005).

340. Dormans, J. *et al.* Correlation of virulence, lung pathology, bacterial load and delayed type hypersensitivity responses after infection with different *Mycobacterium tuberculosis* genotypes in a BALB/c mouse model. *Clin. Exp. Immunol.* **137**, 460–468 (2004).
341. Theus, S., Eisenach, K., Fomukong, N., Silver, R. F. & Cave, M. D. Beijing family *Mycobacterium tuberculosis* strains differ in their intracellular growth in THP-1 macrophages. *Int. J. Tuberc. Lung. Dis.* **11**, 1087–1093 (2007).
342. Palanisamy, G. S. *et al.* Clinical strains of *Mycobacterium tuberculosis* display a wide range of virulence in guinea pigs. *Tuberculosis.* **89**, 203–209 (2009).
343. Aguilar L, D. *et al.* *Mycobacterium tuberculosis* strains with the Beijing genotype demonstrate variability in virulence associated with transmission. *Tuberculosis.* **90**, 319–325 (2010).
344. Ribeiro, S. C. M. *et al.* *Mycobacterium tuberculosis* strains of the modern sublineage of the beijing family are more likely to display increased virulence than strains of the ancient sublineage. *J. Clin. Microbiol.* **52**, 2615–2624 (2014).
345. Wang, C. *et al.* Innate immune response to *Mycobacterium tuberculosis* Beijing and other genotypes. *PLoS. One.* **5**, e13594 (2010).
346. Kato-Maeda, M. *et al.* Beijing sublineages of *Mycobacterium tuberculosis* differ in pathogenicity in the guinea pig. *Clin. Vaccine. Immunol.* **19**, 1227–1237 (2012).
347. Reed, M. B. *et al.* A glycolipid of hypervirulent tuberculosis strains that inhibits the innate immune response. *Nature.* **431**, 84–87 (2004).
348. Tsenova, L. *et al.* BCG vaccination confers poor protection against *M. tuberculosis* HN878-induced central nervous system disease. *Vaccine.* **25**, 5126–5132 (2007).
349. López, B. *et al.* A marked difference in pathogenesis and immune response induced by different *Mycobacterium tuberculosis* genotypes. *Clin. Exp. Immunol.*

- 133, 30–37 (2003).
350. Romero, M. M. *et al.* Clinical isolates of *Mycobacterium tuberculosis* differ in their ability to induce respiratory burst and apoptosis in neutrophils as a possible mechanism of immune escape. *Clin. Dev. Immunol.* **2012**, 152546 (2012).
351. Romero, M. M. *et al.* Outbreaks of *Mycobacterium tuberculosis* MDR strains differentially induce neutrophil respiratory burst involving lipid rafts, p38 MAPK and Syk. *BMC. Infect. Dis.* **14**, 262 (2014).
352. Ordway, D. J. *et al.* *Mycobacterium bovis* BCG-mediated protection against W-Beijing strains of *Mycobacterium tuberculosis* is diminished concomitant with the emergence of regulatory T cells. *Clin. Vaccine Immunol.* **18**, 1527–3 (2011).
353. Jeon, Y. B. *et al.* *Mycobacterium bovis* BCG immunization induces protective immunity against nine different *Mycobacterium tuberculosis* strains in mice. *Infect. Immun.* **76**, 5173–5180 (2008).
354. Levillain, F. *et al.* Preclinical assessment of a new live attenuated *Mycobacterium tuberculosis* Beijing-based vaccine for tuberculosis. *Vaccine.* **38**, 1416–1423 (2020).
355. Herzmann, C. *et al.* Childhood BCG vaccination does not influence control of *Mycobacterium tuberculosis* growth by human bronchoalveolar lavage cells. *Tuberculosis.* **95**, 321–327 (2015).
356. Kilkenny, C., Browne, W. J., Cuthill, I. C., Emerson, M. & Altman, D. G. Improving bioscience research reporting: The arrive guidelines for reporting animal research. *Animals.* **4**, 35–44 (2013).
357. EMI-TB - Home. Available at: <http://www.emi-tb.org/>. (Accessed: 19th October 2020)
358. Barnes, A. G. C., Cerovic, V., Hobson, P. S. & Klavinskis, L. S. *Bacillus subtilis*

- spores: a novel microparticle adjuvant which can instruct balanced Th1 and Th2 immune response to specific antigen. *Eur. J. Immunol.* **36**, 1538–47 (2007).
359. Siddiqi, S. H. & Rüsç-Gerdes, S. *FIND diagnostics MGIT procedure manual for BACTEC™ MGIT 960™ TB System (Also applicable for Manual MGIT)*. (2006).
360. Brennan, M. J. *et al.* The Cross-species Mycobacterial Growth Inhibition Assay (MGIA) Project 2010-2014. *Clin. Vaccine. Immunol.* **24**, e00142-17 (2017).
361. Tanner, R., O’Shea, M. K., Fletcher, H. A. & McShane, H. *In vitro* mycobacterial growth inhibition assays: a tool for the assessment of protective immunity and evaluation of tuberculosis vaccine efficacy. *Vaccine.* **34**, 4656–4665 (2016).
362. Amaral, E., Lassunskaja, E. & D’Imperio-Lima, M. Isolation of lung infiltrating cell in mice. *BIO-PROTOCOL.* **5**, (2015).
363. Moro, K., Ealey, K. N., Kabata, H. & Koyasu, S. Isolation and analysis of group 2 innate lymphoid cells in mice. *Nat. Protoc.* **10**, 792–806 (2015).
364. Conesa, A. *et al.* A survey of best practices for RNA-seq data analysis. *Genome. Biol.* **17**, 13 (2016).
365. QIAGEN. RNeasy Mini Handbook. Available at: <https://www.qiagen.com/gb/resources/resourcedetail?id=14e7cf6e-521a-4cf7-8cbc-bf9f6fa33e24&lang=en>. (Accessed: 15th April 2020).
366. New England Biolabs. NEBNext® Ultra™ II RNA Library Prep. Available at: <https://international.neb.com/nebnext-ultra-ii-rna/nebnext-ultra-ii-rna-library-prep-directional-and-non-directional/nebnext-ultra-ii-directional-rna-library-prep-ultra-ii-directional-rna-workflow>. (Accessed: 15th April 2020).
367. Stark, R., Grzelak, M. & Hadfield, J. RNA sequencing: the teenage years. *Nat. Rev. Genet.* **20**, 631–656 (2019).
368. Harvard Chan Bioinformatics Core. Introduction to RNA-seq using high-

- performance computing (HPC). Available at: https://github.com/hbctraining/Intro-to-rnaseq-hpc-O2/blob/master/lessons/03_alignment.md. (Accessed: 10th April 2020).
369. Iowa State University, G. I. F. RNASeq analysis walk-through. Available at: <https://gif.biotech.iastate.edu/rnaseq-analysis-walk-through>. (Accessed: 11th April 2020).
370. Harvard Chan Bioinformatics Core. Differential gene expression workshop using Salmon counts. Available at: https://github.com/hbctraining/DGE_workshop_salmon/tree/master/lessons. (Accessed: 12th April 2020).
371. Andrews, S. FastQC: a quality control tool for high throughput sequence data. (2010). Available at: <http://www.bioinformatics.babraham.ac.uk/projects/fastqc/>. (Accessed: 29th November 2020).
372. Bushnell, B. BBTools. Available. at: <https://sourceforge.net/projects/bbmap/>. (Accessed: 29th November 2020).
373. Introducing BBDuk: Adapter/Quality Trimming and Filtering - SEQanswers. Available at: <http://seqanswers.com/forums/showthread.php?t=42776>. (Accessed: 11th April 2020).
374. Bolger, A. M., Lohse, M. & Usadel, B. Trimmomatic: a flexible trimmer for Illumina sequence data. *Bioinformatics*. **30**, 2114–2120 (2014).
375. Martin, M. Cutadapt removes adapter sequences from high-throughput sequencing reads. *EMBnet. journal*. **17**, 10 (2011).
376. Dobin, A. *et al.* Sequence analysis STAR: ultrafast universal RNA-seq aligner. *Bioinformatics*. **29**, 15–21 (2013).
377. Kim, D., Paggi, J. M., Park, C., Bennett, C. & Salzberg, S. L. Graph-based genome

- alignment and genotyping with HISAT2 and HISAT-genotype. *Nat. Biotechnol.* **37**, 907–915 (2019).
378. Kim, D. *et al.* TopHat2: Accurate alignment of transcriptomes in the presence of insertions, deletions and gene fusions. *Genome. Biol.* **14**, R36 (2013).
379. Patro, R., Duggal, G., Love, M. I., Irizarry, R. A. & Kingsford, C. Salmon provides fast and bias-aware quantification of transcript expression. *Nat. Methods.* **14**, 417–419 (2017).
380. Bray, N. L., Pimentel, H., Melsted, P. & Pachter, L. Near-optimal probabilistic RNA-seq quantification. *Nat. Biotechnol.* **34**, 525–527 (2016).
381. Patro, R., Mount, S. M. & Kingsford, C. Sailfish enables alignment-free isoform quantification from RNA-seq reads using lightweight algorithms. *Nat. Biotechnol.* **32**, 462–464 (2014).
382. Baruzzo, G. *et al.* Simulation-based comprehensive benchmarking of RNA-seq aligners. *Nat. Methods.* **14**, 135–139 (2017).
383. Cunningham, F. *et al.* Ensembl 2019. *Nucleic. Acids. Res.* **47**, D745–D751 (2018).
384. Wang, L., Wang, S. & Li, W. RSeQC: quality control of RNA-seq experiments. *Bioinformatics.* **28**, 2184–2185 (2012).
385. Aronesty, E. ea-utils: command-line tools for processing biological sequencing data. (2011). Available at: <https://github.com/ExpressionAnalysis/ea-utils>. (Accessed: 11th April 2020).
386. Broad Institute. Picard Tools. Available at: <http://broadinstitute.github.io/picard/>. (Accessed: 29th November 2020).
387. Genome Browser Utilities. Available at: <https://genome.ucsc.edu/util.html>. (Accessed: 11th April 2020).

388. Liao, Y., Smyth, G. K. & Shi, W. Sequence analysis featureCounts: an efficient general purpose program for assigning sequence reads to genomic features. *Bioinformatics*. **30**, 923–930 (2014).
389. Anders, S., Pyl, P. T. & Huber, W. HTSeq - a Python framework to work with high-throughput sequencing data. *Bioinformatics*. **31**, 166–169 (2015).
390. Germain, P.-L. *et al.* RNAontheBENCH: computational and empirical resources for benchmarking RNAseq quantification and differential expression methods. *Nucleic. Acids. Res.* **44**, 5054–5067 (2016).
391. Shi, W. & Liao, Y. Rsubread/Subread Users Guide. 1–67 (2019). Available at: <https://bioconductor.org/packages/release/bioc/vignettes/Rsubread/inst/doc/SubreadUsersGuide.pdf>. (Accessed: 10th April 2020).
392. Love, M. I., Anders, S. & Huber, W. Analyzing RNA-seq data with DESeq2. Available at: <http://bioconductor.org/packages/release/bioc/vignettes/DESeq2/inst/doc/DESeq2.html#input-data>. (Accessed: 12th April 2020).
393. Moolenaar, B. Vim. Available at: <https://github.com/vim/vim>. (Accessed: 10th April 2020).
394. Ewels, P., Magnusson, M., Lundin, S. & Källér, M. MultiQC: summarize analysis results for multiple tools and samples in a single report. *Bioinformatics*. **32**, 3047–8 (2016).
395. Costa-Silva, J., Domingues, D. & Lopes, F. M. RNA-Seq differential expression analysis: An extended review and a software tool. *PLoS. One*. **12**, e0190152 (2017).
396. Anders, S. & Huber, W. Differential expression analysis for sequence count data. *Genome. Biol.* **11**, R106 (2010).
397. Love, M. I., Huber, W. & Anders, S. Moderated estimation of fold change and

- dispersion for RNA-seq data with DESeq2. *Genome. Biol.* **15**, 550 (2014).
398. Hardcastle, T. J. & Kelly, K. A. BaySeq: empirical Bayesian methods for identifying differential expression in sequence count data. *BMC. Bioinformatics.* **11**, 422 (2010).
399. Leng, N. *et al.* EBSeq: an empirical Bayes hierarchical model for inference in RNA-seq experiments. *Bioinformatics.* **29**, 1035–1043 (2013).
400. Robinson, M. D., Mccarthy, D. J. & Smyth, G. K. edgeR: a Bioconductor package for differential expression analysis of digital gene expression data. *Bioinformatics.* **26**, 139–140 (2010).
401. Law, C. W., Chen, Y., Shi, W. & Smyth, G. K. Voom: Precision weights unlock linear model analysis tools for RNA-seq read counts. *Genome. Biol.* **15**, R29 (2014).
402. Tarazona, S. *et al.* Data quality aware analysis of differential expression in RNA-seq with NOISeq R/Bioc package. *Nucleic. Acids. Res.* **43**, 140 (2015).
403. Li, J. & Tibshirani, R. Finding consistent patterns: a nonparametric approach for identifying differential expression in RNA-Seq data. *Stat. Methods. Med. Res.* **22**, 519–536 (2013).
404. Trapnell, C. *et al.* Differential analysis of gene regulation at transcript resolution with RNA-seq. *Nat. Biotechnol.* **31**, 46–53 (2013).
405. Pimentel, H., Bray, N. L., Puente, S., Melsted, P. & Pachter, L. Differential analysis of RNA-seq incorporating quantification uncertainty. *Nat. Methods.* **14**, 687–690 (2017).
406. Sonesson, C. & Delorenzi, M. A comparison of methods for differential expression analysis of RNA-seq data. *BMC. Bioinformatics.* **14**, 1–18 (2013).
407. Dong, K., Zhao, H., Tong, T. & Wan, X. NBLDA: negative binomial linear

- discriminant analysis for RNA-Seq data. *BMC. Bioinformatics*. **17**, 369 (2016).
408. Bullard, J. H., Purdom, E., Hansen, K. D. & Dudoit, S. Evaluation of statistical methods for normalization and differential expression in mRNA-Seq experiments. *BMC. Bioinformatics*. **11**, 94 (2010).
409. Love, M. DESeq2 or edgeR. (2016). Available at: <https://mikelove.wordpress.com/2016/09/28/deseq2-or-edger/>. (Accessed: 13th April 2020).
410. Lin, B. & Pang, Z. Stability of methods for differential expression analysis of RNA-seq data. *BMC. Genomics*. **20**, 35 (2019).
411. Storey, J. D. & Tibshirani, R. Statistical significance for genomewide studies. *Proc. Natl. Acad. Sci. U. S. A.* **100**, 9440–9445 (2003).
412. Benjamini, Y. & Hochberg, Y. Controlling the false discovery rate: a practical and powerful approach to multiple testing. *J. R. Stat. Soc. B.* **57**, 289–300 (1995).
413. Bland, J. M. & Altman, D. G. Multiple significance tests: the Bonferroni method. *Br. Med. J.* **310**, 170 (1995).
414. Yu, L., Fernandez, S. & Brock, G. Power analysis for RNA-Seq differential expression studies. *BMC. Bioinformatics*. **18**, 234 (2017).
415. Stephens, M. False discovery rates: a new deal. *Biostatistics* **18**, 275–294 (2017).
416. Pagès, H., Carlson, M., Falcon, S. & Li, N. AnnotationDbi: manipulation of SQLite-based annotations in Bioconductor. R package version 1.50.3. (2020).
417. Carlson, M. org.Mm.eg.db: Genome wide annotation for Mouse. R package version 3.8.2. (2019).
418. Aranday Cortes, E., Kaveh, D., Nunez-Garcia, J., Hogarth, P. J. & Vordermeier, M. H. *Mycobacterium bovis*-BCG vaccination induces specific pulmonary

- transcriptome biosignatures in mice. *PLoS. One.* **5**, e11319 (2010).
419. Phipson, B., Lee, S., Majewski, I. J., Alexander, W. S. & Smyth, G. K. Robust hyperparameter estimation protects against hypervariable genes and improves power to detect differential expression. *Ann. Appl. Stat.* **10**, 946–963 (2016).
420. Smyth, G. K. *et al.* limma: linear models for microarray and RNA-Seq data user's guide. Available at: <https://www.bioconductor.org/packages/release/bioc/vignettes/limma/inst/doc/usersguide.pdf>. (Accessed: 28th June 2020).
421. Wickham, H. *ggplot2: Elegant Graphics for Data Analysis*. (Springer-Verlag New York, 2016).
422. Singhania, A. *et al.* Transcriptional profiling unveils type I and II interferon networks in blood and tissues across diseases. *Nat. Commun.* **10**, 1–21 (2019).
423. Yoshida, H. *et al.* The cis-regulatory atlas of the mouse immune system. *Cell.* **176**, 897-912.e20 (2019).
424. Mouse models of infection and inflammation. Available at: <https://ogarra.shinyapps.io/MouseModules/>. (Accessed: 26th June 2020).
425. Weiner, J. & Domaszewska, T. tmod: an R package for general and multivariate enrichment analysis. *PeerJ.* **4**, 1–9 (2016).
426. Gupta, S. *et al.* Sex differences in neutrophil biology modulate response to type I interferons and immunometabolism. *Proc. Natl. Acad. Sci. U. S. A.* **117**, 16481–16491 (2020).
427. Yamaguchi, K. D. *et al.* IFN- β -regulated genes show abnormal expression in therapy-naïve relapsing-remitting MS mononuclear cells: gene expression analysis employing all reported protein-protein interactions. *J. Neuroimmunol.* **195**, 116–120 (2008).

428. Meng, H., Yaari, G., Bolen, C. R., Avey, S. & Kleinstein, S. H. Gene set meta-analysis with Quantitative Set Analysis for Gene Expression (QuSAGE). *PLOS Comput. Biol.* **15**, e1006899 (2019).
429. Painter, H. *et al.* Adaption of the *ex vivo* mycobacterial growth inhibition assay for use with murine lung cells. *Sci. Rep.* **10**, 1–9 (2020).
430. World Health Organization. *Global Tuberculosis Report 2018*. (2018).
431. World Health Organization. *The End TB Strategy*. (2015).
432. Abebe, F. & Bjune, G. The emergence of Beijing family genotypes of *Mycobacterium tuberculosis* and low-level protection by bacille Calmette-Guérin (BCG) vaccines: is there a link? *Clin. Exp. Immunol.* **145**, 389–397 (2006).
433. Thomas, Z. M. & Mcshane, H. Aerosol immunisation for TB: matching route of vaccination to route of infection. *Trans. R. Soc. Trop. Med. Hyg.* **109**, 175–181 (2015).
434. Parsons, L. M. *et al.* Rapid and simple approach for identification of *Mycobacterium tuberculosis* complex isolates by PCR-based genomic deletion analysis. *J. Clin. Microbiol.* **40**, 2339–2345 (2002).
435. Sable, S. B. *et al.* Cellular immune responses to nine *Mycobacterium tuberculosis* vaccine candidates following intranasal vaccination. *PLoS One.* **6**, e22718 (2011).
436. Kent, P. T. & Kubica, G. P. *Public health mycobacteriology. A guide for the level III laboratory*. (1985).
437. Niemann, S., Richter, E. & Rüsç-Gerdes, S. Differentiation among members of the *Mycobacterium tuberculosis* complex by molecular and biochemical features: Evidence for two pyrazinamide- susceptible subtypes of *M. bovis*. *J. Clin. Microbiol.* **38**, 152–157 (2000).
438. Giri, P. K., Verma, I. & Khuller, G. K. Protective efficacy of intranasal vaccination

- with *Mycobacterium bovis* BCG against airway *Mycobacterium tuberculosis* challenge in mice. *J. Infect.* **53**, 350–356 (2006).
439. Chen, L. *et al.* Single intranasal mucosal *Mycobacterium bovis* BCG vaccination confers improved protection compared to subcutaneous vaccination against pulmonary tuberculosis. *Infect. Immun.* **72**, 238–246 (2004).
440. Leisching, G. *et al.* RNAseq reveals hypervirulence-specific host responses to *M. tuberculosis* infection. *Virulence.* **8**, 848–858 (2017).
441. Krishnan, N. *et al.* *Mycobacterium tuberculosis* lineage influences innate immune response and virulence and is associated with distinct cell envelope lipid profiles. *PLoS. One.* **6**, e23870 (2011).
442. Carpenter, C. *et al.* A side-by-side comparison of T cell reactivity to fifty-nine *M. tuberculosis* antigens in diverse populations from five continents. *Tuberculosis. (Edinb).* **95**, 713–721 (2015).
443. Sharpe, S. A. *et al.* Establishment of an aerosol challenge model of tuberculosis in rhesus macaques and an evaluation of endpoints for vaccine testing. *Clin. Vaccine. Immunol.* **17**, 1170–1182 (2010).
444. Tchilian, E. Z. *et al.* Immunogenicity and protective efficacy of prime-boost regimens with recombinant (delta)ureC hly+ *Mycobacterium bovis* BCG and modified vaccinia virus ankara expressing *M. tuberculosis* antigen 85A against murine tuberculosis. *Infect. Immun.* **77**, 622–631 (2009).
445. Williams, A. *et al.* Evaluation of vaccines in the EU TB vaccine cluster using a guinea pig aerosol infection model of tuberculosis. *Tuberculosis.* **85**, 29–38 (2005).
446. Williams, A. *et al.* Boosting with poxviruses enhances *Mycobacterium bovis* BCG efficacy against tuberculosis in guinea pigs. *Infect. Immun.* **73**, 3814–3816 (2005).
447. Vordermeier, H. M. *et al.* Viral booster vaccines improve *Mycobacterium bovis*

- BCG-induced protection against bovine tuberculosis. *Infect. Immun.* **79**, 2134 (2011).
448. Home Office. *Guidance on the Operation of the Animals (Scientific Procedures) Act 1986*. (2014).
449. Lamorte power calculator. Available at: http://www.uml.edu/Images/LaMorte_calculator_tcm18-37802.xls. (Accessed: 29th November 2020).
450. Shitikov, E. *et al.* Evolutionary pathway analysis and unified classification of East Asian lineage of *Mycobacterium tuberculosis*. *Sci. Rep.* **7**, 1–10 (2017).
451. Cha, S. Bin *et al.* Repeated aerosolized-boosting with gamma-irradiated *Mycobacterium bovis* BCG confers improved pulmonary protection against the hypervirulent *Mycobacterium tuberculosis* strain HN878 in mice. *PLoS. One.* **10**, e0141577 (2015).
452. Coscolla, M. & Gagneux, S. Does *M. tuberculosis* genomic diversity explain disease diversity? *Drug. Discov. Today. Dis. Mech.* **7**, e43–e59 (2010).
453. Barczak, A. K. *et al.* *In vivo* phenotypic dominance in mouse mixed infections with *Mycobacterium tuberculosis* clinical isolates. *J. Infect. Dis.* **192**, 600–606 (2005).
454. Manabe, Y. C. *et al.* Different strains of *Mycobacterium tuberculosis* cause various spectrums of disease in the rabbit model of tuberculosis. *Infect. Immun.* **71**, 6004–6011 (2003).
455. Marquina-Castillo, B. *et al.* Virulence, immunopathology and transmissibility of selected strains of *Mycobacterium tuberculosis* in a murine model. *Immunology.* **128**, 123–133 (2009).
456. Rutaihwa, L. K. *et al.* Multiple introductions of *Mycobacterium tuberculosis* lineage 2–Beijing into Africa over centuries. *Front. Ecol. Evol.* **7**, 112 (2019).
457. Ajawatanawong, P. *et al.* A novel ancestral Beijing sublineage of *Mycobacterium*

- tuberculosis* suggests the transition site to modern Beijing sublineages. *Sci. Rep.* **9**, 1–12 (2019).
458. Kaufmann, E. *et al.* BCG educates hematopoietic stem cells to generate protective innate immunity against tuberculosis. *Cell.* **172**, 176-190.e19 (2018).
459. Orme, I. M. & Henao-Tamayo, M. I. Trying to see the forest through the trees: deciphering the nature of memory immunity to *Mycobacterium tuberculosis*. *Front. Immunol.* **9**, 1 (2018).
460. Misharin, A. V., Morales-Nebreda, L., Mutlu, G. M., Budinger, G. R. S. & Perlman, H. Flow cytometric analysis of macrophages and dendritic cell subsets in the mouse lung. *Am. J. Respir. Cell Mol. Biol.* **49**, 503–510 (2013).
461. Yu, Y.-R. A. *et al.* A protocol for the comprehensive flow cytometric analysis of immune cells in normal and inflamed murine non-lymphoid tissues. *PLoS. One.* **11**, e0150606 (2016).
462. Zelmer, A. *et al.* High monocyte to lymphocyte ratio is associated with impaired protection after subcutaneous administration of BCG in a mouse model of tuberculosis. *F1000Research.* **7**, 296 (2018).
463. Ritz, N., Hanekom, W. A., Robins-Browne, R., Britton, W. J. & Curtis, N. Influence of BCG vaccine strain on the immune response and protection against tuberculosis. *FEMS. Microbiol. Rev.* **32**, 821–841 (2008).
464. Lúcia Moreira-Teixeira, Mayer-Barber, K., Sher, A. & O’Garra, A. Type I interferons in tuberculosis: foe and occasionally friend. *J. Exp. Med.* **215**, 1273–1285 (2018).
465. Mayer-Barber, K. D. *et al.* Host-directed therapy of tuberculosis based on interleukin-1 and type i interferon crosstalk. *Nature.* **511**, 99–103 (2014).
466. Dorhoi, A. *et al.* Type I IFN signaling triggers immunopathology in tuberculosis-

- susceptible mice by modulating lung phagocyte dynamics. *Eur. J. Immunol.* **44**, 2380–2393 (2014).
467. Zhang, G. *et al.* A proline deletion in IFNAR1 impairs IFN-signaling and underlies increased resistance to tuberculosis in humans. *Nat. Commun.* **9**, 85 (2018).
468. Zak, D. E. *et al.* A blood RNA signature for tuberculosis disease risk: a prospective cohort study. *Lancet.* **387**, 2312–2322 (2016).
469. Berry, M. P. R. *et al.* An interferon-inducible neutrophil-driven blood transcriptional signature in human tuberculosis. *Nature.* **466**, 973–977 (2010).
470. Ottenhoff, T. H. M. *et al.* Genome-wide expression profiling identifies type 1 interferon response pathways in active tuberculosis. *PLoS. One.* **7**, e45839 (2012).
471. Penn-Nicholson, A. *et al.* RISK6, a 6-gene transcriptomic signature of TB disease risk, diagnosis and treatment response. *Sci. Rep.* **10**, 1–21 (2020).
472. Donovan, M. L., Schultz, T. E., Duke, T. J. & Blumenthal, A. Type I interferons in the pathogenesis of tuberculosis: molecular drivers and immunological consequences. *Front. Immunol.* **8**, 1633 (2017).
473. Kuchtey, J., Fulton, S. A., Reba, S. M., Harding, C. V. & Boom, W. H. Interferon- $\alpha\beta$ mediates partial control of early pulmonary *Mycobacterium bovis* bacillus Calmette-Guérin infection. *Immunology.* **118**, 39–49 (2006).
474. Denis, M. Recombinant murine beta interferon enhances resistance of mice to systemic *Mycobacterium avium* infection. *Infect. Immun.* **59**, 1857–1859 (1991).
475. Rivas-Santiago, C. E. & Guerrero, G. G. IFN-alpha boosting of *Mycobacterium bovis* bacillus Calmette Güerin-vaccine promoted Th1 type cellular response and protection against *M. tuberculosis* infection. *Biomed. Res. Int.* **2017**, 8796760 (2017).
476. Kuleshov, M. V. *et al.* Enrichr: a comprehensive gene set enrichment analysis web

- server 2016 update. *Nucleic. Acids. Res.* **44**, W90–W97 (2016).
477. Venkatasubramanian, S. *et al.* IL-21-dependent expansion of memory-like NK cells enhances protective immune responses against *Mycobacterium tuberculosis*. *Mucosal. Immunol.* **10**, 1031–1042 (2017).
478. Suliman, S. *et al.* Bacillus Calmette–Guérin (BCG) Revaccination of adults with latent *Mycobacterium tuberculosis* infection induces long-lived BCG-reactive NK cell responses. *J. Immunol.* **197**, 1100–1110 (2016).
479. Dhiman, R. *et al.* NK1.1+ cells and IL-22 regulate vaccine-induced protective immunity against challenge with *Mycobacterium tuberculosis*. *J. Immunol.* **189**, 897–905 (2012).
480. Junqueira-Kipnis, A. P. *et al.* NK cells respond to pulmonary infection with *Mycobacterium tuberculosis*, but play a minimal role in protection. *J. Immunol.* **171**, 6039–6045 (2003).
481. Lucas, M., Schachterle, W., Oberle, K., Aichele, P. & Diefenbach, A. Dendritic cells prime natural killer cells by trans-presenting interleukin 15. *Immunity.* **26**, 503–517 (2007).
482. Olsen, A. W., Brandt, L., Agger, E. M., Van Pinxteren, L. A. H. & Andersen, P. The influence of remaining live BCG organisms in vaccinated mice on the maintenance of immunity to tuberculosis. *Scand. J. Immunol.* **60**, 273–277 (2004).
483. Kaveh, D. A., Carmen Garcia-Pelayo, M. & Hogarth, P. J. Persistent BCG bacilli perpetuate CD4 T effector memory and optimal protection against tuberculosis. *Vaccine.* **32**, 6911–6918 (2014).
484. Gleeson, L. E. *et al.* *Mycobacterium tuberculosis* induces aerobic glycolysis in human alveolar macrophages that is required for control of intracellular bacillary replication. *J. Immunol.* **196**, 2444–2449 (2016).

485. Shi, L. *et al.* Infection with *Mycobacterium tuberculosis* induces the Warburg effect in mouse lungs. *Sci. Rep.* **5**, 18176 (2015).
486. Huang, L., Nazarova, E. V., Tan, S., Liu, Y. & Russell, D. G. Growth of *Mycobacterium tuberculosis in vivo* segregates with host macrophage metabolism and ontogeny. *J. Exp. Med.* **215**, 1135–1152 (2018).
487. Zhao, S., Fung-Leung, W.P., Bittner, A., Ngo, K. & Liu, X. Comparison of RNA-seq and microarray in transcriptome profiling of activated T cells. *PLoS. One.* **9**, e78644 (2014).
488. Chrominski, K. & Tkacz, M. Comparison of high-level microarray analysis methods in the context of result consistency. *PLoS. One.* **10**, e0128845 (2015).
489. Schaum, N. *et al.* Single-cell transcriptomics of 20 mouse organs creates a Tabula Muris. *Nature.* **562**, 367–372 (2018).
490. Ordway, D. J., Sonnenberg, M. G., Donahue, S. A., Belisle, J. T. & Orme, I. M. Drug-Resistant Strains of *Mycobacterium tuberculosis* Exhibit a Range of Virulence for Mice. *Infect. Immun.* **63**, 741–743 (1995).
491. Manca, C. *et al.* *Mycobacterium tuberculosis* CDC1551 induces a more vigorous host response *in vivo* and *in vitro*, but is not more virulent than other clinical isolates. *J. Immunol.* **162**, 6740–6746 (1999).
492. Zhang, M. *et al.* Enhanced capacity of a widespread strain of *Mycobacterium tuberculosis* to grow in human macrophages. *J. Infect. Dis.* **179**, 1213–1217 (1999).
493. Li, Q. *et al.* Differences in rate and variability of intracellular growth of a panel of *Mycobacterium tuberculosis* clinical isolates within a human monocyte model. *Infect. Immun.* **70**, 6489–6493 (2002).
494. Park, J. S., Tamayo, M. H., Gonzalez-Juarrero, M., Orme, I. M. & Ordway, D. J. Virulent clinical isolates of *Mycobacterium tuberculosis* grow rapidly and induce

- cellular necrosis but minimal apoptosis in murine macrophages. *J. Leukoc. Biol.* **79**, 80–86 (2006).
495. Theus, S. A., Cave, M. D. & Eisenach, K. D. Intracellular macrophage growth rates and cytokine profiles of *Mycobacterium tuberculosis* strains with different transmission dynamics. *J. Infect. Dis.* **191**, 453–460 (2005).
496. Newton, S. M. *et al.* A deletion defining a common Asian lineage of *Mycobacterium tuberculosis* associates with immune subversion. *Proc. Natl. Acad. Sci. U. S. A.* **103**, 15594–15598 (2006).
497. Sohn, H. *et al.* Induction of cell death in human macrophages by a highly virulent Korean isolate of *Mycobacterium tuberculosis* and the virulent strain H37Rv. *Scand. J. Immunol.* **69**, 43–50 (2009).
498. Koo, M. S., Subbian, S. & Kaplan, G. Strain specific transcriptional response in *Mycobacterium tuberculosis* infected macrophages. *Cell. Commun. Signal.* **10**, 2 (2012).
499. Tram, T. T. B. *et al.* Virulence of *Mycobacterium tuberculosis* clinical isolates is associated with sputum pre-treatment bacterial load, lineage, survival in macrophages, and cytokine response. *Front. Cell. Infect. Microbiol.* **8**, 417 (2018).

9 Appendix

9.1 Appendix 1. Published MGIA protocols and results.

First author, year [ref]	Species / sample type	Method	Culture method	Mycobacteria	Quantification method	Observation	Vaccine arm?
Youmans, 1979 [301]	Murine (ns) splenocytes + peritoneal MΦ	<ol style="list-style-type: none"> Splenocytes stimulated with mycobacteria to produce lymphokines. Naïve MΦs co-culture ± lymphokines. 	Multi-well plate	MTB		MTB growth inhibition in the presence of lymphokines.	No
Crowle, 1981 [265]	Human PBMCs	<ol style="list-style-type: none"> Lymphocytes stimulated (3 days) with antigen to produce lymphokines. Mycobacteria and MΦ co-culture ± 	Multi-well plate	BCG, Erdman	Morphological comparisons, acid-fast stain, [³ H]thymidine incorporation	Intracellular bacillary replication inhibited in the presence of lymphokines. Lymphokines only produced by TST ⁺ and	Yes

		lymphokines (7 days).				BCG-vaccinated donors, not TST ⁻ .	
Rook, 1985 [302]	Murine (ns) peritoneal MΦ (pooled) + T cells	Naïve MΦ and MTB co-cultured (4 days) ± tuberculin-responsive T-cells.	Multi-well plate	MTB clinical isolate, <i>M scrofulaceum</i> , <i>M kansasii</i>	[³ H]uracil incorporation	+ T cells: growth inhibition dependent on MHC I-A locus compatibility and mediated by soluble factors. + T-cell lymphokine preparations: growth inhibition MHC locus independent.	Yes
Rook, 1986 [266]	Human mono	Mono co-cultured with MTB (4 days) ± cholecalciferol metabolites, rIFN γ .	Multi-well plate	MTB	[³ H]uracil incorporation	Cholecalciferol metabolites inhibited mycobacterial growth in MΦ.	No
Rook, 1986 [267]	Murine (BALB/c) peritoneal MΦ or	Naïve MΦ co-cultured with mycobacteria (4 days) ± iron, rIFN γ or lymphokines.	Multi-well plate	BCG Glaxo, H37Rv	[³ H]uracil incorporation	Both cell types inhibited BCG and MTB growth. Addition of rIFN γ or lymphokines further	No

	human mono					enhanced growth inhibition in murine MΦ.	
Steele, 1986 [268]	Murine (ns) peritoneal MΦ or human alveolar MΦ	Naïve MΦ co-cultured with mycobacteria (4 days) ± rIFN γ or lymphokines.	Multi-well plate	MTB clinical isolate	[³ H]uracil incorporation	Both cell types inhibit MTB growth. Addition of rIFN γ or lymphokines further enhances growth inhibition in murine MΦ only.	No
Crowle, 1987 [269]	Human PBMCs	Mono differentiated into MΦ (7 days), followed by co-culture with MTB for 4 and 7 days ± 1,25D.	Multi-well plate	Erdman	CFU	1,25D activation of MΦ tuberculoimmunity.	Yes
Flesch, 1987 [303]	Murine (C57BL/6) BMM	Naïve MΦ co-cultured with mycobacteria ± rIFN γ or rIFN γ ⁺ supernatants from stimulated T cells.	Multi-well plate	BCG Phipps, H37Rv, Middelburg	[³ H]uracil, CFU	rIFN γ stimulation inhibited growth of BCG and H37Rv but not Middelburg.	No

Cheng, 1988 [270]	Human PBMCs	Mono co-cultured with mycobacteria and pulsed with antigen-stimulated autologous lymphocytes (3 days).	Multi-well plate	<i>M microti</i>	CFU	Growth rate in post-vaccination (8 weeks) PBMCs and lymphocytes lower vs pre-vaccination.	Yes
Denis, 1991 [304]	Murine (BALB/c) peritoneal MΦ	Naïve MΦ incubated with IFN γ , arginine and/or acetate salt (18 hours) before infection with mycobacteria (4 days).	Multi-well plate	H37Rv	[³ H]uracil	IFN γ pulsing inhibited mycobacterial growth vs untreated infected MΦ. Mediated by nitric oxide.	No
Cheng, 1993 [271]	Human PBMCs	[270].	Multi-well plate	<i>M microti</i>	CFU	Mycobacterial growth inhibition 8 weeks post-BCG vs with pre-vaccination in British school children but not South Indian.	Yes
Carpenter, 1997 [292]	Cattle PBMCs	NACs from vaccinated and unvaccinated animals incubated with autologous BCG-infected MΦ \pm IFN γ .	Multi-well plate	BCG	[³ H]uracil	BCG growth inhibition in vaccinated and unvaccinated animals.	Yes

Silver, 1998 [272]	Human PBMC	Mono co-cultured with mycobacteria (1:1) for 1 hour, 4 days and 7 days \pm TNF α , IFN γ or autologous NACs.	Multi-well plate	H37Rv	CFU	Growth inhibition: IFN γ , 0.9-fold reduction; autologous NACs 6- (PPD $^{+}$) and 10.6- (PPD $^{-}$) fold reduction. CD4 $^{+}$ T cells required for PPD $^{+}$ NAC-mediated growth inhibition (recall response). CD4 $^{-}$ CD8 $^{-}$ NAC contribute to innate immunity to MTB.	No
Kampmann, 2000 [274]	Human WB	Diluted WB co-cultured with mycobacteria (0-4 days).	Bijou tubes, platform shaker at 20 rpm	BCG Montreal lux	RLU, CFU	Optimisation of assay: RLU and CFU demonstrate similar growth pattern, 1 CFU = 10 RLU. Growth inhibition in PPD $^{+}$ vs PPD $^{-}$	No

						individuals, associated with increased TNF α and IFN γ levels.	
Worku, 2000 [290]	Human PBMCs	<ol style="list-style-type: none"> 1. PBMCs incubated (7 days) \pm BCG, MTBWL, TT. 2. Mono removed and matured (6 days). 3. Co-culture with BCG \pm expanded effector cells (3 days) from step 1. 	Multi-well plate	BCG	CFU, radiometric labelling	BCG growth inhibition following PBMC incubation with BCG or whole lysate vs control of TT. BCG vaccination enhanced this observation in some individuals.	Yes
Brill, 2001 [273]	Human PBMCs	Mono co-cultured with mycobacteria overnight \pm lymphocytes or NK cell fractions (0–4 days).	Multi-well plate	H37Rv	CFU	Lymphocyte-mediated killing of MTB occurs within 24 hours. Isolated NK cells recapitulated this effect, identified as independent of IFN γ and requiring direct cell-	

						to-cell contact via an alternative apoptotic pathway (non-Fas) in PPD ⁺ and PPD ⁻ .	
Wallis, 2001 [253]	Human WB	Diluted WB co-cultured with mycobacteria (3 days).	Tubes with constant mixing	DS-, MDR-MTB isolates	BACTEC MGIT	Referred to as 'whole blood bactericidal assay' (WBA). Used to determine bactericidal activity of WB collected before or at time points following administration of anti-tuberculosis drugs.	No (drugs)
Cheon, 2002 [254]	Human WB	[274] (0-4 days).	Tubes with constant mixing	H37Ra, BCG lux, H37Rv, attenuated MTB clinical isolate (MP-28)	BACTEC MGIT, RLU	CFU following 4-day co-culture increased with mycobacterial virulence in PPD ⁻ individuals. Repeated BCG vaccination reduced BCG CFU by	Yes

						50% vs baseline. T-cell depletion resulted in loss of growth inhibition of H37Ra, unaffected in MP-28.	
Hoft, 2002 [275]	Human PBMCs and WB	Comparison of three MGIAAs [272,274,290]		H37Rv, BCG, BCG lux	Various	All assays detected enhanced mycobacterial growth inhibition after BCG vaccination. IFN γ production did not correlate with mycobacterial inhibition. Readouts represent independent and complementary immune function information.	Yes
Cowley, 2003 [296]	Murine (C57BL/6/J, 129S1/SvIm	1. Murine lymphocytes primed with low-	Multi-well plate	Erdman	CFU	Growth inhibition of MTB Erdman by spleen and lung lymphocytes	Yes

	J) BMMs + spleen and lung lymphocytes	<p>dose MTB aerosol infection or i.d. BCG (4 weeks) ± chemotherapy (eliminate residual bacteria).</p> <p>2. Naïve BMM isolated and 7-day culture.</p> <p>3. Infection with mycobacteria (2 hours)</p> <p>4. Co-culture with lymphocytes from step 1 (10 days).</p>				<p>from Erdman, CDC1551 and BCG-primed mice was similar vs naïve. Significant portion of CD4 T-cell regulation of mycobacterial growth in absence of IFNγ in lung and spleen. CD4 and CD8 T cells accounted for large portion of growth inhibition in spleen.</p>	
Tena, 2003 [276]	Human WB	[274].		BCG Montreal lux	RLU, CFU	<p>PPD^{+/-} adults: improved control of mycobacterial growth in PPD⁺ vs PPD⁻ largely mediated by CD4⁺ T cells. HIV^{+/-}</p>	No

						children: mycobacterial growth impairment in HIV ⁺ vs HIV ⁻ associated with low CD4 counts and IFN γ .	
Wallis, 2003 [252]	Human WB	[253].		Autologous isolate, MP-28, H37Ra	BACTEC MGIT	Used to monitor drug treatment in TB patients. Bactericidal activity in WB culture correlated with sputum culture conversion and bacillary counts.	No (drugs)
Worku, 2003 [312]	Human PBMCs	<ol style="list-style-type: none"> 1. Mono cultured (6 days) and then infected overnight with BCG. 2. T cells were expanded with various mycobacterial and 	Multi-well plate	BCG Connaught	CFU, radiometric labelling	Enhanced growth inhibition in total PBMC and $\gamma\delta$ T-cell enriched fractions, not CD4 or CD8 T-cell fractions. Growth inhibition did not correlate with antigen-	Yes

		<p>non-mycobacterial antigens, MTBWL or live BCG.</p> <p>3. T cells and mono co-cultured (3 days).</p>				<p>specific IFNγ response. Growth inhibition capacity detected in cells from primary but not secondary BCG vaccination.</p>	
Denis, 2004 [293]	Cattle PBMC	<p>1. Mono cultured (7 days) and infected with mycobacteria.</p> <p>2. Lymphocytes expanded by PPD stimulation.</p> <p>3. Lymphocytes and infected MΦ co-cultured (6 days).</p>	Multi-well plate	<i>M bovis</i>	[³ H]uracil incorporation	<p>Growth inhibition in cultures containing PBMC from immunised and control animals; higher in immunised. Mediated by CD4⁺ T cells in control and CD4⁺ and CD8⁺ T cells in vaccinated.</p>	Yes
Kampmann, 2004 [255]	Human WB	[274].		BCG lux	RLU, CFU	<p>Mycobacterial growth inhibition higher in BCG-vaccinated South African infants vs unvaccinated. Growth</p>	Yes

						rates in infants prior to vaccination were higher vs adults.	
de Vallière, 2005 [314]	Mono, DCs and neutrophils isolated from human WB + sera	BCG preincubated with sera, followed by co-culture with mono, DCs or neutrophils (0–7 days)	Multi-well plate	BCG Connought	[³ H]uracil incorporation, CFU	Inhibitory effects of neutrophils and mono enhanced by BCG-induced antibodies and reversed by preabsorption of IgG with Protein G. BCG-induced antibodies enhanced proliferation and IFN γ production in antigen-specific CD4 and CD8 T cells, and proportion of CD8 T cells.	Yes
Janulionis, 2005 [283]	Human WB	Diluted WB co-cultured with mycobacteria (1–4 days).	Tubes, constant	18 MTB clinical isolates and 5 reference	BACTEC MGIT	PPD ⁻ subjects: replicative capacity of reference strains (low -	No

			slow mixing	strains (HN878, CDC1551, H37Rv, H37Ra, MP-28)		high) H37Ra, MP-28, HN878, H37Rv, CDC1551; clinical isolates varied greatly.	
Kampmann, 2006 [277]	Human WB	[274].		BCG lux	RLU, CFU	Mycobacterial growth control evaluated in BCG-vaccinated HIV-infected children before and after HAART initiation. Post HAART mycobacterial growth reduced.	No
Martineau, 2007 [278]	Human WB	[274].		BCG lux	RLU, CFU	Mycobacterial growth control evaluated in adult TB contacts treated with oral dose of vitamin D. Growth	No

						inhibition following treatment vs control.	
Martineau, 2007 [279]	Human WB	[274].		BCG lux and H37Rv lux	RLU, CFU	UK adult TB contacts evaluated for TB infection and ability to control mycobacterial growth. Neutrophil counts inversely related to TB infection. Neutrophil depletion impaired BCG and MTB growth inhibition.	No
Sada-Ovalle, 2008 [297]	Murine (C57BL/6) splenocytes and peritoneal MΦ	<ol style="list-style-type: none"> 1. Naïve MΦ infected with MTB (2 hours), washed and incubated overnight. 2. Co-cultured with splenocytes (or 	Multi-well plate	H37Rv	CFU	Addition of splenocytes reduces mycobacterial growth in infected MΦ vs MΦ alone. IFN γ produced under these conditions and CD1d-restricted iNTK cells	No

		purified cell subsets) (3 days).				sufficient to reduce MTB growth.	
Kolibab, 2009 [298]	Murine (C57BL/6) splenocytes and BMM	<ol style="list-style-type: none"> 1. Naïve BMM isolated and cultured (7 days). 2. Infection with mycobacteria (2 hours). 3. Splenocytes isolated from mice previously vaccinated with BCG s.c., SD1 protein/adjuvant, SD1-DNA and MVA-4TB and cultured for 2 hours to isolate non-adherent cells. 	Multi-well plate	INH ^r BCG	CFU	Development of a BSL2 growth inhibition assay. INH ^r used to differentiate between residual BCG and BCG in the assay. Vaccine-induced growth inhibition correlated with <i>in vivo</i> MTB protection. INH ^r and MTB growth inhibition similar but differences in vaccine-induced cytokine responses found.	Yes

		4. Splenocytes (5×10^6) co-cultured with infected BMM (1×10^7) for 4, 7 or 11 days.					
Parra, 2009 [299]	Murine (C57BL/6) splenocytes and BMM	[299]. Mice vaccinated with BCG s.c., <i>DsecA2</i> mutant, SD1-DNA, MVA-4TB, E6-85B.	Multi-well plate	Erdman	CFU (TCH added to plates to quantify MTB only)	Vaccine-induced mycobacterial growth inhibition at 1 week of co-culture correlated with <i>in vivo</i> protection 28 days post-challenge. Upregulated cytokines: IFN γ , GDF15, IL-21, IL-27 and TNF α .	Yes
Wallis, 2009 [284]	Human WB	[253]		Patient-specific isolates, H37Ra, MP-28	BACTEC MGIT	Cured TB patients vs PPD $^-$ healthy volunteers. TB patients able to control growth of their own clinical strain, as well as MP-28 vs	No

						healthy volunteers. No differences in control of H37Ra.	
Burl, 2013 [280]	Human WB	[274] Adapted		BCG lux	RLU, CFU	Two-fold reduction of blood volume (to make assay more suitable for paediatric studies) did not affect bacterial growth ratios.	No
Fletcher, 2013 [256]	Human WB and PBMCs	WB [253] PBMCs ‘direct’ MGIA: 1. Cryopreserved PBMCs thawed and rested overnight. 2. 1×10^6 co-cultured with 600 CFU mycobacteria (4 days).	Rotating 2-mL screw-cap tubes	BCG Pasteur	BACTEC MGIT	Head-to-head comparison of the ability of WB and PBMC assays to detect variations in mycobacterial growth inhibition following primary vaccination and revaccination in a UK adult population. PBMC MGIA detected	Yes

						improvement in growth inhibition following primary BCG vaccination, consistent with epidemiological data in population. No improvement following revaccination in WB or PBMC MGIA.	
Marsay, 2013 [201]	Murine (C57BL/6) splenocytes	<ol style="list-style-type: none"> 1. Mice vaccinated with BCG s.c./PBS. 2. Six weeks post vaccination, splenocytes harvested and co-cultured with mycobacteria for 4 days (1×10^6 splenocytes + BCG TTP 6.5). 	Rotating 2-mL screw-cap tubes	BCG	BACTEC MGIT	BCG immunisation reduced mycobacterial growth in splenocytes vs control. Growth inhibition corresponded to <i>in vivo</i> protection in MTB challenge. Microarray growth inhibition correlated with IFN γ , NOS2 and IL-17 expression.	Yes

Harris, 2014 [264]	Human WB	[253] 4 days.		BCG Pasteur	BACTEC MGIT	Human BCG i.d. challenge on UK adults: naïve, MVA85A, BCG and BCG + MVA85A. No differences in ability to inhibit mycobacterial growth.	Yes
Kolibab, 2014 [300]	Murine (ns) splenocytes and BMM	[299]. Mice vaccinated with BCG s.c., adenoviral or DNA construct expressing E6-85, the E6-85 protein + TDB/DDA adjuvant or the BCG mmaA4 mutant + TDB/DDA adjuvant.	Multi-well plate	Erdman	BACTEC MGIT, CFU	BACTEC MGIT vs <i>in vivo</i> MTB challenge. BACTEC MGIT TTP values inversely correlate with CFU from challenge. MGIT system is a faster and more straight-forward method.	Yes
Herzmann, 2015 [355]	Human BALMC	BALMC isolated from BAL and co-cultured with mycobacteria for 2 hours or	Multi-well plates	H37Rv, 2x Haarlem clinical isolates	CFU	TB healthcare workers, household contacts and cured TB patients ± previous history of BCG	Yes

		5 days (1 x 10 ⁵ BALMC: 5 x 10 ⁵ mycobacteria)				vaccination. Mycobacterial growth was independent of vaccination status.	
Naranbhai, 2015 [286]	Human WB and mixed leukocytes (25, 50 and 75 th centiles of ML ratio)	[253] 4 days.		BCG Pasteur	BACTEC MGIT	Healthy adult donors: higher ML ratio correlated with higher mycobacterial growth.	No
Zelmer, 2015 [305]	Murine (C57BL/6) splenocytes	1. Mice vaccinated with BCG s.c./PBS. 2. Six weeks post vaccination, splenocytes harvested and co-cultured with mycobacteria for 4 days (cell/bacterial input not specified).	Rotating 2-mL screw-cap tubes	BCG	BACTEC MGIT	Protocol for murine vaccination, splenocyte MGIA and standard curve generation.	Yes

Chen, 2016 [230]	THP-1 cells and sera	THP-1 cells co-cultured with paired sera and infected with mycobacteria (MOI 10) for 1 and 4 days.	Multi-well plates	BCG	CFU	Mycobacterial growth lower in THP-1 cells treated with postvaccination (BCG) vs pre-vaccination sera. Growth inhibition correlated with post-vaccination IgG titers to arabinomannan.	Yes
Fletcher, 2016 [207]	Human PBMC	PBMCs (1×10^6) co-cultured with mycobacteria (600 CFU) for 4 days.	Rotating 2-mL screw-cap tubes	BCG Pasteur	BACTEC MGIT	BCG-vaccinated infants from the MVA85A efficacy trial. Growth inhibition did not correlate with TB risk.	Yes
Hoft, 2016 [257]	Human WB	[253] 4 days.		BCG	BACTEC MGIT	Phase I of the AERAS-422 in healthy BCG-naïve adults. High-dose AERAS-422 vaccination induced growth inhibition	Yes

						<p>compared with baseline. Low-dose AERAS-422 or Tice BCG did not. Transcriptional analysis: growth inhibition positively correlated with T-cell expression modules and negatively correlated with monocyte expression modules.</p>	
Smith, 2016 [258]	Human PBMC	PBMCs (1×10^6) co-cultured with mycobacteria (862 CFU) for 4 days (in presence of pooled human antibody sera).	Rotating 2-mL screw-cap tubes	BCG Danish	BACTEC MGIT	<p>Mycobacterial growth inhibition was observed at 4 months post-BCG vaccination vs unvaccinated. No difference at 12 months. Growth inhibition correlated with frequency of</p>	Yes

						polyfunctional CD4 T cells.	
Yang, 2016 [307]	Murine (ns) splenocytes	<ol style="list-style-type: none"> 1. Mice vaccinated with PBS, BCG, BCG + DDA/TDB or ESAT6-SD1 + DDA/TDB. 2. Six weeks post vaccination, splenocytes pooled within groups (n=3) to generate 5 replicates. Co-cultured with mycobacteria for 4 days (5×10^6 splenocytes + 500 CFU). 	48-well plate	MTB	BACTEC MGIT, CFU	‘Simplified’ MGIA. Growth inhibition observed in vaccinated splenocytes vs control. Quantification comparable using CFU plating or BACTEC. Significant correlation between MTB challenge (4 weeks post-infection) and MGIA.	Yes

Zelmer, 2016 [306]	Murine (C57BL/6) splenocytes	[305].		BCG Danish, BCG PA, <i>M</i> <i>smegmatis</i>	BACTEC MGIT	Growth inhibition of all mycobacterial spp in BCG s.c. vaccinated vs control. <i>M smegmatis</i> reduced experiment length by 7 days. Various CFU and splenocyte inputs used. Reduced CFU input and higher number of splenocytes increased growth inhibition in immunised vs control. Variability increased with lower input. Optimal conditions: 5 x 10 ⁶ splenocytes + 100 CFU. Head-to-head comparison of MGIA with MTB challenge (4	Yes
-----------------------	------------------------------------	--------	--	---	-------------	--	-----

						weeks, 700 CFU) comparable at the group level. Mycobacterial growth increased in IFN γ ^{-/-} mice.	
Baguma, 2017 [287]	Human WB	Diluted WB co-cultured with mycobacteria for 4 days.	Tubes with slow rotation	BCG Danish, H37Rv, HN878, CDC1551	BACTEC MGIT	MTB infection status, age and MTB strain were not associated with differential control of mycobacterial growth.	No
Gurumurthy, 2017 [251]	Human WB	[253].		H37Rv	BACTEC MGIT	Healthy participants administered various drugs combinations of faropenem, amoxicillin/clavulanic acid and RIF. Mycobacterial growth determined at timepoints from baseline to 8 hours.	No (drugs)

Jensen, 2017 [308]	Murine (C57BL/6) splenocytes	[305] with enriched media (sodium pyruvate, non- essential amino acids and BME). Mice vaccinated with BCG, H56:CAF01 or BCG + H56:CAF01.		Erdman	BACTEC MGIT	Improved splenocyte viability at 4 days post co-culture by 25% (21 [305] vs 46%). Growth inhibition observed in vaccinated groups vs control. CD4 ⁺ T-cell count and cytokine expression unchanged ± MTB. IFN γ release correlated with growth inhibition.	Yes
Naftalin, 2017 [250]	Human WB	[253].		H37Rv	BACTEC MGIT	Allopurinol coadministration with PZA had no effect on bactericidal activity vs PZA alone.	No (drugs)
Pepponi, 2017 [294]	Bovine WB and PBMCs	[256] adapted. 1 x 10 ⁶ PBMC or 300 μ L WB +		BCG Pasteur	BACTEC MGIT	No significant difference in growth inhibition between	Yes

		3,500 CFU (1:51 WB, 1:6 PBMC).				BCG-vaccinated and control animals in WB or PBMC MGIA.	
Tanner, 2017 [259]	Human and NHP WB and PBMCs	[256].		BCG Pasteur	BACTEC MGIT	No correlation between mycobacterial growth in the WB and PBMC MGIA. Correlation between haemoglobin / iron levels and mycobacterial growth in the WB MGIA. May provide insight into variation noted in the WB MGIA, as well as the PBMC MGIA.	Yes
Joosten, 2018 [260]	Human PBMC	[256].		BCG	BACTEC MGIT	Mycobacterial growth inhibition high in individuals recently exposed to MTB, modest in BCG	Yes

						vaccinated and absent in long-term LTBI individuals. Control of growth correlated with non-classical mono and T cells and was associated with CXCR3 ligands.	
Naftalin, 2018 [249]	Human WB	[253].		H37Rv	BACTEC MGIT	Healthy participants administered celecoxib \pm standard TB drugs. Mycobacterial growth determined at timepoints from baseline to 8 hours. Celecoxib demonstrated no growth inhibitory effects alone or in combination.	No (drugs)

O'Shea, 2018 [289]	Human WB	[256] 150 CFU mycobacteria.		BCG, MTB	BACTEC MGIT	Mycobacterial growth inhibition highest in individuals with active infection, with a range of responses in LTBI. Control found to correlate with mono (higher ML ratio), memory B cells, IgG1 responses to MTB-specific antigens and specific serum cytokine / chemokine cluster.	No
O'Shea, 2018 [288]	Human WB	[256] 150 CFU mycobacteria.		H37Rv	BACTEC MGIT	Healthy adults screened for LTBI and GI parasite infections. Negative correlation between LTBI and hookworm infection. Mycobacterial growth	No

						inhibition was noted in those infected with hookworm vs uninfected.	
Radloff, 2018 [261]	Human BAL cells and PBMCs	1 x 10 ⁶ BAL cells or PBMCs co-cultured with 5.8 x 10 ⁴ mycobacteria (4 days).	24-well plates	H37Rv	BACTEC MGIT, CFU	No difference in mycobacterial growth in healthy adults before vs after BCG vaccination.	Yes
Basu Roy, 2019 [281]	Human WB	Diluted WB co-cultured with mycobacteria for up to 4 days.	Tubes, rocking incubator	BCG (Danish) -GFP-LuxFO	RLU, CFU	Aimed to improve [274]. Reduced blood volume required previously for BCG lux MGIA. RLU correlated with CFU.	No
Cross, 2019 [248]	Human WB	[253].		H37Rv	BACTEC MGIT	Mycobacterial growth inhibition determined following immuno-magnetic depletion of various cell types ± RIF.	No (drugs)

Dijkman, 2019 [291]	NHP PBMCs	[256] 100 CFU.		BCG Pasteur	BACTEC MGIT	Growth inhibitory capacity of PBMCs from two species of macaque determined pre- and 6- and 12-weeks post MTB infection. Growth inhibition post-infection in both species.	No
Lee, 2019 [262]	Human PBMCs	[256] 100 CFU.		BCG Pasteur	BACTEC MGIT	Growth inhibition was unaffected by various demographical characteristics in historically vaccinated healthy adults. Healthy controls found to control mycobacterial growth to greater extent than those with LTBI.	Yes

Prabowo, 2019 [311]	Human PBMCs	[256] 3×10^6 PBMCs + 100 CFU.		BCG Pasteur	BACTEC MGIT	Growth inhibitory capacity of PBMCs from historically vaccinated individuals \pm INH and RIF. Mycobacterial control by INH was higher in BCG-vaccinated individuals.	Yes
Prabowo, 2019 [174]	Murine (C57BL/6) splenocytes	[305] 5×10^6 splenocytes + 90 CFU. Mice vaccinated with BCG or RUTI.		BCG Pasteur	BACTEC MGIT	Mycobacterial growth inhibition significantly higher in RUTI vaccinated mice vs BCG/control.	Yes
Prabowo, 2019 [247]	Human PBMCs	[256] 3×10^6 PBMCs + 100 CFU.		BCG Pasteur	BACTEC MGIT	The impact of immune cell phenotype, CMV- specific response and sex on mycobacterial growth in healthy BCG- vaccinated and	Yes

						unvaccinated healthy individuals.	
Tanner, 2019 [263]	Human PBMCs	[256] 1 (tubes) or 3 (plates) x 10 ⁶ PBMCs + 500 CFU.	Rotating 2-mL screw-cap tubes or static 48-well plates	BCG Pasteur	BACTEC MGIT	Co-culture in 48-well plates (vs tubes) improved: cell viability on day 4 of co-culture by 23%; IFN γ production increased by 500-fold; intra- and inter-assay, and inter-site variability.	Yes
Basu Roy, 2020 [282]	Human WB	Diluted WB co-cultured with mycobacteria for up to 4 days.	Tubes, rocking incubator	BCG (Danish) -GFP-LuxFO	RLU, CFU	Asymptomatic Gambian children. Reduced mycobacterial control in highly TB-exposed uninfected to highly exposed infected. Cytokine responses mirrored infection status.	No

Tanner, 2020 [199]	Human PBMCs	[256] 3 x 10 ⁶ PBMCs + 500 CFU.	48-well plates	BCG Pasteur	BACTEC MGIT	Biological validation of direct PBMC MGIA. Per individual and per group correlation of <i>ex</i> <i>vivo</i> MGIA growth inhibition with <i>in vivo</i> infection (human challenge model).	Yes
-----------------------	----------------	---	-------------------	-------------	-------------	---	-----

1,25D, 1,25-dihydroxyvitamin D3; BALMC, bronchoalveolar mononuclear cells; BCG, Bacillus Calmette–Guérin; BCG lux, luciferase-labelled BCG; BME, 2-mercaptoethanol; BMM, bone marrow macrophages; CXCL, chemokine (C–X–C motif) ligand; CXCR, C-X-C motif chemokine receptor; DC, dendritic cells; DS, drug sensitive; GI, gastrointestinal; i.d., intradermal; iNKT, invariant natural kill T; IL, interleukin; i.n., intranasal; INH^r, isoniazid-resistant; LTBI, latent tuberculosis infection; MΦ, macrophage; MDR, multidrug resistant; MHC, major histocompatibility complex; ML, monocyte:lymphocyte; MOI, multiplicity of infection; MTB, *Mycobacterium tuberculosis*; MTBWL, MTB whole lysate; NAC, non-adherent cells; NHP, non-human primates; NOS, nitric oxide synthase; ns, not specified; PBMC, peripheral blood mononuclear cell; PZA, pyrazinamide; RIF, rifampicin; rIFN γ , recombinant interferon gamma; RLU, relative light units; s.c., subcutaneous; TCH, 2-thiophenecarboxylic acid hydrazide; TNF, tumour necrosis factor; TST, tuberculin skin test; TT, tetanus toxoid; WB, whole blood.

9.2 Appendix 2. Experimental analysis of host response to infection with strains of the MTB complex and vaccine-induced protection.

Author, year [ref]	Strain of MTB	Species and experimental strategy	Host response to infection	Vaccine-induced protection
Ordway, 1995 [490]	Erdman (L4), 15 clinical isolates (12 x MDR)	Mice, aerosol infection (20 – 50 CFU)	Range of virulence with no clear trend in terms of geographical source, degree of drug resistance, or growth rate <i>in vivo</i> . Increased drug resistance did not associate with loss of virulence.	
Manca, 1999 [491]	CDC1551 (L4), HN60 (L2), HN878 (L2), H37Rv (L4), Erdman	B6D2F1 mice, aerosol infection (200–400 CFU)	Survival significantly higher in CDC1551-infected mice vs others. CDC1551 induced more rapid and robust host response in lung: higher levels of TNF α , IL-6, IL-10, IL-12, IFN γ and well-organised granulomas. Observations confirmed in human PBMCs with H37Rv and CDC1551.	
Zhang, 1999 [492]	17 clinical isolates	hMDM	Community spread in an LA homeless shelter correlated with capacity to replicate in human M Φ s. Production of TNF α , IL-6, IL-10, and IL-12, and susceptibility to ROS intermediates, was unchanged between strains.	

Manca, 2001 [338]	HN878, HN60, NHN5 (L2), H37Rv, CDC1551	B6D2F1, aerosol infection (50–600 CFU)	HN878 hypervirulence - early death due to failed induction of T _H 1 response and lack of immunity associated with induction of type I IFNs.	
Li, 2002 [493]	H37Rv, Erdman, CDC1551, 9 x clinical isolates (4 identified as Beijing [L2])	Human monocytes	Growth capacity in human monocytes was significantly different between isolates. Four most rapidly growing isolates were Beijing family. Infection with H37Rv was more reproducible than Erdman.	
Lopez, 2003 [349]	3 x Beijing, 2 x <i>M canetti</i> , H37Rv, 3 x Haarlem (L4), 4 x Somali (L3)	BALB/c mice, i.t. injection	Beijing, extensive pneumonia, high mortality, early but short induction of TNF α and iNOS; <i>M canetti</i> limited pneumonia, ~100% survival, sustained induction of TNF α and iNOS; others (intermediate); Somali and Haarlem strains, heterogeneous intermediate survival rates.	BCG-induced protection against i.v. infection with Beijing, H37Rv and <i>M canetti</i> . Protection lowest against Beijing.
Manabe, 2003 [454]	Erdman, H37Rv, and CDC1551	New Zealand white rabbits, aerosol infection (various CFU)	Dose required to produce a visible lesion at five weeks post-infection lower for Erdman vs H37Rv. Animals infected with Erdman at 16–18 weeks: 7/15 rabbits healed lesions; 2/15 chronic, progressive cavitory	

			disease; a phenotype generally associated with <i>M bovis</i> infection in rabbits, not MTB.	
Dormans, 2004 [340]	H37Rv, Erdman, <i>M canetti</i> , ‘zero-copy’ ^a , ‘IS-in-Ori’ ^b , less-transmissible, Beijing, Africa, Amsterdam, Haarlem, Somalia	BALB/c mice, i.t. injection (2.5 x 10 ⁵ CFU)	Nineteen strains displayed broad range of virulence, pathology, bacterial load and delayed-type hypersensitivity. Within lineage variations found. Low pathogenicity: H37Rv, <i>M canetti</i> , Beijing-1, ‘zero-copy’; high pathogenicity: Beijing-2,3, Africa and Somalia-2. Severe pathological response correlated with high mortality and high CFU counts in lungs, not delayed hypersensitivity response.	
Manca, 2004 [326]	HN878, CDC1551, W/Beijing isolates	Human PBMC, <i>ex vivo</i> co-culture	Analysis of response to bacilli or lipid products of each strain. L2 isolates induced T _H 2 polarised response; CDC1551 induced T _H 1 protective response. Responses mediated by extracted lipids.	
Reed, 2004 [347]	H37Rv, CDC1551, HN878, NHN5, W4 (L2), 210 (L2)	B6D2F1 mice, aerosol infection (50–100 CFU)	PGL produced by Beijing strains correlated with hyperlethality. Disruption of PGL synthesis resulted in loss of hypervirulent phenotype and increased pro-inflammatory cytokine release.	

Barczak, 2005 [453]	CDC1551, HN878: mixed infection at various ratios	C57BL/6 mice, aerosol infection (50 CFU), BMM	Strain mixtures containing higher fractions of HN878 grew faster during first 5 weeks of infection and associated with increased lethality. In non-activated BMM, HN878 grew faster than CD1551; when activated, growth rate of both strains equal.	
Manca, 2005 [339]	HN878, CDC1551, W4	B6D2F1 mice, aerosol infection (100–200 CFU)	Increased levels of type I IFNs induced by HN878 and W4 strains associated with reduced TNF α , IL-12 and T-cell activation and increased expression of negative regulators of Jak–Stat signalling.	
Park, 2005 [494]	H37Rv, 4 x clinical isolates	C57BL/6 mice BMM	Rapid growth rate and induction of necrotic cell death identified as virulence factors during early infection. Apoptosis of infected cells plays a minimal role.	
Theus, 2005 [495]	13 x clinical isolates	THP-1 cells	Strains isolated from clusters of cases grew faster than those from unique cases; correlated with rapid production of IL-10 and suppression of TNF α in THP-1 cells during early infection.	
Tsenova, 2005 [348]	H37Rv, HN878	New Zealand white rabbits, CNS infection		BCG-induced protection against both strains; eight weeks post-infection CNS detectable HN878

				bacillary load, H37Rv undetectable.
Newton, 2006 [496]	CDC1551, H37Rv, CH (L3)	hMDM, <i>ex vivo</i> co-culture	CH microbiologically attenuated (poor growth in broth) vs CDC1551 and H37Rv but no impairment in ability to grow in hMDM. CH-infected MΦs: reduced IL-12 and increased IL-10 and IL-6.	
Ordway, 2007 [327]	H37Rv, HN878, CSU 123, CDC1551, Erdman	C57BL/6 mice, aerosol infection (50–100 CFU)	Survival lowest in HN878-infected mice, with rapid mycobacterial growth and high lung pathology score. Induction of T _H 1 response following infection with all strains. Unique to HN878 infection was a subsequent reduction in T _H 1 immunity and emergence of T _{reg} population. Type I IFN shown to play inhibitory role in T _H 1 response in all strains tested.	
Theus, 2007 [341]	15 x Beijing strains	THP-1 cells	Range of growth phenotypes over the seven-day infection period. Three grew significantly slower; fastest growth observed in isolates of strain 210 (HN878 also a 210 strain).	
Jeon, 2008 [353]	Erdman, 4 x Beijing (HN878, N4, NHN5, ChS), 4	C57BL/6 mice, aerosol		BCG-vaccinated animals: protection against 9/9 stains at 4 weeks; 6/9 at 6 weeks; 3/9 at 20

	x non-Beijing (C913, CDC1551, NY669, NY920)	infection (200 CFU)		weeks (reduced inflammation in all). Protection at 20 weeks not associated with a specific strain.
Marquina–Castillo, 2009 [455]	8 x MTB clinical isolates from a prospective population study of pulmonary TB patients (no genotyping performed)	BALB/c, i.t. infection (2.5 x 10 ⁵)	Identified four strain phenotypes: i) hypervirulent, non-protective immune response, highly transmissible; ii) virulent, high expression of proinflammatory cytokines, low anti-inflammatory cytokine expression, accelerated death; iii) efficient protective immunity, lower virulence; iv) strong and early MΦ activation with delayed participation of acquired immunity. Phenotypes i and ii were found to correlate with markers of community transmission in human analysis.	
Palanisamy, 2009 [342]	H37Rv, 3 x Beijing W, 2 x non-Beijing; both sets included MDR and drug-sensitive	Harley GP, aerosol infection (20 CFU)	Beijing and non-Beijing clinical isolates exhibited wide range of virulence, with specific isolates causing severe and rapidly progressive pulmonary and extra-pulmonary lesion necrosis. Low level virulence, lesion scores and survival in animals infected with MDR strains.	

Sohn, 2009 [497]	H37Rv, K (hypervirulent L2 Beijing)	THP-1 cells	No difference in growth rate observed and both strains induced cell death. TNF α , IL-6 and IL-12 lower in K-strain-infected cells vs H37Rv. K-strain induced higher levels of necrotic cell death, rather than apoptosis. Numerous anti-apoptotic markers significantly upregulated following infection with K-strain. K-strain reduces cellular apoptosis as a host defence mechanism and induces necrosis.	
Aguilar, 2010 [343]	3 x non-transmitted and 2 x highly transmitted Beijing genotype strains	BALB/c mice, i.t. infection (2.5 x 10 ⁵ CFU)	Beijing strains display spectrum of virulence phenotypes in mice which mimic epidemiological characteristics. Mortality significantly higher with highly transmitted strains, indicative of high virulence phenotypes. High virulence correlated with extensive tissue damage, lower levels of IFN γ and iNOS expression, and high but transient TNF α expression. Both phenotypes induced similar levels of IL-4 expression during early infection; IL-4 higher in high virulence phenotype thereafter.	

Homolka, 2010 [332]	6 x L4 (Haarlem and Uganda), 3 x L2 (Beijing), 3 x L1 (EAI), 3 x L6 (WA2), H37Rv, CDC1551	C57BL/6 mice BMM	RNA extraction from mycobacteria and microarray. Identified lineage-specific transcription patterns and intracellular growth profiles.	
Wang, 2010 [345]	H37Rv and 9 x L2 (Beijing), 12 x L4, 4 x L1	Human MΦs and DCs	Beijing strains induced significantly reduced levels of IL-6, TNF α , IL-10 and GROA compared with H37Rv. Levels were heterogeneously induced by strains of other lineages. Beijing strains did not differ relative to one another in ability to modulate cytokine secretion.	
Krishnan, 2011 [441]	5 x L1, 7 x L2, 6 x L4, H37Rv, HN878	BALB/c mice BMM and DCs; BALB/c, i.n. infection (1 x 10 ⁴ CFU)	L2 and L1 induced higher levels of TNF α and IL-1 β expression in MΦs vs L4. L1 induced higher levels of IL-10 expression vs L2 and L4. Faster growth and dissemination to the blood in L2-infected mice. Lineage-specific variation in cell envelope lipids identified but not shown to drive lineage-specific differences observed.	
Ordway, 2011 [352]	H37Rv, HN878, SA161 (L2)	C57BL/6 mice, aerosol		BCG Pasteur vaccinated mice reduced lung consolidation and

		infection (50–100 CFU)		smaller, more organised granulomas at 30 days vs unvaccinated. Protection against L2 strains observed up to 60 days, with worsening pathology. Vaccinated mice infected with HN878: increased T_{eff} at day 30, followed by increased T_{reg} population at day 30. Protection against H37Rv observed across full time course.
Portevin, 2011 [334]	26 clinical isolates from the Gagneux reference set (representative of L1–6 [23]), BCG and H37Rv	hMDM and DCs, human PBMCS, BALB/c mice BMM	Skewing of modern lineages (L2–4) towards lower inflammatory response in human MΦs. Confirmed in DCs and murine BMMs. Not observed in human PBMCs. Reduced immune response to modern lineages may contribute to increased rate of disease progression and transmission. Range of cytokine responses between strains of the same lineage was marked despite skew.	

Kato– Maeda, 2012 [346]	10 x L2 representing 4 sublineages of Beijing sub-strain	Hartley GP, aerosol infection (20 CFU)	Low-dose infection with all strains resulted in mycobacterial growth and pathology. Differences in pathology were not stark but one strain caused significantly more lung damage than others (RD207), concomitant with increased T _{reg} markers and loss of activated T cells.	
Koo, 2012 [498]	CDC1551, HN878	B6D2F1 mice BMM	Similar intracellular growth rates. Analysis of MΦ and mycobacterial transcriptome. CDC1551 infection: early and robust MΦ activation, concomitant with upregulation of bacterial stress response genes in the CDC1551 transcriptome. HN878 infection: suboptimal MΦ activation and dysregulated host cell lipid metabolism, concomitant with reduced stress response in HN878 transcriptome.	
Romero, 2012 [350]	L4: drug- susceptible and MDR (Ra) LAM strains, drug- susceptible and	Human neutrophils	Strong induction of neutrophil apoptosis and induction of ROS production and p38 induction following infection with LAM strains. M (Haarlem) unable to activate and induce apoptosis due to weak ROS production and anti-apoptosis mechanisms.	

	MDR (M) Haarlem strains, H37Rv			
Sarkar, 2012 [336]	Strains representative of L2–4	hMDMs	Growth phenotypes in liquid culture: L4 fastest growth; L3 low and early growth plateau; L2 intermediate. Cytokine profiles in MΦs: L2 lowest levels of pro-inflammatory TNF and IL-12; L3 high TNF and low IL-12; L4 high IL-12 and intermediate TNF.	
Reiling, 2013 [333]	H37Rv, 3 x L1, 4 x L2, 6 x L4, 2 x L6	Human BAL cells, hMDM; C57BL6 and DBA/2 mice, aerosol infection (200 CFU)	Increased growth in human MΦs and BAL cells. No correlation with specific inflammatory profile identified. Three pathogenic profiles identified: L2 – low uptake, low cytokine induction, high growth rate; L4 – high uptake, high cytokine induction, and high growth rate; L1 – low uptake, low cytokine induction, low growth rate. Murine <i>in vivo</i> studies: C57BL6 H37Rv and L2 growth comparable, L1 100-fold lower. DBA/2 survival highest following L1 infection and lowest with L2.	

Via, 2013 [317]	K04 (L2), CDC1551, N0091 (L6)	Common marmoset, aerosol infection (200 CFU)	Survival significantly lower in animals infected with K04, concomitant with increased volume of dense, diseased lung and high glycolytic activity. Bacterial burden in liver, spleen, lung and lymph node significantly higher in K04-infected animals vs CDC1551- and N0091-infected animals.	
Gopal, 2014 [63]	HN878, H37Rv, CDC1551	C57BL/6 mice, aerosol infection (100 CFU)	IL-17 previously considered to be dispensable for protection against MTB. HN878 requires IL-17 for early protective immunity; H37Rv and CDC1551 do not. Protection against HN878 induced via production of IL-1 β through a TLR-2-dependent mechanism.	
Reyes–Martinez, 2014 [337]	BCG Pasteur, H37Rv, <i>M canetti</i> , Beijing	BALB/c mice BMM	Beijing strain modulates DC activation and function - maturation of DCs inhibited by Beijing strain.	
Ribeiro, 2014 [344]	6 x L2 ‘Ancient’ and ‘modern’ Beijing strains, B0/W148 (hypervirulent and	C57BL/6 mice, i.t. infection (100 or 2,500 CFU); BMM infection	Modern Beijing strains demonstrate highly virulent phenotypes compared with more ancient strains. 2/3 modern Beijing strains highly pathogenic and demonstrated comparable virulence to B0/W148. All ancient Beijing strains demonstrated low or intermediate virulence.	

	epidemic Beijing strain), H37Rv			
Romero, 2014 [351]	M (Haarlem), Ra (LAM)	Human neutrophils	Strain M does not induce ROS in neutrophils due to reduction in phagocytosis and lipid raft coalescence. Hypothesised to benefit intracellular survival.	
Tientcheu, 2014 [329]	29 MTB- and 19 MAF-infected patients	Human whole blood	Differences in T-cell responses to mycobacterial strains with differing virulence. Antigen-specific single TNF α -producing CD4 and CD8 T cells significantly higher and single IL-2-producing T cells significantly lower in patients infected with MAF compared with MTB.	
Henao–Tamayo, 2015 [122]	Set of clinical isolates from the Bay Area (USA; 3 x L2 Beijing) and Western Cape (4 x L2 Beijing, 1 x L4 Haarlem), H37Rv	C57BL/6 mice, aerosol infection (50–100 CFU); Hartley GP, aerosol infection (10–20 CFU)		BCG protection against strains from W Cape and the Bay Area variable and short-term for specific strains. Two profiles: i) infection controlled up to 30 days, thereafter bacterial load plateaued/declined; ii) infection slowed up to 30 days vs control, thereafter increased bacterial load

				and protection lost. Second profile common in Bay Area strains; BCG strongly inhibited W Cape strains. Both W Cape and Bay Area strains highly virulent, differences in BCG protection hypothesised to relate to strain fitness (lower in W Cape strains).
Kim, 2015 [328]	Laboratory strains: H37Rv and H37Ra, K	C57BL/6, aerosol infection (450–500 CFU H37Ra, 150–200 CFU H37Rv/K)	Increased growth of K vs laboratory strains at day 28, with increased lung pathology at days 56 and 112. Analysis of immune cell populations: laboratory strains – increased T _H 1 and T _H 17 populations in the lung; K strain – accumulation of plasmacytoid DCs and Gr1 ^{int} CD11b ⁺ cells, downregulation of T _H 1, upregulation of T _H 2, no induction of T _H 17.	
Leisching, 2017 [440]	Hyper- (R5527) and hypovirulent (R1507) Beijing strains	C57BL/6 mice BMM, THP-1 cells	RNA-seq analysis of murine BMMs identified 69 differentially expressed genes. Hypervirulent infection was associated with activation of the stress-induced and growth inhibitory Gadd45 signalling pathway. Hypovirulent infection was associated with	

			upstream regulators of IFN activation. A robust proinflammatory response was observed following infection of THP-1 cells with the hypervirulent strain.	
Romagnoli, 2018 [26]	2 x L1, 1 x L3, 2 x L4, 1 x L5, H37Rv	hMDMs	L4 associated with higher rate of replication, production of proinflammatory cytokines (IL-1 β , IL-6 and TNF α) and induction of a functional autophagy process (autocrine activity of IL-1 β) vs L1 and L5. Autophagy triggered by inflammatory cytokines correlates with increased mycobacterial replication and may contribute to increased pathogenicity of modern lineages.	
Tram, 2018 [499]	H37Rv, 153 clinical isolates: 78 x L2, 50 x L1, 18 x L4, 7 x unidentified	THP-1 cells, hMDMs	High virulence was associated with increased sputum bacterial load in patients prior to TB therapy, high replication rate in THP-1 cells and hMDMs, lower levels of TNF α and IL-6 and increased levels of IL-1 β . High virulence strongly associated L2 with isolates.	
Mourik, 2019 [319]	H37Rv, Beijing-1585 (L2) and EAI-1627 (L3)	BALB/c mice, i.t. infection (1–1.8 x 10 ⁵)	H37Rv: ‘classical’ T-cell influx in the lungs with increase IFN γ levels; L2 and L3: B-cell influx to lungs, increased IL-4, functional impairment of	

			myeloid cells, reduced iNOS and IL-12 expression levels vs H37Rv infection. Significantly decreased expression of IFN γ , TNF α and IFN β in bone marrow of mice infected with L2 and L3 from three-days post-infection compared with H37Rv-infected mice.	
Levillain, 2020	H37Rv, M2 (L4), HN878	C57BL/6 mice, aerosol infection (200–250 CFU)		BCG Pasteur and GC1237 Rv1503c::Tn Δ phoPR vaccine-induced protection against M4; GC1237 Rv1503c::Tn Δ phoPR vaccine-induced protection against HN878.
Perez, 2020 [24]	W4, HCU3524 (L3) or H37Rv	C3H/HeNRj mice, i.n. infection (200 CFU)		BCG Pasteur, MTBVAC (originally constructed from L4), 2 x candidate vaccines based on MTBVAC: MTBVAC-L2::hyg and MTBVAC-L3::hyg. BCG protected against L2–4. Candidates showed similar or superior protection against L2–4. Protection independent of

				phylogenetic lineage used as template strain for vaccine construction.
--	--	--	--	--

Lineage is indicated on first instance of use where stated or identifiable in the manuscript. ^astrain lacking IS6110 DNA (MTB complex specific insertion element); ^bstrain with insertion of IS6110 element in genomic dnaA-dnaN region (characteristic of Beijing strains). BAL, bronchoalveolar lavage; BCG, Bacille Calmette–Guérin; BMM, bone marrow-derived macrophages; DCs, dendritic cells; GM-CSF, granulocyte-macrophage colony-stimulating factor; GP, guinea pig; hMDM, human monocyte-derived macrophages; IFN γ , interferon gamma; IL, interleukin; i.n., intranasal; i.t. intratracheal; i.v., intravenous; L, lineage; MAF *Mycobacterium africanum*; MDR, multi-drug resistant; MTB, *Mycobacterium tuberculosis*; M Φ , macrophage; NOS, nitric oxide synthase; PGL, phenolic glycolipid; ROS, reactive oxygen species; TNF α , tumour necrosis factor alpha.

9.3 Appendix 3. Solutions, reagents, consumables and equipment.

9.3.1 Solutions

7H9 liquid media: Dissolve 4.7 g 7H9 powder and glycerol (final concentration, 0.2%) in 900 mL deionised water and autoclave at 121°C for 15 minutes. Leave to cool to 37°C. Under sterile conditions, add OADC (final concentration, 10%) and sterile-filtered Tween-80 (final concentration, 0.05%).

7H11 agar: Dissolve 21 g 7H11 powder and glycerol (final concentration, 0.5%) in 900 mL deionised water and autoclave at 121°C for 15 minutes. Leave to cool to 55°C. Under sterile conditions, add OADC (final concentration, 10%). Add 25 mL media to 9-cm Petri dishes.

7H11 agar (TCH): As above with addition of TCH (final concentration, 2 µg/mL) following autoclave step.

ACK lysis buffer: 150 mM NH₄Cl, 10 mM KHCO₃, 100 mM Na₂EDTA in Ultrapure water, Milli-Q; pH 7.2–7.4 with 1M HCl, volume to 1L and autoclave at 121°C for 15 minutes.

Cryopreservation media: 0.85% NaCl, 20% glycerol, volume with Ultrapure water. Autoclave at 121°C for 15 minutes and leave to cool to 37°C. Under sterile conditions, add 0.05% sterile-filtered Tween-80.

FACS buffer: dissolve one PBS tablet per 100 mL distilled water. Autoclave at 121°C for 15 minutes and leave to cool to 37°C. Under sterile conditions, add FBS (final concentration, 1%).

PBS–Tween 80 (PBS–T80): dissolve one PBS tablet per 100 mL distilled water. Autoclave at 121°C for 15 minutes and leave to cool to 37°C. Under sterile conditions, add sterile-filtered Tween-80 (final concentration, 0.05%).

R0L: RPMI-1640 + 2 mM L-glutamine + 50 U/mL penicillin.

R10L: RPMI-1640 + 2 mM L-glutamine + 50 U/mL penicillin + 10% FBS.

R10S: RPMI-1640 + 2 mM L-glutamine + 10% FBS.

Wash buffer: 0.85% NaCl, volume with Ultrapure water. Autoclave at 121°C for 15 minutes and leave to cool to 37°C. Under sterile conditions, add 0.05% sterile-filtered Tween-80.

9.3.2 Reagents

Product	Catalogue number, supplier
2-Mercaptoethanol, BioUltra, for molecular biology, $\geq 99.0\%$ (GC) 14.3 M	63689, Sigma, UK
2-Thiophenecarboxylic acid hydrazide, $\geq 98\%$	T1388, Sigma-Aldrich, UK
ArC Amine Reactive Compensation Bead Kit (for use with LIVE/DEAD Fixable dead cell stain kits)	A10628, Thermo Fisher, UK
Autoclaved <i>B subtilis</i> HU58 spores (SGUL)	Sporegen, UK
BACTEC MGIT tubes	245122, BD, UK
BCG Danish 1331 (1.4×10^8 CFU/mL)	SSI, Copenhagen, Denmark
BCG Pasteur Aeras (1.8×10^7 CFU/mL)	Aeras, Rockville MD, USA
Brilliant Stain Buffer	563794, BD Biosciences, UK
CD16/CD32 Monoclonal Antibody (93), eBioscience	14-0161-82, Thermo Fisher, UK
Deoxyribonuclease I from bovine pancreas (DNase)	D5025-150KU, Sigma, UK
Ethanol, Absolute (200 Proof), Molecular Biology Grade	BP2818, Fisher Scientific, UK
Foetal bovine serum (FBS)	FCS-SA/500-21003H, Labtech

FP-1 (Ag85B-Acr-HBHA) (SGUL)	Lionex GmbH, Germany
Glycerol	G5516, Sigma, UK
Ketalar	Pfizer Ltd, Walton Oaks, UK
L-glutamine	10104042, Fisher Scientific, UK
Liberase TL	05401020001, Sigma, UK
LIVE/DEAD™ Fixable Blue Dead Cell Stain Kit, for UV excitation	L34961, Thermo Fisher, UK
Middlebrook 7H9 Broth	271310, Yorlab, UK
Middlebrook OADC Enrichment	212331, Yorlab, UK
Mycobacteria 7H11 Agar	283210, Yorlab, UK
<i>Mycobacterium tuberculosis</i> Erdman (7 x 10 ⁷ CFU/mL)	BEI Resources, UK
<i>Mycobacterium tuberculosis</i> complex reference set	Sebastian Gagneux, Swiss Tropical and Public Health Institute, Switzerland
NEBNext Ultra II Directional RNA Library Prep Kit for Illumina	E7760, New England Biolabs, UK
NEBNext Poly(A) mRNA Magnetic Isolation Module	E7490, New England Biolabs, UK
Nuclease-Free Water	129114, Qiagen, UK
NextSeq 500/550 High Output Kit v2.5 (75 Cycles)	20024906, Illumina, UK
OneComp eBeads Compensation Beads	01-1111-41, Thermo Fisher, UK
PBS	11540546, Fisher Scientific, UK
Physiological saline solution for irrigation	AKF7123, Baxter, USA
PANTA enrichment	245124, BD, UK
Penicillin G Na Salt	P3032-25MU, Sigma, UK
QIAshredder	79654, Qiagen, UK
RBC lysis buffer	R7757, Sigma, UK
RNeasy Mini Kit	74104, Qiagen, UK
RNAprotect Cell Reagent	76526, Qiagen, UK
RNA ScreenTape Analysis	5067-5581, 5067-5580, 5067-5579 (high sensitivity), 5067-5578, 5067-5577, 5067-5576 (standard) Agilent, UK

RNase-Free DNase Set	79254, Qiagen, UK
RPMI-1640	R5886, Sigma-Aldrich, UK
Trypan blue solution (0.4%)	T8154, Sigma, UK
Tween-80	P4780, Sigma, UK
Water, sterile-filtered, BioReagent, suitable for cell culture	W3500, Sigma, UK
xGen Dual Index UMI Adaptors	Integrated DNA Technologies, USA
Xylazine	Bayer plc, Newbury, UK

9.3.3 Antibodies: flow cytometry

Marker	Colour	Host / target	Isotype	Clone	Catalogue number, supplier	Concentration
B220 (CD45R)	BV510	Rat α -mouse	IgG2a κ	RA3-6B2	103248, Biolegend	1:40
CD11b	BV650	Rat α -mouse	IgG2b κ	M1/70	101259, Biolegend	1:67
CD11b	APC-Cy7	Rat α -mouse	IgG2b κ	M1/70	101225, Biolegend	1:320
CD11c	BV605	Armenian hamster α -mouse	IgG	N418	117334, Biolegend	1:40
CD11c	PE	Armenian hamster α -mouse	IgG	N418	117307, Biolegend	1:37
CD24	BV510	Rat α -mouse	IgG2b κ	M1/69	101831, Biolegend	1:400
CD45	BUV395	Rat α -mouse	IgG2b κ	30-F11	565967, BD	1:160
CD45	PE	Rat α -mouse	IgG2b κ	30.F11	103105, Biolegend	1:100

CD3	APC/Cy7	Rat mouse	α -	IgG2b κ	17A2	100222, Biolegend	1:80
CD64	PE-Cy7	Mouse mouse	α -	IgG1 κ	X54-5/7.1	139314, Biolegend	1:80
Ly-6G	BV711	Rat mouse	α -	IgG2a κ	1A8	127643, Biolegend	1:40
I-A/I-E	APC	Rat mouse	α -	IgG2b κ	M5/114.15.2	107613, Biolegend	1:637
NK1.1 (CD161)	APC	Mouse mouse	α -	IgG2a κ	PK136	108709, Biolegend	1:60
Siglec-F	BV605	Rat mouse	α -	IgG2a κ	E50-2440	740388, BD	1:40

9.3.4 Consumables

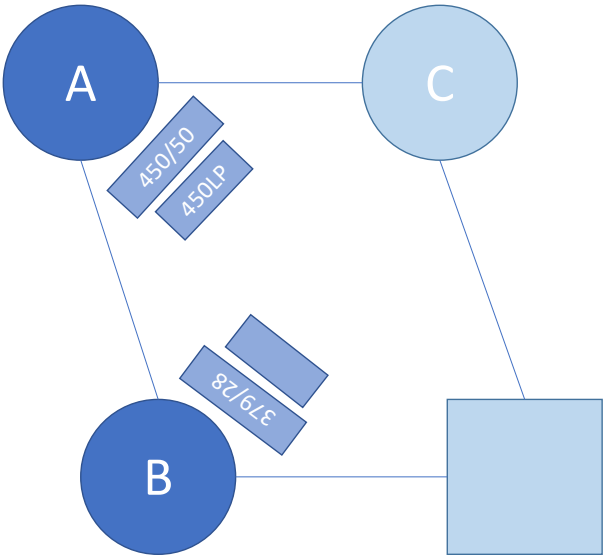
Product	Catalogue number, supplier
Bijou (7 mL)	C129B, VWR, USA
Cell scrapers	22003, Biotium, USA
Cell strainers (100 μ m)	352360, VWR, USA
Collection Tubes (2 mL) for spin-column kits	19201, Qiagen, UK
Disposable counting chambers	BVS100, VWR, USA
Falcon 5 mL polystyrene round-bottom tube	352054, Fisher Scientific, UK
Falcon conical centrifuge tubes (15, 50 mL)	188271 / 227261, Greiner Bio-One, Austria
Multi-well plates	24: 142475, Fisher Scientific, UK 48: 130187, Fisher Scientific, UK
Needles (25G)	SYR6122, Fisher Scientific, UK
Pasteur pipette	LW4006, Alpha Labs, UK
Petri dishes (55, 90 mm)	PET2018 / PET2002, SLS, UK
Screw-cap Eppendorf tubes (2 mL)	72.694.006, Sarstedt, Germany

Sterile filter tips (various)	BT1250, BT200, BT20, BT10, WolfLabs, UK
Syringes (5 mL)	10080264, Fisher Scientific, UK

9.3.5 Equipment

Equipment	Model, manufacturer
BACTEC MGIT 320 mycobacterial detection system	441743, BD, UK
BACTEC MGIT 960 mycobacterial detection system	445870, BD, UK
Bioanalyzer 2100	G2939BA, Agilent, UK
Benchtop refrigerated centrifuge	PK13OR, Thermo, UK
CelCulture CO ₂ incubator	ESCO Medical, Denmark
Cell density meter	WPA CO8000, Biochrom Ltd, UK
LSR II flow cytometer	BD Biosciences, UK Configuration: (Institute for Child Health, UCL, London, UK): shorturl.at/abjlZ
Nanodrop Spectrophotometer	ND2000, Thermo Scientific, UK
NextSeq 500	SY-415-1001, Illumina, UK
PerfectSpin 24 Plus bench-top microcentrifuge	Peqlab, DE, USA
Microscope	NAO.20 WD72, Yenway, UK
Qubit Flex Fluorometer	Q33327, Invitrogen, UK
TapeStation 4200	G2991AA, Agilent, UK

9.5 Appendix 5. LSR II configuration for flow cytometry panel I.



Custom configuration 325 UV laser (325 nm) used at ICH (UCL).

9.6 Appendix 6. RNA-seq I – Library prep input and MultiQC report.

Sample name	Concentration, ng/μL	RINe	% Assigned¹	M Assigned²	% rRNA³	% mRNA⁴	% Aligned⁵	M Aligned⁶	% Dups⁷	% GC⁸	M Seqs⁹
S1-1	25.1	8.9	67.5	17.6	0.3	92.8	85.7	19.0	63.2	50	22.2
S1-3	18.7	9.1	67.7	18.9	0.4	92.7	85.9	20.4	64.8	50	23.7
S1-4	16.9	9.3	67.3	15.8	0.3	92.4	85.2	17.1	62.7	50	20.0
S2-4	14.4	9.3	69.0	23.6	0.3	92.7	86.7	25.5	71.5	50	29.4
S2-5	15.9	9.2	69.0	21.8	0.2	91.7	87.0	23.8	68.0	50	27.3
S2-6	13.2	9.1	67.3	17.0	0.3	90.9	85.5	18.8	68.4	50	22.0
S3-1	21.4	9.5	68.5	15.5	0.3	91.0	86.3	17.1	66.1	50	19.8
S3-3	35.4	9.6	69.5	17.5	0.2	92.7	87.0	18.9	63.8	51	21.7
S3-4	23.3	9.7	69.4	15.4	0.2	92.5	87.1	16.7	61.2	50	19.2
U1-1	30.1	8.4	68.3	21.5	0.3	92.7	86.8	23.3	61.0	50	26.9
U1-3	33.0	9.2	67.2	22.1	0.2	92.3	86.4	24.0	59.8	50	27.7

U1-4	23.2	8.5	68.9	19.2	0.2	92.8	87.2	20.8	59.0	50	23.8
U2-4	8.75	9.0	69.8	17.9	0.2	93.2	87.7	19.3	56.4	50	22.0
U2-5	9.66	8.1	69.8	19.9	0.2	92.3	87.7	21.7	58.7	50	24.8
U2-6	6.48	8.2	69.6	24.8	0.2	93.0	87.6	26.9	63.4	50	30.7
U3-1	15.1	8.7	70.7	18.1	0.7	91.9	87.9	19.9	67.2	51	22.6
U3-3	26.3	9.4	71.6	15.9	0.2	94.1	88.4	17.1	63.8	51	19.4
U3-4	17.8	9.6	72.3	17.9	0.2	94.3	88.9	19.2	61.1	50	21.6

RINe, RNA integrity number equivalent. ¹percent reads mapped to features (featureCounts); ²number (millions) of reads mapped to features (featureCounts); ³percent aligned bases overlapping ribosomal RNA regions (Picard); ⁴percent aligned bases overlapping UTRs and coding regions of mRNA transcripts (Picard); ⁵percent of reads uniquely mapped to genome (STAR aligner); ⁶number (millions) of reads uniquely mapped to genome (STAR aligner); ⁷percent duplicate reads (FASTQC); ⁸average % GC content (FASTQC); ⁹total (millions) sequences (FASTQC).

9.7 Appendix 7. RNA-seq II – Library prep input and MultiQC report.

Sample name	Concentration, ng/μL	RINe	% Assigned ¹	M Assigned ²	% rRNA ³	% mRNA ⁴	% Aligned ⁵	M Aligned ⁶	% Dups ⁷	% GC ⁸	M Seqs ⁹
L1B1	7.77	9.0	61.2	15.6	4.4	82.3	86.2	18.5	53.7	49	21.4
L1B2	26.2	8.4	61.0	12.7	4.0	83.3	85.9	15.0	50.4	48	17.4
L1B3	26.3	8.7	61.8	16.7	3.2	84.8	86.3	19.6	52.6	49	22.7
L1C1	11.1	8.9	63.3	11.1	2.7	86.7	86.1	12.6	48.6	49	14.7
L1C2	12.7	8.3	61.2	14.6	4.0	83.5	85.5	17.1	57.8	50	20.0
L1C3	15.7	8.9	64.9	16.5	0.9	89.3	87.1	18.8	53.0	50	21.6
L2B1	20.5	9.3	61.4	16.8	1.4	87.0	84.9	19.4	56.3	47	22.9
L2B2	11.0	8.5	61.0	15.1	4.1	83.4	85.4	17.6	53.2	49	20.6
L2B3	19.0	9.0	60.6	15.4	4.4	83.2	85.9	18.3	52.7	50	21.3
L2C1	29.6	9.0	62.1	15.0	3.8	84.3	86.0	17.4	54.9	50	20.2
L2C2	15.5	8.5	62.1	13.0	2.2	86.7	85.8	14.9	52.1	49	17.4

L2C3	10.3	8.7	59.3	17.3	3.6	83.8	84.6	20.4	52.5	49	24.1
L4B1	11.8	9.1	61.3	13.3	3.0	84.1	85.8	15.5	56.5	48	18.1
L4B2	17.2	8.6	61.1	13.2	2.9	85.5	85.7	15.3	51.6	48	17.9
L4B3	13.5	8.5	59.2	15.9	3.9	82.1	85.2	19.0	52.1	48	22.3
L4C1	19.4	8.7	59.9	17.8	4.0	82.8	85.7	21.2	54.5	49	24.8
L4C2	40.3	8.5	61.0	14.1	4.3	82.7	85.5	16.5	57.4	49	19.3
L4C3	29.3	9.1	60.9	16.1	2.6	85.9	84.8	18.5	59.2	49	21.8
UB1	17.3	8.8	61.5	14.8	3.7	84.5	86.3	17.4	50.8	49	20.1
UB2	40.0	8.6	61.4	12.0	3.4	84.5	86.2	14.1	50.6	49	16.3
UB3	37.0	8.7	60.5	14.2	4.6	82.8	85.6	16.7	52.2	50	19.5
UC1	7.62	8.6	60.9	14.1	3.1	84.2	86.0	16.6	50.0	48	19.3
UC2	17.4	8.2	60.0	14.4	4.1	83.4	84.9	16.8	55.2	48	19.8
UC3	42.6	8.7	60.7	13.4	5.0	82.7	85.3	15.5	54.9	50	18.2

RINe, RNA integrity number equivalent. ¹percent reads mapped to features (featureCounts); ²number (millions) of reads mapped to features (featureCounts); ³percent aligned bases overlapping ribosomal RNA regions (Picard); ⁴percent aligned bases overlapping UTRs and coding

regions of mRNA transcripts (Picard); ⁵percent of reads uniquely mapped to genome (STAR aligner); ⁶number (millions) of reads uniquely mapped to genome (STAR aligner); ⁷percent duplicate reads (FASTQC); ⁸average % GC content (FASTQC); ⁹total (millions) sequences (FASTQC).

9.8 Appendix 8. DEG lists from Venn diagram intersections (LFC > 1, padj<0.05).

Ensembl gene name	LFC	padj	Symbol	Condition
ENSMUSG00000038179	1.16638856	0.00166445	Slamf7	L1 only
ENSMUSG00000030114	1.3331058	3.82E-06	Klrg1	L1 only
ENSMUSG00000075010	1.26531635	0.00057655	AW112010	L1 only
ENSMUSG00000057123	1.04336997	0.00456058	Gja5	L2 only
ENSMUSG00000029075	1.08790506	0.00023928	Tnfrsf4	L2 only
ENSMUSG00000018341	1.08584655	2.16E-07	Il12rb2	L2 only
ENSMUSG00000023274	1.01225867	7.27E-09	Cd4	L2 only
ENSMUSG00000025929	1.74205338	7.87E-05	Il17a	L4 only
ENSMUSG00000041872	1.75031048	0.00093494	Il17f	L4 only
ENSMUSG00000026011	1.06975405	0.0042876	Ctla4	L4 only
ENSMUSG00000026358	1.08708195	8.47E-05	Rgs1	L4 only
ENSMUSG00000026866	1.32141921	4.85E-05	Kynu	L4 only
ENSMUSG00000028270	1.14911798	4.29E-08	Gbp2	L4 only
ENSMUSG00000028036	1.4008458	0.00210907	Ptgfr	L4 only
ENSMUSG00000039899	1.02116696	0.0004035	Fgl2	L4 only
ENSMUSG00000105096	1.03371211	1.05E-06	Gbp10	L4 only
ENSMUSG00000029436	1.18848508	0.00027944	Mmp17	L4 only
ENSMUSG00000038521	1.00581651	4.03E-09	C1s1	L4 only
ENSMUSG00000030325	1.16842024	0.00403902	Klrb1c	L4 only
ENSMUSG00000067599	1.34805248	0.00114022	Klra7	L4 only
ENSMUSG00000009292	1.18025449	0.00470398	Trpm2	L4 only
ENSMUSG00000082976	2.59247527	0.00033842	Gm15056	L4 only
ENSMUSG00000031548	1.07152477	1.91E-09	Sfrp1	L4 only
ENSMUSG00000031551	1.06078125	0.00033522	Ido1	L4 only
ENSMUSG00000000791	1.11483682	5.94E-05	Il12rb1	L4 only
ENSMUSG00000111229	1.09895845	0.00568411	Gm39323	L4 only
ENSMUSG00000047898	1.00542102	0.00598881	Ccr4	L4 only
ENSMUSG00000020826	1.57701351	0.00033522	Nos2	L4 only
ENSMUSG00000009185	2.04612886	8.47E-05	Ccl8	L4 only
ENSMUSG00000020702	2.31641312	0.00093494	Ccl1	L4 only
ENSMUSG00000021538	1.62725126	0.00157045	Il9	L4 only
ENSMUSG00000050747	1.106666	0.0003458	Trim15	L4 only
ENSMUSG00000035186	1.42557617	0.00045377	Ubd	L4 only
ENSMUSG00000034295	1.56024642	0.00044262	Fhod3	L4 only
ENSMUSG00000090942	1.3346861	2.79E-05	F830016B08Rik	L4 only
ENSMUSG00000039699	1.0634297	0.00014223	Batf2	L4 only
ENSMUSG00000048120	1.29319257	1.79E-05	Entpd1	L4 only
ENSMUSG00000031549	1.0599579	4.34E-05	Ido2	L1 and L2
ENSMUSG00000056091	1.03437095	0.00058401	St3gal5	L1 and L4

ENSMUSG00000044701	1.33415388	0.00059314	Il27	L1 and L4
ENSMUSG00000074695	1.0357834	0.00019539	Il22	L1 and L4
ENSMUSG00000079014	1.07229746	0.00290124	Serpina3i	L1 and L4
ENSMUSG00000038037	1.00975336	3.78E-05	Socs1	L1 and L4
ENSMUSG00000054072	1.06799164	1.37E-05	ligp1	L1 and L4
ENSMUSG00000063388	1.01873046	0.00029198	BC023105	L1 and L4
ENSMUSG00000026009	1.21328515	3.56E-06	Icos	L2 and L4
ENSMUSG00000027718	5.74807658	7.77E-06	Il21	L2 and L4
ENSMUSG00000008153	1.55313372	0.00075345	Clstn3	L2 and L4
ENSMUSG00000030167	1.73863009	0.00044378	Klrc1	L2 and L4
ENSMUSG00000004612	1.72305111	0.00032787	Nkg7	L2 and L4
ENSMUSG00000037202	1.46698147	0.00084243	Prfl	L2 and L4
ENSMUSG00000015437	3.18871324	3.93E-05	Gzmb	L2 and L4
ENSMUSG00000023132	3.0190464	3.93E-05	Gzma	L2 and L4
ENSMUSG00000068227	1.01524296	1.14E-05	Il2rb	L2 and L4
ENSMUSG00000024402	2.36165671	3.34E-06	Lta	L2 and L4
ENSMUSG00000024670	1.2067429	4.12E-05	Cd6	L2 and L4
ENSMUSG00000000817	2.45595444	3.86E-09	Fasl	L1, L2 and L4
ENSMUSG00000053318	1.41130173	0.00051841	Slamf8	L1, L2 and L4
ENSMUSG00000026830	3.95838823	1.26E-06	Ermn	L1, L2 and L4
ENSMUSG00000039521	1.13684424	0.00054044	Foxp3	L1, L2 and L4
ENSMUSG00000027720	5.00324981	5.75E-06	Il2	L1, L2 and L4
ENSMUSG00000028362	1.02647203	0.00075345	Tnfsf8	L1, L2 and L4
ENSMUSG00000029417	1.18485963	0.00316011	Cxcl9	L1, L2 and L4
ENSMUSG00000034438	1.27474687	7.77E-06	Gbp8	L1, L2 and L4
ENSMUSG00000079363	1.09649716	1.69E-06	Gbp4	L1, L2 and L4
ENSMUSG00000046031	1.16632114	3.73E-07	Calhm6	L1, L2 and L4
ENSMUSG00000055170	3.34798195	1.36E-16	Ifng	L1, L2 and L4
ENSMUSG00000111913	2.27528391	0.00037497	Gm49751	L1, L2 and L4
ENSMUSG00000001444	1.68600542	2.80E-07	Tbx21	L1, L2 and L4
ENSMUSG00000053101	1.07799258	0.00400629	Gpr141	L1, L2 and L4
ENSMUSG00000042385	1.85403552	0.00115286	Gzmk	L1, L2 and L4
ENSMUSG00000066363	1.27763468	3.81E-08	Serpina3f	L1, L2 and L4
ENSMUSG00000041481	1.47743703	0.00054346	Serpina3g	L1, L2 and L4
ENSMUSG00000033576	2.31377415	1.35E-11	Apol6	L1, L2 and L4
ENSMUSG00000085977	1.21828801	8.27E-05	Gm5970	L1, L2 and L4
ENSMUSG00000068606	1.23690051	3.93E-05	Gm4841	L1, L2 and L4
ENSMUSG00000118051	4.98699758	2.12E-21	Gm8714	L1, L2 and L4

9.9 Appendix 9. DEG lists from Venn diagram intersections (LFC < -1, padj < 0.05).

Ensembl gene name	LFC	padj	Symbol	Condition
ENSMUSG00000046470	-1.0362263	4.61E-06	Sox18	L1 only
ENSMUSG00000024440	-1.4089517	2.39E-05	Pcdh12	L1 only
ENSMUSG00000000253	-1.0656348	3.93E-05	Gmpr	L2 only
ENSMUSG00000038530	-1.0503636	3.91E-05	Rgs4	L4 only
ENSMUSG00000048142	-1.8644317	2.56E-05	Nat8l	L4 only
ENSMUSG00000054422	-1.2222666	0.00010469	Fabp1	L4 only
ENSMUSG00000059974	-1.479497	0.00095432	Ntm	L4 only
ENSMUSG00000044338	-1.9898709	7.53E-15	Aplnr	L1 and L2
ENSMUSG00000037010	-1.7650005	3.72E-09	Apln	L1 and L2
ENSMUSG00000054690	-1.1237373	7.95E-08	Emcn	L1 and L4
ENSMUSG00000035896	-1.4197873	1.58E-05	Rnase1	L1 and L4
ENSMUSG00000044338	-1.7740935	8.79E-11	Aplnr	L1, L2 and L4
ENSMUSG00000037010	-1.1185403	0.00013008	Apln	L1, L2 and L4